THE UNIVERSITY *of* EDINBURGH

Electrochemical Control of Reversible DNA Hybridisation:

For future use in nucleic acid amplification

Shahida Nina Syed

A Thesis presented for the degree of
Doctor of Philosophy,
The University of Edinburgh

December 2013

Division of Pathway Medicine
College of Medicine and Veterinary Medicine
The University of Edinburgh

Declaration

I hereby declare that this thesis and the work presented in it are my own.

I confirm that:

- This work was done wholly or mainly while in candidature for a research degree at this University.
- Where any part of this thesis has previously been submitted for a degree or any other qualification at this University or any other institution, this has been clearly stated.
- Where I have consulted the published work of others, this is always clearly attributed.
- Where I have quoted from the work of others, the source is always given. With the exception of such quotations, this thesis is entirely my own work.
- I have acknowledged all main sources of help.
- Where the thesis is based on work done by myself jointly with others, I have made clear exactly what was done by others and what I have contributed myself.

Shahida Nina Syed
University of Edinburgh

Abstract

Denaturation and renaturation is indispensable for the biological function of nucleic acids in many cellular processes, such as for example transcription for the synthesis of RNA and DNA replication during cell division. However, the reversible hybridisation of complementary nucleic acids is equally crucial in nearly all molecular biology technologies, ranging from nucleic acid amplification technologies, such as the polymerase chain reaction, and DNA biosensors to next generation sequencing.

For nucleic acid amplification technologies, controlled DNA denaturation and renaturation is particularly essential and achieved by cycling elevated temperatures. Although this is by far the most commonly used method, the management of rapid temperature changes requires bulky instrumentation and intense power supply. These factors so far precluded the development of true point-of-care tests for molecular diagnostics.

This Thesis explored the possibility of using electrochemical means to control reversible DNA hybridisation by using electroactive intercalators. First, fluorescence-based melting curve analysis was employed to gain an in depth understanding of the reversible process of DNA hybridisation. Fundamental properties, such as stability of the double helix, were investigated by studying the effect of common denaturing agents, such as formamide and urea, pH and monovalent salt concentration. Thereafter, four different electroactive intercalators

and their effect on the thermodynamic stability of duplex DNA were screened. The intercalators investigated were methylene blue, thionine, daunomycin and adriamycin. Absorbance-based melting curve analysis revealed a significant increase of the melting temperature of duplex DNA in the presence of oxidised daunomycin. This was not observed in the presence of chemically reduced daunomycin, which confirmed the hypothesis that switching of the redox-state of daunomycin altered its properties from DNA binding to non-binding. Accordingly this altered the thermodynamic stability of duplex DNA. The difference in the stability of duplex DNA, as a direct result of the redox-state of daunomycin, was exploited to drive cyclic electrochemically controlled DNA denaturation and renaturation under isothermal conditions. This proof-of-principle was demonstrated using complementary synthetic 20mer and 40mer DNA oligonucleotides. Analysis with *in situ* UV–vis and circular dichroism spectroelectrochemistry, as two independent techniques, indicated that up to 80 % of the duplex DNA was reversibly hybridised. Five cycles of DNA denaturation and renaturation were achieved and gel electrophoresis as well as NMR showed no degradation of DNA or daunomycin. As no extreme conditions were implicated, no covalent modification of DNA was required and isothermal conditions were kept, this finding has great potential to simplify future developments of miniaturised and portable bioanalytical systems for nucleic acid-based molecular diagnostics.

Acknowledgements

I would like to express my sincere gratitude to my supervisor PD Dr. Till Bachmann. I truly appreciate that you gave me the opportunity to come to Edinburgh and your research group to pursue a PhD. I will always be grateful for your support and guidance throughout my project, but also for your trust and for all the freedom you gave me over the past years. I would also like to thank my second and third supervisors Prof. Jason Crain and Prof. Andrew Mount for all the invaluable input and insightful discussions on my work.

I would like to thank members of the Bachmann group starting with Dr. Holger Schulze for always being there to answer my never-ending questions, your invaluable input and encouragement over the years and for proof-reading my Thesis. I would like to give Senthil Gandi, G-man, for a long time 'the other PhD student' a special thanks for being an incredible fellow PhD student and friend. I could've not imagined getting through my PhD without our daily venting and your support. I would like to thank fellow PhD student Johannes Brennecke for always being ready to listen and for your encouragement, especially in writing this Thesis. I am truly grateful for having had the opportunity to supervise exchange student Christian Goesswald from Germany, MSc students Daniel Macdonald, Aruna Sridhar and Eleojo Obaje, and summer worker Miglė Petruškevičiūtė during my PhD. It has been a true pleasure to work with each one of you and I have learnt a lot. A special thank you to Eleojo Obaje for your amazing help and great spirit in the lab while I have been writing this Thesis. I owe you! Finally, I would like to thank

former member Dr. Damion Corrigan for all your help during the years you were in our group as well as for being my English proof-reader.

Tea break would've not been tea break without my amazing fellow PhD students and friends Miriam Kaatz, Ramya Gundurao, Fairus Noor Hassim, Wey-Yuan Hsieh, Rui Chen, and Peter Thomas. I would like to thank all of you for your amazing support and making my PhD years full of hilarious, crazy and, at times, odd memories. I would especially like to thank Miriam Kaatz for being an awesome flat mate for four years. I will always treasure our hour long chats in the kitchen about anything and everything which made me keep my sanity at times! Thank you to all the members of Division of Pathway Medicine for all your help around the lab and for making my time ever as exciting.

I would like to acknowledge Dr. Janice Bramham at the Edinburgh Biophysical Characterisation Facility for the priceless help and input on the circular dichroism experiments. Juraj Bella at the Edinburgh Biomolecular NMR Unit is gratefully acknowledged for helping me in conducting the NMR experiments and making sense of the data. Your expertise and patience has been of invaluable help. Lastly, thank you Dr. Paul Murray at the Edinburgh University Inorganic Electrochemistry Group for introducing me to *in situ* UV–vis spectroelectrochemistry.

I would like to take this opportunity to thank some of the most important people in my life, my mother Marja-Leena Lahtinen, my father Mukhtar Syed and my brother and his fiancée Shakir Syed and Maria Andersson. Without your support and trust, I would not be where I am today. You have always encouraged me to follow my own path and be the best I can be, so thank you. Many thanks to my wonderful parents-in-law Robert and Susanna Weir for making our weekend trips to Aberdeen as enjoyable and relaxing as ever (much needed!), and for taking your time to show me around beautiful Scotland.

I would like to thank my closest and oldest friends Jasmin Kaleem Siddiqui, Samina Asad, Sufia Wasim, Reena Chuhan, Muzammil Aslam and Linda Granholm for your patience, incredible support and continuous interest in my academic pursuits,

although, I still think that my work might be a mystery for you… I would not be the person I am today if it wasn't for the life-long friends I made during my University studies, Jill Lundberg, Mikaela Viking, Miriam Landfors, Ylva Rodhe and Brenda Söderbäck. You have always inspired me to broaden my horizons and I will always be thankful for that. Finally, I want to say a special thanks to Emily Gauld for being a true inspiration with your non-scientific ways. Ying and yang! I have truly appreciated all your visits to Edinburgh during my PhD years and all the great things we got up to (Nothing to Declare marathon!), and thank you for being my English proof-reader.

Last but not least, I would like to say a BIG thank you to my fiancé Simon Weir. Your daily support and understanding throughout this whole intellectual, yet emotional journey has been incredible. I'm truly grateful for having been able to share joy, tears, laughter and frustration with you, but also to discuss weird results, papers, error analysis, equations and other mysterious things in the world of science. You have been my rock and will always be. Oh, and you're next!

"It's the possibility of having a dream come true
that makes life interesting."

Paulo Coelho, Alchemist

Table of Content

List of Abbreviations

6-FAM	6-carboxyfluorescein
A	Adenine
AM	Adriamycin
AS	Anti-sense
bp	Base-pair
BHQ	Black hole quencher
C	Cytosine
CD	Circular dichroism
CE	Counter electrode
COSY	Homonuclear correlation spectroscopy
CV	Cyclic voltammetry
DM	Daunomycin
DNA	Deoxyribonucleic acid
dsDNA	Double stranded DNA
FRET	Förster resonance energy transfer
G	Guanine
HMDE	Hanging mercury drop electrode
HPLC	High-performance liquid chromatography
ITO	Indium tin oxide
IR	Infrared
LCR	Ligase chain reaction
LMB	Leucomethylene blue

MB	Methylene blue
μTAS	Micro total analysis system
$NaBH_4$	Sodium borohydride
NAT	Nucleic acid testing
NMR	Nuclear magnetic resonance
NPA	No potential applied
OTTLE	Optically transparent thin-layer electrode
PCR	Polymerase chain reaction
POCT	Point-of-care testing
RE	Reference electrode
ROS	Reactive oxygen species
RNA	Ribonucleic acid
S	Sense
SEC	Spectroelectrochemistry
SSC	Saline-sodium citrate
ssDNA	Single stranded DNA
T	Thymine
Th	Thionine
T_M	Melting temperature
TxR	Texas Red
UV	Ultraviolet
WE	Working electrode

List of Figures

List of Tables

List of Schemes

Chapter 1

Introduction

Deoxyribonucleic acid (DNA) is the molecule of life and plays a key role in the flow of genetic information within a biological system, where it is involved in the transmission, expression and conservation of genetic material.[1] Since the discovery of the double helix in 1953 by Watson and Crick,[2] molecular biology has been revolutionised in terms of providing invaluable tools for detection and exploitation of nucleic acids across many different disciplines. One of the most critical functions of nucleic acids is their ability to undergo conformational change, more precisely the association and disassociation of the double helix. While not only indispensable in the cell, many molecular biology technologies rely on this function. Thus, there is a prevailing interest in further understanding and controlling this process in response to external stimuli.[3]

1.1 The Structure of DNA

DNA is a linear polymer built up by the sequential linkage of four types of nucleotides consisting of a sugar unit, also known as 2′ deoxyribose, a phosphate group and one of four possible uniquely structured bases, as depicted in Figure 1.1. The planar bases adenine (A), cytosine (G), guanine (G) and thymine (T) are covalently linked at a perpendicular angle to the sugar unit through an *N*-glycosidic bond, while the negatively charged phosphate group connects to the sugar unit with

an ester linkage. Unique sequences of these bases are built up by connecting nucleotides to each other through phosphodiester bonds between the phosphate groups. The sugar unit and the phosphate group also form the rigid backbone of the DNA polymer.[1] Apart from a linear sequence of nucleotides, DNA can undergo conformational changes forming secondary and tertiary structures. These include helical arrangements, which are reviewed in detail in Section 1.1.1, or higher-order structures such as condensation and chromosome packing.[4]

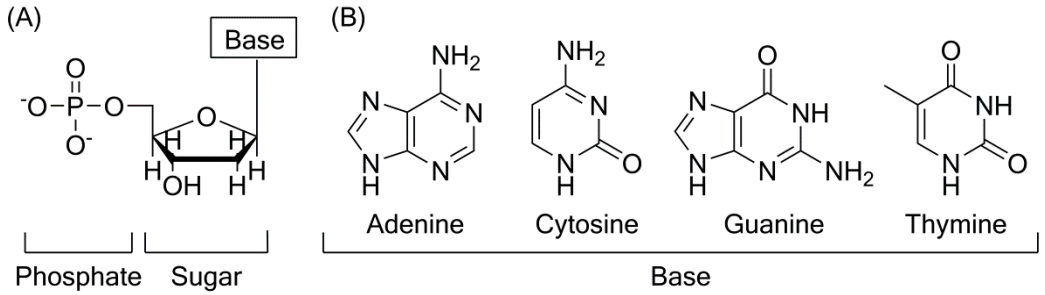

Figure 1.1 Building blocks of DNA. (A) Nucleotide consisting of a phosphate group, sugar unit and a base moiety. (B) The four uniquely structured bases.

1.1.1 The double helix

The existence of DNA in the cell as a double helix was first deciphered by Watson and Crick[2] in 1953 using X-ray diffraction patterns of fibres of DNA generated by Wilkins *et al.*[5] and Franklin and Gosling[6]. They discovered that the double helix consisted of two intertwined polynucleotide chains in antiparallel directions. These chains were interlinked by specific hydrogen bonds in the helix interior and had a sugar-phosphate backbone exterior. The four uniquely structured bases can be divided into two categories. Adenine and guanine are purines, while cytosine and thymine are pyrimidines.[1] Supported by earlier studies by Chargaff[7] in 1950, Watson and Crick realised that purines interact with pyrimidines. That is, guanine was paired with cytosine, while thymine was paired with adenine which confirmed the existence of complementary base-pairing interactions possible through specific hydrogen bonding,[2] see Figure 1.2. This immediately suggested how genetic material was replicated between generations. The sequence of one strand

determines the sequence of the other strand, thus allowing synthesis of complementary strands from a parent strands.[2, 8]

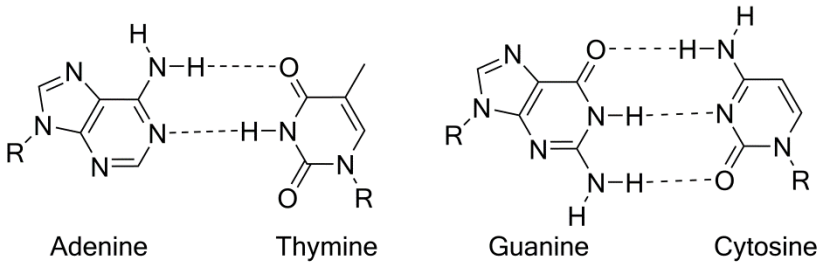

Figure 1.2 Complementary base-pairing in DNA.

In addition to specific hydrogen bonding, bases stack on top of each other allowing the formation of the double helix as illustrated in Figure 1.3. The bases are separated from each other by 3.4 Å with a twist of 36° per base. The helical structure is repeated every 34 Å corresponding to 10 bases per turn undergoing a full 360° turn.[2] The diameter of the helix is 20 Å. Furthermore, the double helix exhibits wide major and narrow minor grooves with widths of 11.7 Å and 5.7 Å, respectively. This occurs as a result of the glycosidic bond between the base and the sugar-phosphate backbone, but also due to the characteristic feature that base-pairs (bp) are not centred at the helix axis but rather displaced by approximately 0.8 Å.[1, 9]

The most common helix conformation of naturally occurring and synthetic DNA is B-DNA with a right-handed twist. However, depending on the environment, different helical arrangements may be adopted. Among others, two common conformations include the right-handed A-DNA and the left-handed Z-DNA.[10] A-DNA can be adopted by any sequence at low hydration levels. It is recognised by its wide and compressed helix with narrow, deep major groves and wide, shallow minor grooves. In contrast, the Z-DNA is characterised by its thin, elongated helix with narrow, deep minor grooves and a convex major groove. It generally occurs with alternating purine and pyrimidine sequences, mainly G and C.[10, 11]

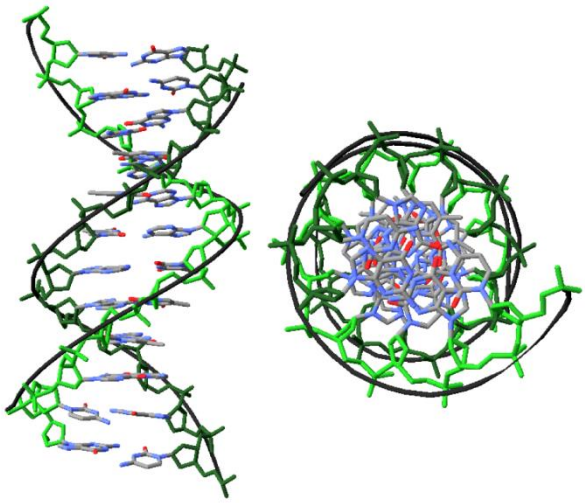

Figure 1.3 Side and top view of the B-DNA double helix. PDB ID: 1D65.[12]

1.1.2 The non-covalent forces of the double helix

The two primary factors responsible for the stability of the DNA double helix are the Watson-Crick hydrogen bonds between base-pairs and the stacking of adjacent bases.[13, 14] The stability and selectivity gained from the hydrogen bonds is essential with respect to the formation and separation of complementary strands.[14]

Despite the critical importance of the Watson-Crick hydrogen bonds, research has demonstrated that the dominating stabilising factor of the double helix is base stacking.[13, 15] Also known as π-π stacking or aromatic stacking, this complex interaction is governed by several non-covalent forces. Base stacking refers to the vertical, face-to-face arrangement of bases in which their aromatic ring structures overlap. As a result, the π-systems of the aromatic rings are in direct contact. Furthermore, dispersion and electrostatic effects, such as van der Waals and dipole-dipole interactions, play a crucial role in attracting and stabilising overlapping bases. Although these interactions are relatively weak, the cumulative effect in a large double helix is substantial.[14, 16, 17] In addition, base-stacking is stabilised by the hydrophobic effect. The hydrophobic nature of the bases results in the minimisation of contact with water, which consequently leads to exposure of the negatively charged, hydrophilic sugar-phosphate backbone on the outside.[9, 14, 17] However, it is

worth emphasising, that the dominating force of base-stacking is still under debate.[13] While Luo and co-workers[18] reported that the non-electrostatic interactions dominate, Newcomb and Gellman[19] found that the dominating force driving base-stacking is the attractive interactions between partial charges on the bases. On the other hand, Guckian *et al.*[17] suggested that the main force responsible for base-stacking is the solvation-driven hydrophobic effect.

Purine-purine stacks are the most stable forms, followed by pyrimidine-purine and pyrimidine-pyrimidine stacks. However, the stacking energy is also influenced by the sequence. Table 1.1 shows the stacking energies of ten unique dimer combinations in B-DNA. The strongest base-stacking occurs between dimers containing G·C base-pairs. Therefore, DNA with high G·C-content generally forms more stable duplexes.[9]

Table 1.1 Stacking energies for ten unique dimers in B-DNA.†

Stacked dimers	Stacking energies (kcal mol^{-1})
AA/TT	−1.00
AT/TA	−0.88
TA/AT	−0.58
CA/GT	−1.45
GT/CA	−1.44
CT/GA	−1.28
GA/CT	−1.30
CG/GC	−2.17
GC/CG	−2.24
GG/CC	−1.84

† Measured in 1 M NaCl at 37 °C.[20]

While Watson-Crick hydrogen bonds and base-stacking act as stabilising forces, other forces exert a negative contribution towards the stability. The electrostatic repulsion by the negatively charged phosphate groups on the sugar-phosphate backbone is an example of a destabilising force.[14] Consequently, the stability of the

double helix is additionally dependent on the ionic strength, as discussed in Section 1.2.2 within the context of the counterion condensation theory.[13, 15]

1.2 Reversible Hybridisation of DNA

Denaturation and renaturation is the reversible interconversion between double-stranded DNA (dsDNA) and single-stranded DNA (ssDNA). This reversible process is indispensable for the biological function of nucleic acids in many cellular processes, such as transcription for the synthesis of ribonucleic acid (RNA), replication during cell division and regulation of gene expression.[8] It plays an equally essential role in many techniques and applications targeting *in vitro* diagnostics, such as nucleic acid amplification technologies including both the polymerase chain reaction (PCR)[21] and the ligase chain reaction (LCR),[22] DNA microarrays,[23, 24] next generation sequencing[25] and biosensing.[26, 27]

1.2.1 The mechanism of reversible DNA hybridisation

Denaturation and renaturation, also termed DNA melting and hybridisation, involves the break down and formation of interstrand Watson-Crick hydrogen bonds between bases and intrastrand base-stacking interactions, such as van der Waals and dipole-dipole interactions.[13, 14] Under ambient conditions, the renaturation of two DNA single strands is a thermodynamic favourable event, while denaturation of duplex DNA is unfavourable and does not occur spontaneously.[8]

The accepted model for duplex formation consists of two main steps. The first key step involves the formation of a nucleation complex where an unstable single base-pair is initially formed. Only upon the stacking of a second and third base-pair is an appropriate, although still unstable, nucleation complex formed. The second step involves a rapid "zippering up" mechanism of the remaining base-pairs.[28, 29] Since base-pair formation is accompanied by a loss in entropy,[14] the initial nucleation event is energetically unfavourable. However, the formation and stacking of additional base-pairs lead to a negative contribution to the free energy.[9, 15] Thus, the formation of the remaining duplex occurs spontaneously and explains the

cooperative behaviour of DNA renaturation.[9, 28] In a recent coarse-grain modelling study by Sambriski *et al.*, it was suggested that the renaturation event is greatly affected by the nucleotide sequence. The authors confirmed that random nucleotide sequences indeed followed the renaturation pathway involving a nucleation event. In contrast, however, sequences with repetitive motifs seemingly followed a less restrictive pathway involving multiple nonspecific base-pairing sites.[30] The denaturation event is described by two types of models depending on the length of the DNA chain. Denaturation of longer chains is described by Poland-Scheraga type models in which the process occurs by the cooperative melting of domains of various sizes. For example, A·T-rich regions have been shown to denature first followed by more stable G·C-rich regions. Thus, it is assumed that during a denaturation event, the DNA chain consists of both hybridised helical segments and denatured loops.[31-34] Contrarily, short oligonucleotides are considered to denature according to the two-state model. This model is based on an all-or-none assumption that bears the nature of an infinitely cooperative transition where the double helix is either fully dissociated or fully associated.[35, 36]

While theoretical and experimental studies have concluded that denaturation of DNA is a first-order reaction,[31, 33] renaturation is generally regarded to follow second-order kinetics with the initial nucleation event as the rate limiting step. The second-order nature arises from the dependence of two strands associating.[28, 29] However, others have argued that, whereas the initial nucleation event does indeed follow second-order kinetics due to complementary strand recognition, the subsequent "zippering up" mechanism is more likely described by first-order kinetics.[37] This is also commonly assumed when applying the two-state model for treatment of denaturation and renaturation data of short oligonucleotides.[35, 36]

1.2.2 Counterion condensation theory

As detailed in Section 1.1.2, aside from stabilising forces, the stability of the double helix is also governed by destabilising forces as a result of the negatively charged phosphate groups on the sugar-phosphate backbone. DNA is hence a highly negatively charged polyion that strongly interacts with cations, making the stability

of the double helix dependent on the ionic strength.[13, 15] In order to gain further insight and understanding of the denaturation and renaturation equilibrium, the polyelectrolyte behaviour of nucleic acids has been examined both experimentally (Section 1.2.3.2) and theoretically. Several theoretical models, such as the counterion condensation theory,[38, 39] the Poisson-Boltzmann theory[40] and the tightly bound ion theory,[41] have been proposed in order to thermodynamically predict and quantify the interaction and effect of counterions on nucleic acids. Nevertheless, owing to its simplicity, the counterion condensation theory has been widely used, as both the Poisson-Boltzmann theory and the tightly bound ion theory require to be solved numerically.[42, 43]

In the present work, the reversible DNA hybridisation and its dependence on the salt concentration will be discussed in the context of the counterion condensation theory proposed by Manning and Record.[38, 39] This theory assumes a simplified model of a polyelectrolyte of length L and charged groups of valence Z_p. This corresponds to an infinitely long charged linear cylinder where the charges are evenly separated at an average spacing b.[38, 39] The simplified model of a polyelectrolyte holds true as long as the Debye-Hückel screening length κ^{-1}, Eq. (1.1), is less than its persistence length, or contour length L (short polyions).[1, 43] The Debye-Hückel screening length is defined as[1]

$$\kappa^{-1} = \sqrt{\frac{\varepsilon_0 \varepsilon k_B T}{e^2 N_A 2C}} \tag{1.1}$$

where ε_0 is the permittivity in free space 8.854×10^{-12} F m^{-1}, ε is the dielectric constant (78.3 for water at 25 °C), k_B is the Boltzmann constant 1.381×10^{-23} J K^{-1}, T is the temperature in Kelvin, e is the electron charge 1.602×10^{-19} C, N_A is Avogadro's number at 6.022×10^{23} mol^{-1} and C is the concentration of the electrolyte in mol m^{-3}. The persistence length for dsDNA is 50 nm,[44] while the contour length is $L = N_{bp}R_0$, where N_{bp} and R_0 is the number and size of each structural unit (base-pair)[1]. R_0 is 3.4 Å for dsDNA which corresponds to the rise of the helix per base-pair.

The extent of counterion association is independent from the bulk salt concentration in the dilute regime. It is fundamentally determined by the axial charge density parameter of DNA[38, 39]

$$\xi = \frac{e^2}{\varepsilon k_B T b} = \frac{l_b}{b} \tag{1.2}$$

where $l_b = e^2/\varepsilon k_B T$ is the Bjerrum length, which is 7.14 Å in water at 25 °C, and b is the average charge spacing. Sufficient counterions associate if $\xi > 1$, which is true when $b < 7.14$ Å. These associated counterions become territorially bound and confined within 7 Å of the surface of the polyion, but are still free to translate along its surface.[45] Thus, the destabilising forces arising from the repulsion of the phosphate groups are accordingly compensated by the condensed counterions, and the net charge of DNA is reduced. The reduction may be estimated as a fraction of condensed counterions n per structural polyion charge N, i.e. $\theta = n/N = 1 - (\xi)^{-1}$.[38] For dsDNA, the average spacing between two phosphate charges is b = 1.7 Å (since there are two phosphate groups per every 3.4 Å rise along the helix) which gives a charge density of ξ = 4.2 (in aqueous solution at 25 °C) using Eq. (1.2). Consequently, the fraction of a condensed counterion is θ_{ds} = 0.76. For ssDNA, the average charge spacing was estimated to ~ 4.3 Å which yields ξ = 1.7 and θ_{ss} = 0.39.[38]

In addition to the charge compensation through territorially bound counterions, uncondensed counterions in the diffuse ion atmosphere that screen the electrostatic interactions along the polyion can be described by the Debye-Hückel approximation. Therefore, the extent of condensation as well as the screening effect is summarised in the thermodynamic counterion binding parameter[39]

$$\psi = \theta + (2\xi)^{-1} = 1 - (2\xi)^{-1} \tag{1.3}$$

The counterion condensation theory predicts, ψ_H = 0.88 for dsDNA and ψ_C = 0.70 for ssDNA.[39] The main outcome is the immediate realisation that renaturation and denaturation events are accompanied by a net uptake, or release, of counterions.[46] The free energy of the system is the combined free energy of the electrostatic

repulsions between the negatively charged phosphate groups, which are neutralised by counterions, and the free energy of mixing of the condensed counterions through translation or exchange close to the DNA. That is,[38, 43]

$$\Delta G^\circ = \Delta G^\circ_{\text{el}} + \Delta G^\circ_{\text{mix}} \tag{1.4}$$

While the extent of counterion condensation is independent of salt concentration, the free energy from the screening of the phosphate charges with diffuse counterions ($\Delta G^\circ_{\text{el}}$) and the entropy from mixing of condensed counterions ($\Delta G^\circ_{\text{mix}}$) will vary with the salt concentration. Indeed this explains the salt-dependent nature of DNA renaturation and denaturation events.[1, 46, 47]

1.2.3 The melting temperature

As mentioned, denaturation of dsDNA does not occur spontaneously. However, many cellular processes require ssDNA for downstream processing.[8] Hence, denaturation inside the cell is catalysed by enzymes known as helicases that move along the nucleic acid and use adenosine tripohosphate (ATP) to facilitate the hydrolysis of hydrogen bonds between complementary bases.[48] In contrast, simpler methods are utilised to achieve denaturation *in vitro*. The input of thermal energy, in the form of heating, is commonly used which disrupts the Watson-Crick hydrogen bonds at a certain temperature. On the removal of the thermal energy, i.e. cooling, the hydrogen bonds form again. Other common methods include the use of acidic or basic pH[49, 50] or chemical agents, such as urea,[51] formamide,[52] diethlysulfoxide and dimethylsulfoxide.[53]

In order to quantify the renaturation or denaturation process, the melting temperature (T_{M}) is commonly determined. It is defined as the temperature at which 50 % of dsDNA is in a denatured state.[54] This parameter can easily be determined using various methods such as ultraviolet (UV) absorption or fluorescence emission.[36] A detailed description is found in Section 1.5. As the melting temperature reflects a conformational change, it allows the determination of structure stability which has found its use in any nucleic acid-based research, assay

design or application.[36, 55] Therefore, the parameters influencing the stability, and consequently the reversible hybridisation of DNA, have been studied for several decades.[35, 36, 56-58] In accordance with studies on the stabilising forces of DNA (see Section 1.1.2), it has been deduced that the melting temperature is influenced by base sequence and length, as well as the salt concentration of the medium.[9] Furthermore, due to the bimolecular nature of the renaturation event, the duplex stability is additionally influenced by the DNA concentration.[36]

1.2.3.1 Base sequence

An early study by Marmur and Doty established the linear relationship between fraction of G·C base-pairs and the melting temperature.[59] It showed that G·C-rich DNA denatured at higher temperatures compared to A·T-rich DNA. Studies have since confirmed that the formation of G·C base-pairs is enthalpically more favourable.[60, 61] A common misconception has involved the assumption that the stability of G·C versus A·T arises from the difference in number of Watson-Crick hydrogen bonds, as depicted in Figure 1.2. However, as outlined in Section 1.1.2, the key stabilising factor for duplex DNA is undoubtedly the base stacking. Hence, sequence-dependent stability has been analysed in terms of nearest-neighbour base-pair interactions. As a consequence of the rules for base-pairing, only ten unique stacking dimer combinations exist. Their thermodynamic contribution has been unravelled by comparing the melting temperatures from several melting studies using repeating copolymers,[58] long restriction fragments[62] and short oligonucleotides[20, 63] with varying G·C-content. In a comparison study, SantaLucia presented a unified view of the stacking energies found in the literature.[56] The published stacking energies by SantaLucia *et al.*,[20, 56] presented in Table 1.1, allows the melting temperature to be predicted for any DNA sequence.[63] Furthermore, they clearly show that G·C stacks are more favourable.

1.2.3.2 Salt concentration

Due to the polyelectrolyte nature of nucleic acids, the strong interaction with cations has been rigorously examined theoretically (Section 1.2.2) as well as experimentally. Indeed, early on Schildkraut and Lifson observed a linear dependence of the

melting temperature of bacterial DNA with salt concentration which increased upon increasing sodium ion concentration.[64] As verified by numerous other systematic studies utilising plasmid DNA,[34] short DNA hairpin structures[65] and short oligonucleotides,[55, 66, 67] this behaviour can also be described in the context of the counterion condensation theory. Assuming a two-state transition of the interconversion between the dsDNA double helix (H) and the ssDNA coil (C) form, the following chemical equilibrium is true[39, 46]

$$H \rightleftharpoons C + (\Delta n)\mathrm{M}^{+} \tag{1.5}$$

where Δn is the net release of counterion M^+ per denatured helix, as deduced from the counterion condensation theory in Section 1.2.2. Since the fraction of condensed counterions n per phosphate charge N is $\theta = n/N = 1 - (\xi)^{-1}$, together with Eq. (1.3) which takes into account both binding and screening contributions, the number of released counterions will be[39]

$$\Delta n = n_{\mathrm{H}} - n_{\mathrm{C}} = (N/2)\left(\xi_{\mathrm{C}}^{-1} - \xi_{\mathrm{H}}^{-1}\right) = N(\psi_{\mathrm{H}} - \psi_{\mathrm{C}}) \tag{1.6}$$

However, since the oligonucleotides in this work do not contain a terminal phosphate, $N = 2(N_{\mathrm{bp}} - 1)$.[55] Through the use of thermodynamic relationships and the equation above, the following equation can be derived which describes the monovalent salt-dependent T_{M}, that is[38, 39]

$$\frac{\partial T_{\mathrm{M}}}{\partial \ \ln[\mathrm{Na}^{+}]} = -\frac{\alpha R {T_{\mathrm{M}}}^{2}}{\Delta H^{\circ}} \Delta n \tag{1.7}$$

or in terms of the reciprocal T_{M} with insertion of Eq. (1.6)[55]

$$\frac{\partial\left(\frac{1}{T_{\mathrm{M}}}\right)}{\partial \ \ln[\mathrm{Na}^{+}]} = \frac{\alpha R}{\Delta H^{\circ}} \Delta n = \frac{\alpha R}{\Delta H^{\circ}} 2\left(N_{\mathrm{bp}} - 1\right)\Delta\psi \tag{1.8}$$

where ΔH° is the renaturation enthalpy that can either be measured or estimated using the nearest-neighbour parameters in Table 1.1. R is the ideal gas constant at

8.314 J mol^{-1} K^{-1}. α is the correction term for the sodium ion activity coefficient γ which equals to $\left(1 + \partial \ln \gamma / \partial \ln[\mathrm{Na}^+]\right)$ and is regarded as constant at 0.92 over the range of 1–100 mM NaCl.[39, 66] It is worth noting, that while the counterion condensation theory predicts a linear relationship between the logarithm of sodium ion concentration and the melting temperature up to 100 mM Na^+,[38, 39, 68] Owczarzy and colleagues[55, 57] reported a nonlinear behaviour above 200 mM Na^+.

Besides association with monovalent cations, nucleic acids additionally bind a number of divalent metal ions.[9] Whereas some ions such as Cu^{2+} decrease the melting temperature[69] others, like Mg^{2+}, exercise a stabilising effect and raise the melting temperature[46, 57, 67]. Unlike the monovalent cations, magnesium ions both stabilise nucleic acids and facilitate its formation of the double helix as well as tertiary structures.[70] Additionally, the stabilising potential of magnesium ions is significantly larger compared to sodium ions.[57, 67] Both theoretical[39] and experimental[46, 57, 67] studies have suggested a nonlinear dependence where the increase in the melting temperature plateaus with increasing magnesium ion concentration. Moreover, in a mixture with sodium ions, magnesium ions exhibit a competitive behaviour. As the magnesium ion concentration increases, the stabilising effect of sodium ions has been shown to decrease because condensation of magnesium ions occurs.[46, 57, 71]

1.3 Towards Point-of-Care Testing

The discovery of DNA, and understanding the thermodynamics behind the reversible hybridisation, has enabled the development of powerful molecular diagnostic tools important for many applications. Besides the frequent use for diagnosis of diseases and assessment of therapies, they have also been applied in other areas such as environmental monitoring, the food and agricultural industry as well as forensics profiling.[72, 73] Nucleic acid testing (NAT) technologies are based on the interrogation of specific DNA sequences, thus, offering higher specificity and sensitivity over traditional microbiological detection methods. However, many of these *in vitro* diagnostic platforms today are purpose-built for centralised

laboratories. They are frequently expensive bench-top sized instruments with high energy usage and, thus, struggle to meet the requirements of the increasing demands on decentralised testing. As a result, the interest in making diagnostics cheaper, faster and user-friendly has in recent years generated a focus on miniaturisation and integration of laboratory operations, such as sample preparation, nucleic acid amplification and detection, into fully automated lab-on-a-chip devices or micro total analysis systems (μTAS).[74-77]

First described by Manz *et al.*,[78] μTAS are miniaturised, simplified devices that make use of less reagents, enable faster reaction and analysis times, are easy to fabricate and have reduced energy consumption.[79, 80] The properties and development of μTAS has brought the possibility of decentralised portable analysis within reach.[73, 81, 82] Point-of-care testing (POCT) is the concept of bringing molecular diagnostics testing conveniently to the site or near the patient, thereby leading to a cost-effective approach as results can be obtained faster. The emergence of POCT is of great interest as diagnostics can be made more patient-centric in terms of, for example, easy monitoring of disease progression or tailoring treatment to individual patients.[83] It furthermore opens the possibility of bringing standard molecular diagnostic tools to geographically remote settings and developing countries, where limitations in well-established laboratory facilities are being faced.[82]

1.3.1 Integration of PCR into point-of-care testing

NAT technologies utilise different types of strategies for detection. However, often only small amounts of nucleic acid analyte are present in the sample. Therefore, many strategies rely on amplification of nucleic acids to increase the amount of the target of interest.[72, 74] Figure 1.4 illustrates the conventional nucleic acid amplification technology PCR.[21] This reaction relies on the repeated cycling of heating and cooling for denaturation of DNA, primer hybridisation and extension by utilising a heat stable DNA polymerase. Primers are short DNA fragments that flank the sequence to be amplified. Aside from being performed in bulky bench-top instruments, conventional PCR suffers from large reaction volumes. As a consequence of large thermal mass, heating and cooling rates are slow leading to

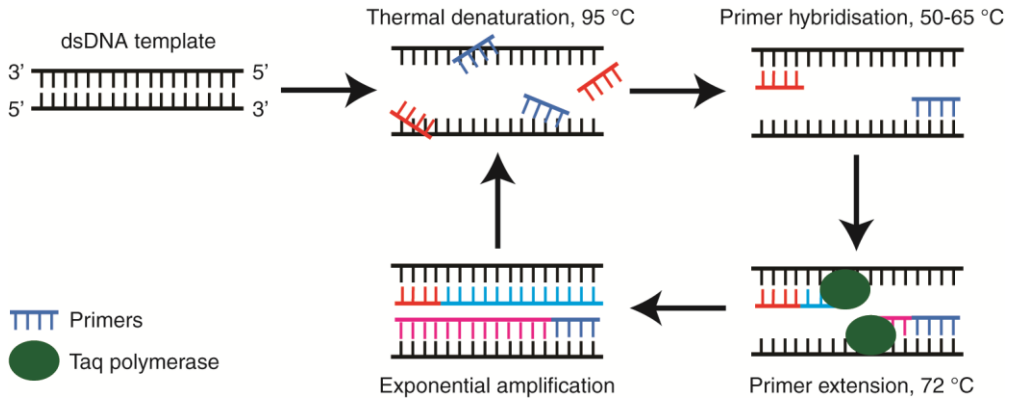

Figure 1.4 DNA amplification with PCR. By cycling three different temperatures, DNA can be exponentially amplified in the presence of primers and DNA polymerase.

lengthy PCR reactions.[79] Since the conventional PCR format is unsuitable for portable diagnostic devices, substantial research towards the miniaturisation of PCR has been carried out.[79, 84] Reduced thermal mass and smaller reaction volumes have made rapid heat transfer possible. Consequently, this has facilitated quicker heating and cooling rates, which in turn reduces assay time and energy consumption.[84] For example, Kopp and co-workers described the fastest continuous-flow miniaturised PCR chip. The glass chip was placed on three copper blocks, with different temperatures. Depending on the flow rate, a 2–20 min amplification of a 176 bp fragment from *Neisseria gonorrhoeae* was obtained (20 cycles). However, this system suffered from low sensitivity.[85] Since then, to balance sensitivity and assay time, numerous research groups have described a variety of miniaturised PCR platforms as recently reviewed by Ahmad and Hashsham[86] and Zhang and Ozdemir.[79]

The combination of miniaturised PCR with microfluidics has enabled the construction of sample-to-result devices, as parallel operations may also be integrated.[79, 86-90] Nevertheless, integration with both sample preparation and detection into a cost-effective and robust POCT device remains challenging.[73]

1.3.2 Challenges of PCR integration into point-of-care testing

Despite the fact that PCR has been miniaturised and integration into μTAS has been realised in different formats, only one commercial POCT platform exists on the

market today.[72, 73] The Cepheid GeneXpert® is a self-contained portable sample-to-answer system which combines sample preparation with real-time PCR amplification and detection.[91] Nonetheless, driving conventional PCR requires the precise and repeated cycling of heating and cooling which has rendered integration of miniaturised PCR into μTAS complex. A considerable amount of research has therefore been dedicated to the high-energy consuming temperature-control issue of miniaturised PCR.[84, 86, 92] This has led to the development of different types of heating elements, such as external heaters, thin metallic integrated heaters or non-contact heaters based on e.g. infrared (IR) light. Owing to high thermal mass, some solutions have not managed to improve the heating and cooling efficiency. While others have shown to be more efficient, the direct measurement of the temperature uniformity within the sample has proved challenging due to small dimensions.[84, 86, 92] Thus, issues associated with temperature-monitoring have equally been addressed. While various methods have been developed, many suffer from only providing readings from a few discrete points. Also, some do not record the actual temperature inside the sample as it is rather extrapolated from heat transfer laws or confer PCR inhibition. Moreover, developing cost-effective disposable heating elements has appeared to be difficult due to high fabrication or substrate material costs.[84, 92] As size becomes smaller, circumventing thermal cross-talk between different regions of the chip must be taken into consideration. Additionally, using high temperatures in conjunction with small reaction volumes has been reported to cause issues with sample evaporation and air bubble formation. The latter is able to cause large temperature differences within the sample.[84, 93]

Technical limitations associated with conventional PCR for μTAS integration have been recognised. In order to circumvent these limitations, isothermal amplification techniques have been considered as they do not rely on the precise thermal cycling mechanism for nucleic acid amplification.[74, 77] Fang *et al.* reported on a microfluidic-based loop-mediated isothermal amplification (LAMP) system for detection of pseudorabies virus. The amplification proceeded at 63 °C and detection was achieved within 1 hour.[94] Gulliksen *et al.* employed nucleic acid sequence-based amplification (NASBA), integrated in a microfluidic chip, to detect human papilloma virus. The amplification alone was accomplished within 2.5 h at 41 °C.[95]

Other integrated isothermal amplification technologies include rolling circle amplification (RCA)[96] and helicase-dependent amplification (HDA), which commonly take place at 30–60 °C and 60–65 °C,[97] respectively. Apart from HDA, which utilises a helicase enzyme for denaturation of dsDNA,[97] many of the aforementioned isothermal techniques rely on initial denaturation of the template at 95 °C to reach desired sensitivities or to work at all.[74] LAMP, for example, requires an elevated temperature to stop.[98] Furthermore, many methods still require incubating the reaction at higher temperatures making them energy consuming for POCT platforms.[99] Since the temperature-requirement persists for amplification of nucleic acids, Liu *et al.*[99] and others[81, 98] have reported on self-heating systems which make use of exothermic reactions to provide heat in order to drive isothermal amplification. Comprising the desirable characteristic of circumventing the need for an external power, exothermic heaters have shown to be fairly independent of the environment temperature. Nevertheless, substantial efforts towards regulating and maintaining the temperature are still being made.[81, 98, 100]

1.3.3 Electrochemistry-based sensing—a suitable option

Over the past decades, numerous applications have been described and developed in the field of electrochemical DNA biosensors.[26, 72, 101-103] Electrochemical biosensor is the definition of a device which couple recognition events, between biological recognition elements and specific target analyte, to an electrode transducer that converts it into an electrical signal for read-out.[104] Characteristics such as high sensitivity, simple operation, easy miniaturisation, fast response and low cost, makes electrochemical-based sensing an active area of research towards integration into μTAS and, consequently, the development of POCT platforms.[26, 72, 80]

While different types of electrochemical-based sensing strategies have been reported for detection of a variety of nucleic acids, many groups have focused on the sequence-specific detection of PCR product.[72, 105-107] However, to make the electrochemical detection of PCR product more efficient and compatible with portable diagnostic devices, it would be highly desirable to monitor product formation in real-time. Fluorescence-based real-time PCR is already a well-

established technology. It makes use of fluorescent reporter molecules that bind to dsDNA, such as SYBR Green,[108] or sequence-specific oligonucleotide probes, such as molecular beacons[109] or TaqMan® probes.[110] However, fluorescence-based methods require complex instrumentation and are expensive, thus, not ideal for decentralised portable systems.[73]

In 2006, Yeung and co-workers pioneered with reporting on the first chip-based real-time electrochemical monitoring of a PCR.[111, 112] The working principle was based on solid-phase PCR with simultaneous solution-phase PCR. Ferrocene-labelled nucleotides were incorporated into the amplified DNA and captured by immobilised primers on an indium tin oxide (ITO) electrode. Further extension of the primers resulted in accumulation of redox-active ferrocene at the electrode surface, which was monitored via differential pulse voltammetry. Deféver *et al.*, on the other hand, employed the inherent redox-activity of an analogue guanine base coupled to a redox-active osmium tripyridine-based mediator. Upon PCR amplification, the decrease in free analogue guanine nucleotides was indirectly monitored real-time using cyclic voltammetry.[113] More recent methods, by the same author[114] and Fang *et al.*,[115] exploited redox-active DNA intercalators for real-time chip-based detection. As the amplification proceeded, the intercalator bound to dsDNA and became less electrochemically available. Both methods employed square wave voltammetry for detection. While Fang *et al.* utilised methylene blue (MB) as a redox-active intercalator, Deféver and co-workers screened the suitability and efficiency of five different compounds, namely MB and four different osmium-based complexes. It is worth emphasising that all electrochemical real-time PCR methods described exploited thermal cycling to control strand separation and hybridisation and, accordingly, drive the amplification.

1.3.4 Alternative control of reversible DNA hybridisation

Thus far, the temperature-dependent amplification has undoubtedly caused significant issues for the incorporation into μTAS. Especially, the requirement for denatured DNA in all amplification methods remains a challenge to overcome. As realised from previous Sections, most existing techniques use thermal control for

denaturation and, by definition, renaturation. Thus, efforts have been put into realisation of alternative ways to control reversible DNA hybridisation. Wang and colleagues recently demonstrated an electrochemically-driven pH alteration method for the cyclic denaturation and renaturation of 290 bp long DNA fragments. The cycling was obtained by changing the bulk pH between 5.2 and 11.4. The pH was altered by applying an overall cell current, and the same current of reverse polarity, to inject and remove HCl. Four cycles of denaturation and renaturation were shown with a cycle time of 300 s. However, slight degradation of the DNA was observed.[116] The utilisation of pH-induced reversible DNA hybridisation has also been described in conjunction with self-assembled DNA nanostructures. Generally, bulk pH was changed between 5 and 8 by repeated additions of 1 M HCl and 1 M NaOH to switch a self-assembled DNA nanostructure between opened and closed state. The open state represented duplex DNA. The closed state characterised the ssDNA state where the single strands were self-assembled to an *i*-motif. Liu and Balasubramanian reported 30 cycles of denaturation and renaturation at a cycle time of 2 min using Förster resonance energy transfer (FRET).[117]

Asanuma *et al.* investigated photoregulation of reversible DNA hybridisation. Photoresponsive azobenzene units were covalently attached to short 8–9 bp long DNA oligonucleotides. Upon irradiation with UV or visible light, the azobenzene units underwent reversible isomerisation from a planar intercalating *trans* form to a non-planar, non-intercalating *cis* form. This facilitated the DNA denaturation and renaturation, of which two full cycles were demonstrated with UV monitoring, each cycle requiring 40 min.[118, 119] Light-controlled reversible DNA hybridisation based on the isomerisation of azobenzenes has been studied extensively.[120] For example, Dohno *et al.* exploited molecular glue with integrated azobenzene ligands to circumvent the need for covalent modification of DNA. Molecular glue is a mismatch binding ligand that facilitates duplex formation between mismatched DNA. On the association of molecular glue with an azobenzene unit, denaturation and renaturation of a mismatch-bearing 11 bp DNA oligonucleotide was accomplished. This was demonstrated both in solution and on a gold surface employing UV monitoring and surface plasmon resonance, respectively.[121, 122] In a different approach by Andersson and co-workers, spiropyrans were employed as

means for reversible DNA hybridisation. Avoiding the covalent binding of spiropyrans to DNA, calf thymus DNA was reversibly denatured and renatured based on the same photochromic working principle as azobenzenes. Two cycles were demonstrated with a cycle time of 10 min.[123]

Electronic control of reversible DNA hybridisation was demonstrated by Hamad-Schifferli and co-workers. This application was based on the induced heating of DNA-modified gold nanoparticles by a radio-frequency magnetic field. Utilising an alternating magnetic field, the local temperature surrounding the gold particles increased and denaturation was observed. Upon turning the magnetic field off, the heat dissipated and the 7 bp long DNA oligonucleotide renatured. Confirmed using FRET and UV monitoring, it was expected that cycling of reversible DNA hybridisation was achieved within seconds.[124]

While elegant approaches to achieve alternative ways for the control of reversible DNA hybridisation have been described, only one approach, to the best of our knowledge, makes use of electrochemistry. Albeit, as means for ultimate pH-dependent control.[116]

1.4 DNA Intercalators—the Alternative to Heat

A wide range of small molecules can strongly interact with DNA covalently or non-covalently. The two main modes of interaction are through intercalation or groove binding. However, it is noteworthy that these binding modes may also occur simultaneously. Intercalators are generally planar aromatic molecules that insert themselves between stacked DNA base-pairs. Grove binders generally comprise of at least two aromatic moieties to allow flexibility of the molecule in order to accommodate the crescent-shape of the minor groove upon binding. In this work, DNA intercalators that bind non-covalently will be considered.[125] Intercalators have been utilised for a range of different purposes. They often exhibit antitumor and antibiotic activity vital for medical applications,[126] however many equally possess fluorescent and electroactive properties. Both of these characteristics have been

vastly exploited for the fluorescent[127] and electrochemistry-based[26, 102, 105, 107, 128, 129] detection of nucleic acids.

1.4.1 Conformational effects of intercalation

The insertion of an intercalator causes conformational changes of the double helix, such as unwinding of 10–30°, lengthening of 3.4 Å per intercalation site and increasing rigidity.[1, 125] Furthermore, the spacing between the negative phosphates charges on the DNA backbone increase resulting in a reduced charge density of duplex DNA. Thus, as described by the counterion condensation theory, ligand binding or intercalation is energetically favourable, since the event is accompanied by a release of counterions. Positively charged compounds are even more favourable compared to uncharged ones.[39, 130] Due to the release of counterions, the binding is dependent on the salt concentration. That is, upon increasing salt concentration, the entropy gain from the release of counterions is reduced and thus weakens their binding.[1] Furthermore, the binding of an intercalator is restricted according to the neighbour exclusion principle. The model dictates that each binding site has equal potential to be an intercalation site. However, once an intercalator has bound, the binding of the next molecule between neighbouring base-pairs is hindered.[131] The neighbour exclusion binding isotherm by McGhee and von Hippel can be written as[132]

$$\frac{r}{C_\mathrm{f}} = K_\mathrm{i}(1-nr)\left[\frac{(1-nr)}{1-(n-1)r}\right]^{n-1} \tag{1.9}$$

where r is the ratio of the concentration of bound intercalator to total available base-pairs binding sites, C_f is the concentration of free intercalator, K_i is the intrinsic binding constant and n is the exclusion parameter in base-pairs. Based on the simplest thermodynamic model for drug–DNA interactions by Scatchard,[133] Eq. (1.9) does not take sequence specificity of the intercalator into account. Instead, this binding isotherm considers DNA as a one-dimensional lattice with several binding sites and no end effects, to which ligands bind in a non-cooperative fashion.[132] It is not entirely clear which effects lead to the exclusion of intercalators binding at

neighbouring sites, though, it is presumed that steric hindrance effects and decrease in electrostatic potential may play important roles.[125, 130]

The binding of an intercalator is not only confined to geometrical changes. If the binding favours duplex DNA, the helix–coil equilibrium is shifted towards the helix form resulting in higher melting temperatures of the ligand–DNA complex.[134, 135] Conversely, destabilisation of duplex DNA, resulting in a lower melting temperature, occurs when the single stranded form is preferred for binding.[136]

Intercalation can be confirmed using several different techniques, such as viscosity or sedimentation measurements, nuclear magnetic resonance (NMR) shift, recording the melting temperature of DNA as well as measuring UV–vis absorption and fluorescence emission.[125] Upon intercalation, the absorption peak of the intercalator commonly displays a hypochromic shift together with a considerable red-shift of the peak maxima. Furthermore, fluorescence quenching or enhancement upon binding may also be detected in the case of fluorescing compounds. High-field shift of the signals corresponding to the aromatic protons, on the other hand, confirms intercalation in ^{1}H-NMR.[137]

1.4.2 The energetics of intercalation

A systematic study by Breslauer *et al.* showed that the intercalative binding mode is generally exothermic ($-\Delta H°$). Furthermore, the investigation revealed large variations in $\Delta H°$, yet similar $\Delta G°$. According to the standard expression of free energy, $\Delta G° = \Delta H° - T\Delta S°$, it is clear that the binding mode is driven by an enthalpy-entropy compensation.[138] However, the interactions governing the binding mode of an intercalator, with potential side groups, are a mixture of forces. While it is not entirely clear exactly which forces drive the intercalation, it may be assumed that the factors contributing to the stabilising free energy of the binding of an intercalator are the following:[139]

$$\Delta G_{\mathrm{obs}} = \Delta G_{\mathrm{conf}} + \Delta G_{\mathrm{r+t}} + \Delta G_{\mathrm{pe}} + \Delta G_{\mathrm{hyd}} + \Delta G_{\mathrm{mol}} \qquad (1.10)$$

where ΔG_{obs} is the observed binding free energy, ΔG_{conf} is the cost in free energy due to conformational changes in DNA to accommodate an intercalator, ΔG_{r+t} is the cost due to loss in rotational and translational degrees of freedom, ΔG_{pe} is the free energy arising from the hydrophobic effect that transfer the intercalator into the DNA to minimise contact with the polar environment, ΔG_{hyd} is the free energy arising from the polyelectrolyte behaviour which leads to release of counterions upon intercalation and finally ΔG_{mol} is the free energy contribution from all the non-covalent molecular interactions once intercalated, such as hydrogen bonding, electrostatic and dipole-dipole interactions, dispersive interactions and π-stacking with the base-pairs of the DNA.[139-142] Furthermore, despite being a debated subject, studies have shown that hydration effects may have significant impact on the binding of intercalators. However, the exact role and contribution to the free energy of the binding process remains to be determined.[143] Qualitative studies by Chaires *et al.* demonstrated that the binding affinity of different intercalators decreased as water activity reduced. This indicated water uptake upon intercalation, which seemingly had a negative effect of the binding.[144]

1.4.3 Mechanism of intercalation

Research has been conducted on the elucidation of the important driving forces of intercalation. However, despite this knowledge, little is known of the actual mechanism. Based on kinetic studies of daunomycin (DM), Chaires *et al.* suggested a three-state mechanism which included an initial binding of the intercalator to the outside of DNA, intercalation and a final re-adjustment of the intercalator within the DNA.[145] Recently, Wilhelm and co-workers performed a systematic molecular dynamics study of DM intercalation based on minimum free energy calculations, which also indicated a three-state mechanism. As suggested by Chaires *et al.*, the molecular dynamics study confirmed initial binding of the intercalator to the outside of DNA, in the case of DM, to the minor groove. However, the second step involved the formation of a metastable intermediate between a rotated intercalator and a kinked DNA. The bending of the double helix facilitated the opening between two base-pairs. Full intercalation was obtained in the final step by further rotation of the intercalator and straightening the double helix to re-establish base stacking.[146]

1.4.4 Intercalators relevant to this study

1.4.4.1 Methylene blue

Methylene blue (MB) in Scheme 1.1 is a phenothiazine dye that interacts non-covalently with DNA. It is a simple polyaromatic, positively charged compound that is mainly used for staining of nucleic acids.[147] Whereas MB has been shown to bind alternating G·C sequences with a higher affinity,[148] it has long been disputed whether the binding mode is in fact intercalative.[149] Studies have indicated that the binding mode is highly dependent on ionic strength, sequence of DNA and the binding ratio.[147-149] However, systematic studies confirmed that intercalation is the predominant binding mode at low ionic strength with low binding ratios,[149] while different conditions promote groove binding[148] and electrostatic interactions.[150] Absorbance-based titration studies have indicated that one MB binds per every three to four base-pairs.[147] The intercalator possesses well-known electrochemical properties and can undergo a reversible $2e^-$ reduction to leucomethylene blue.[151] Furthermore, the oxidised form of MB has been found to stabilise duplex DNA and increase T_M up to 6 °C.[150]

1.4.4.2 Thionine

Thionine (Th) in Scheme 1.1 is a phenothiazine dye that binds non-covalently to DNA. Similar to MB, this intercalator is used for staining nucleic acids and carries one positive charge. While an early study[152] reported that thionine does not exhibit sequence-specific binding, both Chang *et al.*[153] and Paul *et al.*[154, 155] observed a greater binding affinity to G·C-rich sequences, specifically alternating G·C-sequences. The mode of binding has further been confirmed through intercalation.[155, 156] Like in the case of MB, thionine binds every third to fourth base-pair[154] and can undergo a reversible $2e^-$ reduction to leucothionine.[129] Additionally, the oxidised form of thionine has been found to increase the T_M of DNA up to 10 °C.[155]

1.4.4.3 Daunomycin

DM, depicted in Scheme 1.1, is an anthracycline antibiotic originally isolated from a *Streptomyces* strain. It is a potent chemotherapeutic agent and is primarily used for

treatment of leukemia.[157, 158] Comprising an aglycone unit with a fused amino sugar ring, this intercalator has been shown to interact reversibly with DNA.[139] Crystallographic studies by Quigley *et al.* revealed that, while the aglycone unit intercalates between stacked base-pairs, the sugar ring resides in the minor groove. It was additionally discovered that one DM binds per every three base-pairs which, alongside several van der Waals interactions, is stabilised by four hydrogen bonds.[159, 160] The sequence-specificity of DM has been a matter of debate. Whereas binding to both G·C and A·T regions have been demonstrated, an early study by Chaires *et al.* concluded that DM showed slight preference for G·C.[161] Finally, in an extensive DNA footprinting study by the same author, results indicated that the optimal binding site for DM is a triplet sequences of two adjacent G·C base-pairs flanked by one A·T base-pair.[162] The electroactive aglycone unit contains an oxidisable hydroquinone ring and a reducible quinone ring. In an aqueous solution, DM can undergo a reversible $2e^-$ reduction of the quinone to a full hydroquinone.[163] The oxidised form of DM has a profound impact on the stability of dsDNA revealed by an increase of 30 °C in the T_M of DNA.[161]

1.4.4.4 Adriamycin

Adriamycin (AM) in Scheme 1.1 is also an anthracycline antibiotic originally produced by a *Streptomyces* strain. Similar to DM, this intercalator possesses chemotherapeutic activity and has been used as treatment for a variety of cancers.[157, 158] Binding non-covalently to DNA, it comprises an intercalating aglycone unit and a minor groove binding amino sugar ring. In fact, the only structural difference from DM is a substitution of a hydrogen to a hydroxyl group at C14.[164] X-ray diffraction studies of AM and DNA by Fredrick *et al.* revealed that van der Waals interactions and four hydrogen bonds stabilise the complex. However, unlike DM, additional solvent interactions were observed with the hydroxyl group at position C14. It furthermore revealed binding of one AM per three base-pairs.[164] Thus, it may be implied that AM displays a higher affinity for DNA compared to DM[162] and investigations have furthermore confirmed a G·C preference.[164] AM can undergo a reversible $2e^-$ reduction of the quinone to a full hydroquinone,[163] with the oxidised form stabilising dsDNA through the increase of T_M by 13 °C.[165]

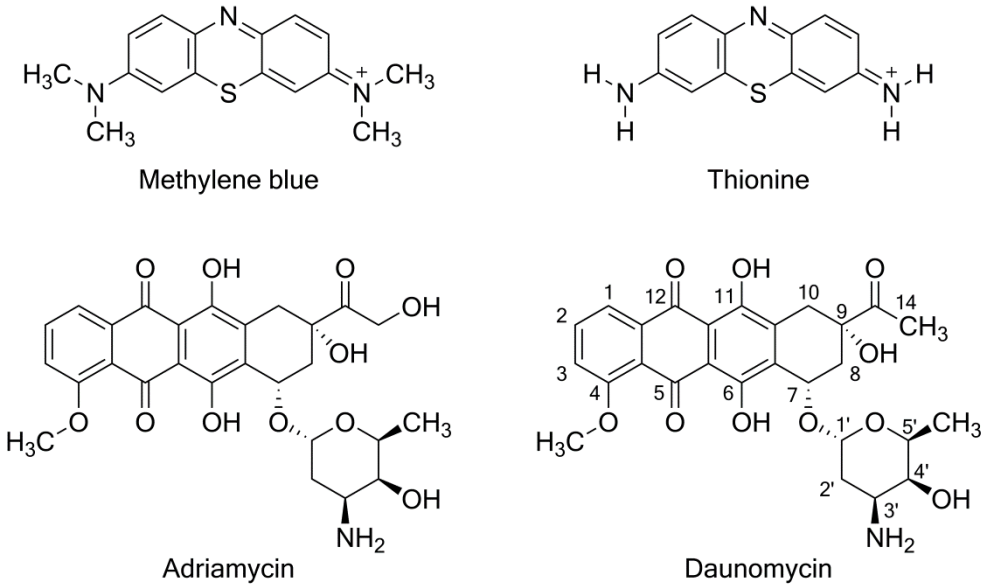

Scheme 1.1 DNA intercalators relevant to this study.

Based on the available literature, it is obvious that the effect of the oxidised forms of these intercalators has been well-documented in terms of structural studies and binding properties. Similar systematic studies regarding the impact of their respective reduced forms have not been published.

1.5 Melting Curve Analysis

1.5.1 Absorbance-based melting curve analysis

The temperature-induced transition between the double and the single stranded form of nucleic acids can be monitored using UV absorption. Aromatic rings in the bases absorb UV light and, thus, stacked bases absorb less UV light than unstacked bases. This effect is known as hypochromicity and is a measure of the amount of formed base-pairs and base stacking in the secondary structure. That is, the single stranded form of nucleic acids absorbs more than the double stranded form. Hence, denaturation of duplex DNA, upon increasing the temperature, is accompanied by an increase in absorption that approaches the sum of the absorbance of its nucleotides.[35, 36, 166, 167] Absorbance is commonly monitored at 260 nm and both renaturation and denaturation profiles are recorded to ensure that the studied system is in thermodynamic equilibrium.[36] Melting curves allow both qualitative

and quantitative information to be extracted. While the hyperchromicity yields information about the number of broken base-pairs, the concentration dependence of the T_M informs about the stoichiometry of the transition. Further analysis for the determination of thermodynamic parameters yields information about the T_M and the stability of the system. While the most common method to record melting curves is by UV–vis, other interrogation techniques may also be used. These include for example fluorescence, NMR, circular dichroism (CD) and calorimetry.[36, 166, 167]

1.5.2 Fluorescence-based melting curve analysis

As mentioned, the transition between the single and double stranded form of nucleic acid can also be detected by fluorescence.[168-170] Whereas different strategies are available, as reviewed by Marras,[171] one common strategy involves the attachment of a fluorescent dye to one strand of the duplex DNA and a quencher to the other strand. When the fluorescent dye and the quencher are in close proximity, the fluorescence of the dye is quenched through FRET. As the distance between the dye and the quencher increases, the fluorescence of the dye returns.[171] This process is depicted in Figure 1.5 where an increase in the fluorescence is observed upon the denaturation of duplex DNA.

The advantage of using fluorescence-based detection over absorbance-based detection is gain in sensitivity. Thus, lower concentrations of nucleic acids can be used. However, fluorescence is well known to be sensitive to changes in the environment, such as in temperature, pH or ionic strength.[168, 172] Moreover, certain fluorophore-quencher combinations may lead to slightly altered thermodynamic behaviour of the nucleic acid.[173] As a result, it has been more common to restrict the analysis to melting temperatures due to disagreement between thermodynamic data extracted from absorbance-based and fluorescence-based melting curves. However, You and co-workers suggested that short oligonucleotides (<16 bp), which are likely to melt in a two-state fashion, are less prone to altered thermodynamic behaviour as a result of the labels.[168] Indeed, thermodynamic data has been extracted from fluorescence-based melting curves.[169, 174] However, as underscored by You *et al.*, the choice of the fluorescent dye and quencher is essential to obtain accurate data.

Therefore, thermodynamic parameters from fluorescence-base melting curves are not extracted in this work.

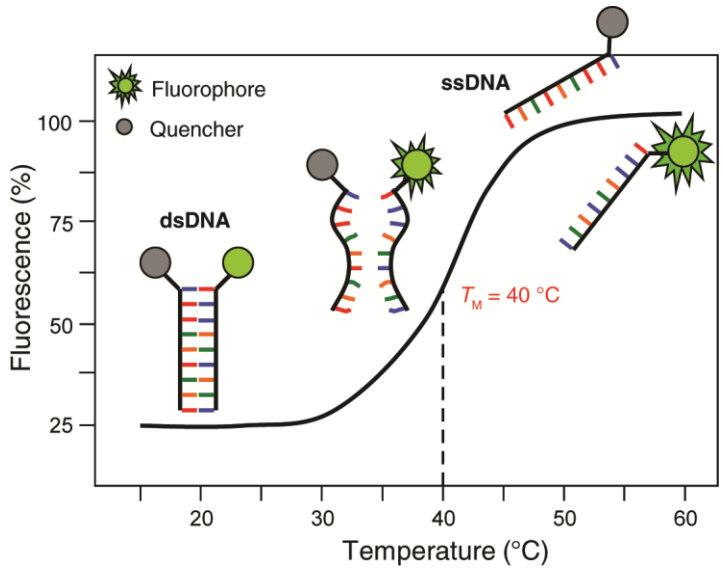

Figure 1.5 Reversible DNA hybridisation by FRET. Complementary DNA strands are attached to a fluorophore and a quencher, respectively. As the temperature is increased, DNA denatures which can be monitored by the increase in fluorescence.

1.5.3 Determination of T_M

The melting temperature can be determined from melting curves using different methods. However, to extract the true T_M values the interrogation signal, for example absorbance or fluorescence, is converted into fraction (f) of formed duplex DNA and plotted versus temperature. The fraction of duplex form is additionally normalised between 0 and 1 where $f = 0.5$ equals T_M.[36, 54] This conversion is carried out by determining an upper and a lower baseline for the linear regions at the start and the end of a melting curve and has been described in detail by Mergny and Lacroix.[36]

1.5.3.1 T_M by the first derivative method

A simple way, and one of the more common methods, to determine the T_M is to calculate the first derivative of the fraction of duplex form with respect to the temperature.[54] T_M is defined at the maxima of the calculated first derivative, that is

$$T_{\mathrm{M}} = \left(\frac{df}{dT}\right)_{max} \tag{1.11}$$

However, it is well established that using the first derivative method for T_{M} determination does not yield entirely accurate values. Essentially the inflection point of a sigmoidal curve is being determined. However, melting curves do not exhibit symmetrical behaviour. Hence, the T_{M} is systematically overestimated.[36, 54] Owczarzy investigated the discrepancy in determination of T_{M} by recording melting curves of 15–40 bp oligomers. The results indicated differences in the T_{M} values of up to 1.5 °C using the first derivative method.[54] However, in the context of this work, exact T_{M} values were not required as the relative difference was of interest. Hence, the first derivative method was mainly used for determination of T_{M} values from fluorescence-based melting curves.

1.5.3.2 T_M by van't Hoff analysis

In order to derive accurate T_{M} values as well as thermodynamic parameters from absorbance-based melting curves, van't Hoff analysis can be applied. For the analysis to be valid, the denaturation and renaturation must be assumed to proceed in a two-state (all-or-none) fashion. Furthermore, this assumption presumes that the transition enthalpy is temperature-independent and consequently the change in heat capacity $\Delta C_{\mathrm{p}}°$ is zero.[15, 35, 167, 175] The two-state model is generally only valid for oligonucleotides shorter than 20 bp. Duplexes longer than 20 bp are not likely to melt in a two-state fashion.[55] For the calculation of the parameters, the following bimolecular equilibrium was considered,

$$[\mathrm{S}_1] + [\mathrm{S}_2] \leftrightharpoons [\mathrm{D}] \quad \text{and} \quad K_{\mathrm{a}} = \frac{[\mathrm{D}]}{[\mathrm{S}_1][\mathrm{S}_2]} \tag{1.12}$$

where S_1 and S_2 are the two single strands, D is the duplex form and K_{a} is the binding constant. The fraction of formed duplexes can be written as

$$f = \frac{2[\mathrm{D}]}{C_{\mathrm{T}}} \tag{1.13}$$

where C_T is the total concentration of single strands, i.e. C_T=[S_1]+[S_1]+2[D]. At equal concentrations of single strands, the initial concentration $C_0 = C_T/2$. Hence, the binding constant K_a can be calculated through the expression in f, that is[36]

$$K_a = \frac{f}{C_0(1-f)^2} \tag{1.14}$$

Obtaining K_a allows the construction of the van't Hoff representation, that is ln K_a as a function of $1/T$ (in Kelvin). The representation was limited to $0.15 \leq f \leq 0.85$ in order to ensure that only the most accurate K_a values were included in the calculation.[167] Providing that $\Delta H°$ and $\Delta S°$ are temperature-independent, the transition enthalpy $\Delta H°$ can be obtained using the van't Hoff relationship[36]

$$\frac{\partial \ln K_a}{\partial(1/T)} = -\frac{\Delta H°}{R} \tag{1.15}$$

where R is the ideal gas constant 8.314 J mol^{-1} K^{-1}. The free energy $\Delta G°$ and entropy $\Delta S°$ may be derived from the standard thermodynamic equation

$$\Delta G° = -RT \ln(K_a) = \Delta H° - T\Delta S° \tag{1.16}$$

Finally, combining Eq. (1.14) with Eq. (1.16) and assuming $f = 0.5$, the T_M can be calculated using the following equation,

$$T_M = \frac{\Delta H°}{\Delta S° + R \ln(C_0/2)} \tag{1.17}$$

1.6 *in situ* Spectroelectrochemistry

Electrochemistry can provide a wealth of information on the thermodynamics and kinetics of reactions involving electron-transfer. However, molecular identification of new electroactive species can be ambiguous and only yield indirect information on structural changes occurring as a result of the redox reaction.[176, 177]

Spectroelectrochemistry (SEC) is the combination of a physical spectroscopic technique and electrochemistry.[178] Using electrochemistry, the redox-state of an electroactive compound may be changed while simultaneously interrogating the electrochemical changes spectrally. Therefore, spectroelectrochemical techniques can provide a plethora of additional information as a function of potential, time and mass transport.[179] While quantitative measurements are possible, often spectroelectrochemistry is used as a qualitative technique for structural characterisation of redox species.[177] A range of spectroscopic techniques can be coupled to electrochemistry, such as UV–vis and near-infrared spectrophotometry, CD and mass spectrometry, fluorescence and Raman spectroscopy and NMR.[180, 181] Different *in situ* spectroelectrochemical techniques have been utilised to study the redox chemistry of inorganic, organic and biological molecules.[176, 177, 182]

Typically, *in situ* spectroelectrochemistry involves bulk electrolysis of a redox-active species in a small volume. However, to enable fast electrolysis, which additionally permits spectroscopic interrogation, the design of the SEC cell and the electrodes becomes critical. While both electrochemistry and spectroscopy comprise standard cell setups, there is no equivalent standard setup in spectroelectrochemistry.[176, 179] However, a prerequisite for spectroelectrochemistry is optically transparent, or partially transparent, electrodes that enable light to pass through the electrode and the nearby solution. These electrodes can for example be deposited metals such as indium-tin oxide (ITO), Au or Pt on transparent substrates or minigrid electrodes consisting of a metal micromesh made from noble metals.[178, 179] With transparency efficiency over 50 %, minigrid electrodes have the possibility to enable exhaustive electrolysis of the electroactive species owing to their large surface area.[177] Unlike planar electrodes, such as ITO-coated electrodes, the diffusion behaviour of electroactive species is more complex on minigrid electrodes. This is due to diffusion perpendicular and parallel to the electrode as well as diffusion inside the mesh holes.[183] Although, for simplification, the diffusion behaviour of minigrid electrodes is frequently approximated to a planar electrode since, after a certain time, the individual diffusion events will merge into one planar diffusion front.[179, 183] Equally critical is the geometry and optical pathlength of the SEC cell, which generally determines the thickness of the solution surrounding the electrode. To

minimise electrolysis time, a common feature for SEC cells is small volumes. Ultimately, the cell geometry and the volume surrounding the electrode define whether the electrochemistry is governed by semi-infinite or finite diffusion of electroactive species to the electrode surface.[182, 184, 185]

Spectroelectrochemistry relies on the fundamentals of electrochemistry and thus commonly utilises a conventional three-electrode setup, with a working electrode (WE), counter electrode (CE) and a reference electrode (RE), which is connected to a potentiostat.[177, 186] While electrochemical methods such as cyclic voltammetry (CV) or coulometry can be employed, potential step chronoamperometry is perhaps the most common.[176] In CV, the current is recorded as a function of the potential which is ramped linearly in a triangular waveform as a function of time. Chronoamperometry, on the other hand, involves stepping the potential and recording the current as a function of time.[186] However, obtaining accurate quantitative time-dependent data can be difficult in a SEC cell. Commonly due to poor cell design and arrangement of electrodes within the cell, this often causes a significant ohmic (iR_u) drop that varies across the surface of the working electrode. In other words, homogenous potential distribution is not achieved over the surface of the electrode. However, the ohmic drop becomes negligible in qualitative measurements. Since no kinetic information is required in this type of measurements, the potential is stepped and applied for a sufficiently long time to enable exhaustive electrolysis which can easily be achieved with the chronoamperometric method. Once equilibrium is reached, spectroscopic interrogation is conducted which is the main method employed in this study.[177, 179]

1.6.1 Absorbance-based spectroscopy

Perhaps the most straight-forward spectroelectrochemical technique measures absorbance changes as a function of the redox-state. This is also the main technique utilised in this study. Upon passing a beam of light with a given frequency or wavelength through an absorbing solution, the intensity of light will change. The ratio of incident light intensity (I_0) and transmitted light intensity (I) is the

transmittance T of the solution. Absorbance A is defined as the logarithm of the transmittance, that is $A = \log(I/I_0)$, and accordingly by Beer-Lambert law[1]

$$A = \varepsilon c \ell \tag{1.18}$$

where ε is the molar extinction coefficient in $M^{-1}\,cm^{-1}$, c is the molar concentration and ℓ is the pathlength of the light beam through the solution. The absorbance is dependent on chemical properties of the solution, i.e. concentration and extinction coefficient, and equally on the geometry of the cell, that is the pathlength.

Absorbance can also be measured with CD spectrometry. However, unlike UV–vis spectrophotometry, CD is the difference in absorption A of left (L) and right (R) circularly polarised light, that is[187]

$$CD = A_{\mathrm{L}} - A_{\mathrm{H}} = c\ell(\varepsilon_{\mathrm{L}} - \varepsilon_{\mathrm{H}}) \tag{1.19}$$

While CD is a property that only chiral molecules possess, it is also apparent that it may only be measured where there is absorbance.[187] Both absorbance and CD measurements have been utilised to great extent for the interrogation of nucleic acids. The extinction coefficients at 260 nm for the four nucleotides encompassed in DNA vary between 7 500–15 000 $M^{-1}\,cm^{-1}$.[1] Furthermore, they are chiral, as is the double helix and thus polarise left and right circular light differently.[187]

1.6.2 Thin-layer *in situ* spectroelectrochemistry

It is often desirable to perform faster electrolysis in case of unstable electroactive species, but also to decrease the time for the system to reach equilibrium after an applied potential.[176, 184] This can be achieved by increasing the ratio of the electrode area to solution volume.[177] In a conventional (spectro)electrochemical cell, with a small electrode area to solution volume ratio, electrolysis is governed by semi-infinite diffusion.[185] Upon applying a potential under these circumstances, a current is generated leading to electrolysis which is dependent on the diffusion of the

electroactive species to the electrode surface. Due to concentration differences between the solution close to the electrode and the bulk solution, a diffusion layer arises where electroactive species diffuse from highly concentrated regions to dilute regions. In other words, diffusion attempts to minimise the concentration difference within the solution causing an increase in the diffusion layer thickness, which is growing into the solution from the surface of the electrode.[186, 188] However, confining the solution to a thin layer at the surface of the electrode, which is smaller than the diffusion layer, permits fast electrolysis since it is governed by finite diffusion and convective mass transfer.[177, 182, 189] Consequently, spectroelectrochemical experiments are commonly conducted within the thin-layer regime using optically transparent thin-layer electrodes (OTTLEs), such as minigrid electrodes.[177, 182] General thin-layer electrochemistry confines solution volume to a thin layer of 2–100 µm from the electrode surface.[186] However, the criteria for spectroelectrochemistry differ from conventional electrochemistry in that the absorbance, which is not as sensitive as other techniques, has to be taken into account. Therefore, spectroelectrochemistry commonly involve thin-layer solutions of thicknesses ≤ 0.5 mm.[176, 182, 184, 186] The OTTLE cell utilised in this study can be seen in Figure 1.6. It consists of a quartz cuvette, with a pathlength of 0.5 mm, which is compatible with a standard spectrophotometer. The optical beam of the spectrophotometer is passed directly

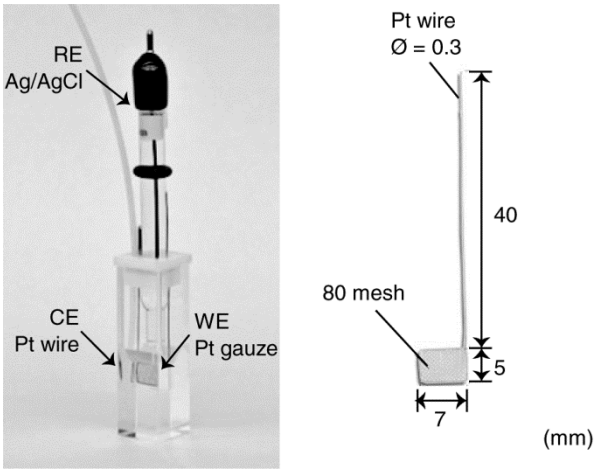

Figure 1.6 Spectroelectrochemical setup. The cell (left) consists of a thin-layer quartz cuvette (pathlength 0.5 mm) with a three-electrode setup utilising a Pt gauze WE (right), Pt wire CE and a Ag/AgCl (3 M NaCl) RE. Images adapted from IJ Cambria Scientific.[190]

through the transparent electrode and the solution. Using a potentiostat, the potential of the system can be controlled via a three-electrode setup.

In thin-layer spectroelectrochemistry, applying a bias potential generates a current flow leading to bulk electrolysis. This permits the whole confined solution to reach equilibrium at a given applied potential within seconds or minutes, depending on the optical pathlength.[177, 191] Thus, a reversible system will follow the Nernst equation,[186] that is

$$E = E^{0'} + \frac{RT}{n_e F} \ln \frac{c_O}{c_R} \tag{1.20}$$

where E is the equilibrium potential, $E^{0'}$ is the formal potential, R is the gas constant 8.314 J mol^{-1} K^{-1}, T is temperature, n_e is number of electrons, F is the Faraday constant 96 485 C mol^{-1} and c_O and c_R are the concentrations of the oxidised and reduced species at the electrode surface. A thin-layer setup has the advantage of rapidly enabling exhaustive electrolysis, as the ratio of the oxidised and reduced species at the surface of the electrode will quickly be reflected in the solution. As a result, the absorbance changes recorded represent the absolute concentrations of the oxidised and reduced specie at various electrode potentials, which can easily be estimated using Beer-Lambert's law, Eq. (1.18).[182, 184, 186] While OTTLE cells enable exhaustive electrolysis in short times mass transport by diffusion may not be completely neglected, in particular if the electrolysis time is shorter than required for exhaustive electrolysis.[186, 192] The total electrolysis time τ can be approximated using the following relationship[185]

$$\tau = \frac{\delta^2}{D} \tag{1.21}$$

where δ is the thin layer thickness and D is the diffusion coefficient in cm^2 s^{-1}.

1.7 Hypothesis and Scope of Thesis

The reversible denaturation and renaturation of DNA is imperative for its function in many cellular processes, such as transcription and replication. Gaining in depth

understanding of the thermodynamics of the reversible process has furthermore rendered it indispensable for many molecular diagnostic techniques such as nucleic acid amplification. In recent years, however, demands on decentralised testing have increased which have generated a focus on miniaturisation and integration of conventional laboratory operations, such as nucleic acid amplification and sample preparation, into automated portable bioanalytical systems. However, many nucleic-acid based diagnostic technologies rely on thermal control for the reversible hybridisation of DNA. For example, amplification of DNA by PCR requires precise control of three different elevated temperatures. Thus, integration into miniaturised bioanalytical systems remains challenging. It is therefore evident, that circumventing the need for a heat source and the implementation of an alternative method to control reversible DNA hybridisation may be vital for the development and commercial success of low-energy consuming portable nucleic acid-based diagnostic platforms. Electrochemistry-based sensing has proven to be highly valuable for the development of point-of-care testing devices as it enables simpler operations suitable for miniaturisation and integration. Therefore, substituting thermal control of reversible DNA hybridisation to isothermal, electrochemical control opens the prospect to achieve miniaturised, integration-friendly bioanalytical systems. This can in turn enable the realisation of truly decentralised nucleic-acid based diagnostics platforms. Despite substantial efforts to describe alternative ways to control reversible DNA hybridisation, no method thus far has proven to accomplish fast, isothermal electrochemical control without dramatic changes of solution conditions, covalent modification or immobilisation of DNA.

Based on the assessment of the integration challenges due to temperature, this Thesis outlines the investigation towards isothermal, electrochemical control of reversible DNA hybridisation through the exploitation of electroactive DNA intercalators, as illustrated in Figure 1.7. We hypothesised that the oxidised form of the electroactive intercalator binds differently to dsDNA compared to the reduced form. We further hypothesised that the difference in binding affects the stability of dsDNA, which is expressed by an altered association constant. Finally, the altered association constant, as an effect of the redox-conversion of the electroactive intercalator, facilitates the reversible denaturation and renaturation of DNA.

In order to demonstrate this proof-of-principle, a model system of complementary 20mer and 40mer synthetic DNA oligonucleotides in a simple buffer was utilised. The first results Chapter focused on exploring and gaining in depth understanding of the concept of reversible DNA hybridisation. This was achieved by studying the effect of different known chemicals and conditions in conjunction with fluorescence-based melting curve analysis. Understanding what affects the stability of DNA, a boundary condition for subsequent studies was defined. This boundary condition comprised the minimum requirement for dsDNA to remain hybridised. The second results Chapter investigated the intercalation and effect of various intercalators on DNA. In order to find the most appropriate candidate, a screening of four different intercalators was conducted employing fluorescence-based melting curve analysis. This included studying the effect of both the oxidised and reduced form of the intercalator. The most successful hit from the screening was then subjected to further melting curve studies based on absorbance for thermodynamic evaluation. The in depth thermodynamic study permitted the estimation of the influence of the intercalator, in its oxidised and reduced form, on the association constant of dsDNA. The final results Chapter exploited the obtained thermodynamic knowledge in order to explore cyclic isothermal, electrochemically controlled DNA denaturation and renaturation by switching the redox-state of the selected DNA intercalator. Primarily investigated with *in situ* UV–vis spectroelectrochemistry, *in situ* CD spectroelectrochemistry was employed as a second independent technique for the validation of the proof-of-principle. Finally, the integrity of both DNA and the selected intercalator was assessed employing gel electrophoresis and NMR.

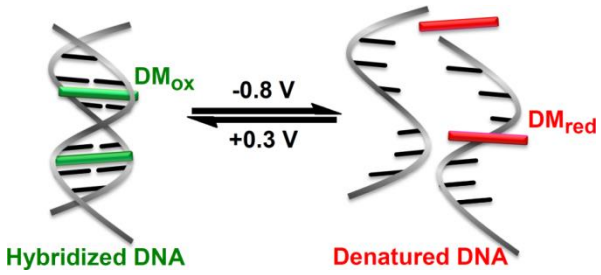

Figure 1.7 Electrochemical control of reversible DNA hybridisation. As postulated, the state of DNA can be electrochemically controlled in a cyclic manner by switching the redox-state of an intercalator.

Chapter 2

Material and Methods

2.1 Materials

2.1.1 Buffers and solvents

All solutions were prepared or diluted with ultrapure water (Milli-Q Synthesis, resistance = 18.2 MΩ cm, Millipore Corp., Bedford, MA, USA). Experiments were conducted in saline–sodium citrate buffer [1× SSC (0.15 M NaCl with 15 mM trisodium citrate), pH 7 adjusted with HCl] from Fisher Scientific (Loughborough, UK) and diluted further as required. Analytical grade ethanol, concentrated nitric acid (HNO_3) and 0.1 M sulfuric acid (H_2SO_4) were used for cleaning and purchased from VWR Laboratories (Lutterworth, UK). 1 M stock solution of HCl (density 1.18) and NaOH, for adjusting pH, 20 M stock solutions of 99.9 % formamide ($HCONH_2$) and 98 % urea ($CO(NH_2)_2$), prepared in 1× SSC and used for melting curve studies, and deuterium oxide (D_2O, 99.9 % D), used for NMR sample preparation, were purchased from Sigma Aldrich (Poole, UK). Hellmanex®III cuvette cleaning detergent was purchased from Scientific Laboratory Supplies (Nottingham, UK). Mineral oil was purchased from Biomérieux (Hapmshire, UK) and used for overlaying samples.

2.1.2 Oligonucleotides

All unlabelled and fluorophore-labelled complementary 20 and 40 bp long oligonucleotides were purchased from Metabion (Martinsried, Germany). Sequences can be found in Table 2.1. Stock solutions were prepared by dissolving lyophilised DNA in water according to the instructions of the supplier and stored at −20 °C. Stock solutions of labelled DNA were stored aliquoted to prevent photo-bleaching. Concentrations were determined using NanoDrop ND-1000 UV–vis spectrophotometer (NanoDrop Technologies, Wilmington, DE, USA).

Table 2.1 Oligonucleotide sequences.

Strand name	Sequence	G·C (%)
20merS	5′-ACA AGG ATG ACA AGC ACA GC-3′	50
20merAS	5′-GCT GTG CTT GTC ATC CTT GT-3′	50
40merS	5′-GTC GGT CAA GAA CGA GCA CTC AAG AGC CTC AGT CAG ACG A-3′	55
40merAS	5′-TCG TCT GAC TGA GGC TCT TGA GTG CTC GTT CTT GAC CGA C-3′	55
20merS-FAM†	5′-**6-FAM**-ACA AGG ATG ACA AGC ACA GC-3′	50
20merAS-BHQ-1†	5′-GCT GTG CTT GTC ATC CTT GT–**BHQ-1**-3′	50
20merS-TxR‡	5′-**TexasRed**-ACA AGG ATG ACA AGC ACA GC-3′	50
20merAS-BHQ-2‡	5′-GCT GTG CTT GTC ATC CTT GT-**BHQ-2**-3′	50

† $\lambda_{em/ex}$(6-FAM) = 495/520 nm, λ_{abs}(BHQ-1) = 480–580 nm

‡ $\lambda_{em/ex}$(TxR) = 595/612 nm, λ_{abs}(BHQ-2) = 560–670 nm

2.1.3 DNA intercalators

Methylene blue (MB) [3,7-bis(dimethylamino)phenazathionium chloride] 0.05 wt% in water and thionine [3,7-diamino-5-phenothiazinium acetate] were purchased from Sigma Aldrich (Poole, UK). Daunomycin (DM) [(8*S*,10*S*)-8-acetyl-10-[(3-amino-2,3,6-trideoxy-α-L-lyxo-hexopyransoyl)oxy]-7,8,9,10-tetrahydro-6,8,11-trihydroxy-1-methoxy-5,12-naphthacenedione hydrochloride] and Adriamycin (AM) [10-[(3-Amino-2, 3, 6-trideoxy-α-L-lyxohexopyranosyl)oxy]-7, 8, 9, 10-tetrahydro-6, 8, 11-trihydroxy-8-(hydroxyacetyl)-5, 12-naphthacenedione hydrochloride] were

purchased from Tocris Bioscience (Bristol, UK). A stock solution of thionine was prepared in water, while MB was used without further preparation. Both stock solutions were stored dark at room temperature. Stock solutions of DM and AM were prepared in water and aliquots were stored dark at −80 °C and −20 °C, respectively. Both stock solutions were used within four months. Concentrations were determined using an Agilent Cary 60 UV–vis spectrophotometer (Agilent Technologies, Wokingham, UK) and a 1 cm path length quartz cuvette. Table 2.2 summarises the molar extinction coefficients of the intercalators. Dilutions of the intercalators were prepared freshly for each experiment.

Table 2.2 Properties of intercalators.

Intercalator	M_W (g mol^{-1})	$\lambda_{em/ex}$(nm)	ε (M^{-1} cm^{-1})
Methylene blue (MB)	319.85	665/682	76 000 at 664 nm[147]
Thionine (Th)	287.34	596/624	54 200 at 598 nm[154]
Daunomycin (DM)	563.98	480/592	11 500 at 480 nm[161]
Adriamycin (AM)	579.98	480/592	11 500 at 480 nm[193]

2.1.4 Reducing agents

Ascorbic acid ($C_6H_8O_6$, M_W = 176.12 g mol^{-1}) and sodium borohydride ($NaBH_4$, M_W = 37.83 g mol^{-1}) were purchased from Sigma Aldrich (Poole, UK). 1 M stock solution of ascorbic acid was prepared by dissolving 1.76 g of powder in 10 mL water followed by vortexing. The stock solution was stored at room temperature and used within a week. 1 M stock solution of $NaBH_4$ was prepared by dissolving 0.3783 g in 10 mL 0.036× SSC, pH 10 (adjusted with 1 M NaOH) and vortexed thoroughly. The stock solution was prepared freshly for each experiment.

2.1.5 Main electrodes and electrochemical setup

Electrochemical and spectroelectrochemical experiments performed in a thin-layer spectroelectrochemical quartz cuvette (pathlength 0.5 mm) made use of a three-electrode setup, consisting of a Pt gauze WE with a Pt wire CE and a single fritted Ag/AgCl (3 M NaCl) RE from IJ Cambria Scientific (Carms, UK). The dimension of

the Pt gauze WE was 7×5 mm with a mesh size of 80 reinforced with a 0.3 mm Pt wire, as seen in Figure 1.6. The gauze wire thickness was 100 μm with a distance of 150 μm between the wires. The estimated surface area was 62.2 mm^2.

2.1.6 Main instruments

Spectrophotometric and spectroelectrochemical experiments were conducted on an Agilent Cary 60 UV–vis spectrophotometer, running the CaryWinUV software, equipped with a Varian Cary Peltier Accessory for temperature control (Agilent Technologies, Wokingham, UK), unless stated otherwise. A Digitron Model 3900 thermocouple (RS Components, Corby, UK) was used to monitor the temperature inside the cuvette. A PalmSens hand-held potentiostat/galvanostat running PSTrace2.4 software (PalmSens, Houten, Netherlands) was used for electrochemical and spectroelectrochemical experiments. All CD experiments were conducted on a Jasco J-810 spectropolarimeter equipped with a Peltier thermoelectric type temperature controller (Jasco International, Great Dunmow, UK), while FluoroMax-3 Spectrofluorometer (Horiba Jobin Yvon Inc., Edison, NJ, USA) was employed for fluorometric measurements. SpectraManager and SpectraAnalysis version 1.53 was employed for control and data handling of the CD spectrometer, while the FluorEssence software was utilised for the spectrofluormeter. Fluorescence-based melting curves were acquired on the Stratagene Mx3000P QPCR Systems (Agilent Technologies, Stockport, UK) running the MxPro QPCR software.

2.2 Methods and Protocols

2.2.1 Cleaning procedures

2.2.1.1 Quartz cuvettes

Quartz cuvettes were routinely cleaned, before each experiment or experimental condition, with ethanol followed by thorough rinsing with water and drying with compressed air. When harsher cleaning was required, cuvettes were soaked overnight at room temperature in 1 % Hellmanex®III cleaning detergent (Scientific

Laboratory Supplies, Nottingham, UK) in water followed by thorough rinsing with water, a quick rinse with concentrated HNO_3 and finally water.

2.2.1.2 Electrodes

The Pt WE and Pt CE were immersed in concentrated HNO_3 for 5 min at room temperature followed by rinsing with water and drying with a stream of N_2. The WE was electrochemically cleaned in 0.1 M H_2SO_4 using cyclic voltammetry. First 1.4 V to −0.2 V was cycled 40 times, followed by 10 times cycling of 1.14 V to −0.24 V, at 50 mV s^{-1}. Electrodes were finally rinsed with water and dried with a stream of N_2 before use.

2.2.2 Sample preparation

2.2.2.1 Hybridisation of unlabelled DNA

DNA experiments were carried out with a 1:1 mixture of complementary ssDNA oligonucleotides (20mer or 40mer) at a base-pair concentration of 200 µM, unless stated otherwise, in 0.036× SSC (7.0 mM Na^+) or 0.1× SSC (19.5 mM Na^+), pH 7. To form dsDNA, oligonucleotides were hybridised by initial denaturation for 5 min at 95 °C while shaking at 450 rpm using a Thermomixer comfort (Eppendorf, Hamburg, Germany). This was followed by cooling down to room temperature over 3.5 h to ensure complete duplex formation. Samples were stored at +4 °C and used within a week.

2.2.2.2 Hybridisation of fluorophore-labelled DNA

Fluorophore-labelled complementary 20mer ssDNA oligonucleotides were mixed 1:1 in varying dilutions of SSC buffer. 6-FAM and BHQ-1 labelled ssDNA were mixed to a final dsDNA-bp concentration of 1 µM, while Texas Red and BHQ-2 labelled ssDNA were mixed to a final dsDNA-bp concentration of 2 µM. Hybridisation was carried out by incubation in the Thermomixer for 30 min at 25 °C, 450 rpm, protected from light. Samples were prepared freshly for each experiment.

2.2.2.3 DNA intercalation

For samples containing an intercalator, an appropriate amount of the compound was added to the hybridised dsDNA to a final concentration based on the required base-pair to intercalator molar ratio. The mixture was incubated in the Thermomixer for 10 min at 25 °C, 450 rpm, protected from light. Intercalation was carried out freshly before each experiment.

2.2.2.4 Chemical reduction of intercalator

For samples requiring the reduced form of the intercalator, chemical reduction was carried out after intercalation by using 1 M ascorbic acid or 1 M sodium borohydride. These reducing agents were added in excess to an appropriate final concentration based on the required molar ratio of [intercalator]:[reducing agent]. Unless stated otherwise, MB and thionine were reduced using ascorbic acid at 150× and 100× excess of the intercalator concentration, respectively. DM and AM were reduced using sodium borohydride at 50× excess of the intercalator concentration. Reduction of MB was carried by incubation for 30 min at 25 °C, whereas the remaining intercalators were reduced by incubation for 1 h at 25 °C. Samples were incubated in the Thermomixer at 450 rpm, except for samples prepared for fluorescence-based melting studies (Section 2.2.6) where an IKA KS501 digital shaker (IKA, Staufen, Germany) was utilised at 96 rpm due to the high number of samples.

2.2.3 Absorbance-based intercalation studies

Intercalation was studied with unlabelled 20mer dsDNA oligonucleotides by keeping the intercalator concentration constant and increasing the DNA base-pair concentration. The interaction was additionally studied in the presence of 20mer ssDNA oligonucleotides as a control. Duplex DNA was prepared according to Section 2.2.2.1 at the appropriate base-pair concentrations. This was followed by intercalation of the probed compound according to Section 2.2.2.3. The base-pair to intercalator molar ratios 1:2, 2:1 and 4:1 (10:1 was only measured for MB) were investigated. Intercalation of 6 μM MB was investigated in the presence of DNA

oligonucleotides at base-pair concentrations of 3, 12, 24 and 60 μM. Thionine was studied at 15 μM with base-pair concentrations of 7.5, 30 and 60 μM, while 40 μM DM was with base-pair concentrations of 20, 80 and 160 μM. All measurements were conducted in 0.1× SSC (19.5 mM Na^+). As an additional control, the absorbance of each intercalator was measured in the absence of DNA. Samples were prepared in triplicates at a total volume of 100 μL each. After blanking with 0.1× SSC buffer, spectra were recorded on a Biomate 5 UV–Vis spectrophotometer by scanning the wavelength range 200–800 nm at the speed setting Intelliscan, which regulates the scan speed and data interval depending on the absorbance (bandwidth 2 nm). Samples were measured in a 1 cm pathlength quartz cuvette at room temperature. The cuvette was cleaned according to Section 2.2.1.1 after each set of three replicates.

2.2.4 Fluorescence-based intercalations studies

Similar to the absorbance-based study in Section 2.2.3, fluorescence-based intercalation was studied with unlabelled 20mer dsDNA oligonucleotides by keeping the intercalator concentration constant and increasing the DNA base-pair concentration. Controls included studying the interaction in presence of 20mer ssDNA oligonucleotides and absence of DNA. Preparation of dsDNA, at the appropriate base-pair concentrations, and subsequent intercalation of the probed compound was carried out according to Section 2.2.2.1 and Section 2.2.2.3. The investigated base-pair to intercalator molar ratios were 1:2, 2:1 and 4:1 (10:1 was only measured for MB). 2 μM MB, thionine or DM was studied in the presence of DNA oligonucleotides at base-pair concentrations of 1, 4 and 8 μM (20 μM was only used for MB) in 0.1× SSC (19.5 mM Na^+). Samples were prepared in triplicates at a total volume of 60 μL each. All emission spectra were acquired on a FluoroMax-3 Spectrofluorometer, at room temperature, using a quartz cuvette of 1 cm pathlength. MB was excited at λ_{ex} = 664 nm and the emission was collected between 670–800 nm, whereas thionine was excited at λ_{ex} = 596 nm and the emission collected between 605–800 nm. Excitation and emission slit widths were 5 nm. DM was excited at λ_{ex} = 480 nm and the emission was collected between 520–720 nm. Emission and excitation slit widths were 7 nm. The fluorescence spectra of 0.1× SSC was additionally recorded, at each respective settings, and subtracted from the

intercalation data. The acquisition interval and integration time were maintained at 1 nm and 0.1 s, respectively. The cuvette was cleaned according to Section 2.2.1.1 after each set of three replicates.

2.2.4.1 Titration-based intercalation study of daunomycin

Properties of the DM and dsDNA interaction were determined, at three different conditions, by titration where a known volume of DNA oligonucleotides was titrated with a known concentration and volume of the intercalator. Duplex DNA was prepared according to Section 2.2.2.1. 6 µM DM was titrated into 20mer or 40mer dsDNA oligonucleotides, at the base-pair concentration of 8 µM, in 0.036× SSC (7.0 mM Na^+) or 0.1× SSC (19.5 mM Na^+). A total volume of 80 µL dsDNA was added to the cuvette followed by 21 titrations with 1-4 µL of DM. Correspondingly, titrations were performed where 1–4 µL of 6 µM DM was titrated into 80 µL of either 0.036× SSC or 0.1× SSC buffer. After each addition, the solution was mixed by pipetting and allowed to equilibrate for 1 min before collecting the emission spectrum with a FluoroMax-3 Spectrofluorometer. Using a quartz cuvette with 1 cm pathlength, at room temperature, DM was excited at λ_{ex} = 480 nm and emission spectra were collected between 520–720 nm. Excitation and emission slit widths were 7 nm. The acquisition interval and integration time were maintained at 1 nm and 0.1 s, respectively. The cuvette was cleaned after each titration according to Section 2.2.1.1.

The binding data was analysed in the form of a Scatchard representation[133] where the ratio of bound molecules to total available binding sites (base-pairs) was plotted versus amount of bound molecules, that is r/C_f versus r. To calculate the amount of bound intercalator, as previously been shown by Chaires *et al.*,[161] the concentration of free intercalator was first estimated through the ratio of the fluorescence intensity of the intercalator in the absence and presence of DNA according to

$$C_f = C_T \frac{I/(I_0 - P)}{(1 - P)} \tag{2.1}$$

where I and I_0 is the fluorescence intensity of DM at λ_{em} = 555 nm in the presence and absence of DNA, C_f is the concentration of free DM, C_T is the total concentration of known added DM and P is the ratio of the observed quantum yield of completely bound intercalator to free intercalator. The concentration of bound intercalator was subsequently acquired by using the following difference

$$C_B = C_T - C_f \tag{2.2}$$

where C_B is the concentration of bound DM. I_0 was experimentally determined by performing the same titration of DM into buffer, as explained above. P was determined by taking the ratio of the fluorescence intensity of DM at 555 nm in the presence and absence of excess of DNA. Upon construction of the Scatchard representation of the binding data, the intrinsic binding constant K_i and the neighbour exclusion parameter n were determined with the neighbour exclusion model of the McGhee–von Hippel binding isotherm in Eq. (1.9). Plots were fitted in the software OriginPro 8.5 (OriginLab Corp., Northampton, UK) and initial values were $K_i = 7 \times 10^5$ M^{-1} and $n = 3$. Upon obtaining K_i, the binding free energy $\Delta G°$ was calculated by using the standard thermodynamic relationship at 20 °C , that is

$$\Delta G° = -RT \ln(K_i) \tag{2.3}$$

2.2.5 Chemical reduction of intercalators

Chemical reduction of intercalators was achieved by using 1 M ascorbic acid or 1 M sodium borohydride stock solutions. These reducing agents were prepared according to Section 2.1.4. To determine the most appropriate reducing agent concentration, chemical reduction of the intercalators was monitored spectrophotometrically over time at different concentrations of the reducing agent. The reducing agents were investigated at a selection of 1×, 50×, 100×, 150×, 200× and 250× in (molar) excess of the intercalator concentration. As a control, the intercalator was measured in the absence of the appropriate reducing agent. Reduction of 50 µM MB or thionine was carried out in 0.036× SSC (7.0 mM Na^+)

using ascorbic acid, while 150 μM DM was reduced with sodium borohydride in the same buffer. The total volume of each sample was 100 μL. Using the UV–vis setting of the NanoDrop ND-1000 UV–vis spectrophotometer, a spectrum of 2 μL sample was recorded at t = 0, 30, 60 and 120 min. The reduction of MB, thionine and DM was followed at 664, 596 and 480 nm, respectively. Prior to measurement, the spectrophotometer was blanked with 0.036× SSC. All measurements were performed at room temperature with a 1 mm pathlength.

2.2.5.1 Time-course reduction of daunomycin

A detailed time-course reduction of 100 μM DM was performed in the absence and presence of unlabelled 20mer dsDNA oligonucleotides, at a base-pair concentration of 200 μM, in 0.036× SSC (7.0 mM Na^+), pH 7 ([dsDNA-bp]:[DM] = 2:1). The preparation of dsDNA and subsequent intercalation of DM is described in Section 1.2.2.1 and Section 1.2.2.3. Reduction of DM was carried out in the presence of 5 mM sodium borohydride (50× in excess) at 25 °C. Upon quickly adding the reducing agent to the sample, 200 uL was transferred to a 0.5 mm pathlength cuvette. A spectrum was recorded at t = 0 min and then every 5 min for 60 min. Spectra were obtained on the Agilent Cary 60 UV–vis spectrophotometer equipped with a Varian Cary Peltier Accessory for temperature control. The wavelength range 800–200 nm was scanned at 4800 nm min^{-1} (bandwidth 2 nm, interval 1 nm). Before the measurement, the spectrophotometer was blanked with 0.036× SSC buffer. The cuvette was cleaned according to Section 2.2.1.1 between each sample. The absorbance at 480 nm was finally plotted versus time.

2.2.6 High-throughput fluorescence-based DNA melting studies

Fluorophore-labelled complementary 20mer DNA oligonucleotides were mixed to form dsDNA according to Section 2.2.2.2. Melting studies making use of 6-FAM and BHQ-1 labelled oligonucleotides were hybridised at a total base-pair concentration of 1 μM. Melting studies utilising TexasRed and BHQ-2 labelled oligonucleotides were hybridised at a total base-pair concentration of 2 μM. To evaluate the effect on the fluorophore, controls with only fluorophore-labelled (6-FAM or TexasRed)

ssDNA were analysed in parallel for each investigated condition. All samples were analysed in, at least, triplicates at a total replicate volume of 20 µL using white 96 well PCR plates. Prior to measurement, the plate was spun down at 1500 rpm (410 g) for 2 min using an Eppendorf centrifuge 5810R (Eppendorf, Hamburg, Germany). Renaturation and denaturation profiles were recorded between 25 and 85 °C, according to the thermal profile in Figure 2.1, on the Stratagene Mx3000P QPCR Systems.

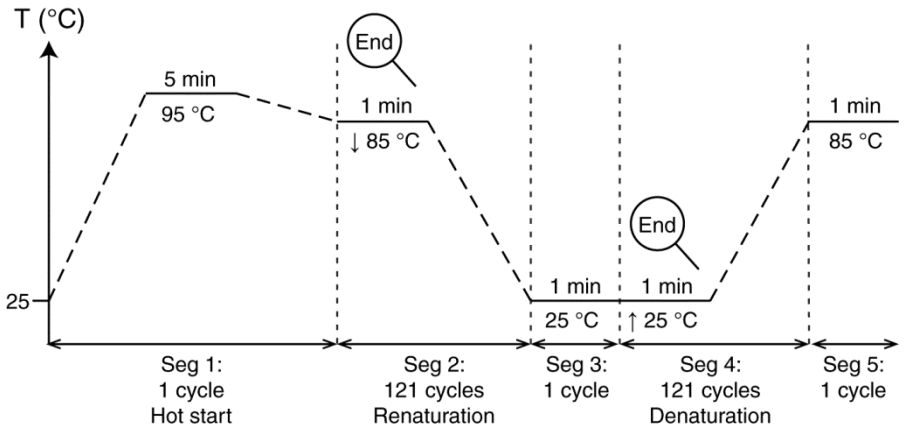

Figure 2.1 Thermal profile for fluorescence-based DNA melting studies. Ramp rate 0.5 °C min^{-1}.

The ramp rate was either 0.5 °C min^{-1} or 1 °C min^{-1} and a measurement was taken at the end of each increment. The processes were followed by FRET employing FAM/SYBR Green I ($\lambda_{ex/em}$ = 492/516 nm) or ROX/TexasRed ($\lambda_{ex/em}$ = 585/610 nm) filter settings.

2.2.6.1 Data analysis

Melting curves were obtained by plotting the raw fluorescence as a function of temperature T. However, to more easily visualise differences in T_M, and extract accurate T_M values from the melting curves, raw data was first background corrected with fluorophore-labelled ssDNA data at the corresponding investigated conditions. This has previously been described by Morrison and co-workers.[169] Briefly, fluorophore-labelled ssDNA data was first normalised to 1 at the maxima. Raw melting curves of the dsDNA samples were then divided by the normalised

data of the fluorophore-labelled ssDNA. Subsequently, each corrected melting curve was smoothed using a 3–5 point FFT filter in OriginPro 8.5. The smoothed dsDNA data was next normalised between 0 (fully hybridised) and 100 % (fully denatured), as described by Owczarzy *et al*.[54] For normalisation, upper and lower baselines were determined corresponding to the linear regions at the start and the end of a melting curve. In order to select the baselines, the second derivative of the smoothed melting curve was plotted. The baselines were selected based on the regions where the second derivative was zero, thus, allowing the linear regions of the smoothed melting curves to be fitted with the linear least square method. Finally, normalisation, expressed as percentage of denatured base-pairs, was obtained using the following relations

$$F_{\mathrm{Norm}}(T) = \frac{F(T) - F(T)_{\mathrm{Lower}}}{F(T)_{\mathrm{Upper}} - F(T)_{\mathrm{Lower}}} \times 100 \tag{2.4}$$

$$F(T)_{\mathrm{Lower}} = b_{\mathrm{Lower}}T + a_{\mathrm{Lower}} \tag{2.5}$$

$$F(T)_{\mathrm{Upper}} = b_{\mathrm{Upper}}T + a_{\mathrm{Upper}} \tag{2.6}$$

where F(T) is the fluorescence at temperature T, $F(\mathrm{T})_{\mathrm{Lower}}$ and $F(\mathrm{T})_{\mathrm{Upper}}$ are the lower and upper baselines with their respective slopes b_{Lower} and b_{Upper} and respective intercepts a_{Lower} and a_{Upper}. T_{M} was calculated by taking the maxima of the first derivative of the normalised melting curve. All T_{M} values were determined from the denaturation profiles.

2.2.6.2 Effect of chemical agents

Melting curves were acquired in the presence of 1–10 M formamide and urea. A 20 M formamide stock solution was prepared by diluting 1.35 mL ultrapure grade formamide in 1× SSC to a total volume of 2 mL, while a 20 M urea stock solution was prepared by dissolving 12.0 g urea in 1× SSC to total volume of 10 mL. The effect of formamide and urea was studied by an appropriate addition of 20 M stock

solution to 6-FAM and BHQ-1 labelled complementary DNA oligonucleotides, before hybridisation took place, in 1× SSC (195 mM Na^+). Controls consisted of recording melting curves of dsDNA in the absence of the chemical agent, and of 6-FAM-labelled ssDNA in the absence and presence of the two chemical agents at 1–10 M. Renaturation and denaturation profiles were recorded at 1 °C min^{-1}.

2.2.6.3 Effect of pH

The effect of pH was studied by recording melting curves at pH 1–13. The pH of 1× SSC was adjusted between pH 1–7 using 1 M HCl, while pH 8–13 was obtained using 1 M NaOH. All pH values were measured on a PL-500 series pH meter (EZDO, Taipei, Taiwan). The effect of different pH values was studied by hybridisation of 6-FAM and BHQ-1 labelled complementary DNA oligonucleotides in pH-adjusted 1× SSC (195 mM Na^+). Controls included 6-FAM-labelled ssDNA in pH-adjusted 1× SSC. Renaturation and denaturation profiles were then recorded at 1 °C min^{-1}.

2.2.6.4 Effect of monovalent salt concentration

The effect of sodium ions was investigated by diluting SSC, the working buffer. Hybridisation of 6-FAM and BHQ-1 labelled complementary DNA oligonucleotides was carried out in 0.01–1× SSC (2.0–195 mM Na^+) at pH 7. Controls included 6-FAM labelled ssDNA in the corresponding dilutions of SSC buffer. Renaturation and denaturation profiles were recorded at 0.5 °C min^{-1}. The experimentally determined T_M values were compared to predicted T_M values generated by two different T_M prediction equations derived by SantaLucia[56] and Owczarzy and co-workers.[55] To assess the goodness-of-fit between the experimental and the predicted T_M values, statistical analysis comprising of estimation of the average error of the T_M predictions, $|\langle T_M \rangle|_{Ave}$, and Pearson's χ^2 was performed. For m number of measured T_M values, the average error and Pearson's χ^2 equals to

$$|\langle T_M \rangle|_{Ave} = \sum_{i=1}^{i=m} (|T_M(\text{predicted}, i) - T_M(\text{measured}, i)|) \Big/ m \qquad (2.7)$$

$$\chi^2 = \sum_{i=1}^{i=m} \frac{\left(T_{\mathrm{M}}(\mathrm{measured}, i) - T_{\mathrm{M}}(\mathrm{predicted}, i)\right)^2}{T_{\mathrm{M}}(\mathrm{predicted}, i)} \quad (2.8)$$

The chi-squared statistics was evaluated in terms of *p*-values using $(m - 1)$ degrees of freedom, where $m = 13$, and were calculated employing the CHISQ.DIST.RT function in Microsoft Excel 2010 (Microsoft Corp., Redmond, USA). The function generated a *p*-value between 0 < *p*-value < 1 where 1 indicated a good fit (difference between measured and predicted data is non-significant) and 0 indicated a poor fit (difference between measured and predicted data is significant).

2.2.6.5 Effect of oxidised and chemically reduced intercalator

Melting curves of complementary 20mer DNA oligonucleotides were acquired in the presence of oxidised and chemically reduced intercalator at 0.036× SSC (7.0 mM Na^+). The base-pair to intercalator molar ratios examined were 1:2, 2:1, 4:1 and 10:1. Following DNA hybridisation, intercalation of the investigated compounds took place as described in Section 1.2.2.3. Effects of MB and thionine were explored with 6-FAM and BHQ-1 labelled DNA oligonucleotides. According to the examined base-pair to intercalator molar ratios, respective intercalator was interrogated at the final concentrations of 0.1, 0.25, 0.5 and 2.0 μM. Effects of DM and AM was studied with TexasRed and BHQ-2 labelled DNA oligonucleotides in the presence of respective intercalator at the final concentrations of 0.2, 0.5, 1.0 and 4.0 μM. For chemical reduction of the intercalators, 1 μL of the appropriate reducing agent was added to the DNA and intercalator mixture, as described in Section 2.2.2.4. MB was reduced with final concentrations of 15, 37.5, 75 and 300 μM ascorbic acid (150× in excess), while reduction of thionine made use of 100, 25, 50, 200 μM ascorbic acid (100× in excess). Reduction of DM and AM was conducted at final concentrations of 10, 25, 50 and 200 μM sodium borohydride (50× in excess). Controls were measured where both intercalator and reducing agent (DNA only), or just the intercalator (DNA and reducing agent), was omitted. Renaturation and denaturation profiles were recorded at 0.5 °C min^{-1}.

2.2.7 Absorbance-based DNA melting studies

Absorbance-based melting curves were acquired for unlabelled 20mer and 40mer dsDNA oligonucleotides in the presence and absence of oxidised and chemically reduced DM in either 0.036× SSC (7.0 mM Na^+) or 0.1× SSC (19.5 mM Na^+). DNA was hybridised, as described in Section 2.2.2.1, to a final base-pair concentration of 200 µM. Intercalation of 100 µM DM took place according to Section 2.2.2.3 ([dsDNA-bp]:[DM] = 2:1). Chemical reduction of DM was achieved by adding 1 M sodium borohydride in excess to a final concentration of 5 mM (50× in excess) as described in Section 2.2.2.4. The sample was degassed for 2.5 min using argon and then overlaid for 1 min to prevent bubble formation at higher temperatures. 300 µL sample was added to the cuvette (pathlength 0.5 mm), overlaid with mineral oil and finally sealed with Teflon tape and parafilm to prevent evaporation. After baseline correction with the appropriate buffer, renaturation, followed by denaturation, was recorded using a spectrophotometer by scanning the wavelength range 800–200 nm at 4800 nm min^{-1} (bandwidth 2 nm, interval 1 nm) between 25 and 95 °C (depending on sample) at 1 °C min^{-1}. The cuvette was cleaned according to Section 2.2.1.1 after each acquired melting curve.

2.2.7.1 Data analysis

Melting curves obtained by plotting the absorbance A at 260 nm as a function of temperature T. The raw melting curves were subsequently smoothed using a 10 point Savitsky-Golay smoothing function in OriginPro 8.5. Prior to normalising the smoothed melting curves between 0 and 1, upper and lower baselines were determined as described in Section 2.2.6.1. Normalised melting curves were expressed as the fraction f of formed duplex, i.e.

$$f(T) = \frac{A(T)_{\mathrm{Upper}} - A(T)}{A(T)_{\mathrm{Upper}} - A(T)_{\mathrm{Lower}}} \tag{2.9}$$

where $f = 1$ for fully hybridised DNA and $f = 0$ for fully denatured DNA, $A(\mathrm{T})$ is the absorbance at temperature T and $A(\mathrm{T})_{\mathrm{Upper}}$ and $A(\mathrm{T})_{\mathrm{Lower}}$ are the determined upper and lower baselines, respectively. T_{M} and thermodynamic parameters were

calculated using van't Hoff analysis, as described in Section 1.5.3.2, which assumes a two-state model where the DNA is either single-stranded or double-stranded.[36, 167] The parameters were derived from the van't Hoff representation, that is $\ln K_a$ as a function of $1/T$ (in Kelvin), Eq. (1.15), where the analysis interval was restricted to $0.15 \leq f \leq 0.85$.[167] The data points were fitted with the linear least square method with a slope of $-\Delta H°/R$ and an intercept of $\Delta S°/R$. Determination of $\Delta H°$ and $\Delta S°$ permitted the calculation of $\Delta G°$ (at T_M) and K_a (at T_{work}) using Eq. (1.16). T_M was subsequently calculated with Eq. (1.17). If the two-state model was not fulfilled, T_M was calculated based on the first derivative of the normalised melting curves (in fraction f of formed duplex). The hyperchromic shift H for each melting curve was calculated according to

$$H_{260\text{ nm}}^{\text{Thermal}}(\%) = \frac{A_{\text{T, upper}} - A_{\text{T, lower}}}{A_{\text{T, lower}}} \times 100 \tag{2.10}$$

where the recorded absorbance at the highest and lowest temperature corresponds to $A_{\text{T, Upper}}$ and $A_{\text{T, Lower}}$, respectively.

2.2.7.2 Endpoint-melting studies

Absorption spectra were recorded on a Biomate 5 UV–vis spectrophotometer equipped with a thermostatic cell holder (Thermo Spectronic, Cambridge, UK) connected to a waterbath with a Grant Optima GD120 immersion thermostat (Grant Instruments (Cambridge), Shepreth, UK) for temperature control. The temperature inside a quartz cuvette of 1 cm pathlength was monitored using a Digitron temperature probe. Unlabelled complementary 20mer DNA oligonucleotides were hybridised to a final base-pair concentration of 20 µM according to Section 2.2.2.1 utilising 1× SSC (195 mM Na^+) at pH 1-4 and pH 7 as buffer. The sample volume was 200 µL. Denaturation was recorded at 260 nm by endpoint-measurement after increasing the temperature from 25 to 85 °C. As a control, denaturation was measured in 1× SSC at pH 7. Further controls included measuring ssDNA, at a base-pair concentration of 20 µM in 1× SSC (195 mM Na^+) between pH 1-4 and pH 7. The absorption was measured three times at the initial and final temperature.

2.2.8 Circular dichroism-based DNA melting studies

CD was employed to record the denaturation and renaturation by endpoint measurement of samples containing 200 µM unlabelled 20mer dsDNA oligonucleotides in the presence and absence of 100 µM oxidised DM at 0.036× SSC (7.0 mM Na^+), pH 7 ([dsDNA-bp]:[DM] = 2:1). Samples were prepared as described in Section 2.2.2.1 and 2.2.2.3. Each sample was degassed for 2.5 min using argon and then overlaid for 1 min to prevent bubble formation at higher temperatures. 300 µL sample was added to a cuvette (1 mm pathlength). Using a CD spectrometer, CD spectra were recorded at 25 °C, 85 °C, and then 25 °C again by scanning the wavelength range 200-400 nm at 100 nm min^{-1} (data pitch 0.1 nm, response time 1 s, bandwidth 1 nm). A spectrum of the buffer (blank) was recorded at the end of the experiment which was subtracted from the spectrum of the sample. The cuvette was cleaned according to Section 2.2.1.1 after measured sample.

2.2.9 Cyclic voltammetry

The redox behaviour of 100 µM DM was studied in the presence and absence of 200 µM unlabelled 20mer dsDNA at 0.036× SSC (7.0 mM Na^+), pH 7 ([dsDNA-bp]:[DM] = 2:1). Duplex DNA preparation and DM intercalation was carried out according to Section 2.2.2.1 and Section 2.2.2.3, respectively. CV was recorded at 25 °C by scanning the potential range from +0.3 to −0.8 V vs. Ag/AgCl RE with a starting potential of +0.3 V. The scan rate was varied between 1 and 30 mV s^{-1}, while the number of scans varied between 1 and 10. Prior to the measurement, the electrodes were cleaned as described in Section 2.2.1.2. The solution was degassed for 2.5 min with argon and then overlaid for 1 min to remove oxygen. Next, 300 µL of the sample was added to the SEC cuvette (pathlength 0.5 mm) followed by electrode assembly. To prevent evaporation, the sample was overlaid with mineral oil and finally sealed with Teflon tape and parafilm. Between each sample, the cuvette was cleaned according to Section 2.2.1.1. PSTrace2.4 software was used to extract peak potentials (E_{pa}, E_{pc}) and peak currents (i_a, i_c) used for further analysis.

2.2.10 Switch experiments with *in situ* UV–vis spectroelectrochemistry

Hybridised unlabelled 20mer and 40mer dsDNA at 200 µM with 100 µM DM ([dsDNA-bp]:[DM] = 2:1) was prepared as in Section 2.2.2.1 and 2.2.2.3 in either 0.036× SSC (7.0 mM Na^+) or 0.1× SSC (19.5 mM Na^+). Prior to the measurement, the electrodes were cleaned as described in Section 2.2.1.2. The sample was degassed for 2.5 min with argon and then overlaid for 1 min to remove oxygen. After baseline correction with the electrodes and appropriate buffer, 300 µL sample was added to the SEC cuvette (pathlength 0.5 mm). Electrodes were assembled and the sample was overlaid with mineral oil to prevent evaporation. The cuvette was finally sealed with Teflon tape and parafilm. A spectrum was first recorded at 25 °C and then 58–65 °C without applying a potential to ensure that the dsDNA was not denatured at the selected working temperature (T_{work}; see Table 4.3). This was followed by applying successive reduction (E_{red} = −0.8 V) and oxidation potentials (E_{ox} = +0.3 V) at T_{work} five times. The first cycle consisted of applying E_{red} and E_{ox} for 120 s each, while a 60 s application time was used for subsequent cycles. While the current was recorded continuously using a potentiostat, a spectrum was recorded after every 60 s of potential application using a spectrophotometer. The spectra were collected within 10 s to minimize risk of DNA damage through UV radiation by scanning the wavelength range from 800–200 nm at 4800 nm min^{-1} (bandwidth 2 nm, interval 1 nm). A final reduction/oxidation potential sequence was then conducted at the respective heat denaturation temperature, 85–95 °C (T_{heat}; see Table 4.3), as an internal control. At this temperature the DNA was expected to be denatured regardless of the redox-state of DM. To confirm that the dsDNA remained intact, a final spectroscopic scan was performed at 25 °C without applying a potential. As controls, the same experiment was carried out omitting either DNA or DM, or performing the experiment at 25 °C where the DNA is expected to be hybridised regardless of the DM redox-state. Samples and controls were measured at least three times. Between each sample, the cuvette was cleaned according to Section 2.2.1.1.

The exclusive switching effect from DNA was calculated using

$$A^{\mathrm{DNA}}_{260\,\mathrm{nm}}(T_{\mathrm{work}}) = A^{\mathrm{DNA+DM}}_{260\,\mathrm{nm}}(T_{\mathrm{work}}) - \bar{A}^{DM}_{260\,\mathrm{nm}}(T_{\mathrm{work}}) \tag{2.11}$$

where $A_{260\,\mathrm{nm}}^{\mathrm{DNA+DM}}(T_{\mathrm{work}})$ is the observed absorbance for DNA in the presence of DM at T_{work} and $\bar{A}_{260\,\mathrm{nm}}^{DM}(T_{\mathrm{work}})$ is the mean absorbance obtained from switching of DM alone at T_{work}. The exclusive absorbance from DNA was then used to calculate the hyperchromic shift using

$$H_{260\,\mathrm{nm}}^{\mathrm{Echem}}(\%) = \frac{A_{\mathrm{red}}^{\mathrm{DNA}} - A_{\mathrm{ox}}^{\mathrm{DNA}}}{A_{\mathrm{ox}}^{\mathrm{DNA}}} \times 100 \tag{2.12}$$

where $A_{\mathrm{red}}^{\mathrm{DNA}}$ and $A_{\mathrm{ox}}^{\mathrm{DNA}}$ is the exclusive absorbance of DNA at 260 nm upon applying a reduction and oxidation potential, respectively. Finally, the hyperchromic shifts obtained from the electrochemically controlled reversible DNA hybridisation were compared to the benchmark hypochromic shifts obtained by thermal means

$$\text{Electrochemically controlled DNA (\%)} = \frac{H_{260\,\mathrm{nm}}^{\mathrm{Echem}}}{H_{260\,\mathrm{nm}}^{\mathrm{Thermal}}} \times 100 \tag{2.13}$$

2.2.11 Switch experiments with *in situ* CD spectroelectrochemistry

200 µM unlabelled 20mer dsDNA with 100 µM DM in 0.036x SSC (7.0 mM Na^+), pH 7 ([dsDNA-bp]:[DM] = 2:1) was prepared as in Section 2.2.2.1 and 2.2.2.3. The experimental procedure and controls were kept identical to the switch experiment performed with *in situ* UV-Vis spectroelectrochemistry, see Section 2.2.10. CD spectra were recorded on a CD spectrometer, under positive N_2 pressure, by scanning the wavelength range 400-200 nm at 500 nm min^{-1} (data pitch 1 nm, response time 0.125 s, bandwidth 2 nm). Sample and controls were measured in triplicates. Buffer (blank) was recorded at the end. Prior to further analysis, all spectra were first normalised to a linear region between 380–400 nm. Thereafter all replicates of the buffer, sample and controls, respectively, were averaged to minimise the noise. The averaged buffer spectra were subtracted from the averaged spectra of the sample and the controls. However, to visualise the changes in the CD spectra arising exclusively from the switching of the DNA, the changes in the CD spectra arising from DM was subtracted according to

$$\overline{CD}^{\mathrm{DNA}}_{\mathrm{Spectrum}} = \overline{CD}^{\mathrm{DNA+DM}}_{\mathrm{Spectrum}} - \overline{CD}^{DM}_{\mathrm{Spectrum}} \quad (2.14)$$

where $\overline{\overline{CD}}^{\mathrm{DNA+DM}}_{\mathrm{Spectrum}}$ is the mean buffer corrected spectra observed for DNA in the presence of DM and $\overline{\overline{CD}}^{\mathrm{DM}}_{\mathrm{Spectrum}}$ is the mean buffer corrected spectra obtained from switching of DM alone. After appropriate corrections, all spectra were smoothed in OriginPro8.5 using the Savitsky-Golay function (convolution width = 15).

2.2.12 Nucleic magnetic resonance

The stability of DM was studied using NMR. All 1D and 2D measurements were performed in standard 5 mm NMR tubes using a minimum sample volume of 0.5 mL at a main frequency of 800 MHz. Measurements were performed on a Bruker AVIII 800 MHz NMR Spectrometer fitted with 5-mm cryogenic probes (Bruker Biospin, Ettlingen, Germany). Standard 1H and homonuclear correlation spectroscopy (COSY) measurements were carried out at 25 °C. 300 μM DM in deuterated 0.036× SSC (7.0 mM Na^+) was measured before and after redox cycling. 0.6 mL of the before sample was prepared by diluting an appropriate amount of DM in the appropriate concentration of the SSC buffer. The after sample was obtained by subjecting DM to redox cycling at 58 °C using identical procedures as described in Section 2.2.10. However, due to contamination risk in the NMR analysis, mineral oil was not used to prevent sample evaporation. Thus, upon addition of the sample to the SEC cuvette (pathlength 0.5 mm) and electrode assembly, only Teflon tape and parafilm was used to seal the cuvette. Using a Hamilton syringe, the sample was recovered after the redox cycling and pooled from two consecutive switch measurements to achieve at least 0.5 mL. NMR was measured on the same day of redox cycling in order to prevent potential effects caused by overnight storage. As a control, 0.036× SSC, 10 % (v/v) D_2O was measured before and after redox cycling. Typical parameters for the NMR experiments were; 90° pulse sequences, spectral width 12019 Hz, acquisition time 1.36 s, relaxation delay (D1) 1.5 s, scans 64-128, points to process spectra (S1) 32768. Presaturation was used for water suppression.

2.2.13 Capillary gel electrophoresis

Gel electrophoresis analysis of DNA was carried out with a microchip on an Agilent 2100 Bioanalyzer (Agilent Technologies, Palo Alto, USA) using the DNA 1000 Series II kit for the detection of fragments between 15-1000 bp. Unlabelled 20mer dsDNA in the presence of DM at 0.036× SSC (7.0 mM Na^+), pH 7 ([dsDNA-bp]:[DM] = 2:1) was analysed before and after redox cycling (as described in Section 2.2.10). The chip was prepared according to the supplier's instructions. Briefly, 9 µL of a fluorescent dye-DNA gel matrix mixture was added to a well on the chip. The mixture was distributed over the chip by applying pressure using a chip priming station. Following the addition of 9 µL of the gel-dye mix to two more wells, 5 µL marker was added to all wells (upper and lower marker at 1500 bp and 15 bp, respectively). Next, 1 µL of ladder was added to one well which was followed by subsequent addition of 1 µL sample to twelve sample wells. The chip was vortexed for 60 s at 2400 rpm on an IKA MS 3 Bioanalyzer Chip vortexer (IKA, Staufen, Germany) and finally measured. Results were visualised as electropherograms and compared to the ladder in Figure 2.2.

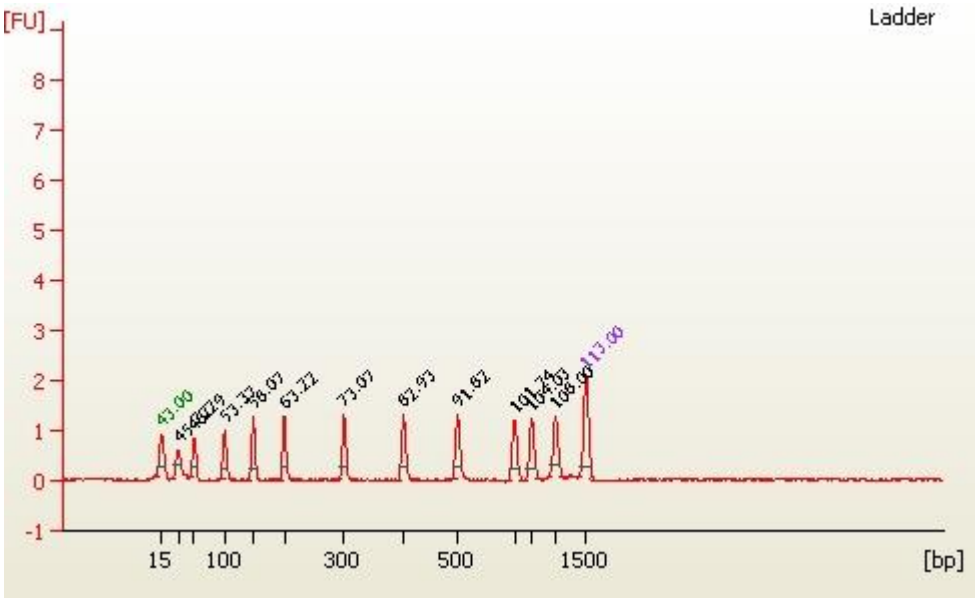

Figure 2.2 Ladder used in the Bioanalyzer DNA 1000 Series II kit. For detection of fragments between 15–1500 bp.

Chapter 3

Probing DNA Hybridisation

3.1 Introduction

Denaturation and renaturation is indispensable for the biological function of nucleic acids in many cellular processes, such as DNA replication and regulation of gene expression.[8] Moreover, many molecular biology technologies rely on the fundamental process of reversible hybridisation, such as nucleic acid amplification technologies (e.g. PCR or LCR),[21, 22, 74] microarrays,[23, 24] next generation sequencing[25] and biosensing.[26, 27] Owing to the self-assembly properties of DNA, this reversible process has additionally found its use in materials science for the production of e.g. DNA origami structures.[194] Thus, there is a prevailing interest in gaining an in depth understanding of what governs the behaviour of reversible hybridisation of DNA through the investigation and development of methods that control and alter this process.[30, 57]

Due to its significance in experimental molecular biology, extensive efforts have been put into the realisation of predictive algorithms and equations that can accurately estimate the thermodynamics and the melting temperature of DNA. Current algorithms predict T_M at desired salt concentrations by scaling down from a known reference point, which is either a measured or theoretically calculated T_M value at 1 M Na^+.[55] While a wide range of different prediction equations exists, as

summarised by Owczarzy and co-workers,[55] this study will consider the two common T_M prediction equations by SantaLucia[56] and Owczarzy.[55] The T_M prediction equation in Eq. (3.1) by SantaLucia[56] is based on the unified nearest-neighbour model which utilises the unified nearest-neighbour parameters found in Table 1.1. Owczarzy[55] on the other hand derived the equation in Eq. (3.2) empirically from a systematic evaluation of 92 oligonucleotides with various lengths and G·C-content in different sodium ion concentrations. While the SantaLucia equation accounts for the sequence length (N_{bp}),[20, 56] the Owczarzy equation is dependent on the base sequence (f(G·C)).[55]

$$\frac{1}{T_M(2)} = \frac{1}{T_M(1)} + \frac{0.368 N_{bp}}{\Delta H^\circ} \ln \frac{[Na^+]_2}{[Na^+]_1} \tag{3.1}$$

$$\frac{1}{T_M(2)} = \frac{1}{T_M(1)} + (4.29 f(GC) - 3.95) \times 10^{-5} \ln \frac{[Na^+]_2}{[Na^+]_1} + 9.40 \times 10^{-6} (\ln^2 [Na^+]_2 - \ln^2 [Na^+]_1) \tag{3.2}$$

where $T_M(1)$ is the measured or predicted melting temperature, using the unified nearest-neighbour parameters, in Kelvin at $[Na^+]_1$ = 1 M and $T_M(2)$ is the estimated scaled down melting temperature at $[Na^+]_2$. In both equations, enthalpy was assumed independent.

This Chapter aims to gain in depth understanding of the concept of reversible DNA hybridisation. The study further aims to elucidate how this reversible process can be manipulated by the variation of well-known and well-defined factors. Revealing the associated underlying chemistry will serve as a basis for understanding electrochemical control of reversible DNA hybridisation explored in later Chapters. This study explored the effect of three common parameters on reversible DNA hybridisation; (1) addition of additives, (2) change in pH and (3) change in the monovalent salt concentration. The first parameter was investigated by addition of two commonly used chemical agents, namely formamide and urea, in a range of concentrations. The second parameter was studied by changing the pH of the buffer in which the experiments were conducted. The last parameter was investigated by

dilution of the buffer to the desired concentration of monovalent salt. Investigating the effect of the monovalent salt concentration furthermore served as the basis for determination of a boundary condition for subsequent studies. At this condition, hybridisation of DNA was maintained yet denaturation could easily be achieved. Due to the importance of establishing correct boundary conditions, the monovalent salt concentration study was further validated by comparing the acquired results with two common T_M prediction equations. The investigation was based on fluorescence-based melting curve analysis where renaturation and denaturation was monitored via FRET, see Figure 1.5.

3.2 Results

3.2.1 The effect of chemical agents on reversible hybridisation

Figure 3.1A and C show the renaturation and denaturation for 20mer dsDNA at 195 mM Na^+ in the presence of 1–10 M formamide and urea, respectively. For full experimental procedures, see Section 2.2.6 and Section 2.2.6.2. To clearly visualise the effect on DNA, melting curves were background corrected and normalised between 0 and 100 % as described in Section 2.2.6.1. The results revealed a single melting transition for all curves, unaffected in sharpness, which consistently shifted towards lower temperatures with increasing concentration of the chemical agent indicating destabilisation of the duplex DNA. The fluorescence of 6-FAM remained largely intact over the whole concentration range as depicted in Figure 3.1B and D for formamide and urea, respectively, and thus did not impact the characterisation of the melting behaviour of the 20mer dsDNA. Further inspection of Figure 3.1A and C revealed no significant effect on the thermodynamic equilibrium, as the renaturation and denaturation curves overlapped in the presence of up to 6 M formamide or urea. Slight hysteresis was however observed at concentrations above 6 M in conjunction with a slight broadening of the melting transition on the renaturation curves.

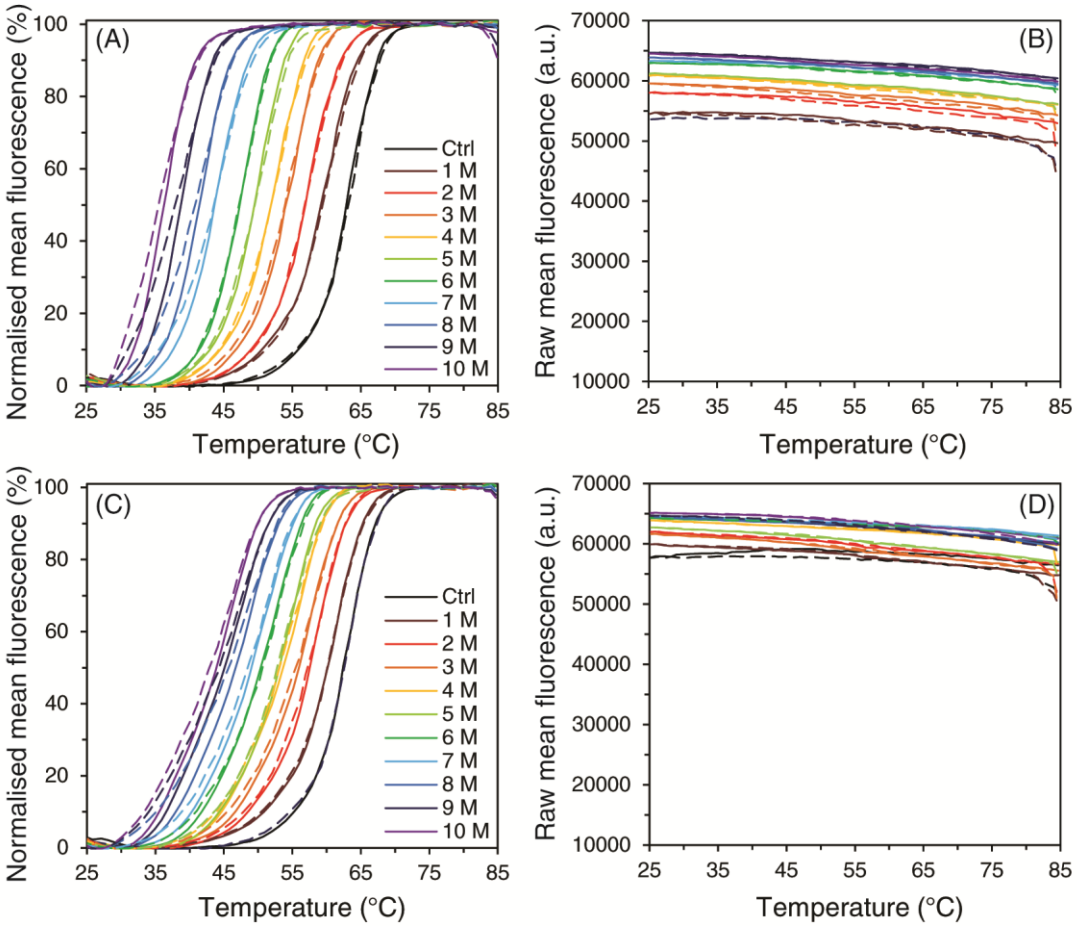

Figure 3.1 Effect of formamide and urea on reversible DNA hybridisation. Normalised renaturation (dashed line) and denaturation (solid line) curves of 20mer dsDNA in SSC buffer at 195 mM Na^+, pH 7, in the presence of 1–10 M (A) formamide and (C) urea. The control (Ctrl) contained no formamide/urea. The melting transition shifted towards lower temperatures with increasing concentrations of chemical agent, indicating destabilisation of dsDNA. The raw fluorescence of 6-FAM labelled ssDNA, in the corresponding experimental conditions, for (B) formamide and (D) urea showed no significant change.

Figure 3.2 shows the summarised plot of the calculated T_M values as a function of formamide and urea in molar concentrations. T_M values were determined from the denaturation curves and were based on the maximum of the first derivative of the normalised melting curves as described in Section 2.2.6.1. As can be seen, increasing concentrations of either formamide or urea lowered the T_M of the 20mer DNA fragment linearly. The mean experimental error in T_M was less than 0.3 °C. The two data sets were fitted with the linear least squares method and a decrease of T_M with

2.7 °C per molar formamide (correlation coefficient R^2 = 0.996) and 1.6 °C per molar urea (correlation coefficient R^2 = 0.974) was obtained.

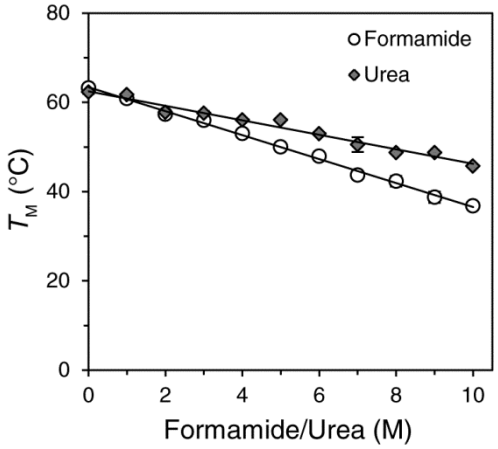

Figure 3.2 Influence of formamide and urea on T_M. T_M of 20mer dsDNA in SSC buffer at 195 mM Na^+, pH 7, decreased linearly with an increasing concentration of formamide or urea. Error bars represent standard deviation ($n \geq 3$).

3.2.2 The effect of pH on reversible hybridisation

Figure 3.3A shows the renaturation and denaturation profiles for 20mer dsDNA at 195 mM Na^+ in the presence of acidic, neutral and alkaline pH ranging from 1–13. An overview of the experimental setup can be found in Section 2.2.6 with a detailed explanation in Section 2.2.6.3. As described in Section 2.2.6.1, for ease of comparison, melting curves were background corrected and subsequently normalised between 0 and 100 %. As seen, the melting behaviour proceeded in a single melting transition, and was only observed between pH 5–11. Results furthermore indicated no significant change in the thermodynamic equilibrium between renaturation and denaturation, apart from at pH 11 which showed slight hysteresis. The sharpness of the melting transitions did not change significantly. A considerable shift of the transition towards lower temperatures was only visible at pH 11, indicating destabilisation of duplex DNA, while a lack of a melting transition at pH 12 and 13 indicated that the 20mer DNA fragment was left in a denatured state at highly alkaline pH. Likewise, no melting transition was observed between pH 1–4. However, inspection of Figure 3.3B, depicting the effect of pH on the fluorescence of

6-FAM labelled ssDNA, revealed that the fluorophore was considerably affected by the acidic pH as the fluorescence was completely quenched between pH 1–4.

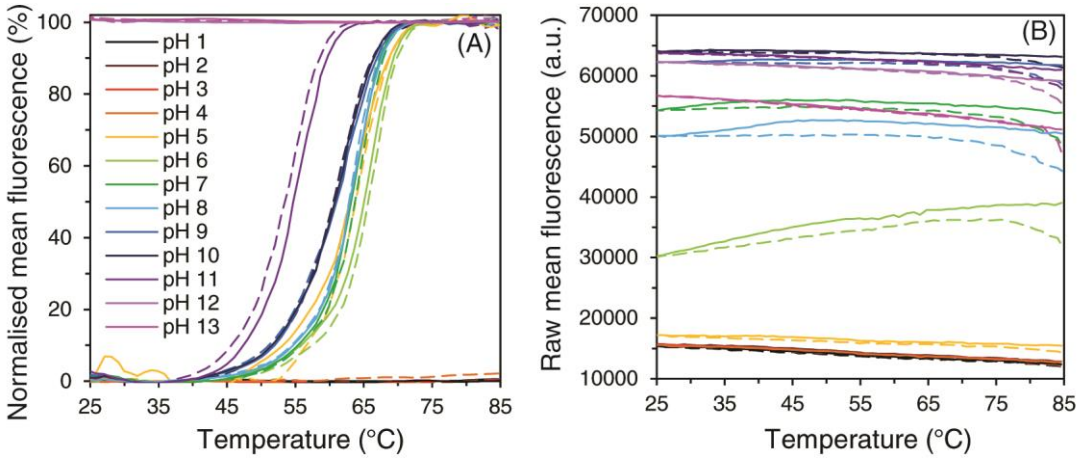

Figure 3.3 Effect of pH on reversible DNA hybridisation. (A) Normalised renaturation (dashed line) and denaturation (solid lines) curves of 20mer dsDNA in SSC buffer, 195 mM Na^+, at pH 1–13. A melting transition was observed at pH 5–11 and the lack thereof at pH < 5 and pH > 11. (B) The fluorescence of the 6-FAM labelled ssDNA in the corresponding experimental conditions was significantly affected by pH and completely quenched in highly acidic conditions.

Therefore, to be able to elucidate whether reversible hybridisation was in fact occurring at pH 1–4, denaturation of the 20mer dsDNA fragment was characterised using unlabelled 20mer DNA oligonucleotides. The process was followed by endpoint-measurement of the absorbance at 260 nm at the initial and final temperature of 25 °C and 85 °C. A detailed description of the procedure can be found in Section 2.2.7.2. Figure 3.4 depicts the measured absorbance as a function of pH. With a hyperchromic shift of 29.2 %, calculated according to Eq. (2.10) in Section 2.2.7.1, denaturation of the 20mer DNA fragment was confirmed at pH 4 and the lack thereof at pH 1–3. Figure 3.4 further revealed that the absorbance at 25 °C and 85 °C for pH 1–3 corresponded to the absorbance observed at 25 °C for pH 4. Thus, the results indicated that the 20mer fragment was not in a denatured state at pH 1–3, but rather degraded.

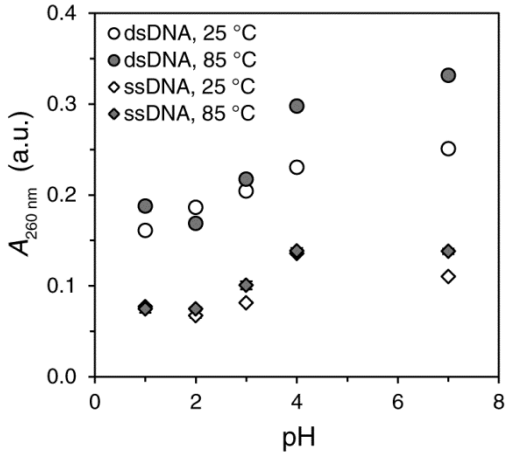

Figure 3.4 Absorbance-based end-point DNA melting study at pH 1–4. Unlabelled 20mer dsDNA and ssDNA (control) in SSC buffer, 195 mM Na^+, at pH 1–4 and pH 7. No increase in $A_{260\ nm}$ was observed at pH 1–3 indicating the lack of reversible hybridisation.

Figure 3.5 represents a summary of the calculated T_M values from the denaturation curves as a function of solution pH. The values were based on the maximum of the first derivative of the normalised melting curves. For details on the determination of T_M, see Section 2.2.6.1.

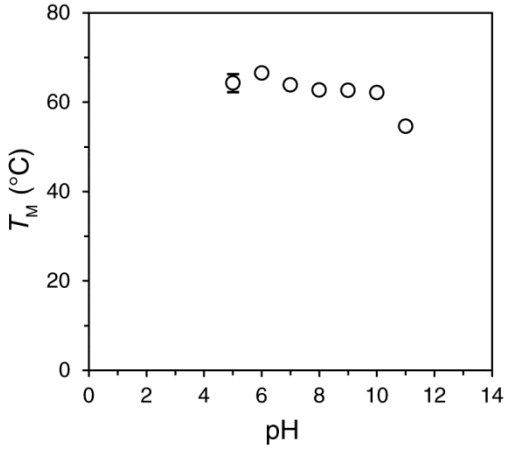

Figure 3.5 Influence of pH on T_M. T_M values for 20mer dsDNA in SSC buffer, 195 mM Na^+, at pH 5–11. No significant change was observed between pH 5-10, while a slight decrease in T_M was observed at pH 11. Error bars represent standard deviation ($n \geq 3$).

T_M values were only determined between pH 5–11, as no reversible hybridisation was detected at pH < 4 and pH > 11. Despite confirming denaturation of the 20mer

DNA fragment at pH 4, T_M could not be calculated since the detection method was based on endpoint-measurements. As realised, with a variation of 1.6 °C, the T_M was largely independent of the solution pH between pH 5–10. Meanwhile, highly alkaline conditions (pH 11) lowered the T_M with an average of 9.1 °C.

3.2.3 The effect of monovalent salt on reversible hybridisation

Figure 3.6A shows the normalised renaturation and denaturation profiles for 20mer dsDNA, at pH 7, in SSC buffer at varying sodium ion concentrations between 2.0 and 195 mM. For details on the full experimental procedure, see Section 2.2.6 and Section 2.2.6.4. Again, melting curves were background corrected and normalised between 0 and 100 % to obtain a straight-forward comparison on the effect on DNA. This was carried out according to Section 2.2.6.1. The melting behaviour was characterised as a single melting transition. While the melting transition evidently shifted towards lower temperatures with decreasing sodium ion concentration indicating destabilisation of duplex DNA, the thermodynamic equilibrium between renaturation and denaturation was likewise affected. The equilibrium persisted at higher sodium ion concentrations (195 and 97.5 mM Na^+). However, hysteresis and a broadening of the melting transitions were observed at concentrations below 20 mM Na^+ indicating a slower renaturation rate. Closer inspection of Figure 3.6A revealed melting transitions, for both renaturation and denaturation curves, until 7.0 mM Na^+. However, at 6.4 mM Na^+ and below a melting transition was only detectable for denaturation. Due to hysteresis, the corresponding renaturation curve exhibited a melting transition too small and diffuse to perform any reliable analysis on. Below 4.7 mM Na^+ the melting transitions were absent, thus, indicating that the 20mer DNA fragment was already in a denatured state at 25 °C (i.e. $T_M < 25$ °C) and hence below the detection limit of the instrument. Examination of Figure 3.6B, displaying the effect of the sodium ion concentration on the fluorescence of 6-FAM, showed a significant decrease in the fluorescence with the decreasing sodium ion concentration. Moreover, the curves exhibited a non-linear temperature-dependent fluorescence.

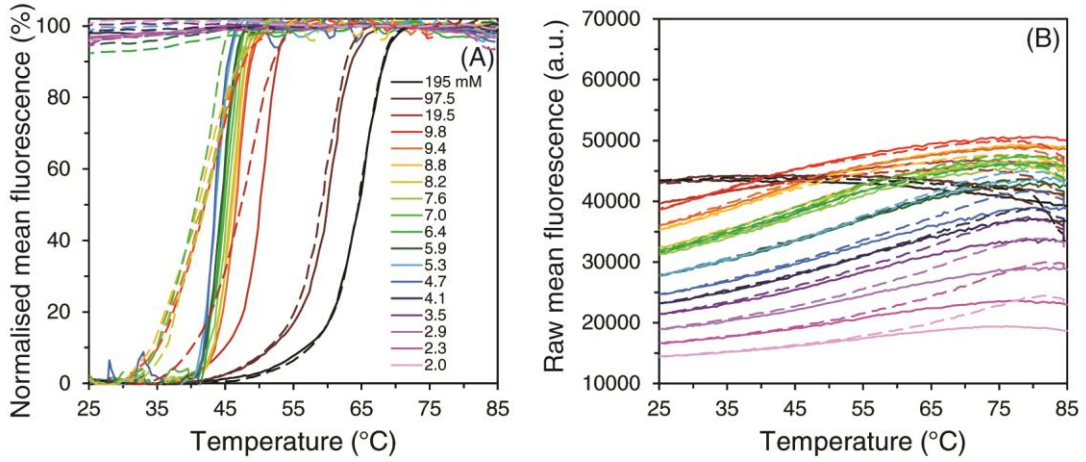

Figure 3.6 Effect of salt concentration on reversible DNA hybridisation. (A) Normalised renaturation (dashed line) and denaturation (solid lines) curves of 20mer dsDNA in SSC buffer, pH 7, at varying $[Na^+]$ between 2.0–195 mM. Significant effect on the thermodynamic equilibrium for renaturation/denaturation was observed at $[Na^+] < 20$ mM. (B) The fluorescence of the 6-FAM labelled ssDNA in the corresponding experimental conditions was significantly lowered with decreasing $[Na^+]$.

The calculated reciprocal T_M values were plotted against the logarithm of the sodium ion concentration as seen in Figure 3.7. T_M values were determined from the denaturation curves and represent the maximum of the first derivative of the normalised melting curves. A detailed description on the calculation is found in Section 2.2.6.1. The mean experimental error for the calculated T_M values was less than 0.5 °C. As can be seen, the plot exhibited a linear dependence of the T_M with decreasing sodium ion concentration in the range studied. The slope $\partial(1/T_M)/\partial \ln[Na^+]$ was determined to -5.45×10^{-5} K^{-1} using the linear least squares method (correlation coefficient $R^2 = 0.996$). For further comparison, the sodium ion concentration dependence was additionally quantified in terms of $\partial T_M/\partial \log[Na^+]$. The data set was re-plotted as a function of $\log[Na^+]$ and subsequently fitted with the linear least squares method, see Figure A.1 in Appendix A. A slope of $\partial T_M/\partial \log[Na^+] = 13.4$ °C was determined with a correlation coefficient of $R^2 = 0.996$.

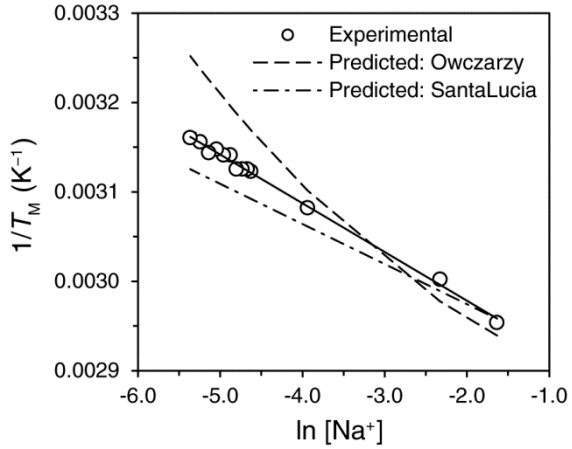

Figure 3.7 Influence of ln [Na⁺] on $1/T_M$. Decreasing [Na⁺] lowered T_M for 20mer dsDNA in SSC buffer, pH 7, as a function of ln [Na⁺] between 7.0–195 mM Na⁺. Besides the experimental data, the effect of sodium ion on T_M is also shown by two common T_M prediction equations by Owczarzy *et al.*[55] and SantaLucia.[56] Correspondence between experimental and predicted data with the SantaLucia equations was observed. Error bars are too small to be visible, however they represent standard deviation (n = 3).

3.2.3.1 Data analysis

Figure 3.7 further provides a graphical representation of predicted T_M values for the sodium ion concentration range studied. The T_M prediction equations used were the SantaLucia[56] equation in Eq. (3.1) and the Owczarzy[55] equation in Eq. (3.2). The SantaLucia equation was solved for the 20mer DNA fragment using N = 19 bp, $T_M(1)$ = 73.5 °C (at 1 M Na⁺) and $\Delta H°$ = −155.7 kcal mol⁻¹, whereas the Owczarzy equation was solved using $T_M(1)$ = 73.5 °C (at 1 M Na⁺) and f(G·C) = 0.5. The parameters at 1 M Na⁺ were theoretically predicted using IDT Biophysics' DNA thermodynamics & hybridization calculator[195] which utilises the nearest neighbour model[56] for the prediction of thermodynamic parameters. T_M was subsequently derived from Gibb's free energy relationship $\Delta G° = \Delta H° - T\Delta S°$.

Closer examination of the Figure 3.7 revealed that the experimentally determined T_M values deviated significantly from the predicted values using the Owczarzy equation. Statistical analysis was performed in order to deduce the goodness-of-fit. The average error $|\langle T_M \rangle|_{Ave}$ was estimated using Eq. (2.7), while the chi-square values χ^2 were calculated employing Eq. (2.8). The estimated parameters and the

corresponding p-values are found in Table 3.1. A detailed description of the statistical analysis is found in Section 2.2.6.4.

Table 3.1 Statistical analysis of goodness-of-fit for predicted T_M values.

Prediction	Equation	$\lvert\langle T_M\rangle\rvert_{Ave}$ (°C)	χ^2	p-value
SantaLucia	(3.1)	5.5	11.9	0.455
Owczarzy	(3.2)	2.9	2.4	1.000

3.2.3.2 Definition of the boundary condition

Based on the results above, a boundary condition for subsequent experiments attempting the control of the reversible DNA denaturation and renaturation was defined. This boundary condition defined the lowest sodium ion concentration where denaturation and renaturation was still detectable. From Figure 3.6 it was evident that this occurred at $[Na^+]_{boundary}$ = 7.0 mM.

3.3 Discussion

The reversible hybridisation of DNA in the presence of changing solution conditions was studied using high-throughput fluorescence-based melting curve analysis. The investigation showed that chemical agents, such as formamide and urea, lowered the T_M of duplex DNA with increasing concentrations while highly acidic and basic pH inhibited reversible hybridisation. Lastly, decreasing the monovalent salt (Na^+) concentration accordingly lowered the T_M of duplex DNA. This latter condition is discussed within the context of the predictions by the counterion condensation theory regarding the salt-dependent behaviour of DNA.

3.3.1 The effect of chemical agents on reversible hybridisation

In this study, the effect of two chemical agents, formamide and urea, on reversible DNA hybridisation was investigated as shown in Figure 3.1A and Figure 3.1C. In correlation with previous findings,[51, 52, 196] the present study demonstrated a linear decrease in T_M of DNA, and thus the duplex stability, with increasing

concentrations of both formamide and urea. However, as also evident, both chemical agents affected the denaturation and renaturation thermodynamic equilibrium. A slight broadening of the melting transition for the renaturation curve indicated a decrease in the renaturation rate at concentrations higher than 6 M. Likewise, Hutton observed a decrease in the renaturation rate upon increasing concentrations of formamide and urea. The author related and demonstrated that the observed effect was a result of the increased solution viscosity.[51] The viscosity has immediate implications on the nucleation rate as the renaturation rate for DNA is inversely proportional to the viscosity of the solution.[197]

In accordance to the findings seen in Figure 3.2, Blake and Delcourt conducted a systematic investigation on the destabilising effect of formamide using plasmid DNA which revealed a decrease in T_M of 2.4–2.9 °C per molar formamide.[52] A single-molecule study on the reaction between DNA and formamide by Bhattacharyya and Feingold showed that the denaturation effect of formamide involves the replacement of Watson-Crick hydrogen bonds via the direct hydrogen bonding of formamide to nucleotides leading to disruption of the double helix.[198] Blake and Delcourt further observed that the destabilisation was, to a certain extent, additionally dependent on base sequence, conformation of helix and state of hydration.[52] Formamide is a strongly associating liquid which can form up to four hydrogen bonds. Thus, the authors proposed that in addition to hydrogen bonding with nucleotides, at concentrations up to 1 M, formamide displaced duplex stabilising weakly groove-bound water molecules leading to alterations in the local ionic strength. Consequently, the amount of condensed counterions changed in the immediate vicinity of the double helix.[52] As a result, the displacement at lower formamide concentrations destabilised the double helix, while at higher concentrations it competed with the nucleotides for the Watson-Crick hydrogen bonds. Consequently, it was concluded that the single stranded state was stabilised leading to perturbations in the helix-coil transition enthalpy and consequently T_M.[52, 198, 199] The authors further went on to show that variations in the G·C-content only gave rise to small differences in the denaturing capability of formamide. Poly(dA·dT) sequences, on the other hand, displayed lower sensitivity towards

destabilisation. This was correlated to the sequence which exhibits an altered B-DNA helix with narrower minor grooves resulting in more tightly bound water.[52]

Urea has been found to affect the stabilisation of DNA in a similar manner as formamide. At lower concentrations, up to 2 M, urea was shown to mainly destabilise the double helix by displacement of surrounding water molecules and accordingly condensed counterions.[200] Upon increasing the concentration, additional competition with the nucleotides for the Watson-Crick hydrogen bonds was seen.[200] Hong *et al.*[196] and Nordstrom and co-workers[201] observed that destabilisation of duplex DNA occurred through favourable interactions and accumulation of urea on the surface of ssDNA upon denaturation. Guinn *et al.* recently quantified the interaction of urea with the functional groups of nucleic acids.[202] The authors showed that destabilisation occurred mainly due to the preferential interaction, i.e. hydrogen bonding, of urea with the heterocyclic aromatic rings of the nucleotides as well as the methyl group on thymine. Unlike formamide, Nordstrom *et al.* found that urea destabilised A·T-rich dsDNA regions to a greater extent compared to G·C-rich regions due to more efficient dehydration of adenine and thymine nucleotides.[201] Similar observations were made by Guinn *et al.* who observed less interaction between urea and DNA with increasing G·C-content.[202] Hutton[51] and Klump and Burkart[203] quantified the destabilisation effect of urea on DNA using genomic DNA. The studies reported a decrease in T_M of 2.3–2.5 °C per molar added urea which is slightly higher than the linear decrease shown in Figure 3.2. This slight discrepancy may be related to the chosen sodium ion concentration of 195 mM at which the experiments were conducted. It has previously been demonstrated that an increasing ionic strength reduced the preferential interaction of urea with DNA, thus, diminishing the denaturing effect of urea.[199, 201] Accordingly, a decrease in the reduction of T_M per molar added urea may be expected. As a comparison, Klump and Burkart obtained a decrease in T_M of 2.5 °C per molar added urea for calf thymus and salmon sperm DNA at a total sodium ion concentration of 11 mM.[203]

3.3.2 The effect of pH on reversible hybridisation

The effect of pH on reversible DNA hybridisation was examined as seen in Figure 3.3A. The investigation revealed that, while a solution pH 4–11 did not substantially affect the reversible hybridisation of DNA, acidic pH (< 4) and basic pH (> 11) destabilised the double helix completely leaving it in a denatured or degraded state. Extracted T_M values summarised in Figure 3.5 indicated that the change in solution pH between 5 and 10 did not affect the duplex stability significantly as the T_M values showed very little variation. However, with a lower T_M value, pH 11 demonstrated a destabilising effect on duplex DNA. Comparable observations were made in previous studies. Owczarzy *et al.*[57] reported a variation of 0.5 °C in the T_M for 10–30 bp long oligomers between pH 6.5–8, which was similarly observed by Plum and Breslauer[204] for DNA hairpin structures as well as by Wetmur and Davidson[197] for T4 phage DNA. The latter study further confirmed a decrease in T_M at pH > 9.[197]

In agreement with the investigation by Ageno and co-workers[49] on the alkaline denaturation of T2 phage DNA, Figure 3.3A indicated a fully denatured state of the double helix at pH > 11. This was concluded on the basis of a constant increased fluorescence observed throughout the measured temperature range of 25–85 °C. Scheme 3.1 details the pK_a values of the four nucleosides, which confirms deprotonation of N1 guanine and N3 thymine at pH > 11. Thus, alkaline denaturation is the result of an increased repulsion between the charges of the two DNA strands, which finally induces disruption of the Watson-Crick hydrogen bonds between the base-pairs in the double helix.[1] Similarly, deprotonation was observed by Lando *et al.* who studied the effect of acidic and alkaline pH on the reversible hybridisation of *E. coli* and calf thymus DNA. However, it was further deduced that the deprotonation occurs in both the single and the double stranded form. Results indicated that the deprotonation of guanine in duplex DNA, at pH > 8, slightly increased the stabilisation of the duplex due to an increase in the DNA charge density. However, the destabilisation gained from the deprotonation of the single stranded form at pH > 11 resulted in a net decrease in duplex stabilisation and finally denaturation.[50]

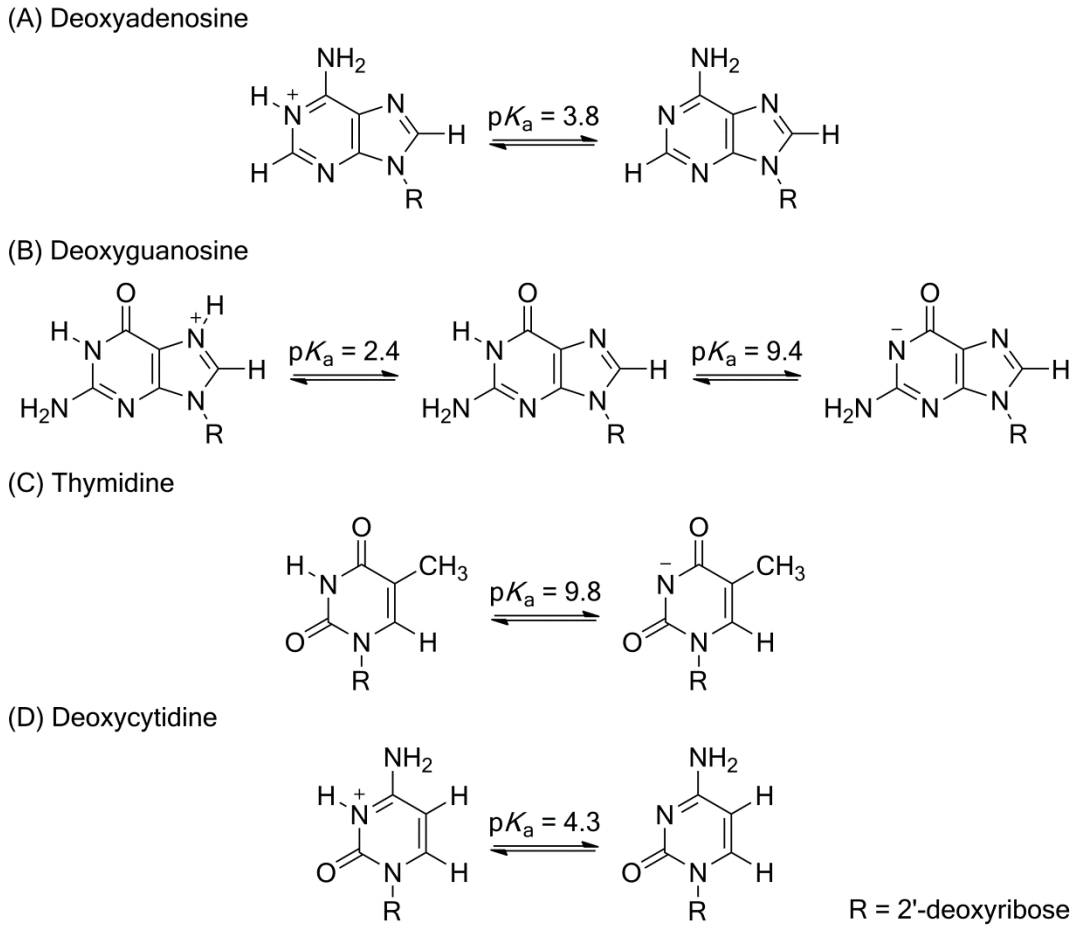

Scheme 3.1 pK_a values of the four nucleosides found in DNA. In nucleotides, the presence of phosphate groups increases the pK_a with ~0.5 pH units. Bases are neutral at pH 7.[205]

While it is well known that alkaline denaturation up to pH 12.5 can be reversed by pH neutralisation,[49, 206] irreversible denaturation is observed in highly acidic solution pH. Upon decrease of the solution pH, melting transitions were no longer visible at pH < 5 as the fluorescence was seemingly quenched, see Figure 3.3A. However, as revealed in Figure 3.3B, the fluorophore 6-FAM was subjected to complete quenching of fluorescence at pH < 5. The strong pH-dependent behaviour of the fluorescein dye is well known and has been characterised previously.[168, 172, 207] You *et al.* showed that 6-FAM, covalently attached to short single stranded oligomers, exhibited optimum fluorescence above pH 7. Studies confirmed that 6-FAM is protonated at pH < 7,[207] which was shown to result in a decreased fluorescence followed by a complete disappearance at pH < 5.[168] The acidic solution pH used in the present study rendered 6-FAM inadequate and thereby the

fluorescence-based melting curve analysis. However, a control experiment measuring the absorbance of unlabelled DNA was able to elucidate the occurrence of denaturation at pH 4 and the lack thereof at pH 1–3, see Figure 3.4. These results indicated that acidic denaturation took place at pH < 4, which is in excellent agreement with the findings of Dubey and Tripathi,[208] as well as others,[50] investigating the acidic denaturation of *E. coli* DNA using laser light scattering to follow the reversible hybridisation of DNA. As realised from Scheme 3.1, the acidic denaturation of duplex DNA is a result of the protonation of N1 adenine, N7 guanine and N3 cytosine and, thus, disruption of the Watson-Crick hydrogen bonds. Since previous studies confirmed that protonation occurred to a higher extent in single compared to double stranded form, the single stranded form was favoured.[1, 50] However, in contrast to the expected behaviour of denatured DNA, which is signified by an increased absorbance at 260 nm, the absorbance recorded at pH 1–3 in Figure 3.4 remained stationary despite the temperature increase to 85 °C. In highly acidic pH, DNA may undergo acid-catalysed hydrolysis where *N*-glycosidic bonds, between the base and the sugar, and covalent bonds, between the sugar-phosphate groups, are cleaved leading to depurination and degradation.[209-211] Lindahl and Nyberg demonstrated that the rate of release of guanine and adenine in *Bacillus subtilis* DNA increased with one order of magnitude per decreasing pH unit at pH < 6. Additionally, the depurination was found to be four times faster for denatured DNA. It was further observed that the depurination was accompanied by a decrease in the absorbance at 260 nm, and thus, may serve as an explanation to the undetected hyperchromic shift for the 20mer DNA fragment at pH 1–3.[209]

3.3.3 The effect of monovalent salt on reversible hybridisation

A linear relationship between decreasing sodium ion concentration and destabilisation of duplex DNA was found between 2.0 and 195 mM Na^+, see Figure 3.7. The linear salt dependence of duplex stabilisation, or T_M, has been predicted by the counterion condensation theory up to 100 mM Na^+[38, 39, 68] and confirmed experimentally.[64, 67, 68] Based on the counterion condensation theory, described in detail in Section 1.2.2, DNA is modelled as an infinitely long charged linear polyelectrolyte that is surrounded by tightly bound (condensed) and weakly bound

cationic counterions, such as e.g. Na^+. These bind, in a delocalised manner, non-specifically to the double helix and account for the neutralisation of the negative phosphate groups on the DNA backbone. However, as predicted by the counterion condensation theory and confirmed experimentally, the fraction of condensed counterions is independent of the bulk salt concentration in the dilute regime. The double helix has an estimated sodium ion concentration around 1.2 M in the immediate vicinity of its surface. This has shown to be constant over a wide range of bulk salt concentration from 3 mM to 1.3 M.[1, 38, 39] As realised from Eq. (1.2), the charge density of dsDNA is greater than ssDNA, since the average charge spacing is smaller for dsDNA than ssDNA. Consequently, the interconversion between the double and the single stranded form is accompanied by a net release of sodium ions, as shown in Eq. (1.5) and Eq. (1.6). Upon this release, the condensed counterions mix with the bulk solution with an entropy gain of[1]

$$\Delta S° = R \ln(c_{\text{condensed}}/c_{\text{bulk}}) \tag{3.3}$$

where $\Delta S°$ is the entropy, R is the ideal gas constant 8.314 J mol^{-1} K^{-1}, $c_{\text{condensed}}$ is the concentration of condensed counterions and c_{bulk} is the concentration of counterions in the bulk solution. In other words, the entropy of mixing increases with decreasing bulk salt concentration. Given the thermodynamic relationship, $\Delta G° = \Delta H° - T\Delta S°$, and owing to the high maintenance of such entropy gain, it is evident that the free energy for the transition from dsDNA to ssDNA decreases with decreasing salt concentration resulting in destabilisation of duplex DNA and a decreasing T_M.[1, 47]

3.3.3.1 Impact of the length of DNA

The net release of sodium ions Δn upon denaturation of the 20mer DNA fragment was calculated using Eq. (1.8). With the slope $\partial(1/T_M)/\partial \ln[Na^+]$ determined from the experimental T_M values plotted in Figure 3.7, $\Delta H° = -155.7$ kcal mol^{-1} and $\alpha = 0.92$, a net sodium ion release of $\Delta n = 2.32$ was obtained. The enthalpy was theoretically predicted as stated in Section 3.2.3.1. This allowed the subsequent determination of the differential thermodynamic counterion binding parameter $\Delta\psi$, which is the release of sodium ions per phosphate group. Using Eq. (1.8), a value of

$\Delta\psi$ = 0.12 was obtained, which deviates slightly from the predicted polyelectrolyte value of $\Delta\psi$ = 0.17 based on the counterion condensation theory. However, similar observations were made in previous studies investigating the salt-dependent melting behaviour of oligomers.[66, 212, 213] Thus, the findings in the present study along with the previously published results suggest that there may be a difference in the melting behaviour of oligomeric and polymeric DNA.

Discrepancy between the present study and previous melting studies utilising polymeric DNA was also found upon comparing the linear variation of T_M with $\log[Na^+]$. Whilst the slope $\partial T_M/\partial \log[Na^+]$ in Figure A.1 in Appendix A was determined to 13.4 °C, previous melting studies of polymeric DNA generated higher dependencies, such as 16.6 °C over the range of 70–120 mM Na^+[64] and 20.5 °C over the range 2.5–100 mM Na^+.[68] Scheffler and co-workers conducted melting studies with d(A·T) hairpin structures and were able to demonstrate that $\partial(T_M)/\partial \log[Na^+]$ decreased from 22.5 °C for polymeric d(A·T) to 11 °C for hairpin oligomers with 18 bases.[65] Thus, Record and Lohman predicted that $\Delta\psi$ varies linearly with $1/N$, where N is the number of phosphate groups.[214] This observation was further substantiated by Shkel and Record[212] as well as Nakano *et al.*[66] who reported a decrease in the release of sodium ions per phosphate group with decreasing oligonucleotide length. Models and simulations of the counterion condensation on duplex DNA have demonstrated that fewer counterions condense at the ends of the polymer due to a lower charge density compared to the interior. Furthermore, it was found that the lengths of the end regions are independent of the polymer length.[39, 43, 214, 215] Fenley *et al.* showed that end effects contribute at low salt concentrations when the Debye length is less, or in the same order of magnitude, as the length of DNA.[43] This was further corroborated by Monte Carlo simulations by Olmsted and co-workers.[215] The authors observed that, at salt concentrations in the range of 10^{-3} M for sufficiently long oligomers (N_{bp} > 20), the fraction of condensed counterions per phosphate charge reaches the predicted polyelectrolyte value of θ_{ds} = 0.76 as a linear function of $1/N$.[43, 215] θ relates to ψ as described by Eq. (1.3).

The contour length of the 20mer DNA fragment in the present study was estimated using $L = N_{bp}R_0$, where N_{bp} and R_0 is the number and size of each structural unit (base-pair)[1]. With R_0 = 3.4 Å for dsDNA (rise of the helix per base-pair) and 20 base-pairs, L = 6.8 nm. Using Eq. (1.1), a Debye length of κ^{-1} = 0.96 nm was obtained for 100 mM Na^+. In other words, the length of the 20mer DNA fragment and the Debye length are already in the same order of magnitude at [Na^+] > 100 mM. Thus, the deviation in $\Delta\psi$ between the present study and the predicted polyelectrolyte value of $\Delta\psi$ = 0.17 is most likely a result of end effects as the studied DNA fragment is only 20 bp long. Thus, it may be concluded that, in conjunction with the literature, current results strongly indicate that oligonucleotides behave differently from polynucleotides with regards to the salt dependence of duplex stabilisation.

3.3.3.2 Impact on the renaturation rate

In agreement with previous spectroscopic and NMR-based melting curve experiments,[67, 197, 213, 216] the reversible hybridisation of DNA experienced hysteresis at [Na^+] < 20 mM, see Figure 3.6A. The renaturation curves displayed broader melting transitions compared to the corresponding denaturation curves demonstrating slower renaturation kinetics.[36] Because the denaturation and renaturation processes were found to be in equilibrium at [Na^+] > 20 mM, results indicated that the system experienced a salt-dependent hysteresis. Using T4 phage DNA, Wetmur and Davidson observed a consistent decrease in the renaturation rate constant upon decreasing the sodium ion concentration from 3.2 M to 60 mM. This resulted in a T_M difference of 20 °C between the denaturation and renaturation process. The authors proposed that the difference arose from changes in the electrostatic interaction between the two DNA strands.[197] Similar findings were made by Kozyavkin and Lyuobchenko using >1 kbp long DNA.[216] In accordance with the renaturation studies making use of polymeric DNA, similar effects were also observed for short oligomers.[67, 213, 217] Furthermore, while the renaturation rate was found to be significantly affected, the denaturation rate was in contrast found to be relatively insensitive to the salt concentration. Williams *et al.* noticed a 10-fold change in the renaturation rate for hexamers, over the range of 12 mM to 1 M Na^+, while only a 3-fold change was observed in the denaturation rate.[67]

One plausible explanation for the observed salt-dependent hysteresis of the 20mer DNA fragment is related to the renaturation process of duplex DNA. As explained in Section 1.2.1, duplex formation consists of two steps; initial base pairing to form a nucleation complex followed by a fast "zippering up" of the remaining base-pairs.[28] It is well known that nucleation formation is the rate limiting step and is strongly dependent on temperature and ionic strength.[28, 217-219] The initial nucleation is hence greatly affected by the electrostatic repulsions between the negatively charged phosphate groups on the DNA strands before molecular recognition occurs.[28, 217] Moreover, based on the counterion condensation theory, renaturation and thus nucleation is an entropy-decreasing process as counterions condense. This results in a positive contribution to the activation free energy through $\Delta G^{\ddagger} = \Delta H^{\ddagger} - T\Delta S^{\ddagger}$, where $\Delta H^{\ddagger}$ is the activation enthalpy.[67, 219, 220] Additionally, as discussed earlier and realised from Eq. (3.3), the entropy of the system is dependent on the bulk salt concentration. Hence, lowering the bulk salt concentration contributes positively to the activation free energy rendering the nucleation step entropically unfavourable. Consequently, a decrease in the renaturation rate would be expected at lower salt concentrations according to the transition state theory

$$k = k_0 e^{-(\Delta G^{\ddagger}/RT)} \tag{3.4}$$

where k is the rate constant, $\Delta G^{\ddagger}$ the activation energy, R is the ideal gas constant 8.314 J mol^{-1} K^{-1} and T the temperature. This was clearly observed in Figure 3.6A as hysteresis only occurred at [Na^+] < 20 mM.

It is worth mentioning however that, in addition to salt concentration, Kozyavkin and Lyuobchenko explored reversibility of DNA hybridisation as a function of the heating and cooling (ramping) rate.[216] The authors conducted absorbance-based melting studies and demonstrated that increasing the ramping rate from 0.05 °C min^{-1} to 0.5 °C min^{-1} resulted in hysteresis at 19.5 mM Na^+, but not at 195 mM Na^+. This evidently suggested that the higher ramp rate was too fast as the system was not given enough time to establish equilibrium at the lower salt concentration.[216] Thus, one could hypothesise that the observed hysteresis in the

present study may have taken place due to the setting of an experimental parameter. In this study, the chosen ramping rate was 0.5 °C min^{-1}. In view of that, the observed hysteresis could have accordingly been avoided by heating and cooling the samples at a slower rate. However, this explanation seems questionable.

Interestingly, unlike the fluorescence-based melting curves at $[Na^+] < 20$ mM in Figure 3.6A, absorbance-based denaturation and renaturation curves of 20mer dsDNA in 7.0 mM Na^+ overlapped indicating thermodynamic equilibrium. This is clearly visualised in Figure 4.11A. Such a discrepancy in the salt-dependent behaviour of the fluorescence- versus absorbance-based melting curves may be an effect of the 100-fold higher DNA-bp concentration utilised for the absorbance-based melting studies. Apart from salt-dependency, the concentration of DNA has been reported to affect hysteresis.[217] This may explain the absence of hysteresis for the absorbance-based melting curves at low salt concentrations. The other possibility is that the discrepancy is the result of the salt- and temperature-dependent variation in the fluorescence of 6-FAM, see Figure 3.6B. The fluorescence of fluorescein and its derivatives is well-known to be sensitive to changes in the solution environment, such as pH, salt concentration, temperature and neighbouring guanine bases.[168, 172] Decreasing salt concentration favours the anionic over the dianionic form of the fluorescein, which shows a weaker absorption in the visible region.[172] Temperature affects the quantum yield and the extinction coefficient of dyes,[168] whereas guanine quenches the fluorescence through orientation- and distance-dependent electron charge transfer.[168, 221] You *et al.* compared DNA hybridisation thermodynamics of FRET-pair labelled short DNA oligomers determined with fluorescence- and absorbance-based melting curve analysis.[168] Evaluating different combinations of FRET-pairs, the authors reported that 6-FAM caused deviations in determination of the thermodynamic parameters ($\Delta G°$, $\Delta H°$ and $\Delta S°$). Due to its complexity, 6-FAM labelled oligomers may have not denatured in a two-state fashion causing deviations. Interestingly, however, the authors found that the extracted T_M values from the fluorescence- and absorbance-based melting curves were in good agreement.[168] Furthermore, others have shown that reliable measurements of the thermodynamic parameters can be performed using fluorescein as the reporter molecule in a FRET-system.[169] Therefore, the

discrepancy observed between the fluorescence- and absorbance-based melting curve analysis is more likely an effect of the DNA concentration.

3.3.3.3 Validation of study by comparison to T_M predicting algorithms

To validate the observed salt dependence of the T_M in Figure 3.7, comparison with two common T_M prediction equations was carried out. As realised from the statistical analysis of the goodness-of-fit in Table 3.1, correlation of the experimentally determined T_M values was found with the SantaLucia prediction equation, see Eq. (3.1). Poor correlation was found with the Owczarzy prediction equation, see Eq. (3.2). SantaLucia[20, 56] derived the T_M prediction equation by collating thermodynamic data for 4–14 bp long oligomers and hairpin structures in the presence of 10–300 mM Na^+. The reported $\partial T_M / \partial \log[Na^+]$ value of 11.7 °C was comparable to the findings in the present study. As calculated from Figure A.1 in Appendix A, the experimentally determined T_M values yielded $\partial T_M / \partial \log[Na^+]$ of 13.4 °C and the predicted T_M values using the SantaLucia prediction yielded 11.1 °C. Previous findings utilising short oligomers showed similar dependencies.[66, 67] The slightly higher dependence observed for the experimentally determined T_M values may have arisen due to differences in the G·C-content of the oligomers used in respective investigations. A systematic examination of 92 oligomers of the length 10–30 bp with varying G·C-content between 20–80 %, in the presence 69 mM to 1.02 M Na^+, was carried out by Owczarzy and colleagues. The authors demonstrated that T_M varies with the G·C-content,[55] an observation similarly reported by Nakano and co-workers.[66]

Unlike Nakano *et al.*,[66] Owczarzy *et al.*[55] observed a non-linear salt-dependent behaviour of T_M above 200 mM Na^+ which most likely accounts for the poor correlation between the predicted (by the Owczarzy equation) and the experimental T_M values, see Figure 3.7. Equally, this behaviour was not captured by SantaLucia[56] and others[67] most likely due to the chosen sodium ion concentration range in which the investigation was carried out. Due to the non-linear nature of the fitted curve, the slope for the Owczarzy prediction was only determined at 195 mM Na^+. Derivation of Eq. (3.2) yielded

$$\frac{\mathrm{d}\left(\frac{1}{T_\mathrm{M}}\right)}{\mathrm{d}\ \ln[\mathrm{Na}^+]} = (4.29f(GC) - 3.95) \times 10^{-5} + 1.88 \times 10^{-5}\ \ln[\mathrm{Na}^+] \tag{3.5}$$

and subsequent substitution of Eq. (1.8) into Eq. (1.7) permitted the calculation of the slope according to

$$\frac{\partial T_\mathrm{M}}{\partial \ln[\mathrm{Na}^+]} = \frac{\partial\left(\frac{1}{T_\mathrm{M}}\right)}{\partial \ln[\mathrm{Na}^+]} T_\mathrm{M}(195\ mM\ \mathrm{Na}^+)^2 \tag{3.6}$$

where $T_\mathrm{M}(195\ \mathrm{mM\ Na^+})$ was the predicted value of 62.7 °C and *f*(G·C) = 0.5. This yielded a value of $\partial T_\mathrm{M}/\partial \log[\mathrm{Na}^+]$ = 12.7 °C, which is comparable with the dependence found for the experimental T_M values. Nevertheless, a poor correlation between the experimental values and the Owczarzy T_M prediction equation remained. Interestingly, the T_M values determined using absorbance-based melting curve analysis corresponded well with the predicted values using the Owczarzy T_M prediction equation. Figure 4.11B shows the T_M values for the unlabelled 20mer DNA fragment at 7.0 mM and 19.5 mM Na^+, while Table A.1 in Appendix G lists the predicted T_M values from IDT Biophysics' DNA thermodynamics & hybridization calculator[195] which is based on the Owczarzy T_M prediction equation, Eq. (3.2). The aforementioned existence of hysteresis, as discussed in Section 3.3.3.2 and seen in Figure 3.6A, is very likely the cause of the observed discrepancy between fluorescence- and absorbance-based melting data. Hysteresis has previously been shown to lead to an under- and overestimation of T_M for the renaturation and denaturation processes, respectively.[36] The experimentally measured T_M values were determined from the denaturation curves. An overestimation of these values, as a result of hysteresis, would indeed result in a poor correlation with the predicted T_M values by the Owczarzy prediction equation. In accordance with the assumption above, Figure 3.7 displayed an increased deviation between the experimentally measured T_M values and predicted values with decreasing salt concentration. Correspondingly, hysteresis was only observed $[\mathrm{Na}^+]$ < 20 mM, see Figure 3.6A. In addition, Owczarzy *et al.* demonstrated that their empirically derived prediction equation accurately predicted T_M values at 1 M down to 11 mM Na^+.[55, 57] Thus, it may be concluded that the correlation of the fluorescence-based T_M values with the

predicted values using the SantaLucia predication equation is inappropriate. According to the results in the present study, and findings in the literature, the salt-dependent behaviour of the 20mer DNA fragment may be more appropriately described by the Owczarzy T_M prediction compared to SantaLucia T_M prediction. Due to the observed discrepancy, thermodynamic evaluation of the reversible DNA hybridisation was only performed on the absorbance-based melting curve data in Chapter 4.

3.3.3.4 Determination of the boundary condition

The boundary condition for subsequent experiments in Chapter 4 and Chapter 5 was determined to $[Na^+]_{boundary}$ = 7.0 mM, see Section 3.2.3.2. This boundary condition was determined on the basis of establishing conditions in which hybridisation of the 20mer DNA fragment persisted, yet denaturation can easily be achieved. Using Eq. (1.1), the obtained Debye length is κ^{-1} = 3.63 nm at 7.0 mM Na^+. In other words, the Debye length is of the same magnitude as the length of the oligomer, i.e. L = 6.8 nm as determined in Section 3.3.3.1. As previously discussed, due to the short length of the oligomer, end effects will make a contribution and affect the fraction of condensed counterions per phosphate charge, see Section 3.3.3.1 and references therein. However, it is worth noting that Fenley *et al.* calculated that the fraction of condensed counterions per phosphate charge is θ = 0.73 for a 20 bp oligomer in 10 mM Na^+.[43] This value is not too different from the counterion condensation limit of 0.76 for a double-stranded polyelectrolyte.[38, 43] Thus, 7.0 mM Na^+ was deemed as an appropriate boundary to establish denaturation favouring conditions, in the subsequent experiments for the electrochemical control of reversible DNA hybridisation, without implicating the intrinsic aspects of salt-dependent duplex stabilisation.

3.4 Summary

This Chapter investigated the effect of three common parameters on reversible DNA hybridisation of short 20mer DNA oligonucleotides. These parameters were addition of additives, here formamide and urea, change in pH and change in the

monovalent salt concentration. It was found that both formamide and urea destabilised duplex DNA linearly with increasing concentrations. A trivial effect of pH 4–11 was observed on the stability of duplex DNA. However, at pH < 4 and pH > 11, no reversible DNA hybridisation occurred as the duplex was in a complete denatured or degraded state. The stability of the duplex DNA was significantly affected by the concentration of monovalent salt, which decreased linearly with a decreasing salt concentration. Comparison with the literature further revealed slightly different melting behaviour between oligomeric and polymeric DNA. Moreover, at very low salt concentrations, the equilibrium of reversible DNA was disturbed. However, the latter finding was concluded to be affected by the experimental setup. Thus, validation of the results by comparison with two common T_M prediction equations revealed that full thermodynamic understanding of the reversible DNA hybridisation, using fluorescence-based melting curve analysis, should be attempted with caution in order to avoid over- or under-estimation of effects. Finally, the boundary condition to be used in subsequent experiments was determined to $[Na^+]_{boundary}$ = 7.0 mM.

Chapter 4

Binding of Oxidised and Reduced Intercalators

4.1 Introduction

First described by Lerman in 1961,[222] intercalators are small, planar aromatic molecules that can interact with DNA non-covalently by insertion between stacked base-pairs of DNA.[125] These molecules have found their use in multiple fields. For example, owing to their often displayed antitumor and antibiotic activity, compounds such as anthracyclines are vital for therapeutic applications.[126] However many equally exhibit fluorescent and electroactive properties, which have made them very useful in diagnostic applications.[26, 125, 223] Both properties have been vastly exploited for fluorescent-[223] and electrochemistry-based[26, 101, 102, 105, 107, 128, 129] detection of nucleic acids. While it is well-known that binding of an intercalator imposes several structural changes on the double helix, such as unwinding and lengthening, less detailed understanding with regards to the thermodynamics and the mechanism of the interaction exists. Thus, due to their versatile use, and the complexity involved with the interaction, gaining an in depth understanding of the binding of an intercalator and its impact on DNA is essential.[143, 146, 224]

This Chapter aims to identify the most suitable intercalator to be exploited for electrochemical control of reversible DNA hybridisation. Thus, the binding and the effect on DNA of methylene blue (MB), thionine, daunomycin (DM) and adriamycin (AM) are examined. However, while the effect of oxidised MB, thionine, DM and AM on DNA has been well-documented, similar systematic studies regarding the impact of their reduced form on DNA have not been published. Furthermore, majority of prior studies on their binding to DNA have concentrated on the characterisation of the drug-binding action. However, the focus in this Chapter is to obtain a profound understanding of the impact of the intercalators' two redox-states on the thermodynamics of the DNA renaturation and denaturation. Therefore, this Chapter aims to provide a detailed characterisation of the impact of oxidised versus reduced intercalator on DNA.[1]

The intercalative binding mode of the four different intercalators was examined and confirmed at various base-pair to intercalator molar ratios using absorbance- and fluorescence-based interrogation. Next, as it was not possible or practical to reduce the intercalators electrochemically for the initial investigation, chemical reduction was explored. Upon confirming intercalation and chemical reduction, the initial effect of oxidised and reduced form of each intercalator on DNA was screened employing fluorescence-based melting curve analysis (see Figure 1.5). Serving as the basis for the decision of the most suitable intercalator, the binding and impact of the selected compound was subjected to further detailed characterisation. Employing fluorescence-based titration, the binding of the selected intercalator to DNA was examined with different lengths of DNA at different salt concentrations. Finally, in depth thermodynamic characterisation of the impact on DNA of the two redox forms, of the selected intercalator, was undertaken. Absorbance-based melting curve analysis in conjunction with van't Hoff analysis (see Section 1.5.3.2 for theory) was employed for the elucidation of the thermodynamic parameters of DNA. This permitted validation of the selected intercalator for subsequent studies on the electrochemical control of reversible DNA hybridisation.

[1] Part of this Chapter was published in Syed, S.N. et al. *J. Am. Chem. Soc.* **135**, 5399–5407 (2013).[3]

4.2 Results

4.2.1 Confirmation of intercalation

The intercalation of MB, thionine[2] and DM[3] into dsDNA was confirmed using UV–vis spectrophotometry and fluorescence spectroscopy, see Section 2.2.3 and Section 2.2.4, respectively, for details on the experimental procedures. Each agent was investigated at a constant concentration while the DNA, in base-pair concentration, was increased according to the base-pair to intercalator molar ratios 1:2, 2:1, 4:1 and 10:1. Spectra were recorded in the presence of both dsDNA and ssDNA. Figure 4.1 displays the absorbance-based spectra of MB in the presence of 20mer dsDNA and ssDNA fragments in SSC buffer (19.5 mM Na^+).

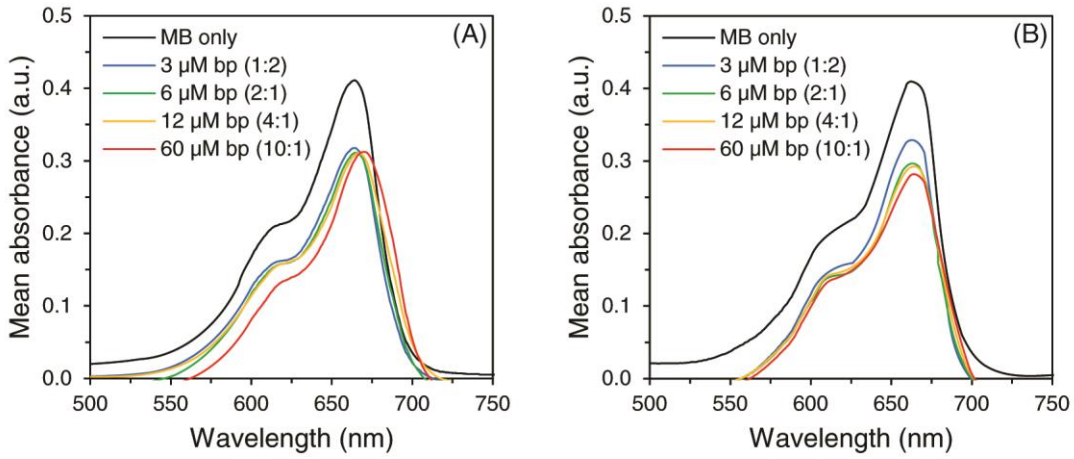

Figure 4.1 Absorbance-based intercalation of MB. Absorption spectra of 6 µM MB in the presence of 3, 12, 24 and 60 µM bp concentration of (A) 20mer dsDNA and (B) 20mer ssDNA. Spectra were recorded in SSC buffer at 19.5 mM Na^+, pH 7. A hypochromic and bathochromic shift was observed in the presence of dsDNA indicating intercalation.

Inspection of Figure 4.1A revealed an absorption peak at 664 nm. Upon increasing the dsDNA concentration, a hypochromic shift of 26.7 ± 6.4 % and bathochromic

[2] Results were generated in an MSc project supervised by Shahida Syed. McDonald, D. Controlling the stringency of DNA hybridization using redox-active DNA intercalating agents. Unpublished MSc thesis. University of Edinburgh (2011).

[3] See Footnote 2.

shift to 669 nm was revealed at the highest concentration (molar ratio 10:1) suggesting intercalation. Figure 4.1B illustrates MB in the presence of an increasing ssDNA concentration. While a hypochromic shift of 31.3 ± 6.7 % was detected for the absorption peak at 664 nm in the presence of the highest ssDNA concentration, no bathochromic shift was observed indicating the absence of intercalation. The results were further substantiated by examining the fluorescence emission spectra of MB in the presence of DNA. Figure 4.2A revealed an emission peak at 683 nm with a significant decrease of 51.7 ± 3.1 % in the fluorescence at the highest concentration of dsDNA. A comparable decrease, reaching only 12.0 ± 8.7 %, did not occur in the presence of ssDNA as seen in Figure 4.2B.

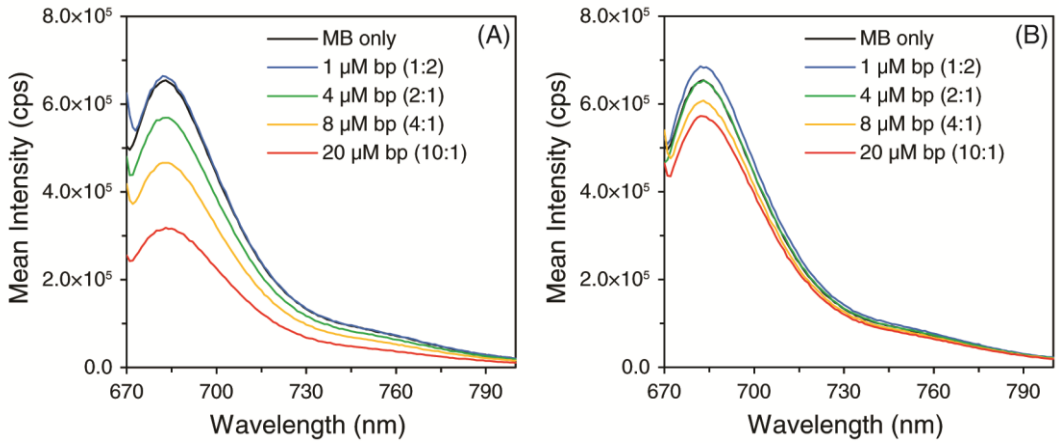

Figure 4.2 Fluorescence-based intercalation of MB. Emission spectra of 2 µM MB in the presence of 1, 4, 8 and 20 µM bp concentration of (A) 20mer dsDNA and (B) 20mer ssDNA. Spectra were recorded in SSC buffer at 19.5 mM Na^+, pH 7 (λ_{ex} = 664 nm). A significant decrease in fluorescence was observed in the presence of dsDNA indicating intercalation.

The characteristics of intercalation were already apparent at the base-pair to intercalator molar ratio 2:1. Thus, Figure 4.3 shows the absorption and fluorescence emission spectra of thionine in the presence of 20mer dsDNA and ssDNA in SSC buffer (19.5 mM Na^+). Figure 4.4 shows the corresponding data for DM. Observed peak maxima, hypochromic and bathochromic shifts for MB, thionine and DM in the presence of dsDNA and ssDNA, at molar ratio of 2:1, are summarised in Table 4.1. In correlation with observations for MB, both thionine and DM showed a hypochromic and bathochromic shift in the presence of dsDNA suggesting

intercalation. On the contrary, both intercalators only displayed a hypochromic shift in the presence of ssDNA, indicating that intercalation was not taking place.

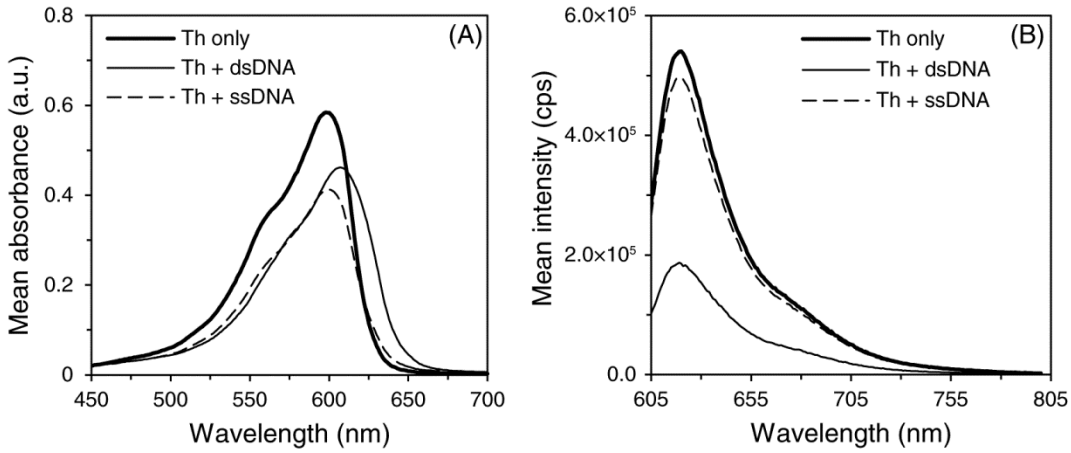

Figure 4.3 Intercalation of thionine. (A) Absorption spectra of 15 μM thionine with 30 μM 20mer dsDNA or ssDNA, in bp concentration. (B) Emission spectra of 2 μM thionine with 4 μM 20mer dsDNA or ssDNA, in bp concentration (λ_{ex} = 596 nm). The hypochromic and bathochromic shift of the absorption peak and a decrease in fluorescence, in presence of dsDNA, confirmed intercalation. Spectra were recorded in SSC buffer at 19.5 mM Na^+, pH 7 (molar ratio 2:1).

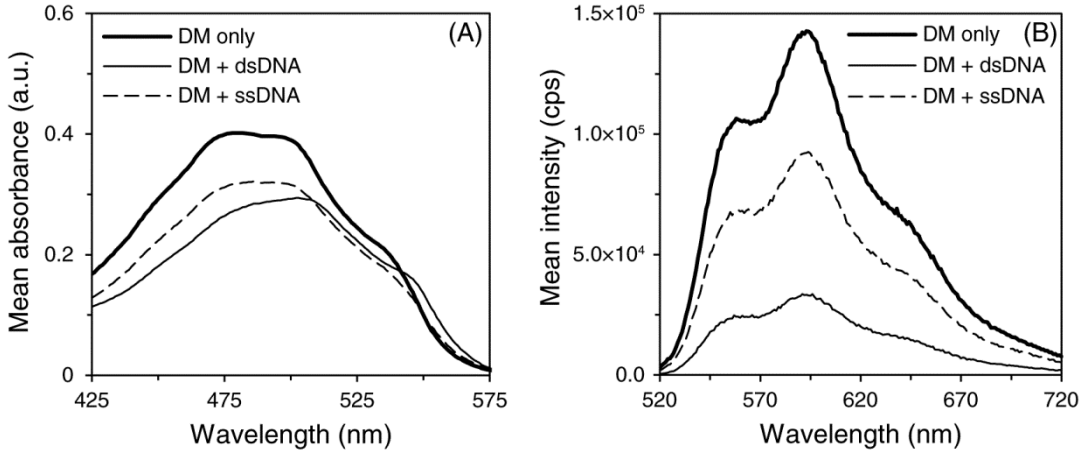

Figure 4.4 Intercalation of DM. (A) Absorption spectra of 40 μM DM with 80 μM 20mer dsDNA or ssDNA, in bp concentration. (B) Emission spectra of 2 μM DM with 4 μM 20mer dsDNA or ssDNA, in bp concentration (λ_{ex} = 480 nm). The hypochromic and bathochromic shift of the absorption peak and a decrease in fluorescence, in presence of dsDNA, revealed intercalation. All spectra were recorded in SSC buffer at 19.5 mM Na^+, pH 7 (molar ratio 2:1).

Table 4.1 Spectral properties of MB, thionine and DM in SSC buffer.†

Sample	UV–vis			Fluorescence	
	λ_{max} (nm)	$\Delta\lambda_{batho}$ (nm)	H_{hypo}‡ (%)	λ_{max} (nm)	H_{hypo}‡ (%)
MB only	664	-	-	683	-
MB + dsDNA	665	1	24.1 ± 5.4	683	12.6 ± 6.6
MB + ssDNA	663	-1	27.3 ± 0.7	683	3.3 ± 3.0
Th only	598	-	-	620	-
Th + dsDNA	607	9	26.4 ± 0.6	620	65.8 ± 1.3
Th + ssDNA	598	0	29.7 ± 1.9	620	7.4 ± 7.3
DM only	478	-	-	594	-
DM + dsDNA	502	24	31.5 ± 4.2	594	76.5 ± 0.8
DM + ssDNA	486	10	20.8 ± 6.7	594	34.8 ± 1.2

† All samples containing DNA are at the base-pair to intercalator ratio of 2:1 at 19.5 mM Na^+. Errors represent standard deviation (n = 3).

‡ Hypochromic shifts (decrease in spectroscopic signal).

4.2.2 Chemical reduction of intercalators

Following the confirmation of intercalation of the oxidised form of the intercalators, their chemical reduction using reducing agents such as ascorbic acid and sodium borohydride was established. Reduction was investigated at a constant intercalator concentration with increasing concentrations of the appropriate reducing agent. The full experimental procedure is described in Section 2.2.5. MB was chemically reduced in the presence of increasing concentrations of ascorbic acid in SSC buffer (7.0 mM Na^+). The concentrations investigated were 100×, 150×, 200× and 250× excess of the concentration of MB. Furthermore, a control containing no ascorbic acid was included. The peak for oxidised MB at 664 nm evidently disappeared after 30 min in the presence of all investigated ascorbic acid concentrations as can be seen in Figure 4.5A. 150× excess of ascorbic acid (7.5 mM) was considered appropriate for complete reduction of MB. The same reducing agent was employed for the reduction of thionine in SSC buffer (7.0 mM Na^+).[4] The studied concentrations of ascorbic acid were 1×, 50×, 100× and 250× the concentration of thionine. Again, a

[4] See Footnote 2 on page 86.

control containing no thionine was included. The peak representing oxidised thionine at 598 nm disappeared after 60 min reduction at higher ascorbic acid concentrations, see Figure 4.5B. 100× excess of ascorbic acid (5 mM) was deemed suitable for the complete reduction of thionine.

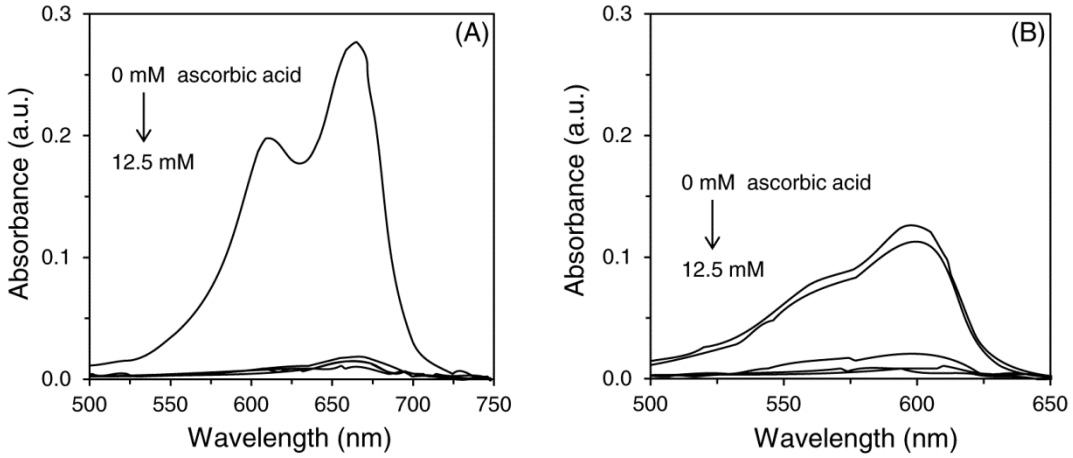

Figure 4.5 Chemical reduction of MB and thionine. (A) 50 µM MB in the presence of 5.0, 7.5, 10.0 and 12.5 mM ascorbic acid in SSC buffer at 7.0 mM Na^+, pH 7. Reduction was achieved after 30 min, which was signified by disappearance of the absorption peak for oxidised MB at 664 nm. (B) 50 µM thionine in the presence of 0.05, 2.5, 5.0 and 12.5 mM ascorbic acid in SSC buffer at 7.0 mM Na^+, pH 7. At higher ascorbic acid concentrations, reduction was achieved after 60 min which was indicated by disappearance of the absorption peak for oxidised thionine at 598 nm.

In comparison to MB and thionine, chemical reduction of DM was carried out with sodium borohydride.[5] Absorption spectra of DM were recorded at sodium borohydride concentrations 1×, 50×, 100× and 250× the concentration of DM in SSC buffer (7.0 mM Na^+). A control containing no sodium borohydride was included. Figure 4.6A revealed the absence of the peak at 480 nm, representing oxidised DM, after 60 min at higher concentrations of sodium borohydride. 50× excess of sodium borohydride (7.5 mM) was selected as the optimum excess concentration for complete reduction of DM. Figure A.2 in Appendix B illustrates the full spectra of DM reduced by sodium borohydride, at 50× excess, over 60 min. For detailed description of the experimental procedure, see Section 2.2.5.1. A spectrum was

[5] Parts of these results were generated in an MSc project, see Footnote 2 on page 86.

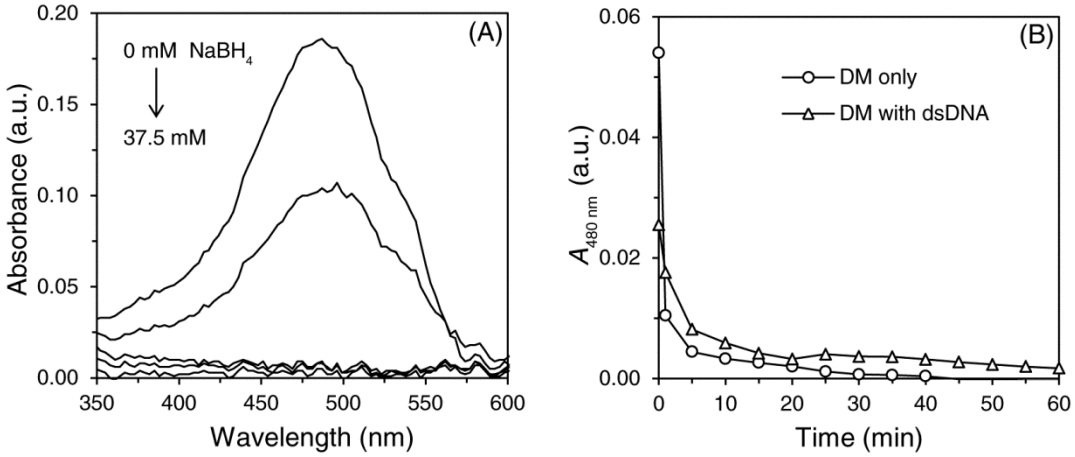

Figure 4.6 Chemical reduction of DM. (A) 150 µM DM in the presence of 0.15, 7.5, 15.0 and 37.5 mM sodium borohydride in SSC buffer at 7.0 mM Na^+, pH 7. Reduction of DM was accomplished after 60 min, which was implied by disappearance of the absorption peak for the oxidised form at 480 nm. (B) A time-course of the reduction of 100 µM DM in the presence and absence of 200 µM 20mer dsDNA (bp concentration) in SSC buffer at 7.0 mM Na^+, pH 7 (molar ratio 2:1). The absorbance at 480 nm was recorded every 5 min over 60 min. Reduction of DM clearly occurred despite intercalation into dsDNA.

recorded every 5 min and the results verified the disappearance of the maximum absorbance peak at 480 nm. In addition, two new peaks and a shoulder at 280, 336 and 420 nm, respectively, were identified which continuously decreased over the course of the reduction. Furthermore, with the purpose of confirming that reduction of the intercalator was taking place despite being bound to dsDNA, the absorbance of DM in the presence of 20mer dsDNA was also monitored. Figure 4.6B shows the reduction of DM, at 480 nm, in the presence and absences of 20mer dsDNA over 60 min. The comparison clearly indicated that, although intercalated into dsDNA, DM still underwent reduction by sodium borohydride at 50× in excess.

4.2.3 Screening of the influence of oxidised and chemically reduced intercalators on DNA stability

Using fluorescence-based melting curve analysis, the influence of oxidised and chemically reduced MB, thionine,[6] DM[7] and AM[8] on DNA stability was screened.

[6] See Footnote 2 on page 86.

Using fluorophore-labelled 20mer dsDNA oligonucleotides in SSC buffer (7.0 mM Na^+), the influence of the intercalator was evaluated in terms of T_M of DNA. As a control, the stability of DNA was additionally evaluated in the absence of an intercalator. The base-pair to intercalator molar ratios investigated were 1:2, 2:1, 4:1 and 10:1. Since the signal from the fluorophore-labelled DNA was interrogated, the DNA concentration was kept constant whilst the intercalator concentration was varied according to the investigated molar ratios. The influence of MB and thionine was studied using the FRET-pair 6-FAM and BHQ-1. Due to crosstalk in the fluorescence between the fluorophore-label and intercalator, the influence of DM and AM was studied with the FRET-pair TexasRed and BHQ-2. Table 2.1 and Table 2.2 provides the excitation and emission information for all involved species, while Section 2.2.6 and Section 2.2.6.5 provides a full description of the experimental procedure.

Figure 4.7 shows denaturation profiles of 20mer dsDNA in the presence of oxidised and chemically reduced DM, at varying concentrations, as a typical example. The denaturation profiles for MB, thionine and AM can be found in Figure A.3 in Appendix C. As established in Section 4.2.2, chemical reduction of MB and thionine was achieved by 150× and 100×, respectively, excess ascorbic acid. Chemical reduction of DM and AM was accomplished by 50× excess sodium borohydride. To visualise the differences in T_M of DNA, all melting curves were normalised between 0 and 100 % according to the method detailed in Section 2.2.6.1. The results revealed a single melting transition across all investigated concentrations for all four intercalators. Further inspection of Figure 4.7 revealed a significant shift of the melting transition towards higher temperatures in the presence of high concentrations of oxidised DM. A comparable shift was not detected in the presence of the reduced form at any concentration.

---

[7] See Footnote 2 on page 86.

[8] Results were generated in an MSc project supervised by Shahida Syed. Sridhar, A. Investigation of the effect of redox active DNA intercalating agents on DNA denaturation and hybridisation. Unpublished MSc thesis. University of Edinburgh (2012).

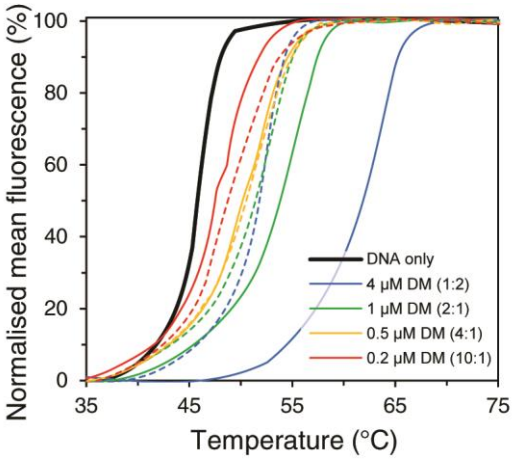

Figure 4.7 Effect of oxidised and chemically reduced DM on DNA stability. Normalised denaturation curves of 2 µM 20mer dsDNA (bp concentration) in the presence of oxidised (solid lines) and chemically reduced (dotted lines) DM, at varying concentrations, in SSC buffer at 7.0 mM Na^+, pH 7. DM was omitted from the control (thick line). All melting curves were recorded at 0.5 °C min^{-1}. Unlike reduced DM, oxidised DM induced a significant increase in T_M of DNA. This was most noticeable at 4 µM DM corresponding to the molar ratio 1:2.

To quantify the influence of the screened intercalators' redox-states, T_M of DNA were extracted from all denaturation curves in Figure 4.7 and Figure A.3. The T_M was based on the first derivative of the normalised melting curves, which was extracted as described in Section 2.2.6.1. A summary of the calculated T_M values for 20mer dsDNA in the presence and absence of the studied oxidised and chemically reduced intercalators, at different molar ratios, can be found in Figure 4.8. Figure 4.8A shows the effect of oxidised and reduced MB on dsDNA. An increase up to 4.6 ± 0.6 °C in T_M of DNA was observed as the concentration of oxidised MB increased. In contrast, the presence of reduced MB did not induce a change in T_M of DNA. However, the difference in T_M between DNA in the presence of oxidised and reduced MB, at any molar ratio, was found insignificant at $\Delta T_M < 1.0 \pm 1.7$ °C. Similar behaviour was observed for thionine in Figure 4.8B. While T_M of DNA increased up to 5.2 ± 0.3 °C in the presence of oxidised thionine, the reduced form yielded an increase up to 3.9 ± 0.9 °C. Thus, the differences in T_M between DNA in the presence of oxidised and reduced thionine were likewise found insignificant at $\Delta T_M < 1.9 \pm 1.4$ °C. The influence of DM in Figure 4.8C, on the other hand, differed

greatly from MB and thionine. Oxidised DM, at the highest concentration (molar ratio 1:2), increased T_M of DNA significantly with values reaching 17.0 ± 1.7 °C. Such significant increase in duplex stability was not observed in the presence of reduced DM, which only increased T_M of DNA up to 7.3 ± 0.8 °C.

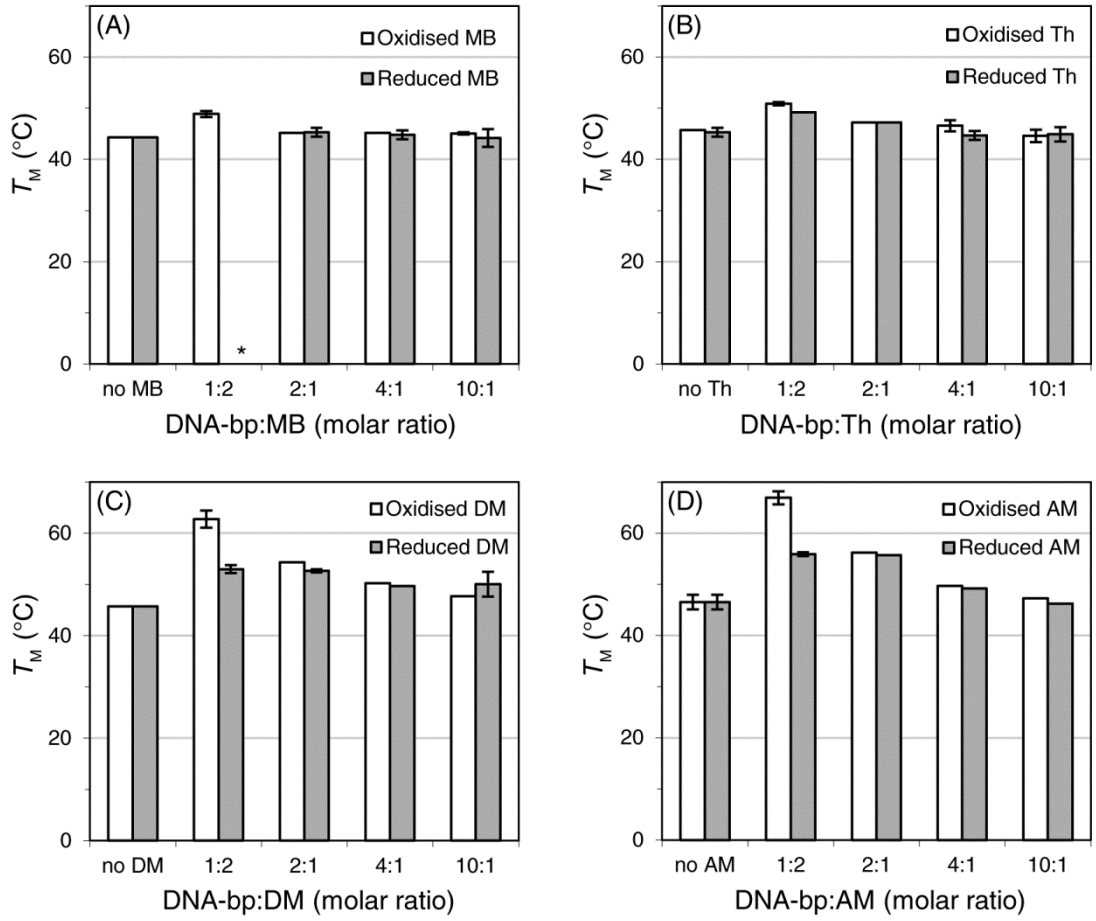

Figure 4.8 Effect of screened intercalators on DNA stability. Oxidised and chemically reduced intercalators were studied in the presence of 20mer dsDNA in SSC buffer at 7.0 mM Na^+, pH 7. The base-pair to intercalator molar ratios studied were 1:2, 2:1, 4:1 and 10:1. The control did not include the intercalator and thus represent the T_M of DNA alone. (A) MB and (B) thionine were studied at 2, 0.5, 0.25 and 0.1 μM, while (C) DM and (D) AM were studied at 4, 1, 0.5 and 0.2 μM. Oxidised DM and AM increased T_M of DNA to a greater extent than oxidised MB and thionine. Furthermore, the difference in T_M between DNA in the presence of oxidised and reduced intercalator, at higher concentrations, was larger for DM and AM than for MB and thionine. Error bars represent standard deviation (n = 3). *T_M not calculated due to absence of a melting transition.

The resulting difference in T_M of DNA in the presence of the highest concentration of oxidised and reduced DM was measured up to $\Delta T_M = 9.8 \pm 1.8$ °C. An equal striking increase in T_M of DNA was observed with the highest concentration of oxidised AM (molar ratio 1:2), see Figure 4.8D, reaching 20.4 ± 1.9 °C. Similar to DM, T_M of DNA with reduced AM increased up to 9.4 ± 1.5 °C. However, a significant difference in T_M of DNA in the presence of the highest concentration of oxidised and reduced AM was still obtained at $\Delta T_M = 11.0 \pm 1.3$ °C.

The impact on the fluorescence of the fluorophore, at the corresponding conditions, was concurrently analysed as a control. Figure A.4 in Appendix D illustrates the effect of the oxidised and chemically reduced intercalators on the fluorescence of 6-FAM and TexasRed labelled 20mer ssDNA oligonucleotides at different molar ratios. Inspection of Figure A.4A revealed that the fluorescence of 6-FAM was moderately affected in the presence of MB. However, at the highest concentration of reduced MB the fluorescence was quenched. This explained the absence of a melting transition at the molar ratio 1:2, as observed in Figure A.3A in Appendix C. Furthermore, Figure A.4B revealed that thionine did not affect the fluorescence of 6-FAM significantly. In contrast, as seen in Figure A.4C and Figure A.4D, the fluorescence of TexasRed was considerably quenched at the higher concentrations of mainly oxidised DM and AM. However, as realised from Figure A.5 in Appendix E, which depicts the raw melting curves of 20mer dsDNA in the presence of oxidised DM and AM, a melting transition was clearly visible throughout all investigated intercalator concentrations. However, it is worth noting that, at the highest concentration of DM and AM (molar ratio 1:2), the fluorescence of TexasRed became quenched as the denaturation of the DNA:intercalator complex proceeded.

In addition, to ensure that the presence of a reducing agent did not affect the T_M of DNA alone, control melting curves of 20mer dsDNA in the presence of ascorbic acid and sodium borohydride were recorded. As shown in Figure 4.9A, no significant impact of ascorbic acid on T_M of DNA was observed at the relevant concentrations. This was likewise the case at the relevant concentrations of sodium borohydride in Figure 4.9B.

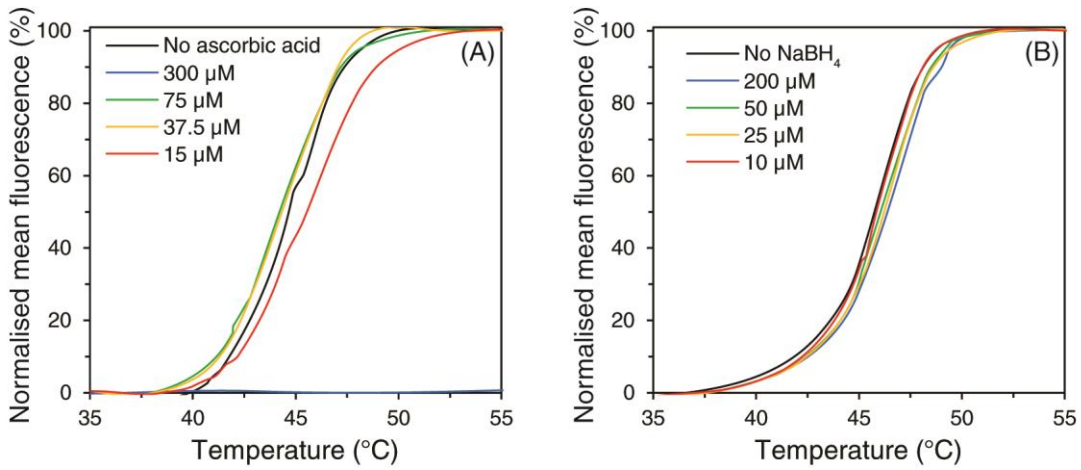

Figure 4.9 Effect of reducing agents on DNA stability. Normalised denaturation curves of 20mer dsDNA in the presence of (A) ascorbic acid and (B) sodium borohydride, at the corresponding concentrations utilised for chemical reduction of the intercalators, in SSC buffer at 7.0 mM Na^+, pH 7. The reducing agent was omitted from the control. No significant impact on T_M of DNA was observed by either reducing agent.

Based on the screening of the influence of oxidised and reduced intercalators on T_M of DNA, summarised in Figure 4.8, it was evident that the oxidised form of DM and AM stabilised duplex DNA considerably more compared to MB and thionine. This was apparent from the vast increase in T_M of DNA. An equal stabilisation of duplex DNA did not take place in the presence of the reduced form for all studied intercalators. Thus, results indicated that the greatest difference in T_M between DNA in the presence of oxidised and reduced intercalator was obtained with DM and AM. Consequently, DM was chosen as a suitable candidate for the investigation of electrochemical control of reversible DNA hybridisation.

4.2.4 Characterisation of daunomycin binding to DNA

4.2.4.1 Binding parameters of daunomycin intercalation

In order to gain further insight of the interaction between DM and DNA, characterisation of the binding was conducted at three different conditions. The interaction was studied in the presence of 20mer dsDNA oligonucleotides at 7.0 mM and 19.5 mM Na^+ as well as 40mer dsDNA oligonucleotides at 7.0 mM Na^+. Fluorescence-based titration studies were performed to deduce the intrinsic binding

constant K_i as well as the neighbour exclusion parameter n for DM. Section 2.2.4.1 gives a comprehensive description of the experimental procedure as well as the accompanying data analysis. Briefly, a known amount of DM was titrated 21 times into a known volume of DNA oligonucleotides. After each titration, the fluorescence of DM was recorded at 555 nm on a fluorometer. Using the titration data, the ratio of the quantum yield of totally bound and free intercalator was determined to $P = 0.02 \pm 0.01$. Establishing this value and using Eq. (2.1) and Eq. (2.2) enabled the calculation of the concentration of bound intercalator. The binding data could thus be analysed in the form of a Scatchard plot as presented in Figure 4.10. Here, the ratio of bound molecules r to total available binding sites (base-pairs) C_f was plotted versus amount of bound molecules r.

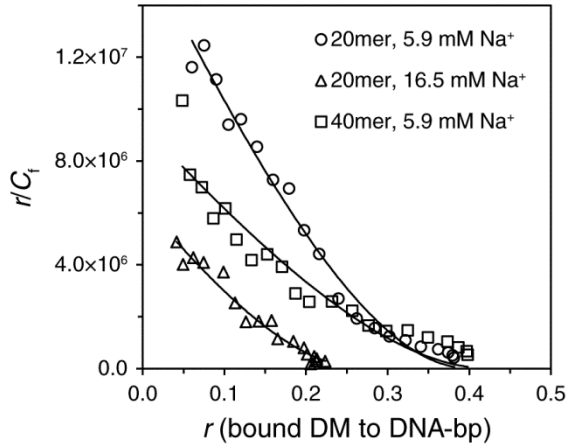

Figure 4.10 Characterisation of the DM–DNA interaction. The binding of 6 µM DM was characterised by 21 titrations of 1–4 µL into 80 µL of 8 µM 20mer and 40mer dsDNA (bp concentration) in SSC buffer at 7.0 mM and 19.5 mM Na^+, pH 7. Fluorescence emission of DM was collected at 555 nm. The data was fitted with the McGhee–von Hippel binding isotherm. The calculated neighbour exclusion parameters and the intrinsic binding constant, for all three conditions, can be found in Table 4.2.

The experimental data was subsequently fitted with the neighbour exclusion binding isotherm by McGhee–von Hippel, Eq. (1.9), which accounts for the observed curvature. K_i and n were obtained, at three different conditions, from the best fit and can be found in Table 4.2 along with their respective correlation coefficients R^2. The uncertainty in the fit, and thus the obtained parameters, was

estimated to below 6 %. The binding free energy $\Delta G°$ was determined by using K_i in the standard thermodynamic relationship in Eq. (2.3). A strong interaction was observed between oxidised DM and DNA. Furthermore, at the lower salt concentration (7.0 mM Na^+), one DM bound per every 2.3–2.5 base-pair, while at the higher salt concentration (19.5 mM Na^+) one DM bound per every 3.4 base-pair.

Table 4.2 Summary of binding parameters for DM to dsDNA.†

Condition	$\Delta G°‡$ (kcal mol^{-1})	K_i (M^{-1})	n (bp/drug)	R^2
20mer, 7.0 mM Na^+	-9.7	1.6×10^7	2.5	0.9843
40mer, 7.0 mM Na^+	-9.4	9.4×10^6	2.3	0.9073
20mer, 19.5 mM Na^+	-9.1	6.4×10^6	3.4	0.9644

† Uncertainty in parameters estimated to < 6 % from the fitting of the McGhee-von Hippel binding isotherm in Eq. (1.9). R^2 signifies the correlation coefficient of the fit.

‡ Calculated at 20 °C.

Based on these findings, a base-pair to intercalator molar ratio 2:1 was deemed suitable for subsequent studies. At this ratio most of the DM was expected to be intercalated.

4.2.4.2 Thermodynamic parameters of DNA with oxidised and reduced daunomycin

To thermodynamically characterise the impact of oxidised and chemically reduced DM on DNA, absorbance-based melting curves of DNA in the absence and presence of DM were recorded at three different conditions. The base-pair to intercalator molar ratio 2:1 was investigated and, as previously established, chemical reduction was achieved by using sodium borohydride at 50× in excess of the concentration of DM. Section 2.2.7 details the complete experimental setup. The absorbance of DNA was monitored at 260 nm and both renaturation and denaturation curves were collected. The recorded hyperchromic shifts of the raw melting curves can be found in Table 4.3 and were calculated according to Eq. (2.10). However, for clear visualisation of the differences in T_M, the melting curves were normalised between 0 and 100 % according to the procedure described in Section 2.2.6.1. Figure 4.11A represents 20mer dsDNA in the presence and absence of oxidised and reduced DM

in SSC buffer (7.0 mM Na^+). The corresponding melting curves for 40mer and 20mer dsDNA in SSC buffer at 7.0 mM and 19.5 mM Na^+, respectively, can be visualised in Figure A.6 in Appendix F. As is seen across all investigated conditions, the renaturation and denaturation melting curves overlapped, within experimental error, and thus confirmed thermodynamic equilibrium of the systems. Furthermore, in contrast to the observed shift in T_M of DNA when interrogated with fluorescence-based measurements (see Figure 4.7), the absorbance-based measurements revealed a much greater shift towards higher T_M values for DNA in the presence of oxidised DM. Indeed, this substantial stabilisation was observed across all three investigated conditions. Further inspection of Figure 4.11A and Figure A.6 revealed that reduced DM only caused a slight shift towards higher T_M values, which was only observed at the lower salt concentration (7.0 mM Na^+).

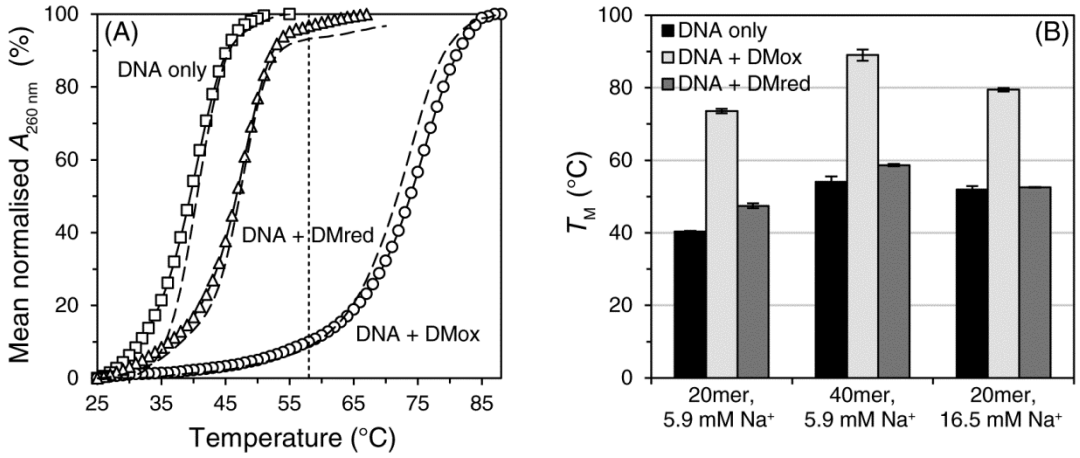

Figure 4.11 Effect of oxidised/reduced DM on DNA stability at three conditions. (A) Normalised absorbance-based renaturation (solid lines with markers) and denaturation (dashed lines) curves of 200 µM 20mer dsDNA (bp concentration) in the presence and absence of 100 µM oxidised and chemically reduced DM (molar ratio 2:1). Melting curves were recorded at 1 °C min^{-1} in SSC buffer at 7.0 mM Na^+, pH 7. The dotted line represents the determined working temperature. Compared to reduced DM, oxidised DM increased T_M of DNA significantly. (B) A summary of T_M of DNA in the presence and absence of oxidised and chemically reduced DM, at three different conditions. Values were based on the renaturation curves for 200 µM dsDNA with 100 µM DM (molar ratio 2:1), pH 7. Throughout all conditions, oxidised DM significantly increased T_M of DNA compared to the reduced form. Error bars represent standard error (n = 3).

Figure 4.11B summarises the extracted T_M values from the renaturation curves of DNA in the absence and presence of oxidised and reduced DM for all three investigated conditions. Two methods were employed for the determination of T_M and a detailed description of the analysis procedure can be found in Section 2.2.7.1. T_M for conditions comprising 20mer dsDNA was determined on the basis of Eq. (1.17), derived from van't Hoff analysis. T_M for conditions involving 40mer dsDNA was based on Eq. (1.11), that is the first derivative of normalised melting curves. An average increase of 31.9 ± 1.3 °C in the T_M of DNA was observed in the presence of oxidised DM across all three conditions. The presence of reduced DM yielded an average increase of only 4.1 ± 1.1 °C. This resulted in a mean ΔT_M of 27.8 ± 1.0 °C between DNA in the presence of oxidised and reduced DM, for all three studied conditions.

The acquired hyperchromic shifts and T_M values served as the basis for the selection of the working temperature (T_{work}) and the heat denaturation temperature (T_{heat}) to be employed in the electrochemical control of reversible DNA hybridisation. The working temperature was selected at the point where the DNA was fully hybridised in the presence of oxidised DM, and fully denatured in the presence of chemically reduced DM. This temperature is represented by the dotted vertical lines displayed in Figure 4.11 and Figure A.6. The heat denaturation temperature was defined as the temperature at which DNA was fully denatured in the presence of oxidised DM. The selected temperatures, for all three conditions, are summarised in Table 4.3.

Finally, thermodynamic evaluation of the effect of oxidised and chemically reduced DM on DNA was performed employing the van't Hoff analysis, which assumes two-state melting. The thermodynamic parameters ΔG°, $\Delta H°$ and $\Delta S°$ and the association constant K_a for DNA were estimated from the absorbance-based renaturation curves according to the analysis procedure described in Section 2.2.7.1. Upon obtaining the van't Hoff representation of $\ln K_a$ versus $1/T$ (in Kelvin), see Figure 4.12 as an example, data points were fitted with the linear least squares method. This enabled the determination of $\Delta H°$ from the slope, according to the van't Hoff relationship in Eq. (1.15), and $\Delta S°$ from the intercept. This facilitated the

calculation of the association constant K_a (at T_{work}) and, in turn, the free energy $\Delta G°$ (at T_M) using the thermodynamic relationship in Eq. (1.16).

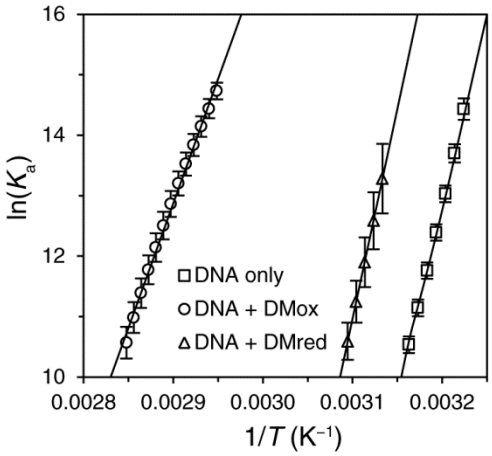

Figure 4.12 van't Hoff representation of the interaction of DM with DNA. Data are shown from the melting curve analysis of 20mer dsDNA in the absence and presence of DM, in SSC buffer at 7.0 mM Na^+. Data points were fitted with the linear least squares method. $\Delta H°$ and $\Delta S°$ were determined from the slope and intercept, respectively, for DNA only (R^2 = 0.9994), DNA with oxidised DM (R^2 = 0.9957) and DNA with chemically reduced DM (R^2 = 0.9999). Error bars represent standard error (n = 3).

Table 4.4 provides a summary of the estimated free energies of the DNA, at three different conditions, while a comparison of the corresponding enthalpies and entropies are found in Figure 4.13A and B. In accordance with the trend of the extracted T_M values in Figure 4.11B, for all three investigated conditions, $\Delta G°$, $\Delta H°$ and $\Delta S°$ remained similar between DNA alone and in the presence of reduced DM. However, a significant change was observed for DNA in the presence of oxidised DM. This change entailed a more favourable $\Delta G°$ term which comprised of a favourable entropy contribution and an unfavourable enthalpy contribution. The results furthermore showed that increasing the salt concentration from 7.0 mM to 19.5 mM Na^+ yielded a more favourable $\Delta G°$ term. A further negative term was observed upon increasing the length of the dsDNA oligonucleotide from 20mer to 40mer. These observations were conserved for DNA in the absence and presence of both oxidised and chemically reduced DM.

Table 4.4 further provides a summary for the corresponding association constants of DNA at the studied conditions. However, instead of evaluating K_a at T_M, the parameter was evaluated at T_{work} for each condition. As mentioned above, this temperature represents the working temperature to be employed for the electrochemical control of reversible DNA hybridisation. Thus, it was necessary to understand how the DNA behaved, in the presence of oxidised and reduced DM, at this temperature for each condition. At the respective working temperatures, results revealed a very large association constant of DNA in the presence of oxidised DM. On the contrary, the DNA exhibited a significantly lower association constant in the presence of reduced DM. Indeed, this value corresponded to the association constants obtained for DNA alone. It is worth noting that some K_a values were accompanied by a large standard error. Nevertheless, the trend in the order of magnitude, between DNA in the presence and absence of oxidised and chemically reduced DM, still remained.

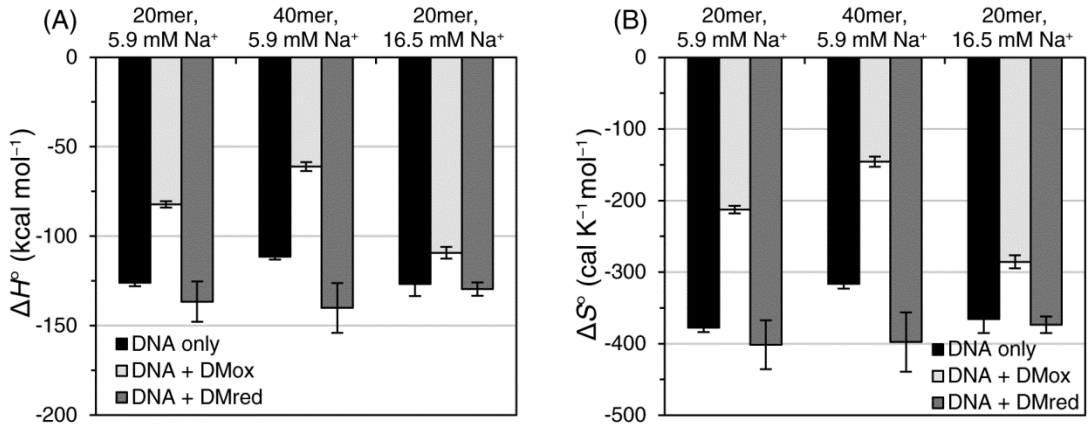

Figure 4.13 Enthalpy and entropy of DNA with oxidised and reduced DM. ΔH° and ΔS° of DNA in the presence and absence of oxidised and chemically reduced DM was determined from absorbance-based renaturation curves, using van't Hoff analysis, for the three tested conditions in SSC buffer at pH 7 (molar ratio 2:1). A similar trend to the extracted T_M values was observed. Reduced DM exhibited ΔH° and ΔS° values similar to DNA alone, whilst the values differed for DNA in presence of oxidised DM. Error bars represent standard error (n = 3).

Table 4.3 Hypochromic shifts of DNA with oxidised and chemically reduced DM.†

Condition	Hyperchromicity H (%)			T_{work} (°C)	T_{heat} (°C)
	DNA	DNA with DM_{ox}	DNA with DM_{red}		
20mer, 7.0 mM Na^+	19.9 ± 0.4	34.0 ± 0.1	17.5 ± 3.7	58	85
40mer, 7.0 mM Na^+	24.4 ± 0.3	33.6 ± 0.5	20.5 ± 2.0	65	95
20mer, 19.5 mM Na^+	22.3 ± 0.1	40.4 ± 1.5	19.8 ± 1.6	60	90

† Values based on renaturation curves. H values were obtained from non-normalised melting curves. Errors represent standard errors (n = 3).

Table 4.4 Free energy and binding constants of DNA with oxidised and chemically reduced DM.†

Condition	DNA		DNA with DM_{ox}		DNA with DM_{red}	
	$\Delta G°$‡ (kcal mol^{-1})	K_a¥ (M^{-1})	$\Delta G°$‡ (kcal mol^{-1})	K_a¥ (M^{-1})	$\Delta G°$‡ (kcal mol^{-1})	K_a¥ (M^{-1})
20mer, 7.0 mM Na^+	−7.6	4.3(±0.8)	−8.4	$5.6(\pm1.1)\times10^7$	−7.8	$2.4(\pm0.3)\times10^2$
40mer, 7.0 mM Na^+	−8.3	$1.0(\pm0.5)\times10^3$	−9.1	$5.2(\pm2.0)\times10^7$	−8.5	$4.4(\pm0.9)\times10^3$
20mer, 19.5 mM Na^+	−7.9	$2.0(\pm0.5)\times10^3$	−8.6	$2.2(\pm0.8)\times10^9$	−7.9	$2.3(\pm0.4)\times10^3$

† Parameters derived from van't Hoff analysis of renaturation curves.

‡ $\Delta G°$ determined at T_M. Standard errors were less than 0.04 kcal mol^{-1}.

¥ K_a determined at T_{work} of each respective conditions. Errors represent standard errors (n = 3).

4.3 Discussion

The primary focus of this results Chapter was to identify the most suitable intercalator to be exploited in the electrochemical control of reversible DNA hybridisation. The studied intercalators were MB, thionine, DM and AM. The mode of intercalation into duplex DNA was first confirmed using absorbance- and fluorescence-based interrogation. Upon investigating the chemical reduction of the intercalators, fluorescence-based melting curve studies were undertaken in order to elucidate an initial impact of the oxidised and reduced form of intercalator on DNA stability. The screening study revealed DM as the most suitable intercalator. The impact of oxidised and chemically reduced DM on DNA stability was finally subjected to comprehensive thermodynamic characterisation using fluorescence-based titration experiments and absorbance-based melting curve studies.

4.3.1 Confirmation of intercalation

The interaction of MB, thionine and DM with dsDNA and ssDNA was examined by means of absorption and fluorescence. A summary of the spectral properties of the intercalators in the absence and presence of dsDNA and ssDNA, at a base-pair to intercalator molar ratio 2:1 can be found in Table 4.1. Figure 4.1A illustrates the progressive spectral changes of MB in the presence of increasing concentrations of 20mer dsDNA oligonucleotides. In accordance with previous findings,[147, 150, 225] MB exhibited a bathochromic and hypochromic shift of the absorption peak at 664 nm in the presence of increasing amounts of dsDNA. While other findings reported slightly larger bathochromic shifts,[147, 150] research has shown that the extent of hypochromic and accompanying bathochromic shifts are dependent on experimental parameters such as salt concentration, temperature and base sequence of the DNA.[147, 150] Quenching of the fluorescence emission maximum at 683 nm for MB in the presence of increasing amounts of dsDNA, as observed in Figure 4.2A, was likewise reported by others investigating the interaction with genomic DNA[225, 226] and synthetic homo- and copolymers[147]. A comparable behaviour to MB was observed for thionine and DM in Figure 4.3 and Figure 4.4, respectively, depicting changes in absorption and fluorescence emission in the absence and presence of

20mer dsDNA oligonucleotides at a base-pair to intercalator molar ratio 2:1. In agreement with previous studies,[154-156, 227] the presence of dsDNA resulted in a bathochromic and hypochromic shift of the absorption peak at 598 nm for thionine (Figure 4.3A), as well as quenching of the fluorescence emission maximum at 620 nm (Figure 4.3B). Similarly, as reported by others,[165, 228, 229] a significant bathochromic and hypochromic shift of the absorbance maximum at 478 nm for DM was observed in the presence of dsDNA (Figure 4.4A). Furthermore, corresponding to previous findings,[161, 165] the fluorescence emission maximum of DM at 594 nm became quenched in the presence of dsDNA (Figure 4.4B).

Spectral analysis of the absorbance and fluorescence signatures of MB, thionine and DM indicated intercalative binding mode with DNA based on the general criteria defined by Long and Barton.[137] Although to different levels, all three studied intercalators revealed pronounced hypochromic and bathochromic shifts in their respective absorbance maximum in the presence of dsDNA. This characteristic behaviour, recognised by Long and Barton[137] and several others,[149, 155, 165, 230] has been interpreted as an effect arising from the close interaction and overlap of the π-electron clouds between the intercalator and DNA base-pairs. Furthermore, the intercalators displayed quenching of their fluorescence emission maximum without an accompanying shift towards longer wavelengths. This distinct feature was likewise ascribed as an effect of intercalation by Long and Barton who suggested that fluorescence-based spectral changes are caused by changes in the excited-state of the electronic structure due to interaction with base-pairs.[137] To provide further evidence for the intercalative binding mode, interaction of MB, thionine and DM was also studied in the presence of 20mer ssDNA oligonucleotides as a negative control. While all three intercalators displayed hypochromic shifts in their respective absorption peaks, in the presence of ssDNA, no distinct bathochromic shifts were observed, see Figure 4.1B, Figure 4.3A and Figure 4.4A. Moreover, although the quenching of the fluorescence emission maximum of DM (Figure 4.4B) was more significant compared to MB (Figure 4.2B) and thionine (Figure 4.3B) in the presence of ssDNA, it was demonstrated to be consistently less significant relative to the presence of dsDNA for all three intercalators. These combined characteristic spectral features are in excellent agreement with previous observations for MB[226, 231]

and thionine.[227] In the case of DM, literature available on the specific spectral changes of DM in the presence of ssDNA is limited. Nevertheless, due to agreement with the MB and thionine data, it may be concluded that all the investigated intercalators evidently interacted with ssDNA, however that the binding mode was not intercalative but rather of electrostatic nature and bound externally.[226, 227, 231]

It is worth noting however that literature data have shown similar spectral characteristics for other types of binding modes and are thus not necessarily exclusive for the intercalative binding mode.[1, 125, 137, 232] For example, at high ionic strength and low base-pair to intercalator ratios, the binding mode for MB has been ascribed as electrostatic. Nonetheless, the interaction still caused a hypochromic shift in the absorbance maximum of MB.[152, 226] Furthermore, Suh and Chaires revealed that the classic groove binder Hoechst 33258 exhibited a bathochromic shift as seen for intercalators.[232] Thus, several critical reviews regarding intercalation have pointed out that additional experiments, to spectral characterisation, are required in order to identify the true binding mode.[137, 232] These additional experiments may comprise examination of the hydrodynamic properties of the intercalator–DNA complex, such as viscometry, sedimentation and electrophoretic techniques.[137, 232] Nevertheless, due to agreement with prior studies, and the distinct spectral differences in the presence of ssDNA, it was concluded that MB, thionine and DM interacted with dsDNA in an intercalative mode under the employed conditions and molar ratios.

4.3.2 Chemical reduction of intercalators

To be able to elucidate a potential differential influence of the intercalators on DNA, depending on their redox-state, the oxidised intercalators had to be reduced. However, as the initial evaluation was based on melting curve analysis, it was neither possible nor practical to reduce the intercalators electrochemically. It was not possible since the effect on DNA was analysed using fluorescence-based melting curve analysis which was performed in a designated instrument. Furthermore, it was not practical or desirable to expose the sample with a reduction potential for more than 3 h when the effect on DNA was studied using absorbance-based melting

curve analysis. Therefore, all studied intercalators were reduced chemically using common reducing agents, such as ascorbic acid and sodium borohydride, in excess.

4.3.2.1 Chemical reduction of methylene blue

Ascorbic acid is a widely used reducing agent for the chemical reduction of MB to leucomethylene blue (LMB). This is a $2H^+$, $2e^-$ reaction, as seen in Scheme 4.1.[233, 234]

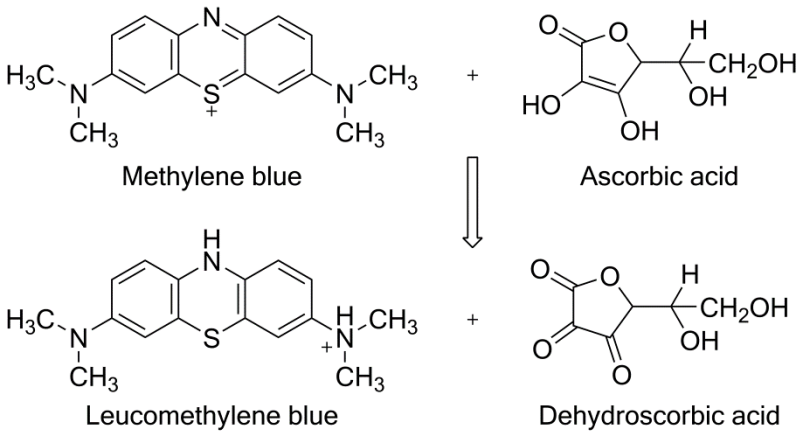

Scheme 4.1 Chemical reduction of MB with ascorbic acid.

Mowry and Ogren investigated the reduction of MB as a function of ascorbic acid and HCl concentration employing absorbance-based measurements.[233] The authors demonstrated that upon reduction, a decrease in the absorbance maximum of MB close to zero was obtained. This spectral characteristic has also been observed using other reducing agents, such as for example thiocyanate.[235] In agreement with Mowry and Ogren, upon treating MB with various concentrations of ascorbic acid the absorption peak for oxidised MB at 664 nm decreased and almost vanished, see Figure 4.5A. Mowry and Ogren further revealed that the reduction followed pseudo first-order decay kinetics which increased with the concentration of ascorbic acid. Interestingly, the authors did not observe a complete reduction of MB, within 13 min, even at an ascorbic acid concentration of roughly 300× excess of MB.[233] Figure 4.5A clearly confirmed complete reduction after 30 min at the selected ascorbic acid concentration of 150× excess of MB. This observed difference in reduction ability may be related to differences in solution pH, since Mowry and

Ogran[233] with others[234] demonstrated faster reduction times in the presence of increasing amounts of HCl.

4.3.2.2 Chemical reduction of thionine

Similar to MB, thionine was chemically reduced by ascorbic acid to leucothionine via a H^+, $2e^-$ reaction, see Scheme 4.2.[236]

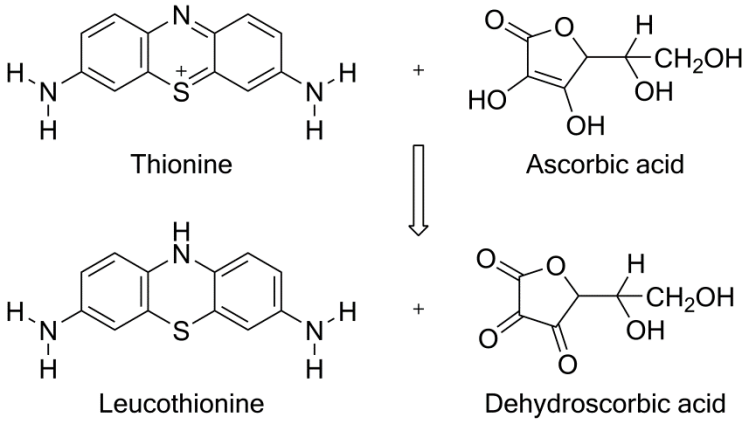

Scheme 4.2 Chemical reduction of thionine with ascorbic acid.

Results in Figure 4.5B displayed a decay of the absorbance for thionine at 598 nm in the presence of increasing concentrations of ascorbic acid. This spectral observation is consistent with previous spectrophotometric studies on the reduction of thionine using ascorbic acid.[236, 237] For example, Pourereza and Mousavi studied the inhibitory effect of vanadium on the ascorbic acid-mediated reduction of thionine. In the absence of vanadium, the authors demonstrated reduction within 10 min by treating thionine with ascorbic acid at 7× in excess. However, it was noted that the authors did not obtain complete reduction at the chosen reaction conditions since an absorption peak for oxidised thionine at 598 nm was still visible.[236] Figure 4.5B confirmed complete reduction of thionine after 60 min at 100× the concentration of the intercalator, as the absorbance maximum at 598 nm had completely vanished at the selected conditions.

4.3.2.3 Chemical reduction of daunomycin

Unlike MB and thionine, reduction of DM was achieved with sodium borohydride via a transfer of H^+, $2e^-$, see Scheme 4.3. This reducing agent has been shown to react both with the quinone ring, for the formation of a hydroquinone, and the carbonyl group at C13.[238] Figure 4.6A shows a decrease in the absorbance of DM at 480 nm with an increasing concentration of sodium borohydride. Schweitzer *et al.* conducted a mechanistic study of the reduction of DM with sodium borohydride in methanol. Confirming the observation in Figure 4.6A and Figure 4.6B, the authors were able to spectrophotometrically detect a decrease in the peak absorption for DM at 480 nm within the first 10 min of the reaction.[238] In agreement with Figure A.2 in Appendix B, the authors furthermore detected a concurrent formation of new peaks at 336 and 430 nm. These peaks were attributed to the formation of borate ester as visualised in Scheme 4.3 and were identified in aqueous medium as well.[238] However, Schweitzer *et al.* further reported on the reappearance of an absorbance maximum at 480 nm. High-performance liquid chromatography (HPLC) analysis showed a mixture of daunomycinol, as seen in Scheme 4.3, and re-oxidised DM.[238] Several publications have reported on the instability of the hydroquinone state of DM and its rapid re-oxidation in the presence of trace amounts of molecular oxygen.[238-240] However, it is evident from Figure A.2 that no reappearance of a peak at 480 nm occurred. In contrast, the characteristic peaks for borate ester disappeared over time. This suggested complete reduction of DM within 60 min by the formation of daunomycinol hydroquinone borate as depicted in Scheme 4.3. An explanation to the observed discrepancy may be related to the amount of sodium borohydride utilised for the chemical reduction. While the present study used sodium borohydride 50× in excess of the concentration of DM, Schweitzer and co-workers used 2× excess. Moreover, Kleyer *et al.* performed a mechanistic reduction study of DM using a different reducing agent, bi(3,5,5-trimethyl-2-oxomorpholin-3-yl), and concluded that at low concentrations of the reducing agent, destruction of the hydroquinone state was faster than its formation.[241]

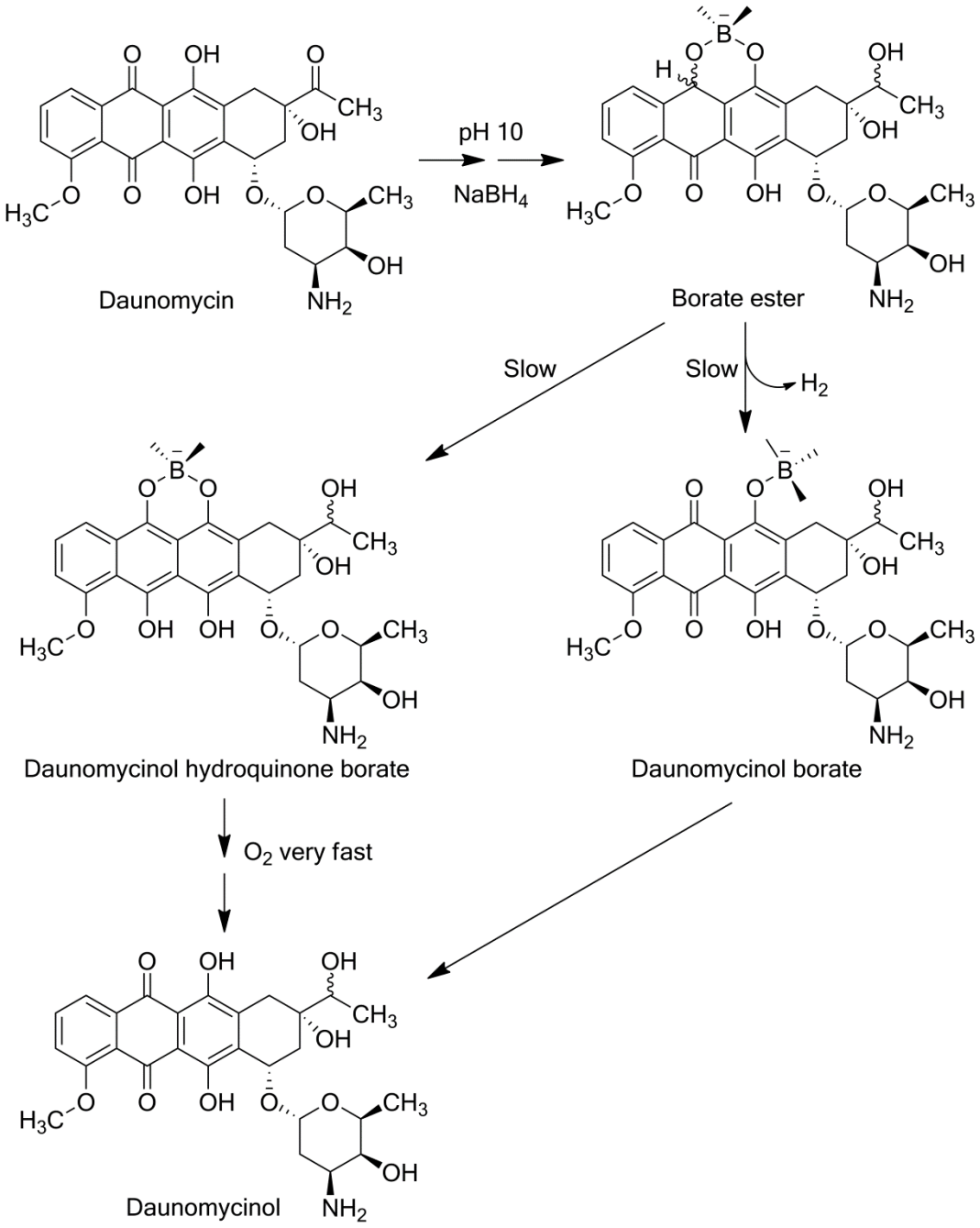

Scheme 4.3 Chemical reduction of DM with sodium borohydride.

It is worth mentioning that, alongside the formation of chemically reduced DM, both Schweitzer *et al.*[238] and Cummings and co-workers[242] observed the formation of daunomycinol borate, see Scheme 4.3. Thus, it is highly likely that the chemical reduction of DM in the present study also formed this additional product. However, further investigation is required for confirmation. It is important to note that because the phenolic OH groups on the hydroquinone have shown to be partially

deprotonated at pH 7,[243] Bird *et al.* further speculated that the hydroquinone undergoes irreversible glycosidic cleavage of the sugar ring.[244] While this irreversible reaction has been demonstrated for the anaerobic reduction of DM,[238-242] neither Schweitzer *et al.*[238] nor Cummings *et al.*[242] observed elimination of the sugar ring upon the aerobic reduction of DM with sodium borohydride. Therefore, based on the high concentration of sodium borohydride used in the present study, it was concluded that chemical reduction of DM mainly yielded reduced DM, that is daunomycinol hydroquinone borate, as well as daunomycinol borate.

4.3.3 Screening of the influence of oxidised and chemically reduced intercalators on DNA stability

Initial assessment of the influence of oxidised and chemically reduced MB, thionine, DM and AM on the stability of 20mer dsDNA in SSC buffer was conducted with fluorescence-based melting curve analysis at the boundary condition (determined in Chapter 3) of 7.0 mM Na^+. To further identify the impact of the concentration of the intercalator on DNA, increasing amounts of each intercalator were examined. The concentrations corresponded to four different base-pair to intercalator molar ratios, namely 1:2, 2:1, 4:1 and 10:1. The extracted T_M values for DNA in the absence and presence of each screened intercalator can be found summarised in Figure 4.8.

While intercalation and chemical reduction was confirmed for MB, thionine and DM, AM was included in the screening based on the assumption that its intercalative and reductive behaviour is essentially identical to DM. AM differs structurally from DM only by an OH group at position C14, see Scheme 1.1. Crystallographic studies by Fredrick *et al.*,[164] along with absorbance- and fluorescence-based spectroscopic studies by others,[165] confirmed that the main mode of interaction between AM and dsDNA is through intercalation. Furthermore, Cummings *et al.* successfully investigated the chemical reduction of AM using sodium borohydride.[242] Thus, based on the existing literature and the experimental results obtained for DNA in the presence of DM (Figure 4.4), intercalation of AM was assumed to take place at the chosen conditions. In addition, in accordance with

the chemical reduction of DM (Figure 4.6), reduction of AM was performed with sodium borohydride at 50× in excess of the concentration of the intercalator.

4.3.3.1 Impact of oxidised intercalators on duplex DNA

As evident from the histograms in Figure 4.8, and the literature,[150, 155, 161, 165] all four intercalators were found to increase T_M of DNA in their oxidised form. However, the observed increase in T_M was dependent on the concentration of the intercalator, with the largest increase at the highest intercalator concentration (molar ratio 1:2). This behaviour was likewise reported by Mudasir *et al.*[150] and Chaires and co-workers.[161] Both authors conducted absorbance-based melting curve studies with calf thymus DNA in the presence of oxidised MB and DM, respectively, at various base-pair to intercalator molar ratios. As in the present study, the authors observed an increased T_M of DNA with higher concentrations of the intercalator. The findings in the current study thus confirmed that the oxidised form of MB, thionine, DM and AM stabilised duplex DNA. However, as revealed by the results, oxidised DM and AM yielded a higher increase in T_M of DNA than MB and thionine. This has similarly been observed in the literature. For example, Mudasir *et al.*[150] found an increase of 5.5 °C in T_M of calf thymus DNA with MB, while Paul *et al.*[155] reported an increase of 6.3–9.4 °C for genomic DNA with thionine. In contrast, Chaires *et al.*[161] revealed a remarkable increase of nearly 30.0 °C in T_M of calf thymus DNA with DM. Furthermore, Ghosh *et al.*[165] demonstrated an increase of 13 °C in T_M of human DNA in the presence of AM. Several studies have shown that the binding of intercalators to DNA is dependent on the base-pair to intercalator ratio,[149, 150, 161] charge on the intercalator[139, 245] and the salt concentration.[155, 161, 246] Thus, due to differences in experimental conditions between the present study and previously conducted studies, it is difficult to compare exact T_M values. Nevertheless, the observed trend of a greater stabilisation of duplex DNA by oxidised DM and AM, relative to MB and thionine, is still evident.

The recorded difference in the stabilisation potential of the studied intercalators is very likely the cause of major structural differences between anthracyclines (DM and AM) and phenothiazines (MB and thionine), see Scheme 1.1. While both

families contain planar aromatic moieties, DM and AM are more complex and comprise an additional sugar ring attached via a glycosidic bond. Crystallographic studies of the DM-DNA[159, 160] and AM-DNA[164] complexes revealed intercalation of the aglycone unit and binding of the sugar ring in the minor groove. Besides stabilisation by several van der Waals interactions, from the structural data it was possible to deduce that the aglycone unit of both compounds was stabilised by several direct and water-bridged hydrogen bonds. It was further confirmed that the sugar ring formed a stabilising hydrogen bond with the solvent, but also via a bridging water molecule to the DNA.[159, 160, 164] While not involved in specific interactions, a mechanistic binding study of DM and AM demonstrated a decreased stability of the intercalative binding mode upon removal of the sugar ring.[247] Corroborated by others,[248] evidence in the present study thus indicated that oxidised DM and AM generated a greater stabilisation of duplex DNA due to the additional sugar ring, which is missing in both MB and thionine.

4.3.3.2 Impact of reduced intercalators on duplex DNA

In contrast to the oxidised form of each intercalator, the corresponding chemically reduced form did not yield a significant increase in the T_M of DNA, as realised from Figure 4.8. Whereas no increase was induced by the presence of reduced MB or thionine, a small concentration dependent increase in T_M of DNA was observed in the presence of reduced DM and AM.

Based on this initial experiment it is not possible to give a detailed explanation for the observation concerning the slight increase in T_M by reduced DM and AM. However, it may be hypothesised that this concentration dependent behaviour in T_M of DNA, in the presence of reduced DM and AM, is a result of an increase in the total salt concentration upon addition of sodium borohydride. As verified in Figure 3.7, increasing salt concentration leads to an increased T_M of DNA. This hypothesis would furthermore correlate well with the absence of an increase in T_M of DNA in the presence of reduced MB and thionine, which are reduced with ascorbic acid. However, a control experiment investigating the effect of sodium borohydride, at increasing concentrations, on DNA stability did not reveal an obvious concentration

dependent upwards shift of T_M. As visualised in Figure 4.9B, the presence of sodium borohydride at the relevant concentrations affected T_M of DNA minimally. Thus, one may instead speculate that the chemical reduction of DM and AM via sodium borohydride may not have been 100 % efficient and therefore led to an increase T_M of DNA. For example, incomplete reduction was obvious in studies employing low concentrations of sodium borohydride with respect to the intercalator.[238] Interestingly, despite using a 1 000× excess of sodium borohydride for the reduction of DM analogues and AM, Cummings *et al.* still detected the presence of oxidised DM via HPLC analysis.[242]

Another possibility is that the reduced form of DM and AM is still interacting with duplex DNA. Recent molecular dynamics studies unravelled the detailed binding mechanism of DM to dsDNA. It was shown that the intercalation step was preceded by an outside bound step where the DM bound in the minor groove.[146, 249] Kinetic studies by Chaires and co-workers indicated that, prior to intercalation, DM formed a weak electrostatic interaction with DNA.[145] Substantiated by Wilhelm *et al.*, this was attributed to the interaction between the sugar ring and the DNA backbone.[146] The sugar ring bears an amine group that is positively charged at pH 7 (pK_a 8.6) and can electrostatically interact with the negatively charged backbone.[248] Moreover, previous melting curve studies demonstrated its importance in conferring stabilisation to the DM-DNA complex.[250] Thus, one may speculate that the minor groove interaction is conserved in both redox-states of DM and AM. This could in turn explain the observed slight increase T_M of DNA in the presence of the reduced form of respective intercalator. With the lack of further evidence, the explanation to the observation remains unclear. However, the experimental data in Figure 4.8 supported the conclusion that the reduced form of MB, thionine, DM and AM did not stabilise duplex DNA to the same extent as their respective oxidised forms.

4.3.3.3 Identification of the hit candidate

The results from the screening study were able to confirm that the two different redox-forms of each intercalator affected the stability of duplex DNA differently. This was expressed as a change in recorded T_M of 20mer dsDNA oligonucleotides.

Based on the calculated T_M values in Figure 4.8, it was evident that the largest difference in T_M between DNA in the presence of oxidised versus reduced intercalator was found for DM and AM. With ΔT_M reaching 9.8 ± 1.8 °C and 11.0 ± 1.3 °C, respectively, DM and AM were deemed as potential candidates for the electrochemical control of reversible DNA hybridisation.

As noticed, a slightly larger ΔT_M was observed with AM. Along the lines of previous thermodynamic studies comparing binding energetics of DM and AM with duplex DNA,[247] oxidised AM was able to induce duplex stabilisation to a higher degree than DM. While surprisingly not observed in some melting curve studies,[165] many drug-DNA binding studies confirmed a tighter binding of AM (1 kcal mol^{-1} more favourable binding free energy).[162, 246, 247, 251] Most scientists have attributed the observed difference to additional interactions between the solvent and the OH group at position C14 in AM, see Scheme 1.1.[164, 246] The thermodynamic binding profile of the two intercalators was established by Chaires and colleagues. These profiles revealed that binding of AM is accompanied by favourable enthalpy and entropy, whereas DM is accompanied by favourable enthalpy and unfavourable entropy.[157] Explaining the stronger binding of AM thermodynamically, Chaires *et al.* argued that the difference between AM and DM binding may be related to other contributions, such as solvent organisation, rather than interactions with the OH group at position C14.[252] Indeed, Yu *et al.* showed that there is an increased water uptake by AM upon binding, which was proposed as a reason for its greater binding affinity relative to DM.[251] However, as the difference in ΔT_M was marginal between DM and AM, DM was chosen as the hit candidate for electrochemical control of reversible DNA hybridisation. This decision was based on the fact that DM has successfully been used in several different biosensing applications,[26, 105] thus, making it an ideal candidate.

Interestingly, while the trend of increasing T_M of DNA in the presence of oxidised DM was observed, a significant discrepancy was found with the aforementioned increase recorded by Chaires and co-workers.[161] The authors, along with others,[250, 253] demonstrated an increase in T_M up to 30 °C at low base-pair to intercalator molar ratios. Thus, an important point to be considered in the interpretation of this data is

that the fluorescence of the fluorophore-labelled ssDNA was highly affected by the presence of the intercalators. Figure 4.9 confirmed that neither ascorbic acid nor sodium borohydride affected the T_M of the 20mer DNA fragment. However, Figure A.4 in Appendix D clearly illustrated the progressive quenching of TexasRed labelled ssDNA in the presence of increasing amounts of oxidised DM and AM. Nonetheless, it is important to underscore that the fluorescence of TexasRed was never completely quenched in any of the conditions investigated. This was easily realised from Figure A.5 in Appendix E showing the raw fluorescence-based melting curves for dsDNA in the presence of oxidised DM and AM. However, at the highest concentration of either intercalator, the fluorescence decreased as the denaturation proceeded. Thus, the results indicated that lower T_M values may have been recorded due to the sensitive fluorescence of TexasRed. Therefore, the observed quenching of fluorescence may serve as a plausible explanation to the observed discrepancy between the T_M values in the present study and the ones determined by, for example, Chaires and co-workers[161]. More importantly it confirmed that, while satisfactory for an initial evaluation, fluorescence-based melting curve analysis was not suitable for a detailed thermodynamic analysis of the binding and impact of DM on DNA.

4.3.4 Characterisation of the DNA and daunomycin interaction

Selecting DM as the candidate redox-active intercalator for the electrochemical control of reversible DNA hybridisation made it essential to characterise the binding and, more importantly, its impact on DNA in detail. A thermodynamic characterisation on the basis of van't Hoff analysis was carried out in three different conditions. These included 20mer dsDNA oligonucleotides at two salt concentrations, low (7.0 mM Na^+) and high (19.5 mM Na^+), and 40mer dsDNA oligonucleotides at the lower salt concentration (7.0 mM Na^+).

4.3.4.1 Evaluation of the binding of oxidised DM to DNA

Figure 4.10 shows the Scatchard plot of the binding data from the fluorescence-based titration, for all three conditions, fitted with the McGhee-von Hippel binding

isotherm in Eq. (1.9). A summary of the calculated binding parameters ($\Delta G°$, K_i, n) can be found in Table 4.2. With energetically favourable negative binding free energies reaching −9.7 kcal mol^{-1} and large intrinsic binding constants reaching 1.6 × 10^7 M^{-1}, oxidised DM displayed a significant binding affinity for dsDNA at all three conditions. Although, increasing the length of the dsDNA oligonucleotide (40mer) indicated a slightly weaker binding of DM. Likewise, a slight further decrease in the binding affinity of DM was observed upon increasing the salt concentration (19.5 mM Na^+). In contrast, the neighbour exclusion parameter stayed essentially constant at 2.7 ± 0.4 bp/drug. Owing to the use of different experimental conditions (such as source of DNA, salt concentration and temperature) and the broad range of binding models, it is difficult to compare exact binding parameters between the present and prior studies.[161, 246, 253-255] Remeta *et al.*, however, collated the results from several binding studies on the DM and DNA interaction, which revealed K_i values ranging from 10^5 to 10^7 M^{-1} in orders of magnitude and exclusion parameters ranging from 2.0 to 9.8.[256] Similar ranges were reported by Chaires and co-workers.[161]

To gain further understanding of the observed variation in the binding parameters of DM, systematic thermodynamic studies on the binding of DM to a series of synthetic co- and homopolymeric, as well as native, dsDNA were undertaken by others.[246, 254] Spectroscopic and calorimetric measurements, analysed with the neighbour exclusion binding model, demonstrated a variation of the binding constant and free energy with the base sequence of DNA.[255, 256] Remeta *et al.* inferred that this behaviour may occur due to the slight G·C preference exhibited by DM.[254] DNA footprinting studies by Chaires *et al.* showed that, whereas DM will intercalate into other sequences as well, the triplet sequence of two adjacent G·C base-pairs flanked by one A·T base-pair is geometrically the most favourable binding site.[162] Thus, it may be suggested that the slightly weaker binding of DM to 40mer dsDNA, at the lower salt concentration (7.0 mM Na^+), may have ensued as a result of a difference in base sequence leading to fewer favourable binding sites.

The observed salt dependency of the binding affinity of DM has likewise been described in several binding studies.[161, 248, 250, 257] For example, a dedicated study

regarding this phenomenon was conducted by Chaires employing fluorescence- and absorbance-based methods to investigate the binding of DM to calf thymus DNA. Using the neighbour exclusion model, the author reported a change in the intrinsic binding constant from 4.9×10^6 M^{-1} to 1.5×10^5 M^{-1} when increasing the sodium ion concentration from 0.05 M to 1.0 M.[257] The author further provided an interpretation of the observation within the context of the counterion condensation theory.[38, 39, 257] Due to the protonated amine group on the sugar ring at pH 7, DM is positively charged and is hence accompanied by a net release of condensed counterions upon binding to DNA. This leads to an increase in entropy.[157, 257] However, at higher salt concentrations, binding of DM will yield less gain in entropy, according to Eq. (3.3).[1, 257] Thus as discussed in Section 3.3.3, given the thermodynamic relationship $\Delta G° = \Delta H° - T\Delta S°$, it is clear that a smaller entropy gain will result in a less favourable binding free energy. This would accordingly reflect a smaller intrinsic binding constant and a weaker binding, which is observed in the present study. Furthermore, the same study by Chaires[257] showed that the binding affinity of DM decreased with temperature, while Lin *et al.*[248] showed the similar behaviour by increasing the pH.

The neighbour exclusion parameter determined for DM, across the three different conditions, correlated well with crystallographic studies on the DM–DNA complex which revealed one bound DM per three base-pair.[159, 160] As mentioned above, the aglycone unit intercalates between the base-pairs while the sugar ring extends into the minor groove. Quigley *et al.* showed that intercalation of DM resulted in complex steric distortion of the binding site in terms of unwinding and lengthening of the double helix.[159] While potentially affecting nearby binding sites, the partial blockage of a third base-pair by the sugar ring was deemed as the cause of the three base-pair exclusion parameter.[159, 161]

The screening study (Figure 4.8) made it possible to identify DM as the hit candidate for electrochemical control of reversible DNA hybridisation. Based on the determined neighbour exclusion parameter of 2.7 ± 0.4 bp/drug for oxidised DM, it was possible to identify the most suitable base-pair to intercalator molar ratio. Despite the fact that the screening study showed the largest difference in stability

(ΔT_M) between oxidised and reduced DM for the molar ratio 1:2 (intercalator in excess), molar ratio 2:1 (base-pair in excess) was deemed as the most suitable one. At this ratio the majority of DM was expected to be intercalated, thus, any effects seen on DNA in future experiments could be assigned to intercalated DM. Furthermore, the intercalative binding mode at this ratio was clearly visible spectrophotometrically (bathochromic and hypochromic shift, see Figure 4.4), which was of importance in the subsequent studies of the electrochemical control of reversible DNA hybridisation.

4.3.4.2 Impact of oxidised and reduced DM on T_M of DNA

To gain further insight into the behaviour of the impact of DM on DNA stability, absorbance-based melting curve analysis was carried out at three different conditions. Melting curves for 20mer dsDNA oligonucleotides, in the presence of oxidised and chemically reduced DM at the molar ratio of 2:1, in the lower salt concentration (7.0 mM Na^+) can be visualised in Figure 4.11A. Figure A.6 in Appendix F depicts the corresponding melting curves for 40mer and 20mer dsDNA oligonucleotides at low (7.0 mM Na^+) and high (19.5 mM Na^+) salt concentration, respectively. A summary of the accompanying hypochromic shifts and calculated T_M values can be found in Table 4.3 and Figure 4.11B, respectively. In accordance with the findings from the Chaires *et al.*[161] and others,[250, 253] T_M of DNA increased substantially in the presence of oxidised DM indicating considerable stabilisation of duplex DNA. In contrast, reduced DM only caused a slight increase in the T_M. Evidently, this resulted in a significant difference in T_M between DNA in the presence of oxidised and reduced DM for all tested conditions. The trend of these findings did not correspond with the observations from the fluorescence-based melting curve study in this work (Section 4.2.3). While both studies showed that oxidised DM confers stabilisation of duplex DNA and reduced DM does not, this was only apparent at a molar ratio 1:2 (DM in excess) in the fluorescence-based melting curve study. Considering the excellent correlation between the observed increase in T_M of DNA with oxidised DM using absorbance-based melting curve analysis and previously reported values,[161] the discussion in Section 4.3.3.3 on the discrepancy between the fluorescence-based data and the literature was validated.

Indeed, with the findings from the absorbance-based melting curve analysis, it clearly confirmed that the quenching of the fluorophore in the fluorescence-based melting curve study affected the outcome of the experiment to a certain degree. While the trend was still apparent, exact T_M values were either over or underestimated.

4.3.4.3 Thermodynamic characterisation of the impact of oxidised and reduced DM on the stability of DNA

Evaluation of T_M of DNA using absorbance provided yet another indication that the different redox-states of DM affected the stability of DNA differently. However, it was essential to thermodynamically characterise and quantify the observed difference in DNA stability. The majority of the existing literature on DM binding to DNA has focused on the characterisation of the thermodynamic profile of the drug-binding action. However, it is important to reiterate that the focus of the present study lies within understanding the effect of the intercalator on the thermodynamics of DNA. Hence, the thermodynamic parameters of DNA, for all three investigated conditions, were calculated on the basis of van't Hoff analysis to provide an in depth understanding of the effects on DNA caused by DM. Figure 4.13 summarises the calculated enthalpies and entropies, while Table 4.4 provides an overview of the free energies and association constants of the renaturation of DNA in absence and presence of DM, at three investigated conditions.

The experimentally determined thermodynamic parameters for 20mer dsDNA alone corresponded well with the predicted values using IDT Biophysics' DNA thermodynamics & hybridisation calculator,[195] see Table A.1 in Appendix G. Furthermore, similar enthalpy, entropy and free energy values to 20mer dsDNA in the presence of oxidised DM were observed by Belozerova and Levicky[258] for the renaturation of short DNA strands in the presence of the minor groove binder netropsin at > 150 mM Na^+. However, discrepancies between experimental and predicted data were found for the 40mer dsDNA alone. A significant underestimation of the experimental values indicated that the reversible hybridisation of 40mer dsDNA may not have followed two-state melting. For the

validity of the van't Hoff analysis, the reversible hybridisation of DNA must be assumed to proceed in an all-or-none manner.[35, 167] However, this assumption is generally only valid for oligonucleotides shorter than 20 bp, as shown by Owczarzy and colleagues.[55] Thus, for true evaluation of the thermodynamics of the 40mer dsDNA, a model-independent method such as calorimetry is required for analysis.[36]

Nevertheless, it was evident from the thermodynamic data of 20mer dsDNA that the two redox-states of DM bound and affected the stability of the double helix differently. As expected for oligonucleotides,[259] a favourable $\Delta G°$ term was observed for duplex formation in the absence of DM. This value was the combination of a favourable enthalpy compensated by an unfavourable entropy. The favourable enthalpy of duplex formation is related to the formation of hydrogen bonds and base stacking, while the unfavourable entropy arises from ordering of the system and uptake of sodium ions and water.[259] Likewise, a similar $\Delta G°$ term was observed for DNA in the presence of reduced DM with a similar enthalpy-entropy compensation. Compared to reduced DM, duplex formation in the presence of oxidised DM exhibited a more favourable $\Delta G°$ term reflecting a more stabilised double helix. Moreover, as realised from Figure 4.13, a less favourable enthalpy contribution was compensated with a more favourable entropy. According to theory, the binding of a ligand involves an entropy gain due to release of water molecules and ions bound to the surface of the DNA. The unfavourable enthalpy, however, arises from disruption of hydrogen bonds between DNA and water molecules or other solvents.[143] While the release of condensed counterions upon ligand binding has been predicted theoretically,[39] studies related to the hydration changes in DNA upon intercalation showed that binding of oxidised DM is in fact accompanied by a net uptake of water molecules.[144, 251, 260] In contradiction to the assumption, the results from the hydration studies clearly indicated that the binding of DM to DNA is very complex involving other factors as well.[143]

Albeit complex binding, with different $\Delta G°$ values and enthalpy-entropy compensations, results undoubtedly indicated that the binding of the two redox-states of DM to dsDNA was different. The evidence was further reflected in the association constant of DNA. When evaluated at the selected working temperature

for respective condition (see Table 4.3), oxidised DM was found to dramatically increase the observed K_a by several orders of magnitude compared to the reduced form. Conversely, in the presence of reduced DM, K_a remained significantly small. The findings in the present study thus confirmed that, at the selected working temperature, oxidised DM facilitated the hybridised state of DNA, while the reduced form promoted the denatured state.

Although, minor differences between the three conditions were visible. As predicted by theory,[38, 39] increasing the salt concentration resulted in a slightly higher T_M and more favourable $\Delta G°$, while increasing the length of the DNA resulted in a further stabilisation. A detailed discussion on these effects, within the context of the counterion condensation theory,[38, 39] can be found in Section 3.3.3. Despite minor differences, DNA indisputably responded in the same manner to oxidised and reduced DM throughout all investigated conditions. Thus, it may be concluded that the observed impact of the redox-state of DM, on the stability of DNA, is not conserved to a certain condition. The differential impact remains although the length of the DNA or the salt concentration increases. Thus, in depth thermodynamic profiling of the impact on DNA at different conditions confirmed the hypothesis of this Thesis. Results clearly indicated that, at the selected working temperature, DM bound differently to dsDNA depending on its redox-state. Accordingly, the stability of dsDNA was affected which was expressed as an altered association constant. In light of current findings, it was furthermore confirmed that DM indeed was a suitable candidate for the electrochemical control of reversible DNA hybridisation.

4.4 Summary

In this Chapter, the intercalative binding mode and chemical reduction was confirmed for a range of intercalators. A subsequent screening study, to explore the initial impact of oxidised and chemically reduced intercalator on DNA, identified DM as a potential hit candidate for the electrochemical control of reversible DNA hybridisation. Absorbance-based melting curve analysis was conducted to validate

DM as a hit candidate. It was concluded that oxidised DM confers substantial stabilisation of duplex DNA while reduced DM does not. Further characterisation of the binding of oxidised DM confirmed a strong interaction with dsDNA. On the basis of van't Hoff analysis, these results were substantiated by a detailed thermodynamic characterisation of the impact of oxidised versus reduced DM on DNA. Relative to DNA in the presence of reduced DM, DNA in presence of oxidised DM exhibited a significantly more favourable free energy of duplex formation with an accompanying difference in the enthalpy-entropy compensation. Examined at three different conditions, the response of the DNA to oxidised and reduced DM remained the same throughout all conditions. Thus, in depth thermodynamic profiling of the impact on DNA at different conditions confirmed the hypothesis of this Thesis that DM binds differently to dsDNA depending on its redox-state. The hypothesis was furthermore confirmed as the affected stability of dsDNA was expressed as an altered association constant. Thus, with current findings, it was concluded that DM was the optimal candidate for electrochemical control of reversible DNA hybridisation in subsequent studies. Additionally, the working temperature and heat denaturation for each investigated condition, to be employed in subsequent experiments, were determined.

Chapter 5
Electrochemical Control of Reversible DNA Hybridisation using DNA Intercalators

5.1 Introduction

Owing to characteristics such as increased sensitivity, simpler operations, easy miniaturisation, fast response and low cost, electrochemical-based biosensors offer an excellent opportunity for integration into μTAS, thus, also for the development of POCT platforms.[26, 72, 80] Whereas electrochemical-based biosensors can detect a variety of analytes, much of the focus has been given towards the detection of DNA and, in particular, PCR product.[72, 103, 105, 261] However, in order to make electrochemical-based sensing strategies of DNA more efficient and compatible with portable diagnostic platforms, it is desirable to monitor the DNA amplification method in real-time. In recent years, electrochemistry-based real-time monitoring strategies of DNA amplification have been developed of which many make use of electroactive DNA intercalators for detection.[112-115, 261] However, many of the published technologies thus far rely on the thermal amplification of DNA, such as for example PCR, and consequently are dependent on cycling elevated temperatures

to control strand separation and hybridisation in order to drive the amplification. Meanwhile, issues regarding incorporation of temperature-dependent amplification strategies into miniaturised bioanalytical systems have been well-documented.[84] Therefore, based on the findings in Chapter 4, developing an electrochemical alternative to thermal control of DNA denaturation and renaturation on the basis of electroactive intercalators has significant merit.

This Chapter aims to characterise the electrochemical behaviour of the selected intercalator DM. It further aims to provide an initial understanding of the impact of electrochemical redox conversion on its stability. Serving as the basis for selection of electrochemical conditions to be employed in the presence of DNA, the main focus of this Chapter lies within providing a proof-of-principle of the electrochemically controlled reversible DNA hybridisation by redox-state switching of DM.[9]

The electrochemical behaviour of DM was characterised by means of cyclic voltammetry in the presence and absence of DNA. Allowing the identification of a suitable reduction and oxidation potential which enabled the complete redox conversion of the intercalator, spectroscopic confirmation was additionally acquired using *in situ* UV–vis spectroelectrochemistry. Next, structural studies employing NMR provided an initial elucidation of the stability of DM upon electrochemical redox conversion. As the electroactivity of DM was established, cycles of electrochemically controlled DNA denaturation and renaturation were examined by means of *in situ* UV–vis spectroelectrochemistry. Different lengths of DNA at different salt concentrations were explored at the working temperatures defined in Chapter 4. Upon deducing the most suitable wavelength to monitor denaturation/renaturation of DNA employing CD-based end-point melting curve analysis, *in situ* CD spectroelectrochemistry permitted validation of electrochemically controlled reversible DNA hybridisation as a second independent technique. Gel electrophoresis was finally used to evaluate the potential degradation of DNA after the redox cycling.

[9] Main results from this Chapter were published in Syed, S.N. et al. *J. Am. Chem. Soc.* **135**, 5399–5407 (2013).[3]

5.2 Results

All (spectro)electrochemical experiments were performed in a quartz cuvette (path length 0.5 mm) with a three-electrode setup (Pt gauze working electrode, Pt wire counter electrode, Ag/AgCl single fritted reference electrode). Figure 5.1 depicts the cyclic voltammogram of a clean Pt gauze working electrode.

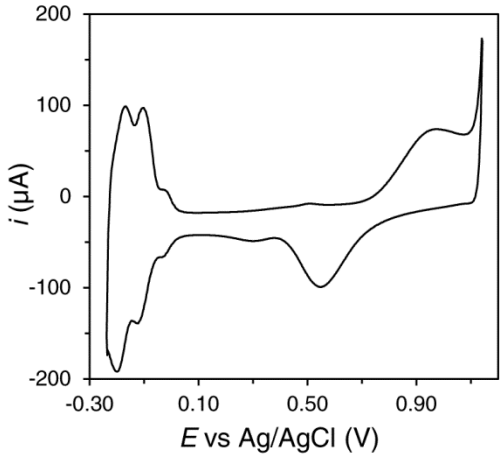

Figure 5.1 CV of the Pt gauze electrode in 0.1 M H_2SO_4. The electrode was cleaned by scanning the potential range −0.2 to 1.14 V at a scan rate of 50 mV s^{-1}.

Characteristic peaks for the formation of an oxide film, and its reduction, were found at > 0.90 V and 0.55 V, respectively. Hydrogen adsorption and oxidation peaks were found at < 0 V. A full description of the electrode cleaning procedure can be found in Section 2.2.1.2.

5.2.1 Electrochemical characterisation of daunomycin

5.2.1.1 Characterisation using cyclic voltammetry

The redox-properties of DM in SSC buffer were primarily characterised by means of cyclic voltammetry. Details on the experimental procedure and data extraction can be found in Section 2.2.9. Figure 5.2 shows a typical voltammogram of DM in the absence and presence of complementary 20mer DNA oligonucleotides in SSC buffer (7.0 mM Na^+), at a base-pair to intercalator ratio 2:1, recorded at scan rate of 10 mV s^{-1}.

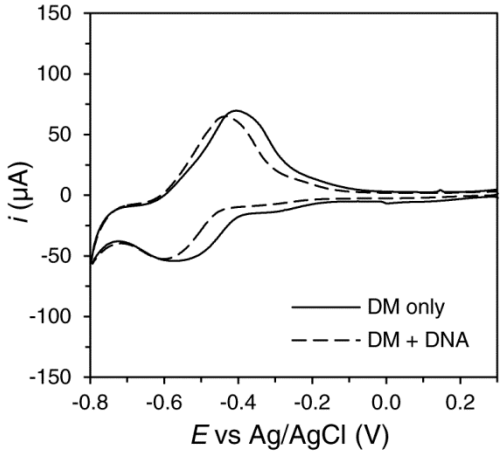

Figure 5.2 CV of DM in the absence and presence of DNA. (B) 100 μM DM in the absence and presence of 200 μM 20mer dsDNA (bp concentration) in SSC buffer (7.0 mM Na^+), pH 7, at 25 °C (molar ratio 2:1). The voltammogram shows the 5th scan and was collected at a scan rate of 10 mV s^{-1}. One redox couple was observed at E_{pa} = −0.41 V and E_{pc} = −0.57 V. The redox peak potentials shifted slightly negative in the presence of DNA.

One set of well-defined redox peaks were identified, where the oxidation and reduction peak potential were E_{pa} = −0.41 V and E_{pc} = −0.57 V, respectively, for DM. The peak potential separation of E_{pa} and E_{pc} was determined to ΔE_p = 168 mV. In the presence of DNA, both redox peaks for DM shifted towards more negative potentials. The new oxidation and reduction peak potentials appeared at E_{pa} = −0.44 V and E_{pc} = −0.60 V. A slightly smaller peak potential separation of ΔE_p = 164 mV was obtained. Additionally, a small decrease in the peak current was observed.

The redox activity of DM was further examined at various scan rates. Figure 5.3A and B depicts the redox activity of DM in the absence and presence of 20mer dsDNA in SSC buffer (7.0 mM Na^+) at scan rates between 1 and 30 mV s^{-1}. As can be visualised in both graphs, the peak potentials were affected by the scan rate. For DM, the oxidation peak potential shifted positively from E_{pa} = −0.46 V to E_{pa} = −0.37 V, while the reduction peak potential shifted negatively from E_{pc} = −0.49 V to E_{pc} = −0.60 V as the scan rate increased. Likewise, in the presence of DNA, with an increasing scan rate, the oxidation peak potential shifted positively

from E_{pa} = −0.49 V to E_{pa} = −0.44 V, while the reduction peak potential shifted negatively from E_{pc} = −0.55 V to E_{pc} = −0.63 V.

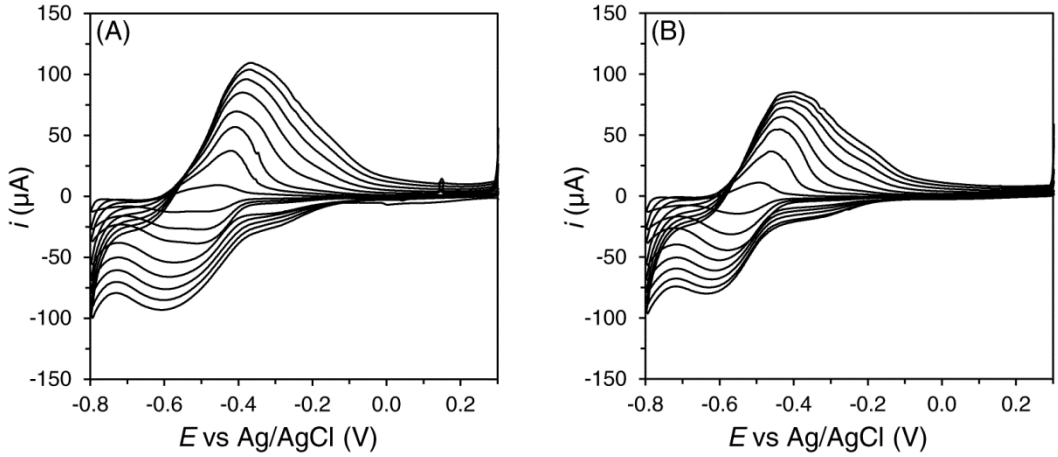

Figure 5.3 CV of DM in the absence and presence of DNA at different scan rates. 100 μM DM in the (A) absence and (B) presence of 200 μM 20mer dsDNA (bp concentration) in SSC buffer (7.0 mM Na^+), pH 7, at 25 °C (molar ratio 2:1). The redox activity was examined at scan rates 1, 3, 5, 10, 15, 20, 25 and 30 mV s^{-1}. Both E_{pa} and E_{pc} of DM were found to be dependent on the scan rate, regardless of the presence of DNA.

The peak potential separation ΔE_p as a function of the scan rate v is quantified in Figure 5.4A. An increasing ΔE_p with an increasing scan rate was clearly observed, thus, indicating a semi-reversible redox couple. Although, it is worth noting that the peak potential separation quickly plateaued at ΔE_p = 204 ± 27 mV and ΔE_p = 185 ± 14 mV for DM in the absence and presence of DNA, respectively, at scan rates above 5 mV s^{-1}. Figure 5.4B, on the other hand, compares the ratio of all peak currents $|i_c/i_a|$ as a function of the scan rate v. Expect at 1 mV s^{-1}, which displayed a ratio close to unity for DM in absence of DNA and unity in the presence of DNA, a slow increase in the ratio towards unity was observed for the remaining scan rates indicating a complicated redox reaction. Furthermore, a larger deviation from unity was observed for DM in the absence of DNA.

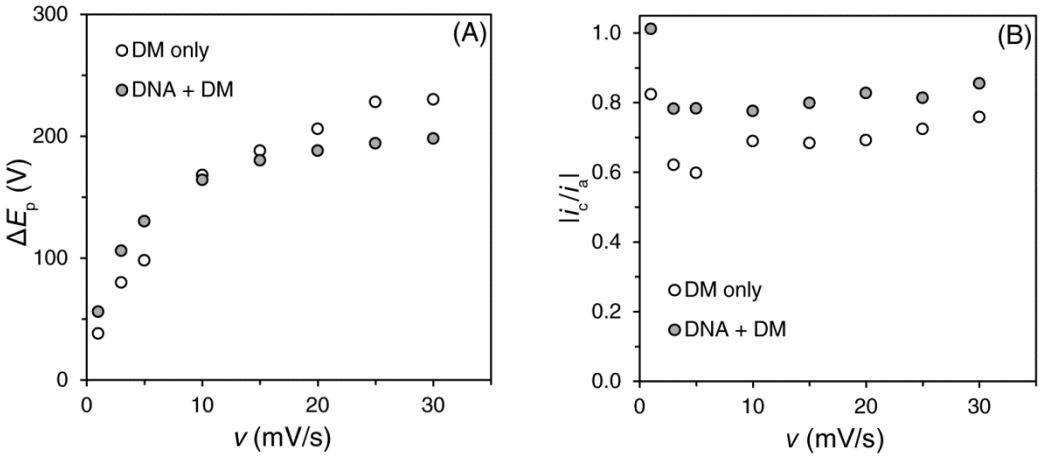

Figure 5.4 Reversibility test of DM in the absence and presence of DNA. (A) The peak potential separation increased with an increasing scan rate for 100 μM DM in the absence and presence of 200 μM 20mer dsDNA (bp concentration) in SSC buffer (7.0 mM Na^+), pH 7 at 25 °C (molar ratio 2:1). (B) An increase in the peak current ratio with the scan rate was likewise observed.

5.2.1.2 Characterisation using in situ UV–vis spectroelectrochemistry

Based on the cyclic voltammetry investigation, −0.8 V and +0.3 V were selected as the reduction and oxidation potential to ensure complete reduction and oxidation upon switching the redox-state of DM in the absence and presence of DNA. The time required for complete electrolysis was first estimated using Eq. (1.21). This estimation was based on measurements of the Pt gauze working electrode found in Section 2.1.5 and the pathlength of the quartz cuvette used (0.5 mm). The thickness of the Pt gauze working electrode was 100 μm. Hence, based on the fact that the electrode resided in the middle of the cell, the distance from the electrode surface to the cell wall was estimated to δ_{wall} = 0.2 mm. However, before a uniform planar diffusion occurs from the gauze electrode towards the cell wall, diffusion occurs first within the grid of the electrode itself as explained in Section 1.6. The distance between two Pt wires within the grid was δ_{grid} = 150 μm. Thus, Eq. (1.21) becomes

$$\tau = \frac{{\delta_{\text{grid}}}^2 + {\delta_{\text{wall}}}^2}{D} \tag{5.1}$$

Using a diffusion coefficient from the literature (8.77×10^{-6} cm^2 s^{-1}),[229] a total electrolysis time of ~70 s was estimated.

Complete reduction and oxidation of DM was confirmed by means of *in situ* UV–vis spectroelectrochemistry and the full experimental procedure can be found in Section 2.2.10. Figure 5.5A shows typical absorption changes of DM in SSC buffer (7.0 mM Na^+) upon cycling −0.8 V and +0.3 V five times at the working temperature 58 °C (as determined in Chapter 4, see Table 4.3). The simultaneously monitored current transients are shown in Figure 5.5B.

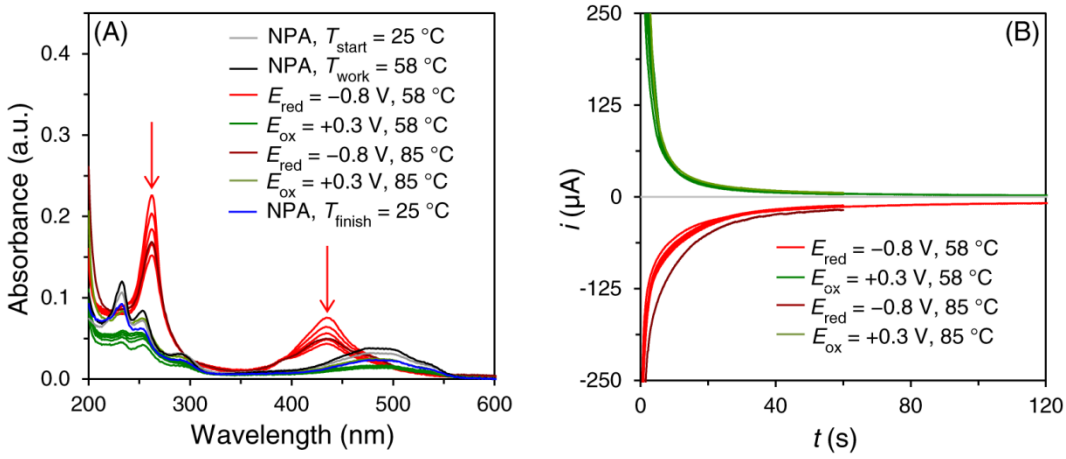

Figure 5.5 *In situ* UV–vis spectroelectrochemical characterisation of DM. (A) Absorption spectra of 100 µM DM in SSC buffer (7.0 mM Na^+), pH 7. Repeated switching of the DM redox-state was observed upon applying the selected redox potentials (−0.8 V/+0.3 V) five times at 58 °C. (NPA = no potential applied). (B) Recorded current transients upon the successive application of the redox potentials in (A). The electrolysis was complete within 120 s for the first reduction/oxidation cycle and within 60 s for the remaining four cycles.

The first reduction/oxidation potential was applied for 120 s. The anodic current decreased to zero as $t \rightarrow \infty$, which indicated the complete oxidation of DM. The cathodic current transient however did not reach zero at $t \rightarrow \infty$, thus, suggesting a background current. Due to the applied reduction potential (−0.8 V), the background current most likely arose from reduction of dissolved oxygen, thus, results suggested the complete reduction of DM. The remaining rounds of reduction/oxidation potentials were applied for 60 s each. Similar to the first

reduction/oxidation cycle, the current decreased to zero at $t \rightarrow \infty$ indicating that the complete oxidation and reduction of DM occurred already within 60 s. The absorption spectra in Figure 5.5A were recorded after complete electrolysis. Initial and finishing spectra recorded at T_{start}, T_{work} and T_{finish}, when no potential was applied, exhibited peaks at 233, 253 and 480 nm for oxidised DM. Upon application of the selected reduction potential (−0.8 V) at T_{work}, new peaks appeared at 262 and 435 nm for reduced DM. A continues decrease in the absorbance for reduced DM was observed upon subsequent reductions. However, at the heat denaturation temperature T_{heat} = 85 °C, the absorbance increased slightly again. Upon application of the selected re-oxidation potential (+0.3 V) at T_{work}, characteristic peaks for oxidised DM re-appeared. Although constant, the peaks for re-oxidised DM were less pronounced. Furthermore, the third peak at 480 nm exhibited a slight shift to 500 nm, which was not observed at T_{heat} = 85 °C.

5.2.1.3 Investigation of the stability of daunomycin using NMR

Owing to the observed continuous decrease in absorbance for reduced DM during the successive reductions at −0.8 V in Figure 5.5, the stability of the intercalator was investigated using NMR. 1D proton NMR spectra and 2D COSY spectra were recorded before and after redox cycling as carried out in Figure 5.5. While 1D NMR spectra plots the signal intensity of each interrogated nucleus vs. the chemical shift, 2D COSY spectra identifies the spin-spin couplings of nuclei separated over 2–3 chemical bonds. Thus, the spectra show the chemical shifts for each nucleus on both axes. Whereas signals with the same chemical shift appear on the diagonal of the plot, signals with different chemical shifts but are spin-coupled appear as cross peaks off the diagonal.

To increase the sensitivity of the NMR spectra, 300 µM DM in deuterated SSC buffer (7.0 mM Na^+) was utilised for the redox cycling at 58 °C. Furthermore, to avoid risk of contamination after sample recovery from the cuvette, mineral oil was omitted as one of the measures against evaporation. More details on the experimental procedure are found in Section 2.2.12. The protons of DM before redox cycling (Scheme 1.1) were assigned on the basis of available literature[262, 263] and the 2D

COSY spectrum (before redox cycling) in Figure 5.7. Figure 5.6 compares the proton NMR spectrum (800 MHz) of DM before and after redox cycling, while the specific chemical shifts are found summarised in Table 5.1. As observed, the signals for the protons of DM after redox cycling were clearly visible and overlapped well with the signals assigned for various protons of DM before redox cycling (insignificant shifts of ≤ 0.09 ppm). Although, a slight decrease in signal intensity was observed. Correspondingly, an excellent correlation was seen between the cross peaks of the spin-spin coupled protons of DM before and after redox cycling in the COSY spectrum in Figure 5.7.

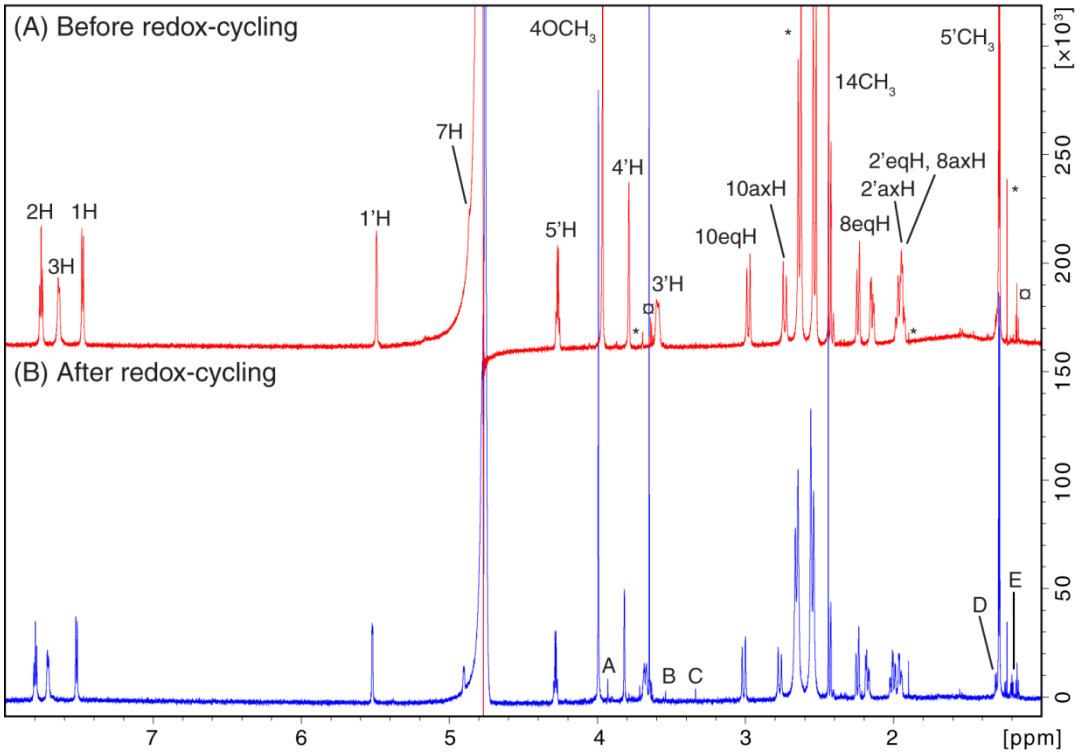

Figure 5.6 800 MHz proton NMR spectrum of DM before and after redox cycling. 300 µM DM in deuterated SSC buffer (7.0 mM Na^+), pH 7, was subjected to five cycles of reduction (−0.8 V) and oxidation (+0.3 V) at 58 °C. Upon recovery, a proton NMR spectrum was recorded of DM before and after redox cycling at 25 °C. Nearly identical chemical shifts were observed in both spectra indicating that DM remained intact after redox cycling. However, five new signals (A–E) appeared after the redox cycling of DM. Signals corresponding to the SSC buffer are marked (*). The sample furthermore showed a slight ethanol (¤) contamination from the cleaning procedures.

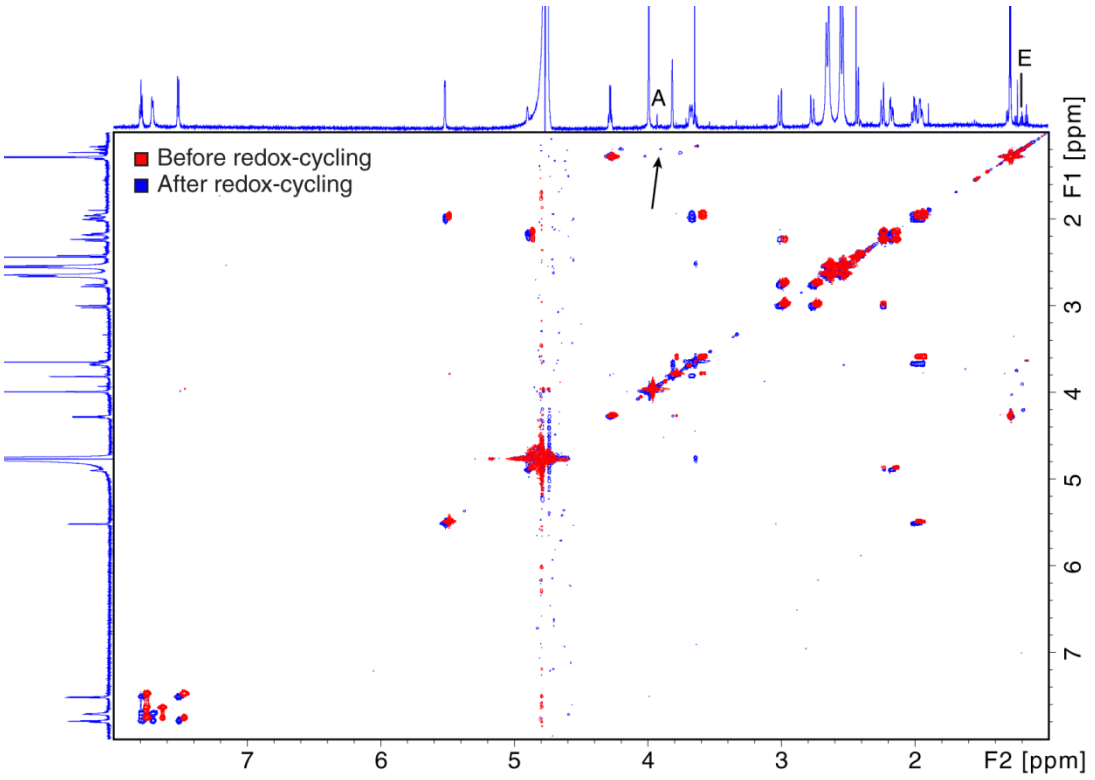

Figure 5.7 800 MHz 2D COSY spectrum of DM before and after redox cycling. 300 μM DM in deuterated SSC buffer (7.0 mM Na^+), pH 7, before and after redox cycling at 58 °C. The COSY spectrum was recorded at 25 °C. The topographical map for DM before and after redox cycling were used to assign the protons of DM. Additionally, a cross peak between the new signals A and E, found after redox cycling of DM, was observed indicating that signal E was related to the buffer.

However, upon further inspection of Figure 5.6B five new signals (marked A–E) were identified and their chemical shifts can be found summarised in Table 5.2. As a control, a proton NMR spectrum was recorded of SSC buffer (7.0 mM Na^+, 10 % v/v D_2O) alone before and after redox cycling, see Figure 5.8A and B. In correlation to the new signals observed for DM after redox cycling, four new signals (marked A*–D*) were identified for SSC buffer after redox cycling. The corresponding chemical shifts are likewise found in Table 5.2. Thus, overlapping chemical shifts suggested that the new signals A–D, observed for DM after redox cycling, could most likely be attributed to the SSC buffer after redox cycling. Upon further inspection of the COSY spectrum of DM after redox cycling in Figure 5.7, a weak intensity cross peak between A and E was revealed. This suggested that the new signal E for DM after

redox cycling could likewise be attributed to the SSC buffer after redox cycling. Consequently, results indicated that DM remained intact after redox cycling.

Table 5.1 Chemical shifts (δ) of protons in DM before and after redox cycling.†

Proton	δ_{before} (ppm)	δ_{after} (ppm)	$\Delta\delta$ (ppm)
1H	7.47	7.52	0.05
2H	7.75	7.79	0.04
3H	7.63	7.71	0.08
4OCH3	3.96	3.99	0.03
7H	4.86	4.90	0.04
8axH	1.95	1.99	0.04
8eqH	2.19	2.21	0.02
14OCH3	2.44	2.44	0
10axH	2.73	2.77	0.04
10eqH	2.98	3.01	0.03
1′H	5.49	5.52	0.03
2′axH	1.95	1.99	0.04
2′eqH	1.95	1.99	0.04
3′H	3.59	3.68	0.09
4′H	3.79	3.82	0.03
5′H	4.27	4.28	0.01
5′CH3	1.28	1.28	0

† Spectra were acquired in deuterated SSC buffer (7.0 mM Na^+) and at 25 °C.

Table 5.2 New signals for DM and SSC buffer after redox cycling.

Signal in DM/SSC buffer	δ_{DM} (ppm)	$\delta_{SSC\ buffer}$ (ppm)
A/A*	3.93	3.91
B/B*	3.54	3.49
C/C*	3.34	3.34
D/D*	1.31	1.30
E	1.20	–†

† Cross-peak (A-E*) observed in the COSY spectrum.

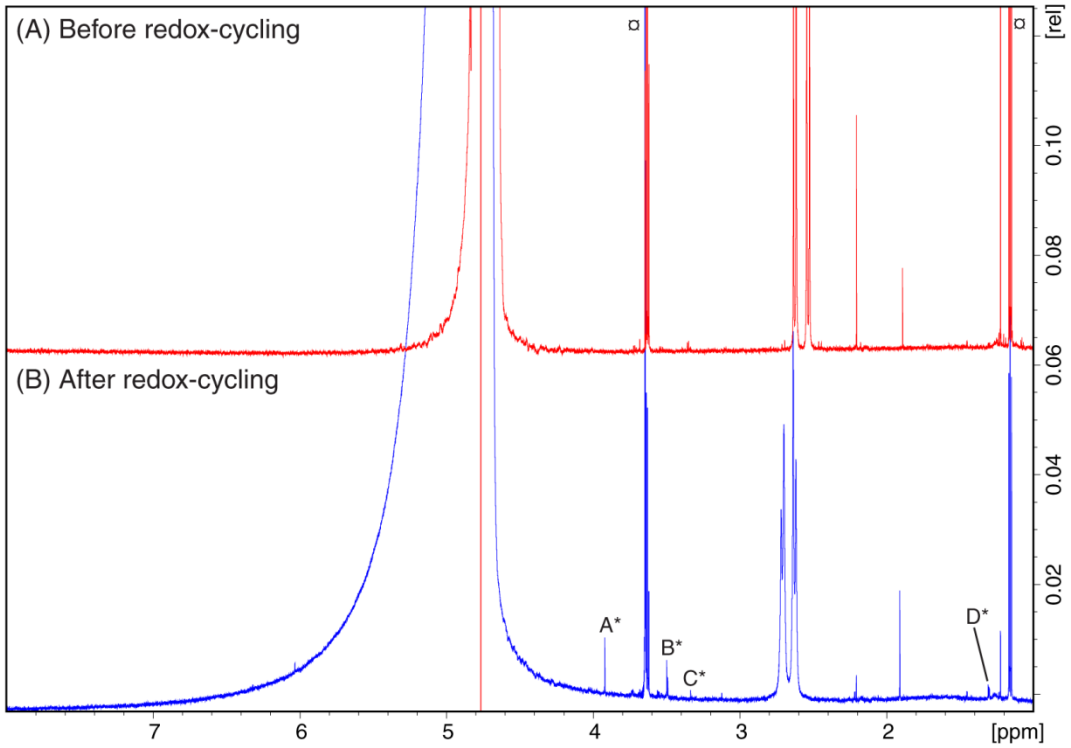

Figure 5.8 800 MHz proton NMR spectrum of SSC buffer before and after redox cycling. A proton NMR spectrum was recorded of SSC buffer (7.0 mM Na^+, 10 % v/v D_2O), pH 7, before and after five cycles of reduction (−0.8 V) and oxidation (+0.3 V) at 58 °C. Four new signals (A*–D*) appeared after the redox cycling of the buffer. Signals marked (¤) indicated an ethanol contamination from the cleaning procedures.

5.2.2 Electrochemical cycling of DNA denaturation and renaturation with daunomycin using *in situ* UV–vis spectroelectrochemistry

Figure 5.9 shows typical *in situ* UV–vis spectroelectrochemical absorption spectra of complementary 20mer DNA oligonucleotides in the presence of the electrochemical cycling of the DM redox-state. Spectra were recorded in SSC buffer (7.0 mM Na^+) at a base-pair to intercalator molar ratio 2:1, with a working temperature of 58 °C (according to Table 4.3). An in depth description of the experimental procedure and data analysis can be found in Section 2.2.10. The initial and finishing absorption spectra, recorded at T_{start}, T_{work} and T_{finish} when no potential was applied, displayed a peak at 260 nm for hybridised DNA and at 500 nm for intercalated oxidised DM. Upon application of the selected reduction potential −0.8 V at T_{work}, a characteristic peak appeared at 435 nm indicating the reduction of DM. Accompanying this peak

was a dramatic hyperchromic shift at 260 nm suggesting denaturation of duplex DNA. Upon application of the selected re-oxidation potential +0.3 V at T_{work}, the hyperchromic shift reversed exhibiting a significant decrease in the absorption at 260 nm, thus, suggesting hybridisation of duplex DNA. Furthermore, the peak for oxidised DM re-appeared at 500 nm.

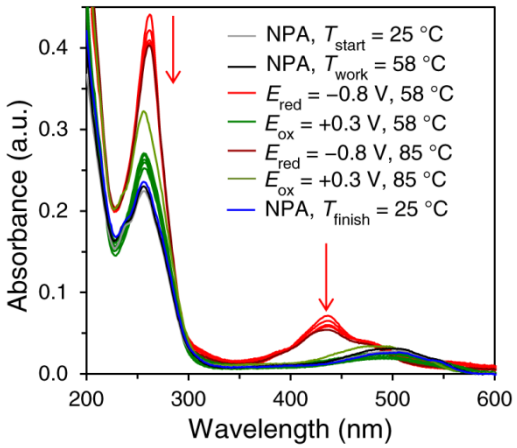

Figure 5.9 Electrochemical control of reversible DNA hybridisation by redox-state switching of DM. Absorption spectra of 200 µM 20mer dsDNA (bp concentration) in the presence of 100 µM DM in SSC buffer (7.0 mM Na^+), pH 7, at T_{work} = 58 °C (molar ratio 2:1). Using *in situ* UV–vis spectroelectrochemistry cyclic denaturation and renaturation of dsDNA was demonstrated. Upon reducing DM at −0.8 V, a significant increase in absorbance at 260 nm was observed indicating denaturation. Switching the potential to +0.3 V re-oxidised DM which resulted in a decrease in absorbance at 260 nm, suggesting hybridisation. (NPA = no potential applied).

As a control, the sample was heated to the heat denaturation temperature T_{heat} = 85 °C (according to Table 4.3) at the end of the experiment. As established by the absorbance-based melting curve experiments (Figure 4.11A), at this temperature the 20mer dsDNA was in a denatured state irrespective of the redox-state of DM. Upon applying −0.8 V at T_{heat} = 85 °C, reduction of DM was achieved alongside with a hyperchromic shift at 260 nm for DNA. This shift corresponded to the hyperchromic shift observed at 260 nm during the reduction of DM at T_{work} = 58 °C. Therefore, results verified that denaturation events of the 20mer dsDNA took place at the working temperature upon reduction of DM. Switching the potential to +0.3 V

at T_{heat} = 85 °C, the absorption at 260 nm for DNA decreased, however, evidently remained higher than during the re-oxidation of DM at T_{work} = 58 °C. Furthermore, the peak for re-oxidised DM appeared blue-shifted at 480 nm with an increased absorbance. As realised from the intercalation study in Figure 4.4, this characteristic behaviour indicated unbound DM. Accordingly, this confirmed re-hybridisation of the 20mer dsDNA at the working temperature upon re-oxidation of DM.

As a further control, the entire experiment was conducted at T_{work} = 25 °C. Realised from the absorbance-based melting curve experiments (Figure 4.11A), at this temperature the 20mer dsDNA was shown to be hybridised irrespective of the DM redox-state. Inspection of Figure 5.10A revealed that, upon applying −0.8 V, a highly unstable peak appeared at 435 nm for the reduction of DM. Likewise, a significantly smaller and less stable hyperchromic shift at 260 nm was obtained.

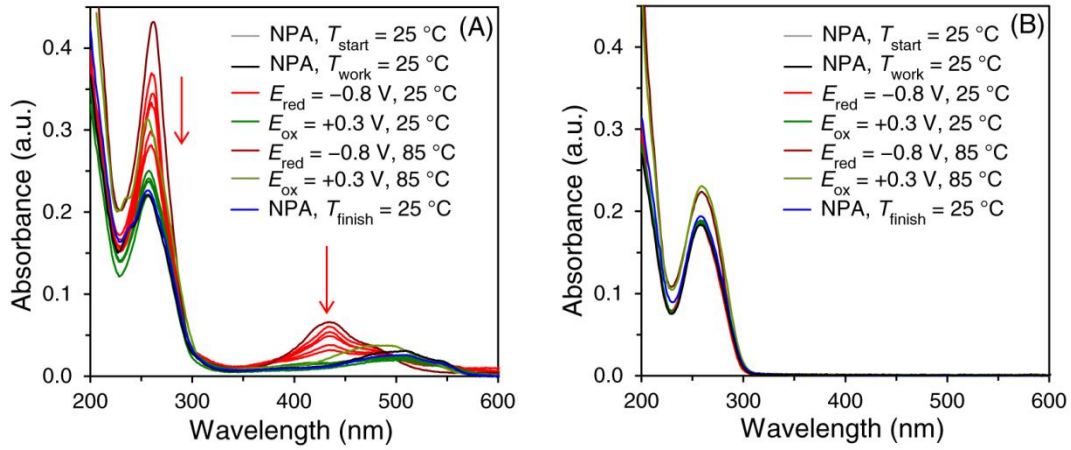

Figure 5.10 Control electrochemical switch experiments. (A) Absorption spectra of 200 µM 20mer dsDNA (bp concentration) in the presence of 100 µM DM in SSC buffer (7.0 mM Na^+), pH 7, at T_{work} = 25 °C (molar ratio 2:1). Upon reduction of DM at −0.8 V, a considerably smaller and less stable increase in the absorbance at 260 nm was observed. This suggested that the DNA was not being denatured. (B) Absorption spectra of 200 µM 20mer dsDNA in SSC buffer (7.0 mM Na^+), pH 7, at T_{work} = 25 °C (molar ratio 2:1). No change in the absorbance at 260 nm was observed upon cycling the redox potentials −0.8 V and +0.3 V. That is, in the absence of DM, the selected redox potentials did not cause any changes in the conformation of DNA. (NPA = no potential applied).

Switching the potential to +0.3 V produced a stable peak at 500 nm for re-oxidised DM, which was accompanied by a stable absorption peak at 260 nm for hybridised DNA. The difference observed in the behaviour of the 20mer dsDNA at 260 nm for T_{work} = 25 °C and 58 °C substantiated that additional changes occurred at T_{work} = 58 °C which clearly affected the absorbance in a reproducible manner. These changes are likely to involve denaturation of the 20mer dsDNA. In order to ensure that the selected reduction and/or oxidation potential did not induce denaturation of DNA, an additional control experiment was conducted where DM was omitted from the sample. As visualised in Figure 5.10B, upon applying successive cycles of −0.8 V and +0.3 V, no change in the absorbance at 260 nm was observed confirming that the DNA remained hybridised despite applied potential.

Electrochemically controlled DNA denaturation and renaturation by redox-state switching of DM was likewise realised for complementary 40mer DNA oligonucleotides in SSC buffer (7.0 mM Na^+) and 20mer DNA oligonucleotides at a higher salt concentration (19.5 mM Na^+). As described in Section 2.2.10, experimental procedures were kept identical to the ones utilised for 20mer DNA in the lower salt concentration (7.0 mM Na^+), apart from the working and heat denaturation temperatures (see Table 4.3). Typical *in situ* UV–vis absorption spectra for the additional conditions, acquired upon the successive application of the redox potentials −0.8/+0.3 V at the respective T_{work}, are displayed in Figure A.7 in Appendix H. In order to numerically evaluate the electrochemically controlled reversible DNA hybridisation, for all three investigated conditions, it is important to note that DM absorbed in the area of 260 nm irrespective of its redox-state. Evident in Figure 5.5, this absorption consequently interfered with the signal obtained for DNA at 260 nm. Therefore, the absolute difference in the absorption at 260 nm ($\Delta A_{260\,nm}$), acquired from the switching of the DM redox-state in the absence and presence of DNA, was analysed. Figure 5.11 shows calculated $\Delta A_{260\,nm}$ for each of the five reduction/oxidation cycles per tested condition. Across all conditions results revealed that upon reduction of DM, a larger difference in the absorption at 260 nm was obtained in the presence of DNA. This served as a further confirmation that additional changes, affecting the absorbance, occurred in the sample containing

DNA. As implied by the results, these additional changes are very likely the effect of denaturation of duplex DNA.

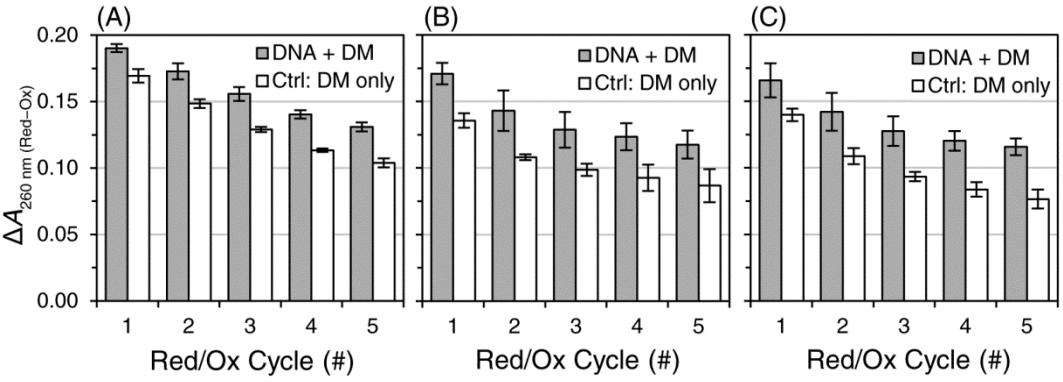

Figure 5.11 Comparison of $\Delta A_{260\ nm}$ obtained from each reduction/oxidation cycle of DM in the absence and presence of DNA. (A) 20mer dsDNA in SSC buffer (7.0 mM Na^+) at T_{work} = 58 °C, (B) 40mer dsDNA in SSC buffer (7.0 mM Na^+) at T_{work} = 65 °C and (C) 20mer dsDNA in SSC buffer (19.5 mM Na^+) at T_{work} = 60 °C. The difference in absorbance at 260 nm is larger for DM in the presence of DNA, thus, reflecting additional contributions from changes in the DNA conformation. Error bars represent standard error ($n \geq 3$).

The reproducibility of the five cycles of electrochemically controlled DNA denaturation and renaturation was established by quantifying the response exclusively assigned to DNA. Using Eq. (2.11), the contribution of the DM absorption at 260 nm was subtracted from the total absorption at 260 nm of DNA in the presence of DM. This resulted in obtaining the absorbance arising exclusively from changes in the DNA conformation, upon switching the redox-state of DM. The acquired values for all investigated conditions can be found summarised in the switch diagram in Figure 5.12A, while the raw data is found in Figure A.8 in Appendix I. A clear stable switching signal was observed which was attributed to cycles of electrochemically controlled DNA denaturation and renaturation. A similar switching behaviour was furthermore observed across all investigated conditions. The best reproducibility was obtained for 20mer dsDNA at the lower salt concentration (7.0 mM Na^+), which was accompanied by a standard error of absorbance within ±0.003. A slight drift in the signal was observed upon increasing the length of the oligonucleotide from 20mer to 40mer. Nonetheless, all conditions demonstrated five cycles of electrochemically controlled reversible DNA

hybridisation with an average cycle time of 144 s. Using Eq. (2.12), the hyperchromic shifts for each of the five reduction/oxidation cycles in Figure 5.12A were calculated and summarised in Figure 5.12B. Results revealed hyperchromic shifts $H_{260\,\mathrm{nm}}^{\mathrm{Echem}} < 20$ %. Table 4.3 shows the benchmark hyperchromic shifts ($H_{260\,\mathrm{nm}}^{\mathrm{Thermal}}$) for DNA alone obtained by thermal means for the corresponding conditions. Compared to the benchmark, using Eq. (2.13), it was deduced that 57–80 % of the total DNA in the sample was electrochemically controlled across all investigated conditions.

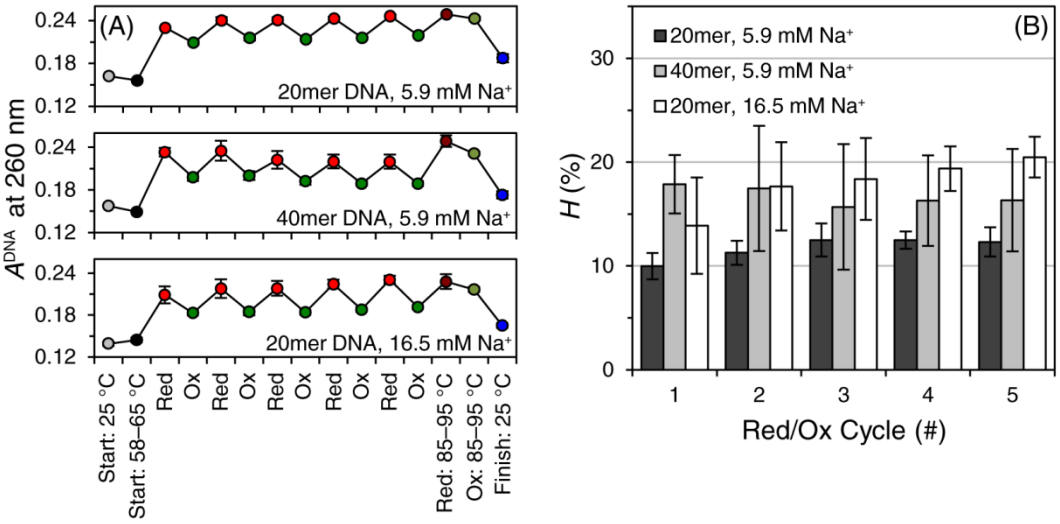

Figure 5.12 Switch diagram of electrochemical control of reversible DNA hybridisation and accompanying hyperchromic shifts. (A) Switch diagram displaying the exclusive absorbance of DNA (Eq. (2.11)) across five consecutive reduction/oxidation cycles at 144 s per cycle. Changes in absorption at 260 nm, at three different conditions, were observed as a result of denaturation (red circles) and renaturation (green circles) of DNA controlled by redox-state switching of DM. (B) Hyperchromic shifts at 260 nm per reduction/oxidation cycle for the quantification of the efficiency of electrochemical controlled reversible DNA hybridisation. Error bars represent standard error ($n \geq 3$).

Finally, in order to examine the potential degradation of DNA as a result of the electrochemical control of reversible hybridisation, capillary gel electrophoretic analysis was conducted following the procedure described in Section 2.2.13. Figure 5.13 depicts the gel electropherogram for complementary 20mer DNA oligonucleotides in the presence of DM, in SSC buffer (7.0 mM Na^+), before and after redox cycling at $T_{\mathrm{work}} = 58$ °C. The peaks at 43.0 s and 112.0 s denote the lower

(15 bp) and upper (1500 bp) ladder marker. Two peaks appeared in the electropherogram before redox cycling. As realised when compared to the ladder in Figure 2.2, the main peak at 44.8 s corresponded to a 20 bp long dsDNA fragment. The smaller peak at 47.6 s corresponded most likely to single strands of the 20 bp long DNA fragment, since single stranded DNA appear larger and with a lower intensity. After redox cycling, the electropherogram displayed one peak at 44.6 s which corresponded to a 20 bp long dsDNA fragment, thus, demonstrating that no degradation of DNA occurred as a result of the redox cycling.

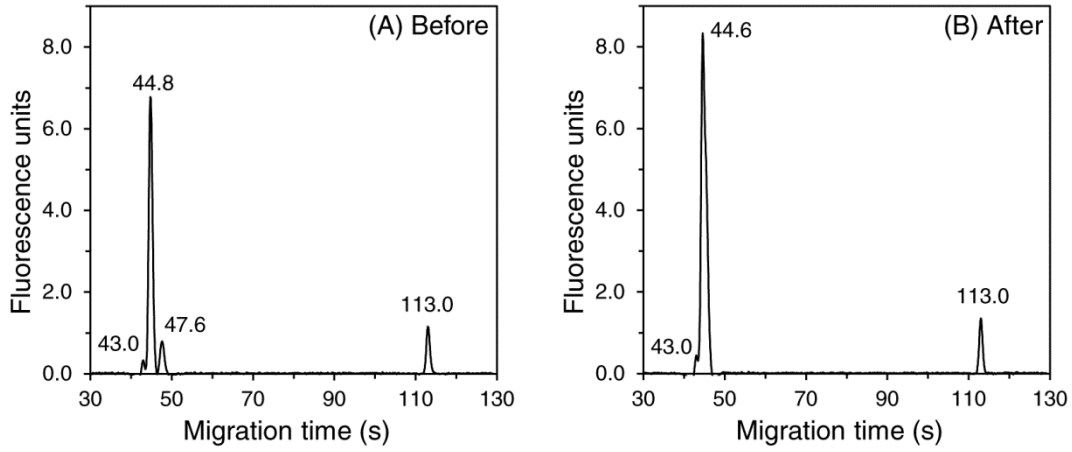

Figure 5.13 Gel electrophoretic analysis of DNA before and after redox cycling. 200 μM 20mer dsDNA (bp concentration) in the presence of 100 μM DM in SSC buffer (7.0 mM Na^+), pH 7, was analysed (A) before and (B) after redox cycling at T_{work} = 58 °C. Peaks at 43.0 and 112.0 s represent the lower and upper ladder marker at 15 and 1500 bp. The peak at ~44 was visible before and after redox cycling and, thus, represented intact 20mer dsDNA.

5.2.3 Validation of electrochemical cycling of DNA denaturation and renaturation with daunomycin using *in situ* CD spectroelectrochemistry

To further validate the observations of electrochemically controlled reversible DNA hybridisation made with *in situ* UV–vis spectroelectrochemistry, the experiments were repeated with *in situ* CD spectroelectrochemistry as a second independent technique. Prior to carrying out the electrochemical switch experiments, the change in CD upon denaturation of complementary 20mer DNA oligonucleotides in SSC buffer (7.0 mM Na^+), in the absence and presence of oxidised DM, was examined by

CD-based end-point melting studies. Further details on the experimental procedure are found in Section 2.2.8. Figure 5.14A displays a CD spectrum of 20mer dsDNA alone recorded at 25 and 85 °C. At 25 °C, when hybridised, the 20mer dsDNA exhibited a strong negative band at 250 nm accompanied by a strong positive band at 275 nm. Upon denaturation, at 85 °C, a decrease in CD at 250 and 275 nm was observed. Figure 5.14B depicts the CD spectrum recorded at 25 and 85 °C of 20mer dsDNA in the presence of oxidised DM at a base-pair to intercalator molar ratio 2:1. A dramatic change in the CD spectrum occurred upon intercalation of DM. At 25 °C, when hybridised, the 20mer dsDNA displayed a dip at 250 nm with a strong positive and negative band at 275 and 300 nm, respectively. Upon denaturation, at 85 °C, the magnitudes of the bands at 275 and 300 nm decreased. Based on these results, it was evident that a decrease in the signal at 275 nm was found upon the denaturation of DNA in the absence and presence of oxidised DM. Thus, this signal was selected for monitoring the conformational state of duplex DNA in the electrochemical switch experiments.

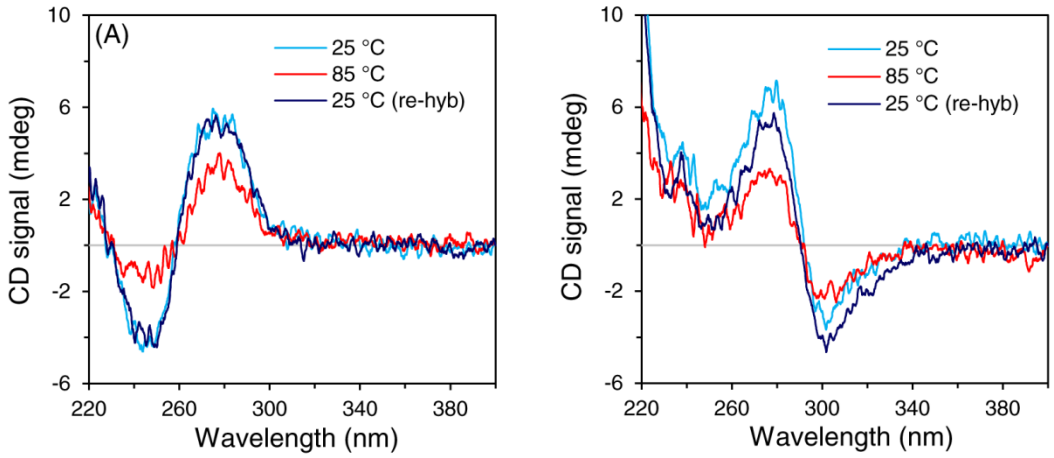

Figure 5.14 CD-based end-point DNA melting study. Upon denaturation at 85 °C, a decrease in CD was observed at 275 nm for 200 μM dsDNA (bp concentration) in SSC buffer (7.0 mM Na^+) in the (A) absence and (B) presence of 100 μM DM (molar ratio 2:1).

Employing identical experimental conditions and procedures as used for the *in situ* UV–vis spectroelectrochemical measurements in Figure 5.9, *in situ* CD spectroelectrochemical spectra of complementary 20mer DNA oligonucleotides, in the presence of the electrochemical cycling of the DM redox-state, were recorded.

Conducted at the working temperature 58 °C (Table 4.3) in SSC buffer (7.0 mM Na^+), and at a base-pair to intercalator ratio 2:1, specific details on the experimental procedure can be found in Section 2.2.11. According to the data analysis described in the same section, all spectra were first normalised and then the averaged buffer spectra were subtracted. Subsequently, to achieve changes in the CD signals exclusively from the DNA, CD spectra obtained from the switching of DM alone were also subtracted according to Eq. (2.14). Thus, Figure 5.15A shows the mean changes in the CD spectra exclusively assigned to 20mer dsDNA upon successive cycling of the redox potentials −0.8 V and +0.3 V, for redox-state switching of DM.

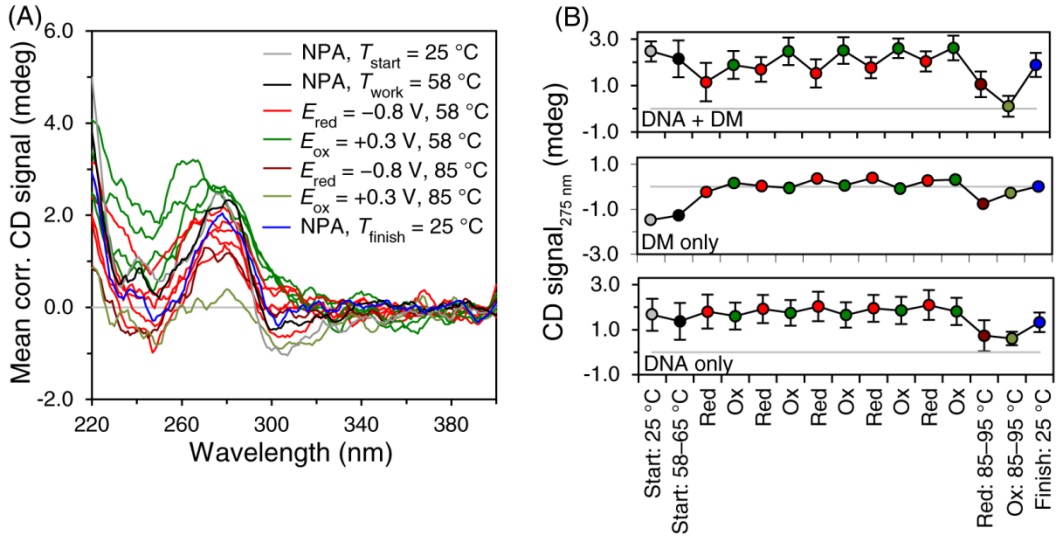

Figure 5.15 Validation of electrochemical control of reversible DNA hybridisation with *in situ* CD spectroelectrochemistry. (A) CD spectra of 200 µM dsDNA (bp concentration) in the presence of 100 µM DM in SSC buffer (7.0 mM Na^+), pH 7, at T_{work} = 58 °C (molar ratio 2:1). The spectra represent changes in CD exclusively from DNA, where a change at 275 nm was observed upon switching the redox-state of DM by cycling −0.8 V and +0.3 V. (B) Switch diagram displaying the change in $CD_{275\ nm}$ for 20mer dsDNA in the presence of DM alongside with two controls of DM alone and DNA alone. Upon cycling −0.8 V and +0.3 V, consistent switching in CD was only observed for DNA in the presence of DM. Error bars represent standard error (n = 3), while DM only was averaged over 2 replicates. (NPA = no potential applied).

A consistent switching in the CD spectrum at 275 nm was observed upon cycling the redox potentials. Similar observations were not made for the controls of DM

alone and DNA alone in Figure A.9 in Appendix J. Upon applying −0.8 V at the final heat denaturation temperature T_{heat} = 85 °C, a fair correlation between the recorded spectrum of heat denatured DNA and the spectra of DNA at T_{work} = 58 °C, during reduction of DM, was noted. However, a slight discrepancy was observed upon switching the potential to +0.3 V at T_{heat} = 85 °C. To clearly visualise the consistent switching, changes in CD at 275 nm obtained exclusively from the 20mer dsDNA in Figure 5.15A were summarised in a switch diagram in Figure 5.15B, along with two controls. Despite larger errors, a clear switching trend in the CD signals was observed for DNA in the presence of DM which was not observed for DM or DNA alone. As can be seen, upon reduction of the DM at T_{work} = 58 °C, the CD signal decreased in a similar manner as observed for thermal melting at T_{heat} = 85 °C. Upon re-oxidising DM, the CD signal increased and correlated well with the signals obtained for hybridised DNA at T_{start} = 25 °C. Thus, results evidently validated the electrochemically controlled DNA denaturation and renaturation by redox-state switching of DM.

5.3 Discussion

The main focus of the last results Chapter was to demonstrate the proof-of-principle of electrochemically controlled reversible DNA hybridisation by redox-state switching of DM. Prior to doing so, the electrochemical behaviour of DM was established using cyclic voltammetry and *in situ* UV–vis spectroelectrochemistry. Furthermore, an NMR investigation confirmed that DM remained intact upon electrochemical redox conversion. These studies permitted the identification of the redox potentials (−0.8 V/+0.3 V) to be employed in subsequent experiments. Finally, the electrochemically controlled reversible DNA hybridisation by redox-state switching of DM was studied, at three different conditions, by means of *in situ* UV–vis spectroelectrochemistry. While CD-based end-point melting studies identified 275 nm as the relevant wavelength to observe changes in the DNA conformation, *in situ* CD spectroelectrochemistry was exploited as a second independent technique in order to validate electrochemically controlled reversible DNA hybridisation. Finally, gel electrophoresis confirmed that DNA did not

undergo degradation as a result of the electrochemical cycling of the DM redox-state.

5.3.1 Elucidating the electrochemical behaviour of daunomycin

In order to establish the electrochemical behaviour of DM, an investigation using cyclic voltammetry was conducted. Figure 5.2 displays the redox activity of DM in the absence and presence of complementary 20mer DNA oligonucleotides in SSC buffer (7.0 mM Na^+) at a molar ratio 2:1. Consistent with previous voltammetric studies on DM in aqueous solutions,[229, 264-266] two well-defined peaks representing the $2e^-$, $2H^+$ reduction and re-oxidation of the anthracycline quinone ring was observed, see Scheme 5.1. While the reduction peak potential E_{pc} was in excellent agreement with previous findings,[229, 264, 265, 267] the oxidation peak potential E_{pa} differed which resulted in a large peak potential separation ΔE_p. However, this observation is very likely an effect of the uncompensated ohmic drop (iR_u) present in the solution, which can be attributed to the design of the spectroelectrochemical cell and the large working electrode generating high currents.[179]

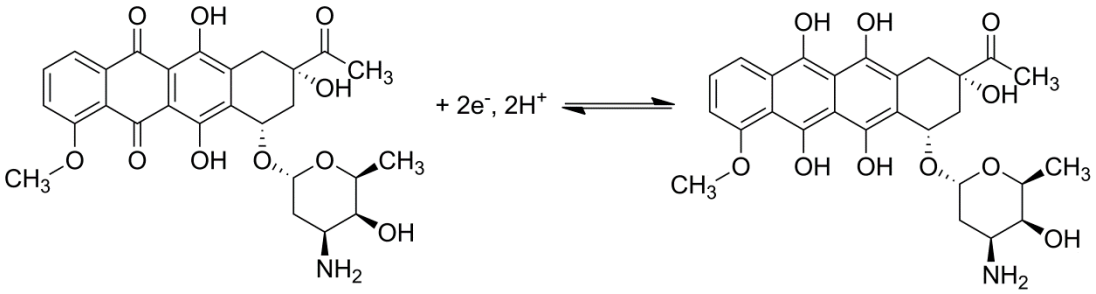

Scheme 5.1 Reversible reduction and oxidation of DM. Under physiological conditions (pK_a 8.6) the amine group on the sugar ring is protonated (NH_3^+).[248]

Further inspection of Figure 5.2 revealed a change in the redox behaviour of DM in the presence of DNA. Two well-defined redox peaks for the $2e^-$, $2H^+$ reduction and oxidation of the anthracycline quinone ring were however still visible. In agreement with previous voltammetric studies,[229, 264, 268, 269] a decrease in the peak current was detected in the presence of DNA. This observation has been attributed to the intercalation of DM, which results from a decreased apparent diffusion coefficient of

the larger and bulkier drug-DNA complex. However, it is worth highlighting that the present study employed a very slow scan rate (10 mV s^{-1}) for interrogation, thus, allowing enough time for redox active species to diffuse to the electrode surface. In contrast, much higher scan rates (> 100 mV s^{-1}) were employed in the previous voltammetric studies, which may serve as an explanation for the smaller decrease observed in the peak current (Figure 5.2) compared to the literature. A shift in the peak potentials was likewise demonstrated in previous voltammetric studies for DM in the presence of DNA. While correlation was found with previous studies[229, 270] on the negative shift of the reduction peak potential upon intercalation, the negative shift of the oxidation peak potential in the present study deviated from previously published data[229, 264] where a positive shift was identified. Carter and co-workers[271] explored the intercalative and electrostatic interaction of metal complexes, such as $Co(bpy)_3^{3+/2+}$ and $Co(phen)_3^{3+/2+}$, with calf thymus DNA. While a positive shift in the reduction and oxidation potential was attributed to intercalation of metal complexes, such as $Co(phen)_3^{3+/2+}$, the authors speculated that a negative shift in the reduction and oxidation potential was observed for species that were mainly electrostatically bound, e.g. $Co(bpy)_3^{3+/2+}$. However, the latter conclusion seems unlikely for DM in the present study, since both intercalation (Figure 4.4) and absorbance-based melting curve studies (Figure 4.11A) confirmed the intercalative binding mode. Thus, in conjunction with the spectroscopic data in Chapter 4, it is reasonable to conclude that the voltammetric response of DM in the presence of DNA in Figure 5.2 described an intercalative binding mode. Moreover, results indicated that DM remained electrochemically active despite being intercalated.[267]

5.3.1.1 Reversibility of the daunomycin redox process

The reversibility of DM in the absence and presence of 20mer dsDNA in SSC buffer (7.0 mM Na^+), at a molar ratio 2:1, was further explored. Figure 5.3A and B shows the voltammetric response at different scan rates. One set of well-defined redox peaks was observed at all scan rates for DM in the absence and presence of DNA for the $2e^-$, $2H^+$ reduction/oxidation of the quinone functionality. However, in general, for an electrochemically reversible redox couple, $\Delta E_p = 59/n$ mV, where n is number of electrons and ΔE_p is independent of the scan rate. In contrast, for a semi-

reversible redox couple, $\Delta E_p > 59/n$ mV and increases with an increasing scan rate due to slow heterogeneous electron-transfer kinetics.[186] Upon inspection of Figure 5.4A, results revealed an electrochemically semi-reversible reduction/oxidation of DM. The electron-transfer seemingly improved slightly in the presence of DNA, indicated by the slightly smaller peak potential separation.[271] The observed semi-reversible nature of DM corresponded well with previous studies investigating the voltammetric activity of DM in solution, using a rotating glassy-carbon disk electrode,[229] and adsorbed to the surface on hanging mercury drop electrodes (HMDE) and carbon paste electrodes.[265] In contrast, however, it is worth noting that others investigating the voltammetric response of DM[272] and other anthracyclines[264, 273] characterised a fully reversible redox couple. Hence, as discussed above, it may be speculated that the apparent semi-reversible nature of DM in the present study can be ascribed to the large ohmic drop iR_u resulting from the design of the spectroelectrochemical cell.[179] As highlighted in a classic cyclic voltammetry study by Nicholson,[274] the impact of a large uncompensated resistance R_u yields qualitatively a similar behaviour in the kinetics of a reversible electroactive species as a semi-reversible electroactive species. That is, an increasing peak potential separation is observed with an increasing scan rate.

Based on the voltammetric study of DM, apparent slow heterogeneous electron-transfer kinetics was revealed. Nevertheless, in the investigated potential range (−0.8 V to +0.3 V), a well-defined reduction and oxidation peak was observed. For the purpose of the method in the current study, it was important to ensure that DM indeed was undergoing complete reduction to a hydroquinone and re-oxidation to a quinone. Therefore, −0.8 V and +0.3 V were selected as E_{red} and E_{ox}, respectively, for the chronoamperometric redox conversion of DM confirmed by means of *in situ* UV–vis spectroelectrochemistry. Figure 5.5A shows typical absorption changes of DM in SSC buffer (7.0 mM Na^+) upon the successive application the selected redox potentials at T_{work} = 58 °C. In agreement with previously reported peak positions, characteristic peaks were observed for the naturally oxidised form of DM[243] when no potential was applied; the fully reduced form of DM[241] upon application of the reduction potential −0.8 V; and the oxidised form of DM[243] upon application of the re-oxidation potential +0.3 V. Figure 5.5B shows the current transients recorded

simultaneously upon potential application. Despite possible slow heterogeneous electron-transfer kinetics of DM, the spectroelectrochemical results clearly indicated that, during the employed time scale for potential application (60 s), a full chemical reversible switching of the redox-state of DM was achieved. Furthermore, this was in agreement with the estimated total electrolysis time using Eq. (1.21).

5.3.1.2 Stability of daunomycin upon redox cycling

Both cyclic voltammetry and *in situ* UV–vis spectroelectrochemical measurements indicated that, in addition to reduction/oxidation of DM, other processes were taking place. Figure 5.4B shows the ratio between the reduction and oxidation peak currents for DM, in the absence and presence of DNA, obtained from the cyclic voltammetry measurement. Deviation from unity (< 1) implied either complications at the electrode surface, such as adsorption, or an unstable reduced species.[186, 271] It is worth noting that slightly less deviation was observed in the presence of DNA. Peak current ratios deviating from unity has been described before. Wang *et al.* observed a ratio < 1 upon the investigation of surface adsorbed DM on HMDE and carbon-paste electrodes.[265] In contrast, investigating the redox behaviour of AM on HMDE, Kano *et al.* described a scan rate dependent variation of the peak current ratio where higher scan rates yielded ratios closer to 1.[275] The authors attributed this observation to irreversible chemical reactions of reduced AM.

Similar to the observations in the cyclic voltammetry investigation, a continuous decrease in the absorbance for reduced DM was observed over the five redox cycles in the *in situ* UV–vis spectroelectrochemical measurement, see Figure 5.5A. In contrast, however, the absorbance for re-oxidised DM remained constant, although the peak was less pronounced and red-shifted. Possible explanations of the decreased absorbance may, like in the cyclic voltammetry investigation, be related to surface adsorption or possible decomposition leading to irreversible chemical reactions of DM. As stated in Chapter 4, the amine group on the sugar ring of DM is positively charged at pH 7 (pK_a 8.6).[248] Therefore, upon successive application of the negative reduction potential (−0.8 V), more positively charged DM may be attracted to the surface each time leading to a decreased absorbance. However, this does not

correlate with the constant absorbance observed for oxidised DM. The other possibility is associated with the irreversible decomposition of the hydroquinone yielding quinone methide intermediates.[239] As previously discussed in Section 4.3.2.3, the hydroquinone is well-known for its unstable nature. Decomposition of DM involves the irreversible glycosidic cleavage of the sugar ring at position C7.[239, 241, 276] This renders an intermediate which can either react with an electrophile to yield a C7-functionalised quinone, or with a nucleophile to yield a C7-functionalised hydroquinone. Often only solvent protons are available for reaction which accordingly yields the aglycone 7-deoxydaunomycinone,[239, 241, 277] see Scheme 5.2.

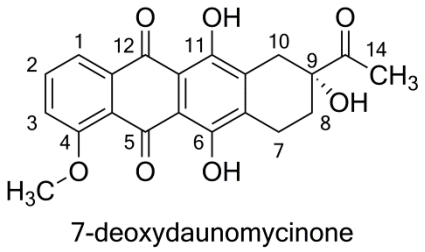

7-deoxydaunomycinone

Scheme 5.2 De-glycosylation of DM yields aglycone 7-deoxydaunomycinone.

While aglycones preserve their redox functionality, they are not readily soluble in water,[239, 272] which may explain the decreased absorbance (Figure 5.5A) and the deviation from unity of the current peak ratio (Figure 5.4B). However, it is important to emphasise that quinone methide formation is likewise a well-characterised anaerobic event. Only when oxygen is absent will the quinone methide persist and undergo such a cleavage.[239] As shown by many,[238-240] even at trace amounts of molecular oxygen, *in vitro* re-oxidation of the hydroquinone is favoured over the irreversible elimination of the sugar ring. It was evident from the cathodic current transients in Figure 5.5B that, although samples were degassed with argon prior to measurement, oxygen was still present to a certain extent. Thus, re-oxidation of the hydroquinone would be expected.

As results were unclear, structural analysis of DM was undertaken in order to confirm whether DM remained intact upon redox cycling. Figure 5.6A and B shows the proton NMR spectrum of DM in SSC buffer (7.0 mM Na^+) before and after five

cycles of redox-state switching at T_{work} = 58 °C (Figure 5.5). The assignments of the protons for DM (before redox cycling) were largely consistent with those reported in the literature.[262, 278] Slight discrepancies in the chemical shifts of specific proton resonances were observed due to differences in solution conditions. With nearly identical spectrum and chemical shifts (Table 5.1) of DM before and after redox cycling, evidence indicated that DM remained intact. While five new signals appeared after redox cycling of DM (Figure 5.6B), these were unambiguously assigned to the SSC buffer as realised from Table 5.2. Arcamone and colleagues[262, 279] conducted an NMR analysis of DM and the two aglycones daunomycinone (OH in position C7) and 7-deoxydaunomycinone (Scheme 5.2) in organic solvents. While the authors found correlation between chemical shifts for various protons of the aglycones and the parent compound DM, a significant difference associated with the protons of C7 was observed. Daunomycinone showed a significant downfield shift of 7H from 5.07 ppm in the parent compound to 5.50 ppm.[262] This was attributed to the existence of a hydroxyl group on the same carbon. On the other hand, 7-deoxydaunomycinone exhibited benzylic 7CH_2 at equivalent chemical shifts found for 10eqH/10axH (~3 ppm). No equally significant shifts in 7H were observed in Figure 5.6B. However, it is essential to reiterate that aglycones have a low solubility in aqueous solutions.[239, 272] It is therefore unlikely that either aglycone compound would have been detected in the NMR spectrum of DM after redox cycling, since measurements were conducted in an aqueous buffer. NMR is however a quantitative technique,[280] hence, further formation of quinone methides from the reduced form of DM and/or precipitation of the aglycones[239] would have significantly affected the intensities of the signals in the spectrum. Slightly lower intensities of the signals for DM after redox cycling were detected. This indicated that some decomposition of reduced DM may have taken place. However, considering that redox cycling of DM proceeded at 58 °C without overlaying the sample with mineral oil (see Section 2.2.12 for the experimental procedure), it was more likely that evaporation and loss of sample occurred. Mineral oil was omitted from the experimental setup due to contamination risk in the NMR analysis, which otherwise served as an essential barrier against evaporation. Thus, initial evidence indicated that DM indeed remained intact after redox cycling. It furthermore suggested that the decreased absorbance observed for DM upon reduction (Figure

5.5) may be related to other processes, such as adsorption of DM to the electrode surface. The electrochemical behaviour of adsorbed DM has been well-studied on mercury,[265, 281] carbon-paste[268] and glassy carbon[267] electrodes. Interestingly, while Kertesz *et al.*[281] noted an increase in the electrode surface charge with oxidised DM, a decrease was observed with reduced DM. That is, in contrast to findings in this study, the authors noted a decrease in the surface coverage when DM was reduced. Thus, whether adsorption of DM was in fact occurring on the Pt electrode in this work remains unclear and further investigation is required.

5.3.2 Electrochemical control of reversible DNA hybridisation

The proof-of-principle of the reversible interconversion between 20mer dsDNA and ssDNA, upon redox-state switching of DM, was confirmed with *in situ* UV–vis spectroelectrochemical measurements. The strength in utilising this technique[179, 184] relates to the fact that the behaviour of both DNA and DM, upon switching the redox potential, can be followed concurrently. As depicted in the cartoon in Figure 5.16, changes in absorbance related to the conformational state of DNA were followed at 260 nm, while changes in absorbance related to intercalation and the redox-state of DM were followed between 400 and 500 nm.

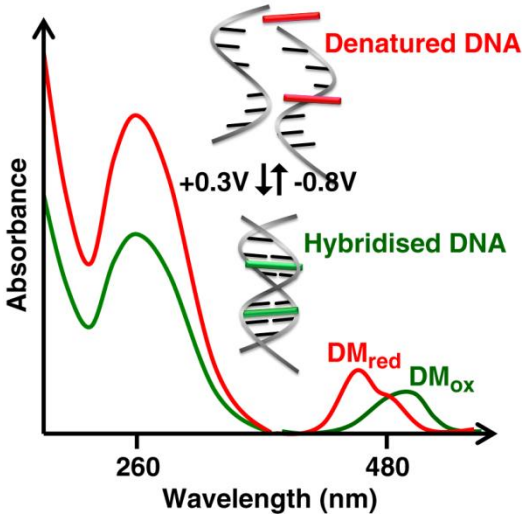

Figure 5.16 Cartoon depicting denaturation and renaturation of dsDNA by redox-state switching of DM.

Figure 5.9 demonstrates the electrochemically controlled DNA denaturation and renaturation, by redox-state switching of DM at −0.8 V and +0.3 V, for 20mer dsDNA in SSC buffer (7.0 mM Na^+) at the working temperature 58 °C (molar ratio 2:1). While cycling the redox-state from oxidised to reduced DM, a consistent hyper- and hypochromic shift was observed for the absorption of DNA at 260 nm. Such spectral changes at 260 nm immediately implicated denaturation and hybridisation events of dsDNA. It is well-known that DNA denaturation leads to an increase in absorbance due to exposure of the aromatic rings in the nucleotides. Conversely, hybridisation of DNA causes a decrease in the absorbance as the aromatic rings are hidden in the stacked nucleotides.[36, 167] Several additional observations confirmed these conformational changes and are listed below:

1. Figure 5.9: Correlation between the absorbance of DNA upon reduction of DM at the working and heat denaturation temperature confirmed that DNA indeed underwent denaturation at the working temperature. Conversely, difference in the absorbance of DNA upon oxidation of DM at the working and heat denaturation temperature confirmed that DNA indeed re-hybridised at the working temperature.

2. Figure 5.9: Difference in the peak maximum and height for DM at the working and heat denaturation temperature further confirmed that DNA indeed underwent re-hybridisation at the working temperature. As was demonstrated in the intercalation study in Section 4.2.1 and by others,[161] intercalation of DM yields a red-shift in the peak maximum at 480 nm as well as a decrease in absorbance.

3. Figure 5.9 and Figure 5.10A: Difference in the magnitude and stability of the DNA absorbance upon reduction of DM at the working temperature (58 °C) and a lower temperature (25 °C; DNA is expected to be hybridised irrespective of the redox-state of DM) substantiated denaturation of DNA at the working temperature.

4. Figure 5.11 and Figure 5.12A: Difference in absorbance of DNA at 260 nm, upon redox cycling of DM, persisted despite removal of the contributing absorbance of reduced and oxidised DM. The remaining difference in the absorbance at 260 nm confirmed the cyclic DNA denaturation and renaturation.

5. Figure 5.10B: No changes in the absorbance of DNA alone upon redox cycling confirmed that the selected redox potentials did not cause denaturation of DNA.

The last point further confirmed that none of the nucleotides were undergoing reduction or oxidation. This conclusion was corroborated by the findings of Nowicka and co-workers. An *in situ* UV–vis spectroelectrochemical study, carried out by the authors, demonstrated that the absorbance of DNA at 260 nm increased upon the oxidation of guanine and adenine at potentials above +0.9 V vs. Pt. While possible changes in the absorbance for thymine and cytosine were not detected, the oxidation potentials were reported being above 1 V vs. Pt.[282] Similar highly positive potentials vs. Ag/AgCl were reported for the separate nucleotides.[283] In contrast, reduction of the nucleotides occur at highly negative potentials (< −1.0 V vs. saturated calomel electrode) and has been observed on mercury electrodes.[284]

Electrochemically controlled DNA denaturation and renaturation was also realised for a longer DNA fragment (40mer dsDNA in SSC buffer at 7.0 mM Na^+) and at a higher salt concentration (20mer dsDNA in SSC buffer at 19.5 mM Na^+), see Figure A.7 in Appendix H. The resulting changes in the absorbance at 260 nm, exclusively obtained from conformational changes in DNA, were summarised for all tested conditions in switch-diagrams in Figure 5.12A. A consistent and highly reproducible switching of the conformational state of DNA was observed over five cycles (144 s/cycle) despite changing the length of DNA or the salt concentration. However, evidence indicated that the efficiency of electrochemical control of reversible DNA hybridisation (Figure 5.12B) was lower than the benchmark of thermal control (Table 4.3). A plausible reason for this observation may be related to incomplete renaturation of DNA due to the low salt concentration (7.0 mM Na^+) utilised which was initially chosen as a boundary condition to favour denaturation (Figure 3.7). This was further implied from the higher salt concentration conditions,

which exhibited more complete renaturation (i.e. lower A^{DNA} values at 260 nm), see Figure 5.12A. The effect of the salt concentration on the renaturation efficiency can be explained in the context of the counterion condensation theory.[38, 39] As discussed in Section 3.3.3, upon the interconversion of dsDNA and ssDNA counterions are released and mixed with the bulk solution which results in an entropy gain. A lower salt concentration yields higher gain in entropy of mixing, which decreases the free energy of the system according to the thermodynamic relationship $\Delta G° = \Delta H° - T\Delta S°$. Accordingly, this results in a destabilisation of duplex DNA which would explain potential incomplete renaturation. The determined working temperatures (see Section 4.2.4.2 for the definition) employed during the switching may be another possible reason for incomplete renaturation of DNA. Upon selection of a working temperature where 100 % of the DNA was in a denatured state, in the presence of reduced DM, it was inevitable to avoid slight denaturation of DNA in the presence of oxidised DM, see Figure 4.11A and Figure A.7A and B in Appendix H. As realised, a combination of both may have led to incomplete renaturation would explain the obtained lower efficiency of the electrochemical control of reversible DNA hybridisation.

5.3.2.1 Stability of DNA upon redox cycling

While antibiotic anthracyclines possess an important antitumor activity, several drugs from this family, including DM, have exhibited a cardiotoxic effect *in vivo*. Over the past three decades substantial efforts have been made in order to elucidate the complex underlying mechanisms for the observed cardiotoxicity. The reduction pathway of DM, and other anthracyclines, to a hydroquinone involves two consecutive one electron reductions with an intermediate semiquinone radical formation. The one electron reduction has long been linked with the generation of reactive oxygen species (ROS) from the *in vivo* reduction of anthracyclines, which can promote damage to DNA.[126, 158, 239, 267, 285-287] Cheng *et al.* conducted an *in situ* UV–vis spectroelectrochemical investigation of the *in vitro* effects of the anaerobic reduction of DM on fish sperm DNA.[288] The authors observed an increase in the absorbance of DNA at 260 nm upon reduction of DM and further speculated that, at a DNA-phosphate to DM ratio of 1:1, DNA fragmentation occurred due to

semiquinone free radical formation of daunomycinone and 7-deoxydaunomycinone, which can equally undergo $2e^-$, $2H^+$ reductions. In the light of these findings, it was essential to investigate whether degradation or fragmentation of the DNA occurred as a result of the redox cycling of DM. Figure 5.13A and B shows gel electrophoretic evaluation of 20mer dsDNA in the presence of DM in SSC buffer (7.0 mM Na^+) before and after redox cycling at T_{work} = 58 °C (Figure 5.9). 20mer dsDNA was clearly visualised after the redox cycling, thus, indicating that no degradation of DNA occurred. These results reflected that perhaps under the conditions in the current study, the potentially DNA damaging semiquinone free radical formation through one electron transfer was largely circumvented. Owing to the large overpotential (−0.8 V) used for the reduction of DM, the reaction equilibrium most likely shifted towards the $2e^-$ reduction for the formation of the hydroquinone.[289] This was further corroborated by Figure 5.5 where spectral characteristics were only observed for the hydroquinone upon the reduction of DM at −0.8 V. Moreover, NMR analysis confirmed that neither daunomycinone nor 7-deoxydaunomycinone was produced as a result of the redox cycling. Abdella and Fisher, on the other hand, speculated that a $2e^-$ reduction of an anthracycline might be favoured whilst intercalated.[239] This speculation was based on findings of Berlin and Haseltine who observed less formation of the semiquinone free radical by NADPH cytochrome P-450 reductase when intercalated into DNA.[290]

5.3.2.2 Validation using a second independent technique

Validation of the reversible interconversion between dsDNA and ssDNA, upon redox-state switching of DM, was obtained by means of *in situ* CD spectroelectrochemistry. Based on an end-point melting curve study, the most suitable wavelength to monitor CD-based DNA denaturation and renaturation was initially identified. Characteristic bands, in Figure 5.14A and B, for 20mer dsDNA in the absence[291] and presence[292] of DM displayed an overall decrease in CD upon thermal denaturation, which has been shown previously for DNA[293]. Implicit from the results was that the most suitable wavelength to monitor was 275 nm. Under identical conditions as in the *in situ* UV–vis spectroelectrochemical experiments (Figure 5.9), electrochemical control of reversible DNA hybridisation was

remarkably also observed with *in situ* CD spectroelectrochemistry for complementary 20mer DNA oligonucleotides in the presence of DM (molar ratio 2:1). While CD spectra for the exclusive spectral changes in DNA are shown in Figure 5.15A, the resulting changes in CD at 275 nm, exclusively obtained from conformational changes in DNA, were summarised in a switch-diagram in Figure 5.15B. Validation of the proof-of-principle was based on several observations. First, correlation was found between CD spectra of DNA, upon reduction of DM, at the working and heat denaturation temperature confirming denaturation events at the working temperature. Second, in excellent agreement with the observations using *in situ* UV–vis spectroelectrochemistry, a consistent switching in CD for DNA upon cycling the redox-state of DM was observed. Third, neither DM alone nor DNA alone showed any sign of such switching.

However, the errors associated with the consistent switching found for DNA in the presence of DM must be noted. In an overview by Garbett *et al.*, on the use of CD spectrometry for interrogation of ligand-DNA interactions, the signal-to-noise ratio of the technique was specified to increase with the square root of the number of scans and response time. In order to maintain a reduction/oxidation cycle time of 144 s, as in the *in situ* UV–vis spectroelectrochemical measurements, CD spectra were collected at a high scan speed and low response time. Thus, an obvious sacrifice in resolution was made for the gain in experimental consistency. Therefore, the errors most likely reflected a systematic error inherent to the technique as a result of the chosen parameters for recording data. This was further evident from the equivalent errors associated with the DNA alone control in Figure 5.15B. Thus, it is reasonable to conclude that as a second independent technique, the *in situ* CD spectroelectrochemical experiments substantiated the electrochemical control of reversible DNA hybridisation by redox-state switching of DM.

5.3.3 Hypothetical considerations for the underlying mechanism

At this point the underlying mechanism for induced DNA denaturation and renaturation, by redox-state switching of DM, is not fully understood. However, the mechanism may be speculated based on the available literature and theories.

According to the crystallographic studies by Quigley *et al.*[159] and Wang *et al.*,[160] four hydrogen bonds stabilises the DM-DNA complex, as shown in Figure 5.17. However, none of these specific hydrogen bonds were observed between DNA and the quinone/hydroquinone functionality of DM. O5 on the quinone is coordinated by a Na^+ and participates in several van der Waals interactions. O12 on the quinone forms hydrogen bonds to water molecules, surrounding the complex, which in turn forms hydrogen bonds to the nucleotides. Considering that the reduction of DM to a fully reduced hydroquinone occurs on the quinone functionality, it is ambiguous whether this would affect the hydrogen bond stabilised interaction of oxidised DM to DNA.

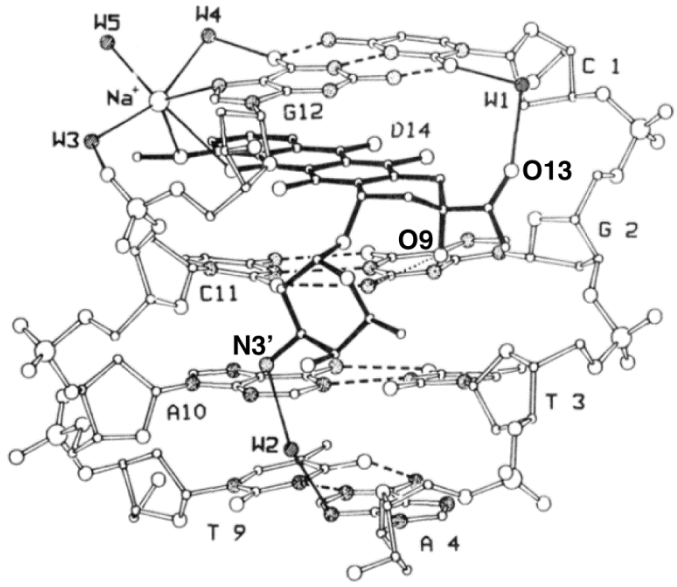

Figure 5.17 Diagram of DM intercalated into d(CGTACG). The intermolecular interactions between the intercalator and a DNA hexamer were solved with X-ray diffraction analysis (resolution 1.2 Å). Hydrogen bonds between base-pairs are represented with dashed lines. Two hydrogen bonds are formed between O9 on DM and G2. A water-bridged (W1) hydrogen bond is formed between O13 on DM and C1, while another one (W2) if formed between N3' on DM and A4. Lastly, Na^+ is coordinated by O4 and O5 on DM, G12 and three water molecules. Adapted with permission from Wang, A.H., Ughetto, G., Quigley, G.J. & Rich, A. *Biochemistry* **26**, 1152–1163 (1987). Copyright (2013) American Chemical Society.

Therefore, one plausible explanation for the electrochemically induced interconversion between dsDNA and ssDNA may be related to the protonation state of DM. Using cyclic voltammetry, Kano *et al.* explored the pH dependency of

adsorbed AM on a mercury electrode surface.[275] The p$K_a$values of the phenolic hydroxyl groups for oxidised and reduced AM were determined to 8.53 and 6.83, respectively. In a review by Bouma and co-workers concerning anthracycline antitumor agents, agreement of pK_a values for oxidised AM and DM from different studies was found.[243] It is important to reiterate that DM differs from AM only by one extra hydroxyl group at position C14 (Scheme 1.1). Therefore, in light of previous studies it may be inferred that reduced DM may exhibit similar pK_a values as reduced AM and, thus, is partially deprotonated at neutral pH. As a consequence of the negatively charged DNA backbone, electrostatic repulsion forces may facilitate de-intercalation of DM. If the working temperature was selected to such that the hybridised state was only maintained by intercalation of the duplex-stabilising oxidised DM, reduction of DM would result in denaturation of dsDNA. This consideration was exactly observed in this study (Figure 5.9). The importance of electrostatic repulsion forces can be realised from the alkaline denaturation of DNA as discussed in Section 3.3.2, but also from an electrochemistry-based intercalation study by Wong and co-workers.[245] Positively and negatively charged intercalators were explored for the electrochemical detection of hybridised synthetic 20mer DNA oligonucleotides on a gold electrode surface. Whereas intercalation was eventually observed for all intercalators, the negatively charged intercalators anthraquinone-2,6-disulfonic acid and anthraquinone-2-sulfonic acid required up to three and six hours, respectively, to bind to DNA. This observation was attributed to electrostatic repulsion forces between the intercalator and the negatively charged DNA. However, the postulated underlying mechanism for electrochemically controlled reversible DNA hybridisation is based on the pK_a values of different functional groups of the DM. It is therefore worth noting that, upon investigating intercalation of the ethidium bromide analogue 3,8-diamino-6-phenyl-phenanthridine, Jones and Wilson observed a shift in the pK_a of the ligand as a function the ionic strength upon binding to DNA.[294] The impact of this finding may be essential in order to understand the system properly.

It is evident that further investigation is required in order to give a reasonable explanation to the underlying mechanism for the observed electrochemically controlled DNA denaturation and renaturation. For example, dissecting the

associated free energy, according to Eq. (1.10), with the postulated de-intercalation process above may be very useful in understanding the exact forces which are driving the process. Furthermore, conducting for example molecular dynamics modelling studies would likewise illuminate the underlying mechanism. Nonetheless, in agreement with the results in Chapter 4, on the impact of oxidised and chemically reduced DM on DNA, the findings in this Chapter likewise provided further evidence for hypothesis of this study. Results clearly indicated that, at an appropriate working temperature, DM evidently bound differently to dsDNA depending on its redox-state. The stability of dsDNA was affected which was reflected in achieving cyclic DNA denaturation and renaturation.

5.4 Summary

In this Chapter, the electrochemical behaviour of DM was characterised as a $2e^-$, $2H^+$ complicated semi-reversible redox reaction. However, redox potentials were identified which permitted the complete reduction and re-oxidation of DM. This was confirmed using *in situ* UV–vis spectroelectrochemistry. An NMR investigation on the stability of DM confirmed that redox cycling did not cause decomposition of the compound. Finally the proof-of-principle of isothermal, electrochemical control of reversible DNA hybridisation, by redox-state switching of DM, was demonstrated. By means of two independent techniques, *in situ* UV–vis and CD spectroelectrochemistry, and three experimental conditions, five cycles of denaturation and renaturation were achieved at 144 s/cycle. Furthermore it was shown that 57–80 % of the total amount of DNA was under electrochemical control. Indeed, this exemplification further verified the hypothesis of this Thesis. That is, depending on the redox-state, DM binds differently to dsDNA which produces a difference in the stabilisation of the double helix. This was reflected in repeated cycles of denaturation and renaturation of dsDNA. Lastly, gel electrophoretic studies confirmed that DNA remained intact. With regards to available literature and theoretical considerations, a hypothesis based on the protonation state and net charge of DM was provided for the underlying mechanism of this alternative, novel method to control the conformation of DNA.

Chapter 6

Conclusion and Outlook

Denaturation and renaturation, the reversible interconversion between double and single stranded DNA, is essential to many nucleic acid-based technologies and applications relevant for molecular diagnostics. Owing to its importance, there is a fundamental interest in gaining an in depth understanding of what governs the behaviour of reversible hybridisation of DNA through the investigation and development of methods that control and alter this process. In conjunction, due to increasing demands on decentralised molecular diagnostics testing, a focus towards miniaturisation and integration of conventional laboratory operations, such as nucleic acid amplification, into automated portable bioanalytical systems has emerged. However, many nucleic-acid based molecular technologies, especially amplification strategies, rely on precise control of elevated temperatures for reversible DNA hybridisation. Integration of such technologies into miniaturised bioanalytical systems has proven challenging in terms of energy consumption, cost and various technical issues. In contrast, enabling simpler and faster operations suitable for miniaturisation and integration, electrochemistry-based sensing has presented invaluable advantages for the development of POCT platforms. Therefore, substituting thermal control of reversible DNA hybridisation to isothermal, electrochemical control opens the prospect of miniaturisation and integration for the development of truly decentralised nucleic-acid based

diagnostics platforms. Thus far, alternative approaches described for the control of reversible DNA hybridisation have not been successful at achieving fast, isothermal electrochemical control without imposing dramatic changes and modifications in the solution environment and of the DNA. Therefore, this Thesis has demonstrated the proof-of-principle of an isothermal method which relies on electrochemical control of reversible DNA hybridisation by means of electroactive DNA intercalators. This novel method was based on the hypothesis that the oxidised form of the electroactive intercalator binds differently to duplex DNA compared to the reduced form. It was further hypothesised to affect the stability of duplex DNA, which would be expressed as an altered association constant and, thus, facilitate the reversible denaturation and renaturation of DNA.

This Conclusion will first provide a synthesis of key findings to provide evidence for the proof-of-principle and the hypothesis. Technical limitations and implications of the developed method are then highlighted in their own sections. Finally, an overview of key aspects to be considered for future research is provided along with a final statement.

6.1 Demonstration of the Proof-of-Principle

This Thesis has demonstrated an alternative method to control the fundamental process of the reversible interconversion between dsDNA and ssDNA. Based on electrochemistry, this isothermal approach made use of switching the redox-state of an electroactive DNA intercalator to drive cycles of denaturation and renaturation. In order to exemplify this alternative method (Chapter 5), a model system of short (20mer and 40mer) complementary DNA oligonucleotides was used. Selection of a suitable intercalator and establishment of important experimental conditions were addressed in Chapter 3, Chapter 4 and Chapter 5. While DM was selected as the most suitable intercalator, conditions such as working temperature of the system and optimal redox potentials for the complete reduction/oxidation of DM were additionally determined.

Renaturation is thermodynamically favourable and occurs spontaneously at ambient temperatures; denaturation is a thermodynamically unfavourable process and does not occur spontaneously. It was therefore important to establish conditions in which one of the processes was favoured only as a result of the redox-state of the intercalator. Thus, based on the melting temperature of duplex DNA in the presence of oxidised and chemically reduced DM determined via absorbance-based melting curve analysis (Section 4.2.4.2), the working temperature of the system was established. This permitted a condition where DNA remained hybridised due to the presence of oxidised DM and entered a denatured state due to the presence of reduced DM. A thermodynamic evaluation at this condition provided strong initial evidence for the hypothesis of this Thesis. In presence of oxidised DM, a large association constant for duplex DNA was revealed. However, in the presence of reduced DM, an association constant of duplex DNA was revealed that was significantly decreased over several orders of magnitude. Since intercalation was demonstrated as the binding mode of oxidised DM (Section 4.2.1), results strongly indicated a difference in the binding of reduced DM owing to the dramatic decrease in the association constant.

Similarly, this was aimed to be achieved electrochemically. That is, by applying an electrochemical trigger (reduction of DM) the thermodynamic stability of the duplex DNA would decrease, which would result in dissociation into single strands. Upon reverting the electrochemical trigger (re-oxidation of DM), the thermodynamic stability of the duplex DNA would be re-established, which would result in association of single strands. Isothermal, electrochemical control of reversible DNA hybridisation, by redox-state switching of DM, was demonstrated by means of *in situ* UV–vis spectroelectrochemistry and validated by *in situ* CD spectroelectrochemistry as a second independent technique (Section 5.2.2 and Section 5.2.3). Results strongly indicated that, at the identified working temperature, denaturation was induced by the reduced form of DM while renaturation was facilitated by the oxidised form. This was in complete accordance with the association constant of dsDNA in the presence of oxidised and chemically reduced DM. Five reproducible cycles (144 s/cycle) of denaturation and renaturation of DNA, at three different experimental conditions, demonstrated robustness of the

method. Furthermore, while several publications have reported on stability issues with DM and damaging of DNA as a result of reduction and oxidation of DM, NMR (Section 5.2.1.3) and gel electrophoretic (Section 5.2.2) analysis strongly indicated that no decomposition of DM or degradation of DNA occurred in this study. Thus, by exemplifying isothermal, electrochemical control of reversible DNA hybridisation, final proof of the hypothesis was provided. Oxidised DM bound differently to reduced DM, which affected the stability of the duplex DNA. This was expressed as an altered association constant which evidently facilitated the reversible denaturation and renaturation of DNA.

In contrast to previous studies on alternative non-thermal based approaches,[116-119] the method presented in this Thesis relied on an electrochemical principle for the control of reversible DNA hybridisation. The original approach presented proved faster and more importantly did not require dramatic changes in the solution composition or covalent modification of the DNA. Feasibility under isothermal conditions in a buffered medium without causing DNA degradation, the method presented in this Thesis offers a viable solution to replace thermal control with electrochemical control of the reversible interconversion between dsDNA and ssDNA in many nucleic acid hybridisation-based molecular biology techniques such as nucleic acid amplification.

6.2 Limitations of the Proof-of-Principle

The behaviour of duplex DNA in the *in situ* spectroelectrochemical measurements corresponded well with the calculated association constant of duplex DNA in the presence of oxidised and chemically reduced DM. However, the association constant was obtained from the thermodynamic parameters which were determined on the basis of van't Hoff analysis. Considering it is a model-dependent method which requires the assumption of two-state melting (all DNA is either denatured or hybridised), it generally only holds true for short DNA strands (< 20 bp). Thus, it would be of relevance to use a model-independent method, such as calorimetry, for the determination of more robust thermodynamic parameters for all lengths of

DNA. Moreover, despite agreement between two techniques, it would be useful to characterise these parameters in the presence of electrochemically reduced DM rather than chemically reduced DM. Chemical reduction of DM was chosen since the technique used for determination of these parameters would have required a prolonged exposure (> 3 h) to a reduction potential which was not desirable.

Also worth highlighting were the unconventional acquisition parameters (low response time and fast scan rate) used for the *in situ* CD spectroelectrochemical measurements, which clearly affected the resolution of the data. While agreement of the behaviour of DNA was observed between the two *in situ* spectroelectrochemical techniques, to increase the strength of the proof-of-principle, validation using a third technique such as *in situ* fluorescence spectroelectrochemistry would be of interest. Lastly, while not inhibiting the electrochemical control of reversible DNA hybridisation, results indicated potential adsorption of DM to the electrode (Section 5.3.1.2). This may have affected the efficiency of the process and, therefore, it would be relevant to investigate different electrode materials or surface modification strategies.

Currently electrochemically controlled denaturation and renaturation has only been demonstrated with short DNA oligonucleotides (20mer and 40mer). Moreover, it is only achieved at an elevated temperature around 60 °C. Furthermore, this working temperature is specific for each condition investigated, as it is based on the melting temperature of the DNA oligonucleotides. Thus, for the application of the method, it will be of vital relevance to address the challenge of longer DNA strands. This will however naturally affect the working temperature of the method, since longer DNA strands will have higher melting temperatures. Although, it is anticipated that this would not result in a higher working temperature than 95 °C, which is the maximum denaturation temperature used in e.g. nucleic acid amplification protocols. Thus, it is evident that addressing the challenge of a lower working temperature is equally essential for the application of the method, but also for making it more energy efficient.

6.3 Implications of the Proof-of-Principle

The novel concept presented in this Thesis addresses an important challenge in the development of truly decentralised nucleic acid-based diagnostic platforms. Miniaturisation and integration of nucleic acid-based molecular technologies, such as nucleic acid amplification strategies, that rely on the precise control of various elevated temperatures for achieving reversible DNA hybridisation, has proven challenging. In contrast, the isothermal concept presented in this Thesis is relieved from the need of repeated cycling of large intervals of elevated temperatures. It is rather based on the original approach of controlling cycles of denaturation and renaturation by means of electrochemistry. Exploiting redox-state switching of DM for electrochemical control, the novel concept presented in this Thesis has great potential to simplify miniaturisation and integration of, for example, nucleic acid amplification which is an integral technology in the field *in vitro* molecular diagnostics. At this stage, compared to a number of existing chip-based miniaturised nucleic acid amplification systems, either incorporating conventional PCR[79, 85, 86] or isothermal-based amplification protocols,[94, 261] the cycle time in the presented method is quite long and thus requires to be addressed in future experiments. Furthermore, in order to lower the power consumption, which is of great relevance for portable molecular diagnostics systems, the working temperature of the method needs to be addressed as well as the length of the DNA strands (see Section 6.2). Nevertheless, no covalent modification of DNA is required, which simplifies the system. Additionally, no dramatic changes in the solution conditions are inflicted, as feasibility in a buffered medium was demonstrated. This is critical since many conventional biomolecular techniques require buffered medium for the optimum performance of various components, such as enzymes[295] or fluorescent labels.[168]

Whereas the immediate application from this new concept may be nucleic acid amplification, it must be emphasised that the reversible process addressed in this Thesis is fundamental to nearly all nucleic acid-based technologies. As such it may provide an alternative solution to control hybridisation events associated with DNA microarrays, next generation sequencing and biosensors as well. Furthermore,

bearing in mind that DM is an antibiotic anthracycline with important antitumor activity, the observed *in vivo* cardiotoxicity potentially arising from the reduction of DM has been a subject for research over the past three decades. Thus, elucidation of the underlying mechanism of the interconversion of dsDNA and ssDNA and further characterisation of the interaction between reduced/oxidised DM with DNA may potentially provide valuable insights for the *in vivo* mechanism of the DM-DNA interaction.

6.4 Future Work

Considering that the electrochemically controlled reversible DNA hybridisation was demonstrated in a model system using short DNA oligonucleotides and a simple buffer, an immediate course of action will be to investigate the feasibility and reproducibility of the method using longer DNA strands and more complex buffers. As this will be of relevance for the future application, DNA strands longer than 100 bp and buffers commonly used for standard nucleic acid amplification reactions, such as PCR, will be examined.

The near future will involve implementation of the concept in this Thesis for the development of electrochemically controlled nucleic acid amplification. While feasibility of electrochemically controlled reversible DNA hybridisation in more complex buffers will be investigated, it will be of equal relevance to investigate the simplification of standard nucleic acid amplification protocols, such as PCR. This will additionally involve identifying or designing a dedicated robust electrochemical cell which permits amplification and easy recovery of sample for further processing, such as purification and detection using e.g. gel electrophoresis.

Future work will also include further investigation and characterisation of the underlying mechanism of electrochemical control of reversible DNA hybridisation, which currently is not well-understood. While a mechanism was postulated based on previous literature and theories (Section 5.3.3), validation and confirmation has not been pursued thus far. This would be of great relevance especially for the

optimisation of the method, such as investigating different conditions, more complex environments or different intercalators. While further experiments such as characterising the binding of reduced DM to DNA using e.g. calorimetry is of importance, further investigation using molecular dynamics modelling would provide invaluable insights for unravelling the mechanism.

6.5 Concluding Statement

This Thesis demonstrated the proof-of-principle of an alternative isothermal method for controlling the reversible DNA hybridisation. Achieving cycles of denaturation and renaturation of DNA on the basis of an electrochemical trigger provides an original contribution to the existing knowledge and understanding of the control of the reversible interconversion between dsDNA and ssDNA. This has moreover significant translational value since a reaction process was addressed which is fundamental to a plethora of nucleic acid-based technologies and applications targeting molecular diagnostics. Electrochemical control of reversible DNA hybridisation, by redox-state switching of DM, was demonstrated under three experimental conditions using two independent techniques. Substituting cycles of elevated temperatures for isothermal, electrochemical control opens the prospect of an electrochemically controlled nucleic acid amplification technology. Although slower than existing conventional techniques and currently requiring an increased constant solution temperature for reversible DNA hybridisation, feasibility in buffered medium was shown and no modification of the DNA was required. Owing to its isothermal and electrochemical nature, the novel concept presented in this Thesis has great potential to simplify the development of truly decentralised nucleic acid-based molecular diagnostics platforms.

Chapter 7

References

1. Bloomfield, V.A., Crothers, D.M. & Tinoco Jr., I. Nucleic acids: structures, properties, and functions. (University Science Books, Sausalito, CA; 2000). pp. 489-500.
2. Watson, J.D. & Crick, F.H.C. Molecular structure of nucleic acids. A structure for deoxyribose nucleic acid. *Nature* **171**, 737-738 (1953).
3. Syed, S.N., Schulze, H., Macdonald, D., Crain, J., Mount, A.R. & Bachmann, T.T. Cyclic denaturation and renaturation of double-stranded DNA by redox-state switching of DNA intercalators. *J. Am. Chem. Soc.* **135**, 5399-5407 (2013).
4. Kornyshev, A., Lee, D., Leikin, S. & Wynveen, A. Structure and interactions of biological helices. *Rev. Mod. Phys.* **79**, 943-996 (2007).
5. Wilkins, M.H.F., Stokes, A.R. & Wilson, H.R. Molecular structure of deoxypentose nucleic acids. *Nature* **171**, 738-740 (1953).
6. Franklin, R.E. & Gosling, R.G. Molecular configuration in sodium thymonucleate. *Nature* **171**, 740-741 (1953).
7. Chargaff, E. Chemical specificity of nucleic acids and mechanism of their enzymatic degradation. *Experientia* **6**, 201-209 (1950).
8. Berg, J.M., Tymoczko, J.L. & Stryer, L. Biochemistry, Edn. 5th. (W. H. Freeman and Company, New York; 2002).
9. Saenger, W. Principles of nucleic acid structure. (Springer-Verlag, New York; 1984).
10. Ghosh, A. & Bansal, M. A glossary of DNA structures from A to Z. *Acta Crystallogr., Sect. D: Biol. Crystallogr.* **59**, 620-626 (2003).

11. Zimmerman, S.B. The three-dimensional structure of DNA. *Annu. Rev. Biochem.* **51**, 395-427 (1982).

12. Edwards, K.J., Brown, D.G., Spink, N., Skelly, J.V. & Neidle, S. Molecular structure of the B-DNA dodecamer d(CGCAAATTTGCG)2. An examination of propeller twist and minor-groove water structure at 2.2 A resolution. *J. Mol. Biol.* **226**, 1161-1173 (1992).

13. Yakovchuk, P., Protozanova, E. & Frank-Kamenetskii, M.D. Base-stacking and base-pairing contributions into thermal stability of the DNA double helix. *Nucleic Acids Res.* **34**, 564-574 (2006).

14. Kool, E.T. Hydrogen bonding, base stacking, and steric effects in DNA replication. *Annu. Rev. Biophys. Biomol. Struct.* **30**, 1-22 (2001).

15. Petersheim, M. & Turner, D.H. Base-stacking and base-pairing contributions to helix stability: thermodynamics of double-helix formation with CCGG, CCGGp, CCGGAp, ACCGGp, CCGGUp, and ACCGGUp. *Biochemistry* **22**, 256-263 (1983).

16. Hunter, C.A. Sequence-dependent DNA structure. The role of base stacking interactions. *J. Mol. Biol.* **230**, 1025-1054 (1993).

17. Guckian, K.M., Schweitzer, B.A., Ren, R.X.F., Sheils, C.J., Tahmassebi, D.C. & Kool, E.T. Factors contributing to aromatic stacking in water: evaluation in the context of DNA. *J. Am. Chem. Soc.* **122**, 2213-2222 (2000).

18. Luo, R., Gilson, H.S., Potter, M.J. & Gilson, M.K. The physical basis of nucleic acid base stacking in water. *Biophys. J.* **80**, 140-148 (2001).

19. Newcomb, L.F. & Gellman, S.H. Aromatic stacking interactions in aqueous solution: evidence that neither classical hydrophobic effects nor dispersion forces are important. *J. Am. Chem. Soc.* **116**, 4993-4994 (1994).

20. SantaLucia, J., Jr., Allawi, H.T. & Seneviratne, P.A. Improved nearest-neighbor parameters for predicting DNA duplex stability. *Biochemistry* **35**, 3555-3562 (1996).

21. Saiki, R.K., Gelfand, D.H., Stoffel, S., Scharf, S.J., Higuchi, R., Horn, G.T., Mullis, K.B. & Erlich, H.A. Primer-directed enzymatic amplification of DNA with a thermostable DNA polymerase. *Science* **239**, 487-491 (1988).

22. Wiedmann, M., Wilson, W.J., Czajka, J., Luo, J., Barany, F. & Batt, C.A. Ligase chain reaction (LCR)--overview and applications. *PCR Methods Appl.* **3**, S51-S64 (1994).

23. Bier, F.F., von Nickisch-Rosenegk, M., Ehrentreich-Forster, E., Reiss, E., Henkel, J., Strehlow, R. & Andresen, D. DNA microarrays. *Adv. Biochem. Eng. Biotechnol.* **109**, 433-453 (2008).

24. Southern, E., Mir, K. & Shchepinov, M. Molecular interactions on microarrays. *Nat. Genet.* **21**, 5-9 (1999).

25. Metzker, M.L. Sequencing technologies - the next generation. *Nat. Rev. Genet.* **11**, 31-46 (2010).

26. Drummond, T.G., Hill, M.G. & Barton, J.K. Electrochemical DNA sensors. *Nat. Biotechnol.* **21**, 1192-1199 (2003).

27. Cagnin, S., Caraballo, M., Guiducci, C., Martini, P., Ross, M., Santa Ana, M., Danley, D., West, T. & Lanfranchi, G. Overview of electrochemical DNA biosensors: New approaches to detect the expression of life. *Sensors* **9**, 3122-3148 (2009).

28. Sambriski, E.J., Schwartz, D.C. & de Pablo, J.J. A mesoscale model of DNA and its renaturation. *Biophys. J.* **96**, 1675-1690 (2009).

29. Wetmur, J.G. Hybridization and renaturation kinetics of nucleic acids. *Annu. Rev. Biophys. Bioeng.* **5**, 337-361 (1976).

30. Sambriski, E.J., Schwartz, D.C. & de Pablo, J.J. Uncovering pathways in DNA oligonucleotide hybridization via transition state analysis. *Proc. Natl. Acad. Sci. USA* **106**, 18125-18130 (2009).

31. Kafri, Y., Mukamel, D. & Peliti, L. Why is the DNA denaturation transition first order? *Phys. Rev. Lett.* **85**, 4988-4991 (2000).

32. Richard, C. & Guttmann, A.J. Poland–Scheraga models and the DNA denaturation transition. *Journal of Statistical Physics* **115**, 925-947 (2004).

33. Record, M.T. & Zimm, B.H. Kinetics of the helix-coil transition in DNA. *Biopolymers* **11**, 1435-1484 (1972).

34. Blake, R.D. & Delcourt, S.G. Thermal stability of DNA. *Nucleic Acids Res.* **26**, 3323-3332 (1998).

35. Marky, L.A. & Breslauer, K.J. Calculating thermodynamic data for transitions of any molecularity from equilibrium melting curves. *Biopolymers* **26**, 1601-1620 (1987).

36. Mergny, J.L. & Lacroix, L. Analysis of thermal melting curves. *Oligonucleotides* **13**, 515-537 (2003).

37. Murugan, R. Revised theory on DNA renaturation kinetics and its experimental verification. *Biochem. Biophys. Res. Commun.* **293**, 870-873 (2002).

38. Manning, G.S. The molecular theory of polyelectrolyte solutions with applications to the electrostatic properties of polynucleotides. *Q. Rev. Biophys.* **11**, 179-246 (1978).

39. Record, M.T., Jr., Anderson, C.F. & Lohman, T.M. Thermodynamic analysis of ion effects on the binding and conformational equilibria of proteins and nucleic acids: the roles of ion association or release, screening, and ion effects on water activity. *Q. Rev. Biophys.* **11**, 103-178 (1978).

40. Fixman, M. The Poisson--Boltzmann equation and its application to polyelectrolytes. *J. Chem. Phys.* **70**, 4995-5005 (1979).

41. Tan, Z.-J. & Chen, S.-J. Nucleic acid helix stability: effects of salt concentration, cation valence and size, and chain length. *Biophys. J.* **90**, 1175-1190 (2006).

42. Stigter, D. Evaluation of the counterion condensation theory of polyelectrolytes. *Biophys. J.* **69**, 380-388 (1995).

43. Fenley, M.O., Manning, G.S. & Olson, W.K. Approach to the limit of counterion condensation. *Biopolymers* **30**, 1191-1203 (1990).

44. Hagerman, P.J. Flexibility of DNA. *Annu. Rev. Biophys. Biophys. Chem.* **17**, 265-286 (1988).

45. Anderson, C.F. & Record, M.T. Polyelectrolyte theories and their applications to DNA. *Annu. Rev. Phys. Chem.* **33**, 191-222 (1982).

46. Record, M.T. Effects of Na+ and Mg++ ions on the helix–coil transition of DNA. *Biopolymers* **14**, 2137-2158 (1975).

47. Manning, G.S. Electrostatic free energy of the DNA double helix in counterion condensation theory. *Biophys. Chem.* **101-102**, 461-473 (2002).

48. Singleton, M.R., Dillingham, M.S. & Wigley, D.B. Structure and mechanism of helicases and nucleic acid translocases. *Annu. Rev. Biochem.* **76**, 23-50 (2007).

49. Ageno, M., Dore, E. & Frontali, C. The alkaline denaturation of DNA. *Biophys. J.* **9**, 1281-1311 (1969).

50. Lando, D., Haroutiunian, S.G., Kul'ba, A.M., Dalian, E.B., Orioli, P., Mangani, S. & Akhrem, A.A. Theoretical and experimental study of DNA helix-coil transition in acidic and alkaline medium. *J. Biomol. Struct. Dyn.* **12**, 355-366 (1994).

51. Hutton, J.R. Renaturation kinetics and thermal stability of DNA in aqueous solutions of formamide and urea. *Nucleic Acids Res.* **4**, 3537-3555 (1977).

52. Blake, R.D. & Delcourt, S.G. Thermodynamic effects of formamide on DNA stability. *Nucleic Acids Res.* **24**, 2095-2103 (1996).

53. Markarian, S.A., Asatryan, A.M., Grigoryan, K.R. & Sargsyan, H.R. Effect of diethylsulfoxide on the thermal denaturation of DNA. *Biopolymers* **82**, 1-5 (2006).

54. Owczarzy, R. Melting temperatures of nucleic acids: discrepancies in analysis. *Biophys. Chem.* **117**, 207-215 (2005).

55. Owczarzy, R., You, Y., Moreira, B.G., Manthey, J., Huang, L., Behlke, M. & Walder, J. Effects of sodium ions on DNA duplex oligomers: improved predictions of melting temperatures. *Biochemistry* **43**, 3537-3554 (2004).

56. SantaLucia, J. A unified view of polymer, dumbbell, and oligonucleotide DNA nearest-neighbor thermodynamics. *Proc. Natl. Acad. Sci. USA* **95**, 1460-1465 (1998).

57. Owczarzy, R., Moreira, B.G., You, Y., Behlke, M. & Walder, J. Predicting stability of DNA duplexes in solutions containing magnesium and monovalent cations. *Biochemistry* **47**, 5336-5353 (2008).

58. Breslauer, K.J., Frank, R., Blöcker, H. & Marky, L.A. Predicting DNA duplex stability from the base sequence. *Proc. Natl. Acad. Sci. USA* **83**, 3746-3750 (1986).

59. Marmur, J. & Doty, P. Determination of the base composition of deoxyribonucleic acid from its thermal denaturation temperature. *J. Mol. Biol.* **5**, 109-118 (1962).

60. Yanson, I.K., Teplitsky, A.B. & Sukhodub, L.F. Experimental studies of molecular interactions between nitrogen bases of nucleic acids. *Biopolymers* **18**, 1149-1170 (1979).

61. Arora, N. & Jayaram, B. Energetics of base pairs in B-DNA in solution: an appraisal of potential functions and dielectric treatments. *J. Phys. Chem. B* **102**, 6139-6144 (1998).

62. Delcourt, S.G. & Blake, R.D. Stacking energies in DNA. *J. Biol. Chem.* **266**, 15160-15169 (1991).

63. Owczarzy, R., Vallone, P.M., Gallo, F.J., Paner, T.M., Lane, M.J. & Benight, A.S. Predicting sequence-dependent melting stability of short duplex DNA oligomers. *Biopolymers* **44**, 217-239 (1997).

64. Schildkraut, C. & Lifson, S. Dependence of the melting temperature of DNA on salt concentration. *Biopolymers* **3**, 195-208 (1965).

65. Scheffler, I.E., Elson, E.L. & Baldwin, R.L. Helix formation by d(TA) oligomers: II. Analysis of the helix-coil transitions of linear and circular oligomers. *J. Mol. Biol.* **48**, 145-171 (1970).

66. Nakano, S., Fujimoto, M., Hara, H. & Sugimoto, N. Nucleic acid duplex stability: influence of base composition on cation effects. *Nucleic Acids Res.* **27**, 2957-2965 (1999).

67. Williams, A.P., Longfellow, C.E., Freier, S.M., Kierzek, R. & Turner, D.H. Laser temperature-jump, spectroscopic, and thermodynamic study of salt effects on duplex formation by dGCATGC. *Biochemistry* **28**, 4283-4291 (1989).

68. Record, M.T., Jr., Zhang, W. & Anderson, C.F. Analysis of effects of salts and uncharged solutes on protein and nucleic acid equilibria and processes: a practical guide to recognizing and interpreting polyelectrolyte effects, Hofmeister effects, and osmotic effects of salts. *Adv. Protein Chem.* **51**, 281-353 (1998).

69. Venner, H. & Zimmer, C. Studies on nucleic acids. VIII. Changes in the stability of DNA secondary structure by interaction with divalent metal ions. *Biopolymers* **4**, 321-335 (1966).

70. Misra, V.K. & Draper, D.E. On the role of magnesium ions in RNA stability. *Biopolymers* **48**, 113-135 (1998).

71. Korolev, N., Lyubartsev, P. & Nordenskiöld, L. Application of polyelectrolyte theories for analysis of DNA melting in the presence of Na+ and Mg2+ ions. *Biophys. J.* **75**, 3041-3056 (1998).

72. Luo, X. & Hsing, I.M. Electrochemical techniques on sequence-specific PCR amplicon detection for point-of-care applications. *Analyst* **134**, 1957-1964 (2009).

73. Niemz, A., Ferguson, T.M. & Boyle, D.S. Point-of-care nucleic acid testing for infectious diseases. *Trends Biotechnol.* **29**, 240-250 (2011).

74. Craw, P. & Balachandran, W. Isothermal nucleic acid amplification technologies for point-of-care diagnostics: A critical review. *Lab. Chip* (2012).

75. Foudeh, A.M., Fatanat Didar, T., Veres, T. & Tabrizian, M. Microfluidic designs and techniques using lab-on-a-chip devices for pathogen detection for point-of-care diagnostics. *Lab. Chip*, 3249-3266 (2012).

76. Lee, S.J. & Lee, S.Y. Micro total analysis system (micro-TAS) in biotechnology. *Appl. Microbiol. Biotechnol.* **64**, 289-299 (2004).

77. Asiello, P.J. & Baeumner, A.J. Miniaturized isothermal nucleic acid amplification, a review. *Lab. Chip* **11**, 1420-1430 (2011).

78. Manz, A., Graber, N. & Widmer, H.M. Miniaturized total chemical analysis systems: a novel concept for chemical sensing. *Sens. Actuators B Chem.* **1**, 244-248 (1990).

79. Zhang, Y. & Ozdemir, P. Microfluidic DNA amplification--a review. *Anal. Chim. Acta* **638**, 115-125 (2009).

80. Xu, X., Zhang, S., Chen, H. & Kong, J. Integration of electrochemistry in micro-total analysis systems for biochemical assays: Recent developments. *Talanta* **80**, 8-18 (2009).

81. Weigl, B., Domingo, G., Labarre, P. & Gerlach, J. Towards non- and minimally instrumented, microfluidics-based diagnostic devices. *Lab. Chip* **8**, 1999-2014 (2008).

82. Yager, P., Edwards, T., Fu, E., Helton, K., Nelson, K., Tam, M.R. & Weigl, B.H. Microfluidic diagnostic technologies for global public health. *Nature* **442**, 412-418 (2006).

83. Pai, N.P., Vadnais, C., Denkinger, C., Engel, N. & Pai, M. Point-of-care testing for infectious diseases: diversity, complexity, and barriers in low- and middle-income countries. *PLoS Med.* **9**, e1001306 (2012).

84. Zhang, C. & Xing, D. Miniaturized PCR chips for nucleic acid amplification and analysis: latest advances and future trends. *Nucleic Acids Res.* **35**, 4223-4237 (2007).

85. Kopp, M.U., de Mello, A.J. & Manz, A. Chemical amplification: continuous-flow PCR on a chip. *Science* **280**, 1046-1048 (1998).

86. Ahmad, F. & Hashsham, S.A. Miniaturized nucleic acid amplification systems for rapid and point-of-care diagnostics: A review. *Anal. Chim. Acta* **733**, 1-15 (2012).

87. Ferguson, B.S., Buchsbaum, S.F., Wu, T.T., Hsieh, K., Xiao, Y., Sun, R. & Soh, H.T. Genetic analysis of H1N1 influenza virus from throat swab samples in a microfluidic system for point-of-care diagnostics. *J. Am. Chem. Soc.* **133**, 9129-9135 (2011).

88. Easley, C.J., Karlinsey, J.M., Bienvenue, J.M., Legendre, L.A., Roper, M.G., Feldman, S.H., Hughes, M.A., Hewlett, E.L., Merkel, T.J., Ferrance, J.P. & Landers, J.P. A fully integrated microfluidic genetic analysis system with sample-in–answer-out capability. *Proc. Natl. Acad. Sci. USA* **103**, 19272-19277 (2006).

89. Oblath, E.A., Henley, W.H., Alarie, J.P. & Ramsey, J.M. A microfluidic chip integrating DNA extraction and real-time PCR for the detection of bacteria in saliva. *Lab. Chip* **13**, 1325-1332 (2013).

90. Kaigala, G.V., Huskins, R.J., Preiksaitis, J., Pang, X.L., Pilarski, L.M. & Backhouse, C.J. Automated screening using microfluidic chip-based PCR and product detection to assess risk of BK virus-associated nephropathy in renal transplant recipients. *Electrophoresis* **27**, 3753-3763 (2006).

91. Cepheid, http://www.cepheid.com/, *Accessed 16 November 2013*.

92. Zhang, C., Xu, J., Ma, W. & Zheng, W. PCR microfluidic devices for DNA amplification. *Biotechnol. Adv.* **24**, 243-284 (2006).

93. Yamanaka, K., Saito, M., Kondoh, K., Hossain, M.M., Koketsu, R., Sasaki, T., Nagatani, N., Ikuta, K. & Tamiya, E. Rapid detection for primary screening of influenza A virus: microfluidic RT-PCR chip and electrochemical DNA sensor. *Analyst* **136**, 2064-2068 (2011).

94. Fang, X., Liu, Y., Kong, J. & Jiang, X. Loop-mediated isothermal amplification integrated on microfluidic chips for point-of-care quantitative detection of pathogens. *Anal. Chem.* **82**, 3002-3006 (2010).

95. Gulliksen, A., Solli, L.A., Drese, K.S., Sorensen, O., Karlsen, F., Rogne, H., Hovig, E. & Sirevag, R. Parallel nanoliter detection of cancer markers using polymer microchips. *Lab. Chip* **5**, 416-420 (2005).

96. Sato, K., Tachihara, A., Renberg, B., Mawatari, K., Tanaka, Y., Jarvius, J., Nilsson, M. & Kitamori, T. Microbead-based rolling circle amplification in a microchip for sensitive DNA detection. *Lab. Chip* **10**, 1262-1266 (2010).

97. Ramalingam, N., San, T., Kai, T., Mak, M. & Gong, H.-Q. Microfluidic devices harboring unsealed reactors for real-time isothermal helicase-dependent amplification. *Microfluid. Nanofluid.* **7**, 325-336 (2009).

98. LaBarre, P., Hawkins, K.R., Gerlach, J., Wilmoth, J., Beddoe, A., Singleton, J., Boyle, D. & Weigl, B. A simple, inexpensive device for nucleic acid amplification without electricity-toward instrument-free molecular diagnostics in low-resource settings. *PLoS One* **6**, e19738-e19738 (2011).

99. Liu, C., Mauk, M.G., Hart, R., Qiu, X. & Bau, H.H. A self-heating cartridge for molecular diagnostics. *Lab. Chip* **11**, 2686-2692 (2011).

100. Liu, C., Geva, E., Mauk, M., Qiu, X., Abrams, W.R., Malamud, D., Curtis, K., Owen, S.M. & Bau, H.H. An isothermal amplification reactor with an integrated isolation membrane for point-of-care detection of infectious diseases. *Analyst* **136**, 2069-2076 (2011).

101. Gebala, M., Stoica, L., Neugebauer, S. & Schuhmann, W. Label-free detection of DNA hybridization in presence of intercalators using electrochemical impedance spectroscopy. *Electroanalysis* **21**, 325-331 (2009).

102. Erdem, A., Kerman, K., Meric, B. & Ozsoz, M. Methylene blue as a novel electrochemical hybridization indicator. *Electroanalysis* **13**, 219-223 (2001).

103. Corrigan, D.K., Schulze, H., Henihan, G., Ciani, I., Giraud, G., Terry, J.G., Walton, A.J., Pethig, R., Ghazal, P., Crain, J., Campbell, C.J., Mount, A.R. & Bachmann, T.T. Impedimetric detection of single-stranded PCR products derived from methicillin resistant *Staphylococcus aureus* (MRSA) isolates. *Biosens. Bioelectron.* **34**, 178-184 (2012).

104. Ronkainen, N.J., Halsall, H.B. & Heineman, W.R. Electrochemical biosensors. *Chem. Soc. Rev.* **39**, 1747-1763 (2010).

105. Marrazza, G., Chiti, G., Mascini, M. & Anichini, M. Detection of human apolipoprotein E genotypes by DNA electrochemical biosensor coupled with PCR. *Clin. Chem.* **46**, 31-37 (2000).

106. Ozsoz, M., Erdem, A., Kerman, K., Ozkan, D., Tugrul, B., Topcuoglu, N., Ekren, H. & Taylan, M. Electrochemical genosensor based on colloidal gold nanoparticles for the detection of Factor V Leiden mutation using disposable pencil graphite electrodes. *Anal. Chem.* **75**, 2181-2187 (2003).

107. Lai, R.Y., Lagally, E.T., Lee, S.-H., Soh, H.T., Plaxco, K.W. & Heeger, A.J. Rapid, sequence-specific detection of unpurified PCR amplicons via a reusable, electrochemical sensor. *Proc. Natl. Acad. Sci. USA* **103**, 4017-4021 (2006).

108. Ririe, K.M., Rasmussen, R.P. & Wittwer, C.T. Product differentiation by analysis of DNA melting curves during the polymerase chain reaction. *Anal. Biochem.* **245**, 154-160 (1997).

109. Tyagi, S. & Kramer, F.R. Molecular beacons: probes that fluoresce upon hybridization. *Nat. Biotechnol.* **14**, 303-308 (1996).

110. Livak, K.J., Flood, S.J., Marmaro, J., Giusti, W. & Deetz, K. Oligonucleotides with fluorescent dyes at opposite ends provide a quenched probe system useful for detecting PCR product and nucleic acid hybridization. *PCR Methods Appl.* **4**, 357-362 (1995).

111. Yeung, S.S.W., Lee, T.M.H. & Hsing, I.M. Electrochemical real-time polymerase chain reaction. *J. Am. Chem. Soc.* **128**, 13374-13375 (2006).

112. Yeung, S.S.W., Lee, T.M.H. & Hsing, I.M. Electrochemistry-based real-time PCR on a microchip. *Anal. Chem.* **80**, 363-368 (2008).

113. Deféver, T., Druet, M., Rochelet-Dequaire, M., Joannes, M., Grossiord, C., Limoges, B. & Marchal, D. Real-time electrochemical monitoring of the polymerase chain reaction by mediated redox catalysis. *J. Am. Chem. Soc.* **131**, 11433-11441 (2009).

114. Deféver, T., Druet, M., Evrard, D., Marchal, D. & Limoges, B. Real-time electrochemical PCR with a DNA intercalating redox probe. *Anal. Chem.*, 1815-1821 (2011).

115. Fang, T.H., Ramalingam, N., Xian-Dui, D., Ngin, T.S., Xianting, Z., Lai Kuan, A.T., Peng Huat, E.Y. & Hai-Qing, G. Real-time PCR microfluidic devices with concurrent electrochemical detection. *Biosens. Bioelectron.* **24**, 2131-2136 (2009).

116. Wang, Y.-C., Lin, C.-B., Su, J.-J., Ru, Y.-M., Wu, Q., Chen, Z.-B., Mao, B.-W. & Tian, Z.-W. Electrochemically-driven large amplitude pH cycling for acid-base driven DNA denaturation and renaturation. *Anal. Chem.* **83**, 4930-4935 (2011).

117. Liu, D. & Balasubramanian, S. A proton-fuelled DNA nanomachine. *Angew. Chem., Int. Ed.* **42**, 5734-5736 (2003).

118. Asanuma, H., Liang, X., Yoshida, T. & Komiyama, M. Photocontrol of DNA duplex formation by using azobenzene-bearing oligonucleotides. *ChemBioChem* **2**, 39-44 (2001).

119. Asanuma, H., Liang, X., Nishioka, H., Matsunaga, D., Liu, M. & Komiyama, M. Synthesis of azobenzene-tethered DNA for reversible photo-regulation of DNA functions: hybridization and transcription. *Nat. Protoc.* **2**, 203-212 (2007).

120. Nishioka, H., Liang, X., Kato, T. & Asanuma, H. A photon-fueled DNA nanodevice that contains two different photoswitches. *Angew. Chem. Int. Ed.* **51**, 1165-1168 (2012).

121. Dohno, C., Uno, S.-N. & Nakatani, K. Photoswitchable molecular glue for DNA. *J. Am. Chem. Soc.* **129**, 11898-11899 (2007).

122. Dohno, C. & Nakatani, K. Control of DNA hybridization by photoswitchable molecular glue. *Chem. Soc. Rev.* **40**, 5718-5729 (2011).

123. Andersson, J., Li, S., Lincoln, P. & Andreasson, J. Photoswitched DNA-binding of a photochromic spiropyran. *J. Am. Chem. Soc.* **130**, 11836-11837 (2008).

124. Hamad-Schifferli, K., Schwartz, J.J., Santos, A.T., Zhang, S. & Jacobson, J.M. Remote electronic control of DNA hybridization through inductive coupling to an attached metal nanocrystal antenna. *Nature* **415**, 152-155 (2002).

125. Ihmels, H. & Otto, D. Intercalation of organic dye molecules into double-stranded DNA general principles and recent developments. *Top. Curr. Chem.* **258**, 161-204 (2005).

126. Minotti, G., Menna, P., Salvatorelli, E., Cairo, G. & Gianni, L. Anthracyclines: molecular advances and pharmacologic developments in antitumor activity and cardiotoxicity. *Pharmacol. Rev.* **56**, 185-229 (2004).

127. Lepecq, J.B. & Paoletti, C. A fluorescent complex between ethidium bromide and nucleic acids: physical—chemical characterization. *J. Mol. Biol.* **27**, 87-106 (1967).

128. Farjami, E., Clima, L., Gothelf, K.V. & Ferapontova, E.E. DNA interactions with a methylene blue redox indicator depend on the DNA length and are sequence specific. *Analyst* **135**, 1443-1448 (2010).

129. Mao, Y., Luo, C. & Ouyang, Q. Studies of temperature-dependent electronic transduction on DNA hairpin loop sensor. *Nucleic Acids Res.* **31**, e108 (2003).

130. Friedman, R.A. & Manning, G.S. Polyelectrolyte effects on site-binding equilibria with application to the intercalation of drugs into DNA. *Biopolymers* **23**, 2671-2714 (1984).

131. Neto, B.A.D. & Lapis, A.A.M. Recent developments in the chemistry of deoxyribonucleic acid (DNA) intercalators: principles, design, synthesis, applications and trends. *Molecules* **14**, 1725-1746 (2009).

132. McGhee, J.D. & von Hippel, P.H. Theoretical aspects of DNA-protein interactions - cooperative and non-cooperative binding of large ligands to a one-dimensional homogeneous lattice. *J. Mol. Biol.* **86**, 469-489 (1974).

133. Scatchard, G. The attractions of proteins for small molecules and ions. *Ann. N. Y. Acad. Sci.* **51**, 660-672 (1949).

134. Adamcik, J., Valle, F., Witz, G., Rechendorff, K. & Dietler, G. The promotion of secondary structures in single-stranded DNA by drugs that bind to duplex DNA: an atomic force microscopy study. *Nanotechnology* **19**, 384016-384016 (2008).

135. Greschner, A.A., Bujold, K.E. & Sleiman, H.F. Intercalators as molecular chaperones in DNA self-assembly. *J. Am. Chem. Soc.* **135**, 11283-11288 (2013).

136. Teulade-Fichou, M.P., Fauquet, M., Baudoin, O., Vigneron, J.P. & Lehn, J.M. DNA double helix destabilizing properties of cyclobisintercaland compounds and competition with a single strand binding protein. *Bioorg. Med. Chem.* **8**, 215-222 (2000).

137. Long, E.C. & Barton, J.K. On demonstrating DNA intercalation. *Acc. Chem. Res.* **23**, 8-10 (1990).

138. Breslauer, K.J., Remeta, D.P., Chou, W.Y., Ferrante, R., Curry, J., Zaunczkowski, D., Snyder, J.G. & Marky, L.A. Enthalpy-entropy compensations in drug-DNA binding studies. *Proc. Natl. Acad. Sci. USA* **84**, 8922-8926 (1987).

139. Chaires, J.B. Energetics of drug – DNA interactions. *Biopolymers* **44**, 201-215 (1997).

140. Ren, J., Jenkins, T.C. & Chaires, J.B. Energetics of DNA intercalation reactions. *Biochemistry* **39**, 8439-8447 (2000).

141. Reha, D., Kabelac, M., Ryjacek, F., Sponer, J., Spooner, J.E., Elstner, M., Suhai, S. & Hobza, P. Intercalators. 1. Nature of stacking interactions between intercalators (ethidium, daunomycin, ellipticine, and 4',6-diaminide-2-phenylindole) and DNA base pairs. *Ab initio* quantum chemical, density functional theory, and empirical potential study. *J. Am. Chem. Soc.* **124**, 3366-3376 (2002).

142. Medhi, C., Mitchell, J.B., Price, S.L. & Tabor, A.B. Electrostatic factors in DNA intercalation. *Biopolymers* **52**, 84-93 (1999).

143. Haq, I. Thermodynamics of drug-DNA interactions. *Arch. Biochem. Biophys.* **403**, 1-15 (2002).

144. Qu, X. & Chaires, J.B. Hydration changes for DNA intercalation reactions. *J. Am. Chem. Soc.* **123**, 1-7 (2001).

145. Chaires, J.B., Dattagupta, N. & Crothers, D.M. Kinetics of the daunomycin--DNA interaction. *Biochemistry* **24**, 260-267 (1985).

146. Wilhelm, M., Mukherjee, A., Bouvier, B., Zakrzewska, K., Hynes, J.T. & Lavery, R. Multistep drug intercalation: molecular dynamics and free energy studies of the binding of daunomycin to DNA. *J. Am. Chem. Soc.* (2012).

147. Hossain, M. & Kumar, G.S. DNA intercalation of methylene blue and quinacrine: new insights into base and sequence specificity from structural and thermodynamic studies with polynucleotides. *Mol. BioSyst.* **5**, 1311-1322 (2009).

148. Rohs, R. & Sklenar, H. Methylene blue binding to DNA with alternating AT base sequence: minor groove binding is favored over intercalation. *J. Biomol. Struct. Dyn.* **21**, 699-711 (2004).

149. Tuite, E. & Nordén, B. Sequence-specific interactions of methylene blue with polynucleotides and DNA: a spectroscopic study. *J. Am. Chem. Soc.* **116**, 7548-7556 (1994).

150. Mudasir, Wahyuni, E.T., Tjahjono, D.H., Yoshioka, N. & Inoue, H. Spectroscopic studies on the thermodynamic and thermal denaturation of the ct-DNA binding of methylene blue. *Spectrochim. Acta. A. Mol. Biomol. Spectrosc.* **77**, 528-534 (2010).

151. Ju, H., Cai, C. & Chen, H. The electrochemical behaviour of methylene blue at a microcylinder carbon fiber electrode. *Electroanalysis* **7**, 1165-1169 (1995).

152. Tuite, E. & Kelly, J.M. The interaction of methylene blue, azure B, and thionine with DNA: Formation of complexes with polynucleotides and mononucleotides as model systems. *Biopolymers* **35**, 419-433 (1995).

153. Chang, T.C., Yang, Y.P., Huang, K.H., Chang, C.C. & Hecht, C. Investigation of thionin-DNA interaction by satellite hole spectroscopy. *Optics and Spectroscopy* **98**, 655-660 (2005).

154. Paul, P. & Kumar, G.S. Toxic interaction of thionine to deoxyribonucleic acids: elucidation of the sequence specificity of binding with polynucleotides. *J. Hazard. Mater.* **184**, 620-626 (2010).

155. Paul, P., Hossain, M., Yadav, R.C. & Kumar, G.S. Biophysical studies on the base specificity and energetics of the DNA interaction of photoactive dye thionine: spectroscopic and calorimetric approach. *Biophys. Chem.* **148**, 93-103 (2010).

156. Lozano, H.J., Garcia, B., Busto, N. & Leal, J.M. Interaction of thionine with triple-, double-, and single-stranded RNAs. *J. Phys. Chem. B* **117**, 38-48 (2013).

157. Chaires, J.B. in *Small molecule DNA and RNA binders: from synthesis to nucleic acid complexes*. (Eds. M. Demeunynck, C. Bailly & W.D. Wilson) Ch. 17, pp. 461-481 (Wiley-VCH Verlag GmbH & Co. KGaA, Weinheim, 2004).

158. Gewirtz, D.A. A critical evaluation of the mechanisms of action proposed for the antitumor effects of the anthracycline antibiotics adriamycin and daunorubicin. *Biochem. Pharmacol.* **57**, 727-741 (1999).

159. Quigley, G.J., Wangt, A.H.J., Ughettott, G., van der Marel, G., van Boom, J.H. & Rich, A. Molecular structure of an anticancer drug-DNA complex: daunomycin plus d(CpGpTpApCpG). *Proc. Natl. Acad. Sci. USA* **77**, 7204-7208 (1980).

160. Wang, A.H., Ughetto, G., Quigley, G.J. & Rich, A. Interactions between an anthracycline antibiotic and DNA: molecular structure of daunomycin complexed to d(CpGpTpApCpG) at 1.2-A resolution. *Biochemistry* **26**, 1152-1163 (1987).

161. Chaires, J.B., Dattagupta, N. & Crothers, D.M. Studies on interaction of anthracycline antibiotics and deoxyribonucleic acid: equilibrium binding studies on

interaction of daunomycin with deoxyribonucleic acid. *Biochemistry* **21**, 3933-3940 (1982).

162. Chaires, J.B., Fox, K.R., Herrera, J.E., Britt, M. & Waring, M.J. Site and sequence specificity of the daunomycin-DNA interaction. *Biochemistry* **26**, 8227-8236 (1987).
163. Guin, P.S., Das, S. & Mandal, P.C. Electrochemical reduction of quinones in different media: a review. *Int. J. Electrochem.* **2011**, 1-22 (2011).
164. Frederick, C.A., Williams, L.D., Ughetto, G., van der Marel, G.A., van Boom, J.H., Rich, A. & Wang, H.-J. Structural comparison of anticancer drug-DNA complexes: adriamycin and daunomycin. *Biochemistry* **29**, 2538-2549 (1990).
165. Ghosh, D., Hossain, M., Saha, C., Dey, S.K. & Kumar, G.S. Intercalation and induction of strand breaks by adriamycin and daunomycin: a study with human genomic DNA. *DNA Cell Biol.* **31**, 378-387 (2012).
166. Jaeger, J.A., Santalucia, J. & Tinoco, I. Determination of RNA structure and thermodynamics. *Annu. Rev. Biochem.* **62**, 255-287 (1993).
167. Puglisi, J.D. & Tinoco, I. Absorbance melting curves of RNA. *Methods Enzymol.* **180**, 304-325 (1989).
168. You, Y., Tataurov, A.V. & Owczarzy, R. Measuring thermodynamic details of DNA hybridization using fluorescence. *Biopolymers* **95**, 472-486 (2011).
169. Morrison, L.E. & Stols, L.M. Sensitive fluorescence-based thermodynamic and kinetic measurements of DNA hybridization in solution. *Biochemistry* **32**, 3095-3104 (1993).
170. Cardullo, R.A., Agrawal, S., Flores, C., Zamecnik, P.C. & Wolf, D.E. Detection of nucleic acid hybridization by nonradiative fluorescence resonance energy transfer. *Proc. Natl. Acad. Sci. USA* **85**, 8790-8794 (1988).
171. Marras, S.A.E. Interactive fluorophore and quencher pairs for labeling fluorescent nucleic acid hybridization probes. *Mol. Biotechnol.* **38**, 247-255 (2008).
172. Sjöback, R., Nygren, J. & Kubista, M. Absorption and fluorescence properties of fluorescein. *Spectrochim. Acta. A. Mol. Biomol. Spectrosc.* **51**, L7-L21 (1995).
173. Moreira, B.G., You, Y., Behlke, M.A. & Owczarzy, R. Effects of fluorescent dyes, quenchers, and dangling ends on DNA duplex stability. *Biochem. Biophys. Res. Commun.* **327**, 473-484 (2005).
174. Yoshida, W., Sode, K. & Ikebukuro, K. Aptameric enzyme subunit for biosensing based on enzymatic activity measurement. *Anal. Chem.* **78**, 3296-3303 (2006).
175. Mergny, J.L. & Lacroix, L. Kinetics and thermodynamics of i-DNA formation: phosphodiester versus modified oligodeoxynucleotides. *Nucleic Acids Res.* **26**, 4797-4803 (1998).

176. Kaim, W. & Fiedler, J. Spectroelectrochemistry: the best of two worlds. *Chem. Soc. Rev.* **38**, 3373-3382 (2009).

177. Keyes, T.E. & Forster, R.J. in *Handbook of Electrochemistry*. (Eds. C.G. Zoski) Ch. 14, pp. 591-635 (Elsevier, Amsterdam, 2007).

178. Kuwana, T. & Heineman, W.R. Study of electrogenerated reactants using optically transparent electrodes. *Acc. Chem. Res.* **9**, 241-248 (1976).

179. Neudeck, A., Marken, F. & Compton, R.G. in *Electroanalytical Methods: Guide to Experiments and Applications* Vol. 2. *UV/Vis/NIR Spectroelectrochemistry* (Eds. F. Scholz) Ch. II.6, pp. 179-200 (Springer, New York, 2010).

180. Anderson, J.L., Coury Jr., L.A. & Leddy, J. Dynamic electrochemistry: methodology and application. *Anal. Chem.* **72**, 4497-4520 (2000).

181. Holze, R. Surface and interface analysis: an electrochemists toolbox. (Springer Berlin Heidelberg, Berlin, Heidelberg; 2009).

182. Schroll, C.A., Chatterjee, S., Heineman, W.R. & Bryan, S.A. Thin-layer spectroelectrochemistry on an aqueous microdrop. *Electroanalysis* **24**, 1065-1070 (2012).

183. Zhu, Y., Cheng, G. & Dong, S. Digital simulation in a thin layer spectroelectrochemical cell with minigrid platinum electrode by microregion approximation explicit finite difference method. *Electroanalysis* **12**, 736-741 (2000).

184. Heineman, W.R. Spectroelectrochemistry - the combination of optical and electrochemical techniques. *J. Chem. Educ.* **60**, 305-308 (1983).

185. Schroll, C.A., Chatterjee, S., Heineman, W.R. & Bryan, S.A. Semi-infinite linear diffusion spectroelectrochemistry on an aqueous micro-drop. *Anal. Chem.* **83**, 4214-4219 (2011).

186. Bard, A.J. & Faulkner, L.R. Electrochemical Methods: Fundamentals and Applications, Edn. 2nd. (Wiley, New York; 2001).

187. Rodger, A. & Nordén, B. Circular dichroism and linear dichroism. (Oxford University Press, Oxford; 1997).

188. Pletcher, D. A first course in electrode processes. (Royal Society of Chemistry, Cambridge; 2009).

189. Dhungana, S. & Crumbliss, A.L. in *Spectroelectrochemistry*. *UV-Vis Spectroelectrochemistry of Selected Iron-Containing Proteins* (Eds. W. Kaim & K. Klein) Ch. 2, pp. 31-67 (The Royal Society of Chemistry, 2008).

190. IJ Cambria Scientific, http://www.ijcambria.com/, *Accessed 16 November 2013*.

191. Wilson, R.A., Pinyayev, T.S., Membreno, N. & Heineman, W.R. Rapid prototyped optically transparent thin-layer electrode holder for spectroelectrochemistry in bench-top spectrophotometers. *Electroanalysis* **22**, 2162-2166 (2010).

192. Xie, Y., Chen, T. & Dong, S. Influende on the thin layer spectroelectrochemistry: diffusion within a thin layer cell. *Electrochim. Acta* **40** (1995).

193. Zeman, S.M., Phillips, D.R. & Crothers, D.M. Characterization of covalent Adriamycin-DNA adducts. *Proc. Natl. Acad. Sci. USA* **95**, 11561-11565 (1998).

194. Seeman, N.C. DNA in a material world. *Nature* **421**, 427-431 (2003).

195. IDT Biophysics, http://biophysics.idtdna.com, *Accessed 16 November, 2013*.

196. Hong, J., Capp, M.W., Anderson, C.F., Saecker, R.M., Felitsky, D.J., Anderson, M.W. & Record, M.T. Preferential interactions of glycine betaine and of urea with DNA: Implications for DNA hydration and for effects of these solutes on DNA stability. *Biochemistry* **43**, 14744-14758 (2004).

197. Wetmur, J.G. & Davidson, N. Kinetics of renaturation of DNA. *J. Mol. Biol.* **31**, 349-370 (1968).

198. Bhattacharyya, a.J. & Feingold, M. Single molecule study of the reaction between DNA and formamide. *Talanta* **55**, 943-949 (2001).

199. Levine, L., Gordon, J.A. & Jencks, W.P. The relationship of structure to the effectiveness of denaturing agents for deoxyribonucleic acid. *Biochemistry* **2**, 168-175 (1963).

200. Hackl, E.V. & Blagoi, Y.P. Urea effect on Cu(2+)-induced DNA structural transitions in solution. *J. Inorg. Biochem.* **98**, 1911-1920 (2004).

201. Nordstrom, L.J., Clark, C.A., Andersen, B., Champlin, S.M. & Schwinefus, J.J. Effect of ethylene glycol, urea, and N-methylated glycines on DNA thermal stability: The role of DNA base pair composition and hydration. *Biochemistry* **45**, 9604-9614 (2006).

202. Guinn, E.J., Schwinefus, J.J., Cha, H.K., McDevitt, J.L., Merker, W.E., Ritzer, R., Muth, G.W., Engelsgjerd, S.W., Mangold, K.E., Thompson, P.J., Kerins, M.J. & Record, M.T. Quantifying functional group interactions that determine urea effects on nucleic acid helix formation. *J. Am. Chem. Soc.* **135**, 5828-5838 (2013).

203. Klump, H. & Burkart, W. Calorimetric measurements of the transition enthalpy of DNA in aqueous urea solutions. *Biochim. Biophys. Acta* **475**, 601-604 (1977).

204. Plum, G.E. & Breslauer, K.J. Thermodynamics of an intramolecular DNA triple helix: a calorimetric and spectroscopic study of the pH and salt dependence of thermally induced structural transitions. *J. Mol. Biol.* **248**, 679-695 (1995).

205. Ts'o, P.O.P. (Ed.) Basic principles in nucleic acid chemistry, Volume 1. (Academic Press, New York; 1974). pp. 462-463.

206. Rush, M.G. & Warners, C. Alkali denaturation of covalently closed circular duplex deoxyribonucleic acid. *J. Biol. Chem.* **245**, 2704-2708 (1970).

207. Klonis, N. & Sawyer, W.H. Spectral properties of the prototropic forms of fluorescein in aqueous solution. *J. Fluoresc.* **6**, 147-157 (1996).

208. Dubey, R.K. & Tripathi, D.N. A study of thermal denaturation/renaturation in DNA using laser light scattering: a new approach. *Indian J. Biochem. Biophys.* **42**, 301-307 (2005).

209. Lindahl, T. & Nyberg, B. Rate of depurination of native deoxyribonucleic acid. *Biochemistry* **11**, 3610-3618 (1972).

210. Jelen, F., Fojta, M. & Palecek, E. Voltammetry of native double-stranded, denatured and degraded DNAs. *J. Electroanal. Chem.* **427**, 49-56 (1997).

211. Suzuki, S., Kimura, T. & Saneyoshi, M. Characterization of DNA polymerase induced by salmon herpesvirus, oncorhynchus masou virus. *J. Gen. Virol.* **67**, 405-408 (1986).

212. Shkel, I.A. & Record, M.T., Jr. Effect of the number of nucleic acid oligomer charges on the salt dependence of stability (DeltaG 37degrees) and melting temperature (Tm): NLPB analysis of experimental data. *Biochemistry* **43**, 7090-7101 (2004).

213. Braunlin, W.H. & Bloomfield, V.A. Proton NMR study of the base-pairing reactions of d(GGAATTCC): salt effects on the equilibria and kinetics of strand association. *Biochemistry* **30**, 754-758 (1991).

214. Record, M.T. & Lohman, T.M. A semiempirical extension of polyelectrolyte theory to the treatment of oligoelectrolytes: application to oligonucleotide helix-coil transitions. *Biopolymers* **17**, 1101-1101 (1978).

215. Olmsted, M.C., Anderson, C.F. & Record, M.T., Jr. Monte Carlo description of oligoelectrolyte properties of DNA oligomers: range of the end effect and the approach of molecular and thermodynamic properties to the polyelectrolyte limits. *Proc. Natl. Acad. Sci. USA* **86**, 7766-7770 (1989).

216. Kozyavkin, S.A. & Lyubchenko, Y.L. The nonequilibrium character of DNA melting: effects of the heating rate on the fine structure of melting curves. *Nucleic Acids Res.* **12**, 4339-4349 (1984).

217. Rougée, M., Faucon, B., Mergny, J.L., Barcelo, F., Giovannangeli, C., Garestier, T. & Hélène, C. Kinetics and thermodynamics of triple-helix formation: effects of ionic strength and mismatches. *Biochemistry* **31**, 9269-9278 (1992).

218. Hoff, A.J. & Roos, A.L.M. Hysteresis of denaturation of DNA in the melting range. *Biopolymers* **11**, 1289-1294 (1972).

219. Chen, C., Wang, W., Wang, Z., Wei, F. & Zhao, X.S. Influence of secondary structure on kinetics and reaction mechanism of DNA hybridization. *Nucleic Acids Res.* **35**, 2875-2884 (2007).

220. Yin, Y. & Zhao, X.S. Kintecis and dynamics of DNA hybridization. *Acc. Chem. Res.* **44**, 1172-1181 (2011).

221. Unruh, J.R., Gokulrangan, G., Wilson, G.S. & Johnson, C.K. Fluorescence properties of fluorescein, tetramethylrhodamine and texas red linked to a DNA aptamer. *Photochem. Photobiol.* **81**, 682-690 (2005).

222. Lerman, L.S. Structural considerations in the interaction of DNA and acridines. *J. Mol. Biol.* **3**, 18-30 (1961).

223. Waring, M.J. Complex formation between ethidium bromide and nucleic acids. *J. Mol. Biol.* **13**, 269-282 (1965).

224. Chaires, J.B. A thermodynamic signature for drug-DNA binding mode. *Arch. Biochem. Biophys.* **453**, 26-31 (2006).

225. Zhang, L.Z. & Tang, G.-Q. The binding properties of photosensitizer methylene blue to herring sperm DNA: a spectroscopic study. *J. Photochem. Photobiol. B* **74**, 119-125 (2004).

226. Tong, C., Hu, Z. & Wu, J. Interaction between methylene blue and calf thymus deoxyribonucleic acid by spectroscopic technologies. *J. Fluoresc.* **20**, 261-267 (2010).

227. Paul, P. & Suresh Kumar, G. Thionine interaction to DNA: comparative spectroscopic studies on double stranded versus single stranded DNA. *J. Fluoresc.* **22**, 71-80 (2012).

228. Chaires, J.B., Dattagupta, N. & Crothers, D.M. Self-association of daunomycin. *Biochemistry* **21**, 3927-3932 (1982).

229. Chu, X., Shen, G.-L., Jiang, J.-H., Kang, T.-F., Xiong, B. & Yu, R.-Q. Voltammetric studies of the interaction of daunomycin anticancer drug with DNA and analytical applications. *Anal. Chim. Acta* **373**, 29-38 (1998).

230. Dougherty, G. & Pigram, W.J. Spectroscopic analysis of drug nucleic-acid interactions. *CRC Crit. Rev. Biochem.* **12**, 103-132 (1982).

231. Ortiz, M., Fragoso, A., Ortiz, P.J. & O'Sullivan, C.K. Elucidation of the mechanism of single-stranded DNA interaction with methylene blue: a spectroscopic approach. *J. Photochem. Photobiol. A* **218**, 26-32 (2011).

232. Suh, D. & Chaires, J.B. Criteria for the mode of binding of DNA binding agents. *Bioorg. Med. Chem.* **3**, 723-728 (1995).

233. Mowry, S. & Ogren, P.J. Kinetics of methylene blue reduction by ascorbic acid. *J. Chem. Educ.* **76**, 970-970 (1999).

234. Snehalatha, T., Rajanna, K.C. & Saiprakash, P.K. Methylene blue - ascorbic acid: an undergraduate experiment in kinetics. *J. Chem. Educ.* **74**, 228 (1997).

235. Pande, S., Ghosh, S.K., Nath, S., Praharaj, S., Jana, S., Panigrahi, S., Basu, S. & Pal, T. Reduction of methylene blue by thiocyanate: kinetic and thermodynamic aspects. *J. Colloid Interface Sci.* **299**, 421-427 (2006).

236. Pourreza, N. & Mousavi, H.Z. Kinetic spectrophotometric determination of vanadium (V) based on its inhibitory effect on the thionine – ascorbic acid reaction. *Anal. Lett.* **33**, 2065-2073 (2000).

237. Liu, Y., Yamamoto, S. & Sueishi, Y. Kinetic studies on oxidations of leucomethylene blue and leucothionine by iron (III) in aqueous solution. *J. Phys. Org. Chem.* **12**, 194-200 (1999).

238. Schweitzer, B.A., Egholm, M. & Koch, T.H. Mechanistic studies of the reduction of daunomycin with sodium borohydride. Formation and reaction of borate esters. *J. Am. Chem. Soc.* **114**, 242-248 (1992).

239. Abdella, B.R.J. & Fisher, J. A chemical perspective on the anthracycline antitumor antibiotics. *Environ. Health Perspect.* **64**, 3-18 (1985).

240. Houée-Levin, C., Gardes-Albert, M. & Ferradini, C. Pulse radiolysis study of daunorubicin redox reactions: redox cycles or glycosidic cleavage. *J. Free Radic. Biol. Med.* **2**, 89-97 (1986).

241. Kleyer, D.L. & Koch, T.H. Mechanistic investigation of reduction of daunomycin and 7-deoxydaunomycinone with bi(3,5,5-trimethyl-2-oxomorpholin-3-yl). *J. Am. Chem. Soc.* **106**, 2380-2387 (1984).

242. Cummings, J., Morrison, J.G. & Willmott, N. Determination of anthracycline purity in patient samples and identification of in vitro chemical reduction products by application of a multi-diode array high-speed spectrophotometric detector. *J. Chromatogr.* **381**, 373-384 (1986).

243. Bouma, J., Beijnen, J.H., Bult, A. & Underberg, W.J.M. Anthracycline antitumour agents A review of physicochemical, analytical and stability properties. *Pharm. Weekbl. Sci.* **8**, 109-133 (1986).

244. Bird, D.M., Boldt, M. & Koch, T.H. Leucodaunomycin, a tautomer of daunomycin hydroquinone. *J. Am. Chem. Soc.* **111**, 1148-1150 (1989).

245. Wong, E.L.S., Erohkin, P. & Gooding, J.J. A comparison of cationic and anionic intercalators for the electrochemical transduction of DNA hybridization via long range electron transfer. *Electrochem. Commun.* **6**, 648-654 (2004).

246. Graves, D.E. & Krugh, T.R. Adriamycin and daunorubicin bind in a cooperative manner to deoxyribonucleic acid. *Biochemistry* **22**, 3941-3947 (1983).

247. Chaires, J.B., Satyanarayana, S., Suh, D., Fokt, I., Przewloka, T. & Priebe, W. Parsing the free energy of anthracycline antibiotic binding to DNA. *Biochemistry* **35**, 2048-2053 (1996).

248. Lin, P.-H., Kao, Y.-H., Chang, Y., Cheng, Y.-C., Chien, C.-C. & Chen, W.-Y. Daunomycin interaction with DNA: microcalorimetric studies of the thermodynamics and binding mechanism. *Biotechnol. J.* **5**, 1069-1077 (2010).

249. Mukherjee, A., Lavery, R., Bagchi, B. & Hynes, J.T. On the molecular mechanism of drug intercalation into DNA: a simulation study of the intercalation pathway, free energy, and DNA structural changes. *J. Am. Chem. Soc.* **130**, 9747-9755 (2008).

250. Patel, D.J. & Canuel, L.L. Anthracycline antitumor antibiotic. Nucleic-acid interactions. *Eur. J. Biochem.* **90**, 247-254 (1978).

251. Yu, H., Ren, J., Chaires, J.B. & Qu, X. Hydration of drug-DNA complexes: greater water uptake for adriamycin compared to daunomycin. *J. Med. Chem.* **51**, 5909-5911 (2008).

252. Chaires, J.B. Calorimetry and thermodynamics in drug design. *Annu. Rev. Biophys.* **37**, 135-151 (2008).

253. Chen, Y.Z. & Prohofsky, E.W. Melting profile and temperature dependent binding constant of an anticancer drug daunomycin-DNA complex. *Eur. Biophys. J.* **24**, 203-212 (1996).

254. Remeta, D.P., Mudd, C.P., Berger, R.L. & Breslauer, K.J. Thermodynamic characterization of daunomycin-DNA interactions: comparison of complete binding profiles for a series of DNA host duplexes. *Biochemistry* **32**, 5064-5073 (1993).

255. Xodo, L., Manzini, G. & Ruggiero, J. On the interaction of daunomycin with synthetic alternating DNAs: sequence specificity and polyelectrolyte effects on the interaction equilibrium. *Biopolymers* **27**, 1839-1857 (1988).

256. Remeta, D.P., Mudd, C.P., Berger, R.L. & Breslauer, K.J. Thermodynamic characterization of daunomycin-DNA interactions: microcalorimetric measurements of daunomycin-DNA binding enthalpies. *Biochemistry* **30**, 9799-9809 (1991).

257. Chaires, J.B. Thermodynamics of the daunomycin-DNA interaction: ionic strength dependence of the enthalpy and entropy. *Biopolymers* **24**, 403-419 (1985).

258. Belozerova, I. & Levicky, R. Melting thermodynamics of reversible DNA/ligand complexes at interfaces. *J. Am. Chem. Soc.* **134**, 18667-18676 (2012).

259. Rentzeperis, D., Medero, M. & Marky, L.A. Thermodynamic investigation of the association of ethidium, propidium and bis-ethidium to DNA hairpins. *Bioorg. Med. Chem.* **3**, 751-759 (1995).

260. Qu, X. & Chaires, J.B. Contrasting hydration changes for ethidium and daunomycin binding to DNA. *J. Am. Chem. Soc.* **121**, 2649-2650 (1999).

261. Hsieh, K., Patterson, A.S., Ferguson, B.S., Plaxco, K.W. & Soh, H.T. Rapid, sensitive, and quantitative detection of pathogenic DNA at the point of care through microfluidic electrochemical quantitative loop-mediated isothermal amplification. *Angew. Chem., Int. Ed.* **51**, 4896-4900 (2012).

262. Arcamone, F., Franceschi, G., Orezzi, P., Penco, S. & Mondelli, R. The structure of daunomycin. *Tetrahedron Lett.* **9**, 3349-3352 (1968).

263. Barthelemy-Clavey, V., Maurizot, J.C., Dimicoli, J.L. & Sicard, P. Self-association of daunorubicin. *FEBS Lett.* **46**, 5-10 (1974).

264. Ibrahim, M.S. Voltammetric studies of the interaction of nogalamycin antitumor drug with DNA. *Anal. Chim. Acta* **443**, 63-72 (2001).

265. Wang, J., Lin, M.S. & Villa, V. Adsorptive stripping voltammetric determination of low levels of daunorubicin. *Analyst* **112**, 1303-1307 (1987).

266. Kelley, S.O., Jackson, N.M., Hill, M.G. & Barton, J.K. Long-range electron transfer through DNA films. *Angew. Chem., Int. Ed.* **38**, 941-945 (1999).

267. Oliveira-Brett, A.M., Vivan, M., Fernandes, I.R. & Piedade, J.A. Electrochemical detection of in situ adriamycin oxidative damage to DNA. *Talanta* **56**, 959-970 (2002).

268. Wang, J., Ozsoz, M., Cai, X., Rivas, G., Shiraishi, H., Grant, D.H., Chicharro, M., Fernandes, J. & Palecek, E. Interactions of antitumor drug daunomycin with DNA in solution and at the surface. *Bioelectrochem. Bioenerg.* **45**, 33-40 (1998).

269. Molinier-Jumel, C., Malfoy, B., Reynaud, J.A. & Aubel-Sadron, G. Electrochemical study of DNA-anthracyclines interaction. *Biochem. Biophys. Res. Commun.* **84**, 441-449 (1978).

270. Plambeck, J.A. & Lown, J.W. Electrochemical studies of antitumor antibiotics V. An electrochemical method of measurement of the binding of doxorubicin and daunorubicin derivatives to DNA. *J. Electrochem. Soc.* **131**, 2556-2556 (1984).

271. Carter, M.T., Rodriguez, M. & Bard, A.J. Voltammetric studies of the interaction of metal chelates with DNA. 2. Tris-chelated complexes of cobalt(III) and iron(II) with 1,10-phenanthroline and 2,2'-bipyridine. *J. Am. Chem. Soc.* **111**, 8901-8911 (1989).

272. Rao, G.M., Lown, J.W. & Plambeck, J.A. Electrochemical studies of antitumor antibiotics III. Daunorubicin and adriamycin. *J. Electrochem. Soc.* **125**, 534-534 (1978).

273. Ibrahim, M.S. Voltammetric behaviour and determination of the anthracycline antitumor drug nogalamycin. *Anal. Chim. Acta* **409**, 105-112 (2000).

274. Nicholson, R.S. Theory and application of cyclic voltammetry for measurement of electrode reaction kinetics. *Anal. Chem.* **37**, 1351-1355 (1965).

275. Kano, K., Konse, T. & Kubota, T. The effets of the pH and the temperature on the oxidation-reduction properties of adriamycin adsorbed on a mercury electrode surface. *Bull. Chem. Soc. Jpn.* **58**, 424-428 (1985).

276. Gaudiano, G. & Koch, T.H. Reaction of the quinone methide from reductive glycosidic cleavage of daunomycin with molecular oxygen. Evidence of semiquinone methide formation. *J. Am. Chem. Soc.* **112**, 9423-9425 (1990).

277. Fisher, J., Abdella, B.R. & McLane, K.E. Anthracycline antibiotic reduction by spinach ferredoxin-NADP+ reductase and ferredoxin. *Biochemistry* **24**, 3562-3571 (1985).

278. Barthwal, R., Mujeeb, A., Srivastava, N. & Sharma, U. A proton nuclear magnetic resonance investigation of the conformation of daunomycin. *Chem. Biol. Interact.* **100**, 125-139 (1996).

279. Arcamone, F., Cassinelli, G., Orezzi, P., Franceschi, G. & Mondelli, R. Daunomycin I. The structure of daunomycinone. *J. Am. Chem. Soc.* **86**, 5334-5335 (1964).

280. Pauli, G.F., Jaki, B.U. & Lankin, D.C. Quantitative 1H NMR: development and potential of a method for natural products analysis. *J. Nat. Prod.* **68**, 133-149 (2004).

281. Kertesz, V., Chambers, J.Q. & Mullenix, A.N. Chronoamperometry of surface-confined redox couples. Application to daunomycin adsorbed on hanging mercury drop electrodes. *Electrochim. Acta* **45**, 1095-1104 (1999).

282. Nowicka, A.M., Zabost, E., Donten, M., Mazerska, Z. & Stojek, Z. Electrooxidation of dissolved dsDNA backed by in situ UV-Vis spectroscopy. *Bioelectrochemistry* **70**, 440-445 (2007).

283. Oliveira-Brett, A.M., Piedade, J.A., Silva, L.A. & Diculescu, V.C. Voltammetric determination of all DNA nucleotides. *Anal. Biochem.* **332**, 321-329 (2004).

284. Paleček, E., Fojta, M., Jelen, F. & Vetterl, V. in *The Encyclopedia of Electrochemistry*. (Eds. A.J. Bard & M. Stratmann) pp. 365-429 (Wiley-VCH Verlag, Weinham, 2002).

285. Gaudiano, G., Frigerio, M., Bravo, P. & Koch, T.H. Reduction of daunomycin in dimethyl sulfoxide. Long-lived semiquinones and quinone methide and formation of an enolate at the 14-Position via the quinone methide. *J. Am. Chem. Soc.* **114**, 3107-3113 (1992).

286. Octavia, Y., Tocchetti, C.G., Gabrielson, K.L., Janssens, S., Crijns, H.J. & Moens, A.L. Doxorubicin-induced cardiomyopathy: from molecular mechanisms to therapeutic strategies. *J. Mol. Cell. Cardiol.* **52**, 1213-1225 (2012).

287. Batchelor-McAuley, C., Dimov, I.B., Aldous, L. & Compton, R.G. The electrochemistry of quinizarin revealed through its mediated reduction of oxygen. *Proc. Natl. Acad. Sci. USA* **108**, 19891-19895 (2011).

288. Cheng, G., Qu, H., Zhang, D., Zhang, J., He, P. & Fang, Y. Spectroelectrochemical study of the interaction between antitumor drug daunomycin and DNA in the presence of antioxidants. *J. Pharm. Biomed. Anal.* **29**, 361-369 (2002).

289. Li, Q., Batchelor-McAuley, C., Lawrence, N.S., Hartshorne, R.S. & Compton, R.G. Semiquinone intermediates in the two-electron reduction of quinones in aqueous media and their exceptionally high reactivity towards oxygen reduction. *ChemPhysChem* **12**, 1255-1257 (2011).

290. Berlin, V. & Haseltine, W.A. Reduction of adriamycin to a semiquinone-free radical by NADPH cytochrome P-450 reductase produces DNA cleavage in a reaction mediated by molecular oxygen. *J. Biol. Chem.* **256**, 4747-4756 (1981).

291. Bishop, G.R. & Chaires, J.B. Characterization of DNA structures by circular dichroism. *Curr. Protoc. Nucleic Acid Chem.* **Chapter 7**, Unit 7 11 (2003).

292. Dalgleish, D.G., Fey, G. & Kersten, W. Circular dichroism studies of complexes of the antibiotics daunomycin, nogalamycin, chromomycin and mithramycin with DNA. *Biopolymers* **13**, 1757-1766 (1974).

293. Baase, W.A. & Johnson, W.C. Circular dichroism and DNA secondary structure. *Nucleic Acids Res.* **6**, 797-814 (1979).

294. Jones, R.L. & Wilson, W.D. Effect of ionic strength on the pKa of ligands bound to DNA. *Biopolymers* **20**, 141-154 (1981).

295. Cline, J., Braman, J.C. & Hogrefe, H.H. PCR fidelity of pfu DNA polymerase and other thermostable DNA polymerases. *Nucleic Acids Res.* **24**, 3546-3551 (1996).

Appendices

Appendix A

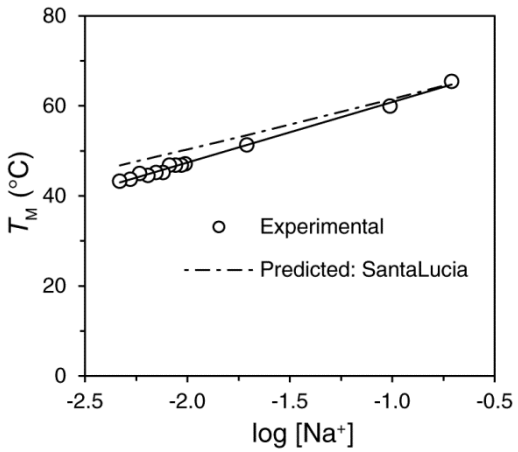

Figure A.1 Influence of log [Na⁺] on T_M. Re-plot of T_M values from Figure 3.7 as a function of log [Na⁺]. A linear decrease of T_M is observed with decreasing [Na⁺] permitting the calculation of the slope $\partial T_M / \partial \log[Na^+]$. Error bars too small to be visible, however they represent standard deviation (n = 3).

Appendix B

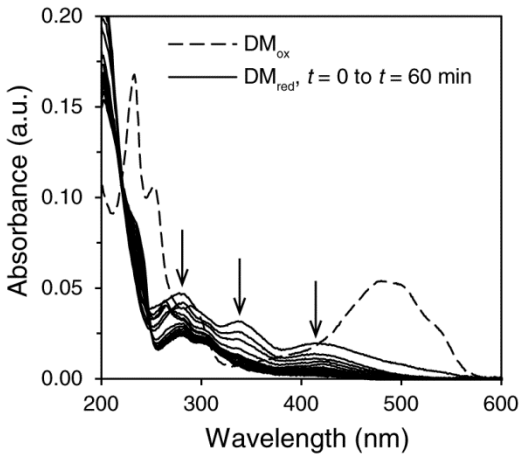

Figure A.2 Time-course reduction of DM with sodium borohydride. 100 μM DM in the presence of 5 mM sodium borohydride (50× in excess) in SSC buffer at 7.0 mM Na^+, pH 7. A spectrum was recorded every 5 min over 60 min. The maximum absorbance peak at 480 nm for oxidised MB disappeared. Instead, two new peaks and a shoulder at 280, 336 and 420 nm, respectively, were identified which continuously decreased over the course of the reduction.

Appendix C

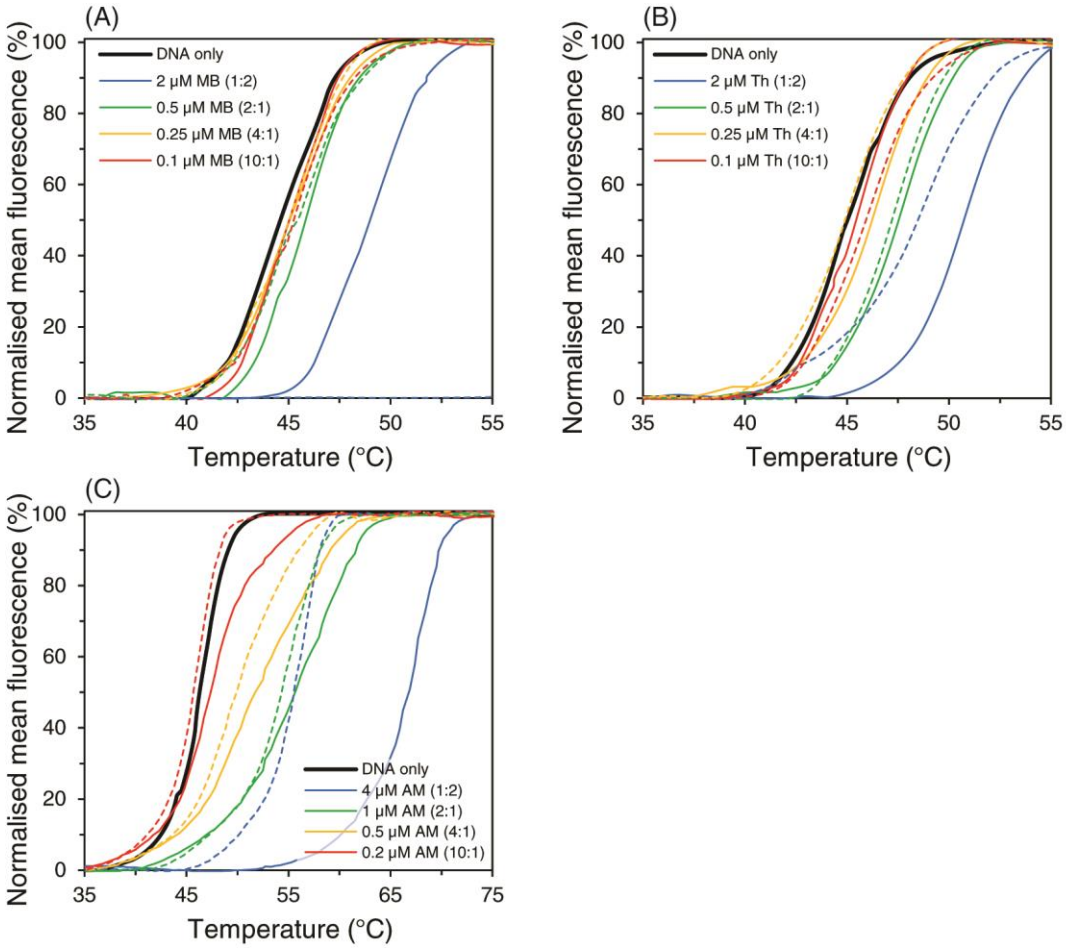

Figure A.3 Effect of oxidised and reduced intercalator on DNA stability. Normalised denaturation curves of 20mer dsDNA in the presence of oxidised (solid lines) and chemically reduced (dotted lines) (A) MB, (B) thionine and (C) AM, at varying concentrations, in SSC buffer at 7.0 mM Na^+. The control (thick line) is recorded in the absence of each intercalator. No significant increase in T_M of DNA was observed in the presence of MB and thionine. Both reduced and oxidised forms of these intercalator generated similar T_M values. However, unlike its reduced form, the highest concentration of oxidised AM increased T_M of DNA considerably (molar ratio 1:2).

Appendix D

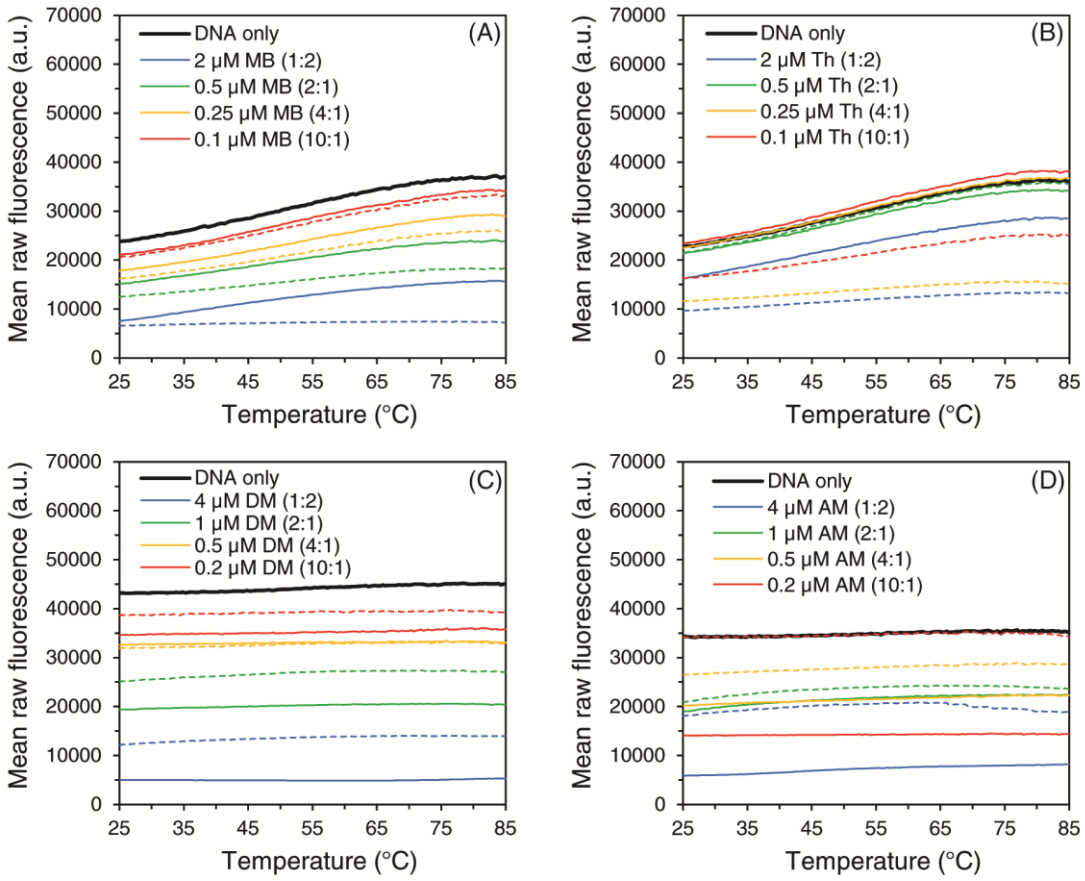

Figure A.4 Effect of oxidised and reduced intercalator on fluorophore-labelled ssDNA. The effect on fluorophore-labelled 20mer ssDNA in the presence of oxidised (solid lines) and chemically reduced (dotted lines) intercalator was investigated in SSC buffer at 7.0 mM Na^+. Impact on 6-FAM was examined in the presence of (A) MB and (B) thionine, while the impact on TexasRed was studied in the presence of (C) DM and (D) AM. The control (thick line) consists of the fluorophore-labelled ssDNA in the absence of an intercalator. Quenching of fluorescence was observed in the presence of the highest concentration of reduced MB and oxidised DM and AM (molar ratio 1:2).

Appendix E

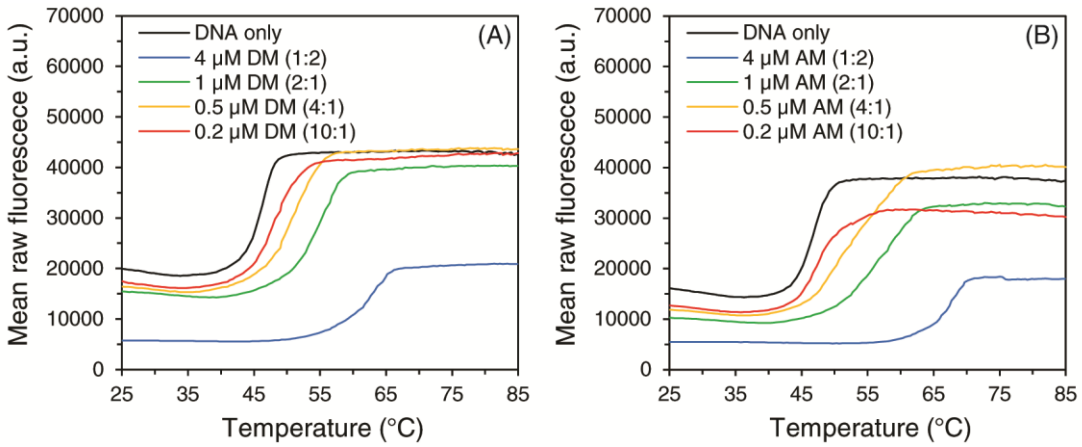

Figure A.5 Raw melting curves of DNA with oxidised DM and AM. Raw denaturation profiles of 20mer dsDNA in the presence of oxidised (A) DM and (B) AM, at varying concentrations, in SSC buffer at 7.0 mM Na^+. The fluorescence of TexasRed became quenched as denaturation of the DNA:intercalator complex proceeded at the highest concentration of respective intercalator (molar ratio 1:2).

Appendix F

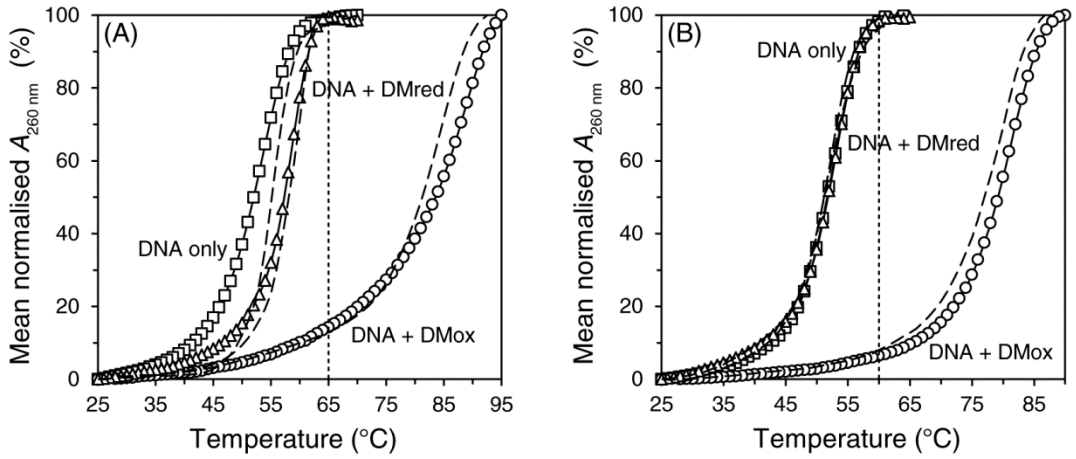

Figure A.6 Effect of oxidised and reduced DM on DNA with UV–vis. Normalised absorbance-based renaturation (solid lines with markers) and denaturation (dashed lines) curves of 200 μM (A) 40mer dsDNA in SSC buffer at 7.0 mM Na^+ and (B) 20mer dsDNA in SSC buffer at 19.5 mM Na^+ in the presence and absence of oxidised and chemically reduced 100 μM DM (molar ratio 2:1). The dotted line represents the determined working temperature.

Appendix G

Table A.1 Predicted thermodynamic parameters for DNA only at investigated conditions.†

Condition	$\Delta H°$ (kcal mol^{-1})	$\Delta S°$ (cal mol^{-1})	$\Delta G°_{37}$ (kcal mol^{-1})	T_M (°C)
20mer, 7.0 mM Na^+	-155.70	-470.23	-9.86	41.73
40mer, 7.0 mM Na^+	-326.00	-974.47	-23.77	53.27
20mer, 19.5 mM Na^+	-155.70	-454.05	-14.87	52.38

† Parameters predicted with IDT Biophysics' DNA thermodynamics & hybridisation calculator.[195]

Appendix H

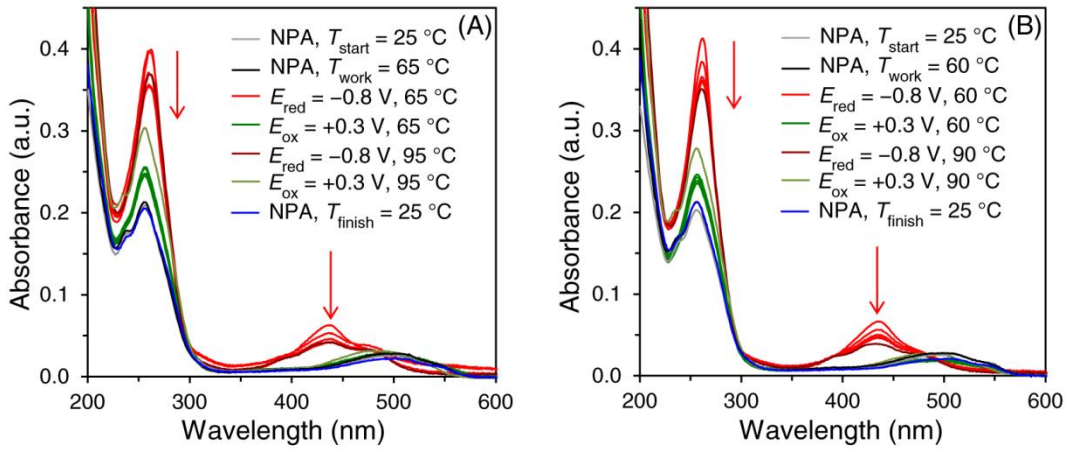

Figure A.7 Additional conditions for electrochemical control of reversible DNA hybridisation by redox-state switching of DM. Absorption spectra of 200 µM (A) 40mer dsDNA at T_{work} = 65 °C and (B) 20mer dsDNA at T_{work} = 60 °C in the presence of 100 µM DM in SSC buffer (7.0 mM Na^+ and 19.5 mM Na^+, respectively), pH 7 (molar ratio 2:1). Cyclic denaturation and renaturation of dsDNA was demonstrated with *in situ* UV–vis spectroelectrochemistry. Upon reducing DM at −0.8 V, a significant increase in absorbance at 260 nm was observed indicating denaturation. This increase was reversed upon switching the potential to +0.3 V for the re-oxidation of DM, thus, suggesting hybridisation. (NPA = no potential applied).

Appendix I

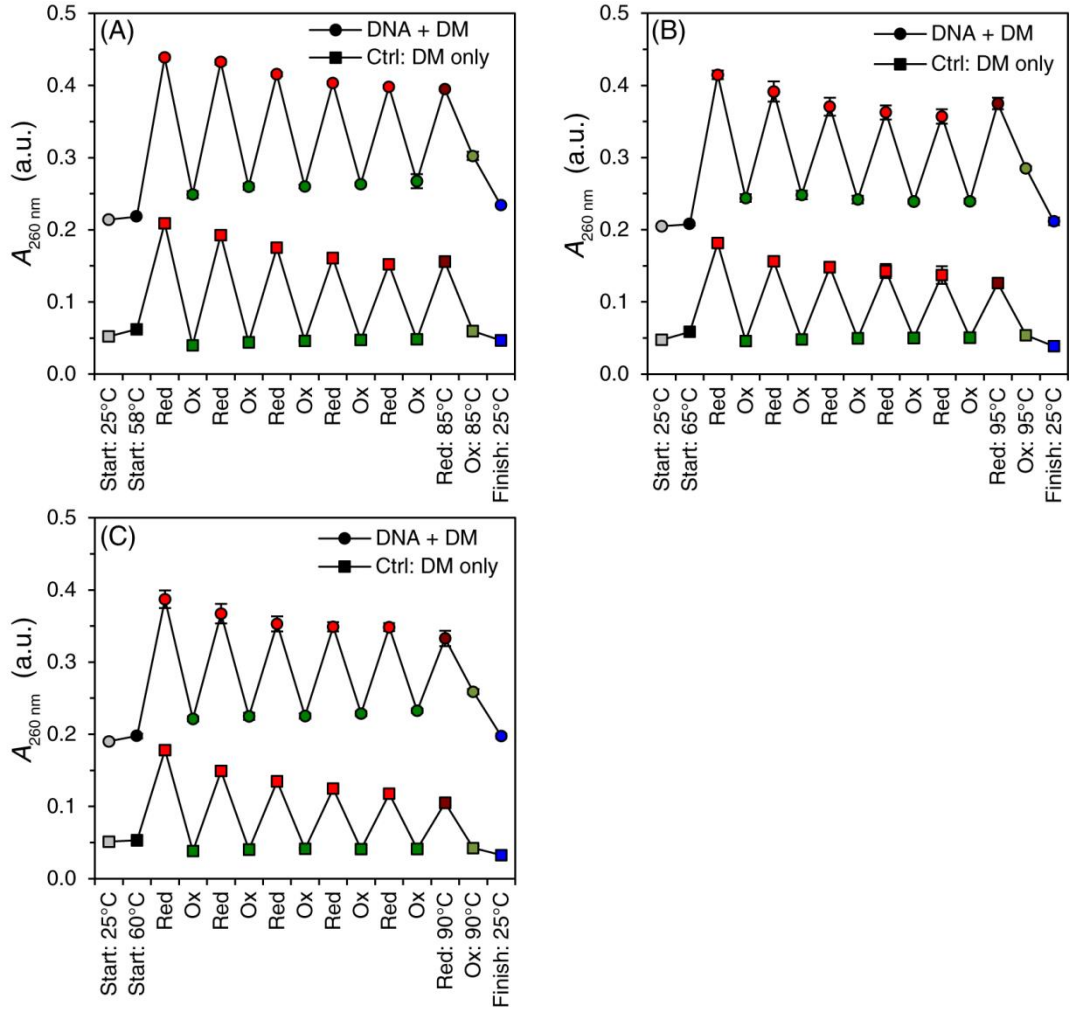

Figure A.8 Raw absorbance values at 260 nm for DNA with DM and DM alone. The raw absorption values at 260 nm for 100 μM DM alone and in the presence of 200 μM (A) 20mer dsDNA (SSC buffer, 7.0 mM Na^+), (B) 40mer dsDNA (SSC buffer, 7.0 mM Na^+) and (C) 20mer dsDNA (SSC buffer, 19.5 mM Na^+). These values were used in Eq. (1.11) in order to obtain the change in absorption exclusively assigned to DNA.

Appendix J

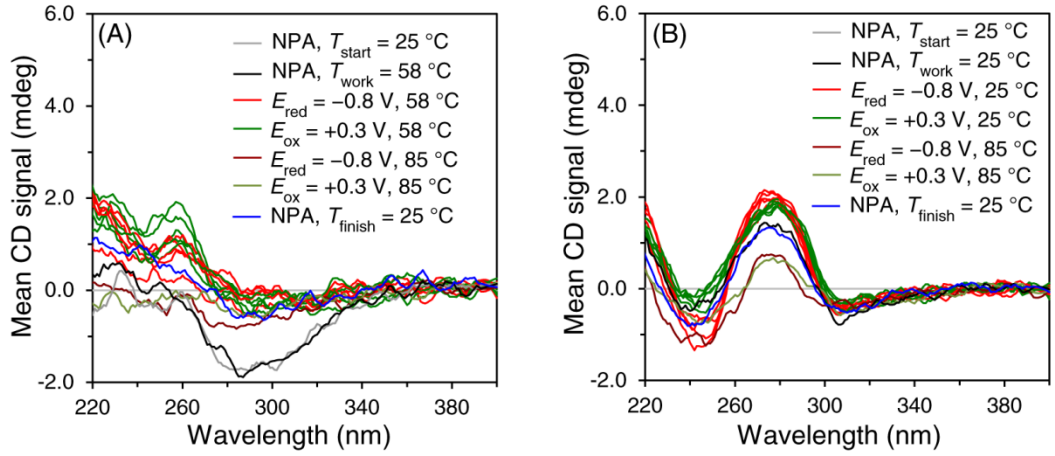

Figure A.9 *in situ* CD spectroelectrochemistry of DM only and DNA only. Changes in the CD spectra of (A) 100 µM DM at T_{work} = 58 °C (B) for 200 µM 20mer dsDNA (bp concentration) at T_{work} = 25 °C in SSC buffer (7.0 mM Na^+), pH 7, upon cycling the redox potentials −0.8 V and +0.3 V. No change in CD was observed for DM and DNA alone at 275 nm. (NPA = no potential applied).

Published Paper

Cyclic denaturation and renaturation of double stranded DNA by redox-state switching of DNA intercalators.

Shahida N. Syed, Holger Schulze, Daniel Macdonald, Jason Crain, Andrew R. Mount, Till T. Bachmann

J. Am. Chem. Soc. **135**, 5399–5407 (2013)

DOI: 10.1021/ja311873t